10-31-2023

On the Origin of AIDS: CARD8's Role in Pathogenesis and Cure

Kolin Clark
Washington University in St. Louis

WASHINGTON UNIVERSITY IN ST. LOUIS
Division of Biology and Biomedical Sciences
Molecular Genetics and Genomics

Dissertation Examination Committee:
Liang Shan, Chair
Siyuan Ding
Makedonka Mitreva
Rachel Presti
Lee Ratner
Nancy Saccone

On the Origin of AIDS: CARD8's Role in Pathogenesis and Cure

by

Kolin Mark Clark

A dissertation presented to
Washington University in St. Louis
in partial fulfillment of the
requirements for the degree
of Doctor of Philosophy

December 2023
St. Louis, Missouri

Table of Contents

List of Figures

List of Tables

Acknowledgments

I would first like to thank my mentor, Liang Shan. It has been an honor to be your first PhD student and to learn from your expertise in HIV immunology and cure research. Your constant support and guidance in ensuring that clinical outcomes be at the forefront of our work have helped me get to where I am and guaranteed that my work has an impact for those affected by HIV. I'd like to thank my colleagues in the lab, Qiankun Wang and Hongbo Gao for answering my questions and teaching me relevant techniques, Ritudwhaj Tiwari and Josh Kim for your repeated assistance on the experiments that I could not accomplish alone, and Toni Sherlinski in keeping the whole Shan lab running through thick and thin. It has also been my pleasure to mentor Hilary Weisburd in her growing interest in HIV research, I see a bright future for you in this field and I hope you take your inquisitive nature with you wherever you go. I would also like to thank my thesis committee for your unwavering support and guidance, and in particular Lee Ratner for your longstanding commitment to the field and for chairing my committee. In addition, Sebla Kutluay offered repeated advice and collaboration for our molecular and biochemical work that was critical in understanding CARD8 activation by HIV protease. My previous mentors Kirby Phillips, Elena Bray Speth, Christine Vogel, and Enoma Omoregie were pivotal in creating and maintaining my desire for a career in biology and public health. The final mentors that I would like to thank are the Molecular Genetics and Genomics program directors Jim Skeath and John Edwards as well as Melanie Relich for your mentorship as a researcher and an individual, I would not have been as successful in my graduate career without you all. I would also like to recognize my funding through the National Institutes of Health F31 fellowship.

I would also like to thank my science policy colleagues in ProSPER and NSPN for providing me with a community where I could thrive in my exploration of a career in Science Policy. Specifically, I would like to thank my SciDEAL team Shane Coffield, Colbie Chinowsky, Anna Dye, and Jacob O'Connor for working tirelessly with me on LGBTQ+ equity in STEM. You provided me with a sense of community and friendship as we worked on a topic we care so much about; I cannot thank you enough. I would also like to thank Ronit Prawer for developing the project and for constantly pushing for a world where LGBTQ+ people can thrive.

Like raising a child, completing a PhD requires a village. My chosen and biological family have been critical to ensuring my success in this process. My parents have always supported my career even without fully understanding what I do. I would not be where I am today without my chosen family and I would like to thank you from the bottom of my heart Becky, Andrew, Erika, Anna, Casey, Ben, Emilee, Landon, Katalin, Dave, Alyssa, and Brie. You keep me going when things are rough and make sure I enjoy life when they are not. Lastly, I would like to thank the LGBTQ+ community for teaching me resiliency, love, compassion, and kindness. We experienced an incalculable loss of our community to the HIV pandemic that can never be regained. This dissertation is for those lives that are no longer with us and their loved ones that experienced their chosen families disappear in a world that did not accept them. I envision a world where one day HIV will be cured, LGBTQ+ people will not experience discrimination, and where we can thrive in STEM.

Kolin Clark

Washington University in St. Louis

December 2023

Dedicated to the millions of LGBTQ+ lives lost to the HIV/AIDS pandemic.

ABSTRACT OF THE DISSERTATION

On the Origin of AIDS: CARD8's Role in Pathogenesis and Cure

by

Kolin Mark Clark

Doctor of Philosophy in Biology and Biomedical Sciences

Molecular Genetics and Genomics

Washington University in St. Louis, 2023

Dr. Liang Shan, Chair

HIV infection remains a major global health burden with 1.7 million new acquisitions and 770,000 deaths in 2018 alone. While these numbers are declining due to antiretroviral therapy, only a handful of individuals have achieved complete remission from HIV. With the advent of antiretroviral therapy, HIV has turned a death sentence into a chronic, manageable condition. However, current antiretroviral therapies have only been studied on their ability to block infection and have not been able to clear the viral reservoir. Additionally, HIV cure strategies often rely upon sensing of highly variable epitopes such as the HIV envelope and have not achieved broad success. We previously identified a novel pattern recognition receptor, the caspase recruitment domain family member 8 (CARD8), that can sense HIV-1 protease activity in infected cells after dimerization by non-nucleoside reverse transcriptase inhibitors. CARD8 can be cleaved by HIV-1 protease and induces Caspase-1 inflammasome activation and pyroptosis of infected cells.

The utilization of NNRTIs to induce CARD8 inflammasome activation offers a promising strategy for eliminating HIV-infected cells in a "Shock and Kill" approach due to its

reliance upon viral protease activity which is less susceptible to mutation than its envelope counterpart. However, this process has reduced efficacy *in vivo* due to high binding affinity of NNRTI's to serum proteins and antiretroviral drug resistance. Therefore, it is imperative to elucidate ways to sensitize the CARD8 inflammasome to NNRTI-induced activation. We show that this sensitization can be achieved through chemical inhibition of the CARD8 negative regulator DPP9. The DPP9 inhibitor Val-boroPro (VbP) kills HIV-1-infected cells without the presence of NNRTIs and acts synergistically with NNRTIs to promote clearance of HIV-1-infected cells *in vitro* and in humanized mice. More importantly, VbP can enhance clearance of residual HIV in $CD4^+$ T cells isolated from people living with HIV (PLWH). We also show that VbP can ameliorate issues with NNRTI serum binding by reducing the threshold for CARD8 activation and can partially overcome NNRTI resistance. This offers a solution to enhance NNRTI efficacy in the elimination of HIV-1 reservoirs in PLWH.

We also recently discovered that CARD8 inflammasome activation, immediately upon HIV-1 viral entry and release of HIV protease, may contribute substantially to $CD4^+$ T cell loss. The loss of non-productively infected $CD4^+$ T cells, known as bystander cell death, is the main contributor to HIV-1 disease progression and AIDS. Until the elucidation of CARD8's role in this process, it was largely unknown how these cells undergo cell death without productive infection. Additionally, disease progression in non-human primate models of SIV infection display stark differences in their ability to recapitulate human disease. Some NHP species, such as those in the *Cercocebus* and *Chlorocebus* genera, do not develop $CD4^+$ T cell loss and AIDS like symptoms in contrast to members of the Macaca genus. These non-pathogenic or "natural" hosts of SIV infection raise questions of CARD8's role in lentiviral disease progression. We discovered loss-of-function mutations in the CARD8-coding genes from these "natural hosts",

which may explain the peculiarly non-pathogenic nature of these infections. These mutations were likely a byproduct of a novel reverse tandem gene duplication in the CARD8 gene of the *Cercopithecoidae* lineage which allows for increased mutational rates. As only the non-pathogenic hosts of SIV infection have naturally experienced SIV infection, it is possible that these loss-of-function mutations were selected to avoid $CD4^+$ T Cell loss in endemic populations. We show that only the pathogenic hosts of infection have functional CARD8 proteins that can be cleaved and activated by SIV protease and that can induce rapid cell death. We propose this mechanism as a potential explanation for the difference in pathogenicity of non-human primate species.

Chapter 1: Introduction

Section 1.2 has been reproduced and adapted from the following publication:

Clark, K.M., Pal, P., Kim, J.G., Wang, Q., Shan, L. The CARD8 inflammasome in HIV infection. *Advances in Immunology* **157**, 59-100 (2023).

Section 1.3.3 was written by Priya Pal, all other sections were written by Kolin Clark

Section 1.4.3 contains writing by Qiankun Wang reproduced and adapted from the following unpublished manuscript the rest of the contents of this manuscript are discussed in Chapter 3:

Wang*, Q., Clark*, K.M., Tiwari, R., Burdo, T.H., Silvestri, G., Shan, L. The CARD8 Inflammasome Dictates HIV/SIV Pathogenesis and Disease Progression.

1.1 Overview of HIV

1.1.1 Introduction to the HIV Pandemic

The HIV pandemic first arose in the 1980's and has since resulted in an estimated 74.9 million people acquiring the causative agent of AIDS and claiming the lives of 32 million. While acquisition rates are decreasing, HIV remains a major global health burden with 1.7 million new infections and 770,000 deaths globally in 2018 alone.[1] Additionally, according to the CDC in 2016, 330,000 LGBTQ+ lives have been lost in the US since the start of the pandemic accounting for 48% of the total deaths. While the LGBTQ+ community comprises a small fraction of the general population, they are disproportionally affected by the HIV pandemic which are compounded in communities of color when observing rates of diagnoses, access to

antiretroviral therapy (ART), and achieving viral suppression.[2] This highlights a distinct issue of who is benefitting from new research, therapeutics, and interventions.

Even with the decline in acquisitions, there are still major obstacles to overcome in stopping the spread of the pandemic. The main barriers involve access to care and prevention, lack of testing and education, and lack of curative treatment or vaccination. The first speaks to socio-economic factors that keep certain communities and countries from access to combined antiretroviral therapy, pre-exposure prophylaxis (PrEP), and post-exposure prophylaxis (PEP) as the majority of HIV incidences affect the global south which have not been allocated proper resources and policies to stem the spread and control of HIV.[3,4] The second again stems from health disparities present in specific communities in the ability to access the necessary education and testing services required to prevent acquisition and spread of the disease.[3] The most important is the third; there is still no vaccine for HIV due to the highly mutagenic nature of the HIV genome and no treatment for eradicating the disease in people living with HIV (PLWH) due to the ability of HIV to establish a latent viral reservoir early on during infection. Current antiretroviral therapies can maintain suppression of viral replication, but HIV can integrate into the genome of $CD4^+$ T-cells, and potentially macrophages, to become latent. The evidence for latency can easily be seen once PLWH are taken off ART and rapidly have rebound of viral replication.[5] This inability to combat infection calls for further investigation into methods of stopping the virus by further understanding how the latent reservoir is established to prevent infection, how disease progresses to AIDS, and novel cure strategies for the eradication of HIV latent reservoirs.

1.1.2 The HIV Life Cycle

The HIV-1 virion contains two copies of a 9kb single-stranded RNA genome encapsulated in a Capsid (*Ca*) core along with the enzymes required for its replication.[6,7] A schematic of the HIV viral genome can be seen in **Figure 1.1**. The HIV-1 life cycle begins by binding of the HIV envelope glycoprotein (*env*) to the CD4 receptor on the surface of $CD4^+$ T cells and macrophages.[8,9] It also necessitates binding to one of two co-receptors depending upon tropism: CCR5 or CXCR4.[8,9] After binding, the HIV envelope fuses with the host cell membrane thereby releasing viral proteins and the capsid core containing the HIV genomic RNA (gRNA).[10] This capsid core is transported to the nucleus where it is uncoated. Prior to capsid uncoating, the gRNA undergoes reverse transcription through its reverse transcriptase enzyme (*RT*) to create double stranded DNA which can integrate into the host genome via the viral integrase enzyme (*IN*).[11-13] After integration, the virus uses host machinery for viral genome replication which produces the gRNA and transcripts for translating the key viral proteins required for viral particle construction.[14] The main proteins necessary for viral replication are encoded by the gag-pol polyprotein. The gag-pol transcript has an open reading frame which begins with translation of the gag protein containing the structural components of the virion. The pol polyprotein contains the key enzymes for viral replication and is translated via a frameshift between gag and pol and results in a 20-fold greater expression of gag to gag-pol proteins.[15] These polyproteins localize at the cell membrane via insertion of the myristolated matrix protein into the membrane which can then bind to HIV gRNA via the nucleocapsid protein (*NC*).[16,17] The virion then buds off the host cell. Finally, particle maturation is mediated via the protease enzyme (*PR*) which cleaves the gag-pol protein in a tightly regulated fashion upon dimerization of at least two gag-pol polyproteins resulting in individual mature viral proteins.[18,19]

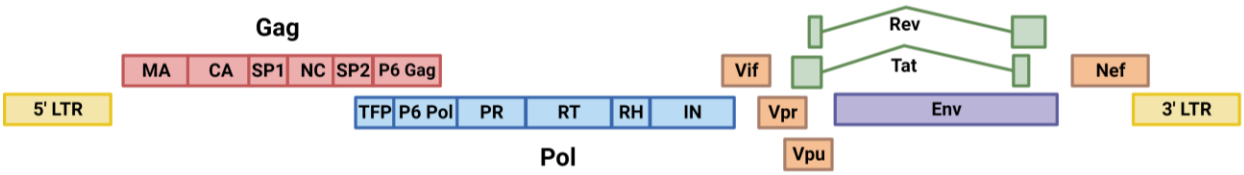

Figure 1.1: Schematic of the HIV Viral Genome

Graphical depiction of the key elements and proteins of the HIV viral genome.

1.1.3 HIV PR as a Target for an HIV Cure

As previously mentioned, the main barrier for an HIV cure is the seeding of the latent viral reservoir in $CD4^+$ T cells and macrophages.[20-22] These latently infected cells harbor intact proviruses and are transcriptionally inactive.[22] However, these latent cells can expand via clonal expansion from homeostatic, antigen-driven, or integration site-driven proliferation which result in persistence of these cell populations.[23-26] This long-lived reservoir of cells is not eliminated by current ART strategies and requires other methods for sustained remission of HIV infection.

Several strategies have been proposed for curing HIV which can be broadly characterized into four groups: hematopoietic stem cell transplantation, CRISPR/Cas9 mediated excision, "block and lock", and "shock and kill".[27] The first has been the only successful method for remission of infection but has only been achieved in a handful of cases.[28-31] Hematopoietic stem cell transplantation relies upon transplanting hematopoietic stem cells from a donor which is naturally resistant to HIV infection via a genetic deletion in the CCR5 co-receptor (CCR5Δ32).[32] However, this method is not a universal strategy for a cure as it requires a matched donor that contains a homozygous CCR5Δ32 mutation, and the exact mechanism of remission is still not fully understood. It is still unclear if irradiation, chemotherapy, drug regimens, or the presence of graft-versus-host disease are required for the sustained remission seen in these case studies.[28-31]

However, it offers promise that a cure is possible. CRISPR/Cas9 mediated excision relies upon editing of the integrated viral genome to inactivate it or to edit the host machinery critical for viral replication.[33] This strategy necessitates high levels of editing efficiency in reservoir cells which is difficult to achieve given the high genetic variability of the genome and issues of targeting all latent reservoirs.[34] Additionally, concerns of off-target effects or on-target effects, such as chromothripsis, present a major concern when delivering this strategy *in vivo.*[35-38] Similarly, the "Block and Lock" strategy attempts to make the integrated provirus fully latent and incapable of reactivation which has largely been unsuccessful and leaves the integrated virus intact in the host genome with the potential of escape and reactivation.[39]

The most popular strategy for an HIV cure is the "Shock and Kill" strategy. This strategy involves reactivation of transcription of the latent provirus and killing infected cells by targeting viral protein expression.[40] The largest barrier for a "Shock and Kill" strategy is finding an LRA that can substantially reactivate the latent reservoir. Numerous LRAs have been proposed for reactivation of the latent reservoir such as epigenetic modifiers (e.g., HDAC inhibitors, HMT inhibitors, bromodomain inhibitors, and P-TEFb activators), PKC agonists, PI3K/Akt pathway modulators, TLR agonists, SMAC mimetics, and TCR activators which have varying degrees of efficacy and off target effects[41]. However, the focus of this dissertation is on improving the second step in this strategy by killing latent reservoirs once they have been reactivated. Most current strategies for the kill approach rely upon inducing apoptosis or clearing latent cells via the adaptive immune response via recognition of viral proteins[41]. The first approach aims to sensitize infected cells to apoptosis but has the critical issue in ensuring no off-target killing of uninfected cells. These pro-apoptotic compounds should only elicit cell death upon the expression of HIV proteins but has encountered barriers as these compounds have issues of

specificity. The adaptive immune targeting of latently infected cells also encounters issues as it relies upon the expression of the highly mutable HIV *Env* protein.[42-44] This protein is one of the most susceptible to genetic variation and can rapidly escape any immune response which highlights the key issues in the development of an HIV vaccine or in the host immune response from being able to maintain suppression of HIV replication on its own. Taken together these pitfalls in the current strategies highlight the need to target HIV proteins that are not as susceptible to genetic variation and that are exclusive to cells producing these viral proteins to eliminate unintended cell death of uninfected cells. Since the HIV pol enzymes PR, RT, and IN are necessary for viral replication they are less susceptible to genetic variation and provide an optimal target for an HIV cure.[45] In this dissertation the focus for an HIV cure strategy relies upon targeting HIV PR activity which cannot be lost by the virion and is not present in uninfected cells again emphasizing its potential for a target for an HIV cure.

1.2 The CARD8 Inflammasome

1.2.1 The Inflammasomes

Inflammasomes were first identified as multiprotein complexes of high molecular weight in the cytosol that mediate the activation of the inflammatory caspases (cysteine-aspartic proteases, cysteine aspartases), such as caspase-1.[46] Caspases are a family of cysteine proteases that are involved in apoptosis (programmed cell death), pyroptosis (inflammatory cell death), and necroptosis (programmed necrosis).[47-52] Caspases play a key role in the removal of infected, senescent, or stressed cells by regulating cell death in response to extracellular and intracellular stressors. Therefore, these regulators of cell death are tightly controlled through their expression as inactive zymogens, or procaspases, which contain an N-terminal pro-domain and a C-terminal

proteolytic domain made up of a large and small subunit.[53-55] Maturation of caspases involves proteolytic cleavage at cysteine residues to remove the pro-domains and transform these procaspases into catalytically active caspases that can cleave their cognate substrates typically after aspartate residues.[53,56,57] The downstream effects of caspase activation culminate in apoptosis or other forms of cell death as well as cytokine release. All active caspases exist as dimers and the exact mechanism of proteolytic cleavage and activation differentiates the various types of caspases. The first type of caspase activation can be seen in caspases-3, -6, and -7, whose procaspases exist as dimers. This type of caspase activation is mediated by either an external cleavage (such as by other caspases) or autoproteolytic cleavage in response to a cellular stressor.[58,59] All other pro-caspases are expressed as monomers, which become activated through oligomerization, which is mediated by docking of adaptor proteins to their pro-domains.[46,60-62] There are two key domains in caspases that are responsible for docking of adaptor molecules to induce activation: the death effector domain (DED) of caspases-8 and -10 and the caspase-like caspase-8 homolog c-FLIP(L) and the CARD domain of Caspases-1, -2, -4, -5, -9, and -12. [56,63-65] Further classification of caspases relies upon their biological function and their position in the apoptotic cascade.[54,56,65] Pro-apoptotic caspases can therefore be classified into extrinsic or initiator caspases, which are more apical in the cascade (caspases-2, -8, -9, -10), and intrinsic or effector caspases, which are more distal (caspases-3, -6, and -7). A third group of caspases include those involved with inflammation such as caspases-1, -4, -5, and -12. These caspases are known to trigger pyroptosis, an inflammatory form of cell death, which is caused by caspase cleavage of GSDMD and other unknown pro-pyroptotic caspase substrates.[46]

The inflammasome is activated upon the sensing of pathogen-associated molecular patterns (PAMPs) or damage-associated molecular patterns (DAMPs) by PRRs, which relay the

signal either directly to the inflammatory caspases or through intermediate signaling molecules.[46,66] The sensing of unique danger signals is a critical component of the innate immune system that allows for greater specificity in the host defense to pathogens.[67] Numerous PRRs have been identified to date and can generally be categorized into five types: NOD-like receptors (NLRs), AIM2-like receptors (ALRs), RIG-I like receptors (RLRs), C-type lectin receptors (CLRs), and Toll-like receptors (TLRs).[68,69] PRRs contain a domain that recognizes the PAMP and a domain that can communicate this sensing such as the death domain (DD) with 37 members, the death effector domain (DED) with 7 members, and the pyrin domain (PYD) with 22 members.[70-73] PAMPs that have been shown to be sensed by PRRs include nucleic acids, metabolites, protein structures, and toxins derived from pathogenic organisms.[68,69] In the context of the inflammasome, activation is commonly mediated through the protein–protein interactions of the CARD domain of the caspase with the CARD domain of a PRR or its adaptor proteins.[45,66,74] Inflammasomes can be broken down into two subgroups based on differences in caspase usage: the canonical and the noncanonical inflammasomes. Canonical inflammasomes are mediated through binding and activation of caspase-1, whereas the non-canonical inflammasome pathway results in caspase-11 or caspase-4 and caspase-5 activation in mouse and humans, respectively.

The canonical inflammasome can be activated upon sensing of myriad PAMPs through a variety of PRRs **Figure 1.2**. Upon activation, caspase-1 cleaves pro-IL1β and pro-IL-18, resulting in the release of their active forms.[46]. Caspase-1 also cleaves GSDMD, triggering pyroptosis. The cleavage of GSDMD causes release of its N-terminal fragment, leading to pore formation and release of the cytosolic contents, thereby promoting inflammation.[75,76] Caspase-1 is activated like other non-effector caspases through docking of adaptor molecules—mediated

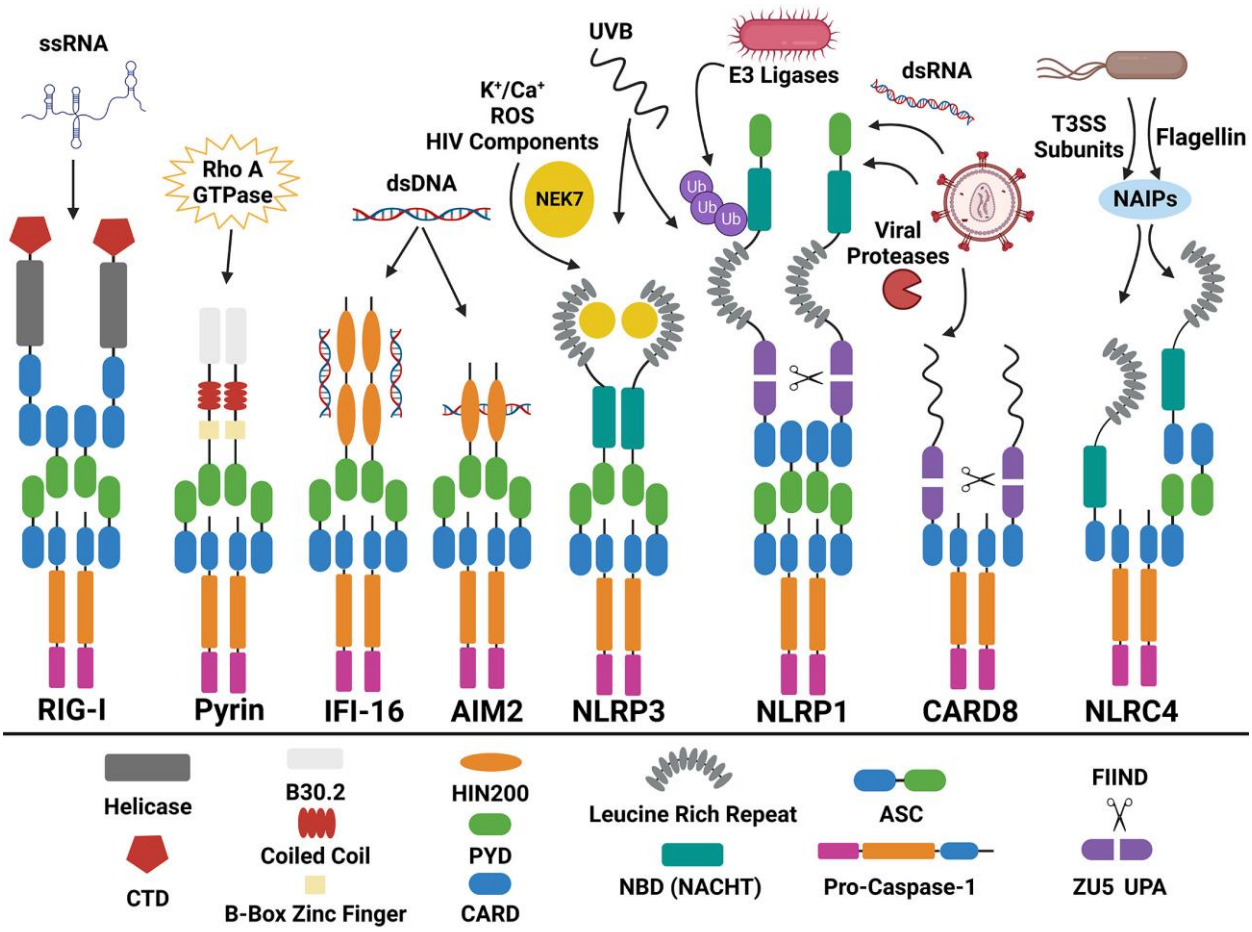

Figure 1.2: The Inflammasomes

Pattern recognition receptors known to activate the canonical inflammasome and their corresponding PAMPs or DAMPs.

through the CARD domain—to induce oligomerization of caspase-1, leading to cleavage of the interdomain linker between its pro-domain and its proteolytic subunits.[46] This releases the proteolytic domain that activates its downstream effectors. Caspase-1 can be activated either directly through the CARD domains of NLRC4 (CARD12) and CARD8 or indirectly through mediation by ASC (CARD5).[77-79] ASC is a small mediator molecule that contains only an N-terminal pyrin domain (PYD) followed by a C-terminal CARD domain.[79] The ASC-dependent

inflammasomes can be activated through members of the nod-like receptor (NLR) family or through AIM2, IFI16, RIG-I or Pyrin.[79-81] Most of these sensors contain a PYD which allows for recruitment of ASC through a protein–protein interaction with the ASC-PYD. ASC is then able to recruit caspase-1 through its CARD domain leading to activation of the inflammasome. AIM2 and IFI16 bind and sense cytosolic DNA via their hematopoietic interferon-inducible nuclear (HIN) domains.[74,80,82,83] While IFI16 oligomerization is mediated through its PYD, AIM2 relies upon binding of multiple monomers to the same molecule of DNA which creates a backbone for oligomerization and recruitment of ASC.[80,82,84] The pyrin inflammasome is activated upon the inactivation of RhoA GTPase by pathogens.[85] This allows for ASC binding to the PYD of pyrin to recruit caspase-1.

The study of NLRP inflammasome sensors—NLR proteins with a PYD—has largely revolved around the NLRP-3 inflammasome. The NLR inflammasomes sense a variety of PAMPs and DAMPs and mediate downstream ASC-dependent activation of caspase-1. NLRs are characterized by the presence of a nucleotide binding domain (NBD) and a Leucine-rich repeat.[86] While the exact mechanism of NLRP-3 activation needs further study, it is well known that binding of NLRP3 through its LRR domain to the kinase NEK7 is necessary for its activation.[87-90] Like the other ASC-dependent sensors, NLRP3 recruits ASC through its PYD for inflammasome activation. The other NLRP inflammasome sensors, such as NLRP1, are thought to directly sense PAMPs and recruit ASC. Notably, NLRP1 contains a CARD domain but still requires ASC for its activation.[86] Mechanisms of NLRP1 activation will be discussed below. Some inflammasome sensors are known to directly interact with caspase-1. Like all NLR proteins, NLRC4 contains an NBD and LRR but differs from the NLRP proteins as it has a C-terminal CARD domain instead of a pyrin domain. NLRC4 activation relies upon another

member of the NLR family: NLR family-apoptosis inhibitory protein (NAIP).[91-95] The PRR in this case is the NAIP that recruits NLRC4 for direct interaction with caspase-1. While NLRC4 is thought to be able to recruit ASC, this is not essential for its function.[77,96] Another ASC-independent sensor, and the focus of this review, is a PRR called CARD8. CARD8 represents a unique activator of the inflammasome as it acts as both the sensor of PAMPs and the activator of caspase-1.[78,97]

1.2.2 Mechanism of CARD8 Inflammasome Activation

Two of the inflammasome sensors we have discussed represent unique members of this family as they contain structural and functional distinctions from their counterparts. The first of these is NLRP1, which consists of an N-terminal PYD followed by the NBD and LRR.[86,98] However, the distinction arises with the presence of the Function-to-Find (FIIND) and CARD domains at the C-terminal end of NLRP1. The presence of the CARD domain makes NLRP1 a unique member of the NLRP family as it contains two protein–protein interaction domains from the DD superfamily: the PYD and CARD domains. Unlike the other NLRP family members, NLRP1 uses its CARD domain for inflammasome formation instead of the PYD.[99,100] Most importantly, NLRP1 contains a unique domain called the FIIND domain.[101] The FIIND domain was found to be homologous to two domains: the ZU5 at the N-terminal side followed by the UPA at the C-terminal end. When initially discovered, this was the first time such a domain had been described. Later, another protein called CARD8 was found to have significant homology with the C-terminal end of NLRP1.[102] CARD8 contains a C-terminal CARD domain like NLRP1 and an N-terminal FIIND domain making it the second and only other protein to contain a FIIND domain.[101] In addition to these two domains, CARD8 has a long unstructured N-terminal tail in place of the PYD, NBD, and LRR of NLRP1. These proteins have a unique way of activating the

inflammasome as they require auto-proteolytic cleavage (autoprocessing) of their FIIND domains in order to be a functional sensor.[99,101,103] This autoprocessing occurs between amino acids 1212 and 1213 for NLRP1 and 296 and 297 for CARD8, however, the exact mechanism of autoprocessing is still not well understood. Autoprocessing of these proteins leads to two non-covalently bound fragments, hereafter termed as the N-terminal and C-terminal fragments. The N-terminal fragments contain the recognition sites for PAMPs whereas the C-terminal fragments contain the UPA-CARD domains which are the downstream activators of the inflammasome.[99-101] Once activated, the UPA-CARD domain is released and undergoes oligomerization which is mediated by UPA–UPA interactions which allow the CARD domain to be exposed for caspase-1 activation.[99,100,104-106] Caspase-1 activation in human NLRP1 is ASC-dependent, while it is ASC-independent in CARD8.[78] However, NLRP1 orthologs in other species, such as NLRP1b in mice, do not necessarily require ASC as an intermediary to caspase-1 activation.[107-109]

The central mechanism for activation of NLRP1 and CARD8 centers on what is called functional degradation.[110,111] The N-terminal fragment is either cleaved or targeted for proteasomal degradation through a PAMP or DAMP. Once NLRP1 or CARD8 has been targeted for degradation, the N-terminal fragment is degraded by the proteasome through what is known as the N-end-rule pathway. The degradation of the N-terminal fragment then allows for release of the UPA-CARD containing C-terminal fragment. The C-terminal fragment is then able to oligomerize and provide a platform for caspase-1 docking either directly, as in the case of CARD8, or indirectly, through ASC.[78,105,106] This is evidenced in many studies that show the usage of proteasome and N-end-rule pathway inhibitors can completely block NLRP1 and CARD8 inflammasome activation.[97,110-113] Most of the work conducted to understand the function and activation of NLRP1 has utilized murine models. While NLRP1 in humans only has

one paralog, mice contain three NLRP1 paralogs termed NLRP1a, b, and c with NLRP1b being the most well studied.[114,115] NLRP1c does not contain the CARD domain and is thought to be a pseudogene. However, it still contains the N-terminal PYD and function mediated through the PYD cannot be ruled out. NLRP1a does contain a CARD domain, but a physiologically relevant PAMP for NLRP1a has yet to be identified. NLRP1b has been the central focus of research on murine NLRP1 activation. Most of these studies have revolved around NLRP1b's ability to sense the Lethal Toxin (LeTx) of *Bacillus anthracis.* LeTX contains two proteins the Lethal Factor Protease (LF) and the Protective Antigen (PA) protein.[116] LF can directly cleave the N-terminal fragment of NLRP1b thereby creating a neo-N-terminus which then is targeted for proteasomal degradation after recognition by N-recognins and ubiquitylation.[114,117-121] This method of targeting the neo-N-terminus and ubiquitylating it for proteasomal degradation is what characterizes the N-end-rule pathway.[110,111,121] After the neo-N-terminus of NLRP1b is degraded, the UPA-CARD is released resulting in the activation of caspase-1 through ASC-dependent or -independent manners. This contrasts with the NLRP1 of humans that requires ASC for caspase-1 activation.[78] Studies on LF activation of NLRP1b demonstrated that cleavage in itself is sufficient for activation of the inflammasome.[120] This is further supported upon swapping the cleavage site for another putative protease cleavage site for the Tobacco Etch Virus (TEV) protease.[122] The swapping of protease sites leads to resistance to LF-mediated inflammasome activation and sensitizes NLRP1b to TEV protease activation. Other studies also showed that LF-mediated pyroptosis could be inhibited through proteasome and N-end-rule inhibitors—that block ubiquitylation—solidifying its mechanism of action.[111,113] In addition to NLRP1b's ability to sense LF protease function, it has also been shown to be activated by the E3 ligases of *Shigella flexneri* which induce its degradation.[111,123]

While human NLRP1 is not cleaved by *Bacillus anthracis* LF, it can be activated through a similar mechanism via sensing viral protease activity. A family of single stranded RNA viruses called *Piconaviridae* contain a family of proteases called 3C proteases.[124,125] It was discovered that NLRP1 contains a putative 3C protease cleavage site in its N-terminal fragment.[125,126] As expected, many members of this family such as Enteroviruses, Rhinoviruses, Coxsackievirus B3, Poliovirus, and Coronavirus can induce NLRP1 inflammasome activation through direct cleavage of NLRP1.[124,126,127] The activation of the human NLRP1 inflammasome, like its murine counterpart, can be inhibited via N-end rule inhibitors, demonstrating a shared mechanism of action with mouse NLRP1b. Human NLRP1 has also been shown to recognize the viral double-stranded RNA of Semliki Forest Virus (SFV).[128] This is instead mediated through direct binding of the RNA to the NBD of NLRP1 which increases its ATPase activity. While the function of the increased ATPase activity and direct mechanism of activation is still unknown, proteasome inhibitors were able to inhibit this mechanism of action indicating that proteasomal degradation is still required. This function is not preserved in mouse NLRP1b, but instead NLRP1b may be able to sense low intracellular ATP levels suggesting that NLRP1 proteins may play a role in sensing intracellular ATP levels during stressed states.[123,129] It has also been shown that NLRP1 can be activated by ultraviolet B (UVB) irradiation.[130-132] In this study, Robinson et al. reported that UVB irradiation induced NLRP1 activation by the ribotoxic stress response kinase ZAKα pathway. Like viral dsRNA and proteases, ZAKα pathway-induced NLRP1 also required N-terminal degradation.[132] However, further studies are needed to fully elucidate this function and how it relates to the functional degradation of NLRP1.

While there have been extensive studies on NLRP1, CARD8 has received far less attention as up until recently the PAMPs that CARD8 sensed were unknown. Additionally, while

mice and rats possess three orthologs to human NLRP1, they do not have any genes orthologous to CARD8 rendering study of CARD8 in murine models impossible. CARD8, also known as TUCAN or CARDINAL, was initially identified in a search for CARD domain containing proteins that interacted with CARD domain containing caspases.[102] Its interaction with caspase-1 was first described by Razmara and colleagues that showed that CARD8 was able to bind to caspase-1, but rather might play a role in inhibition of caspase-1 activation.[133] They hypothesized that its binding to caspase-1 impeded binding by other activators of caspase-1, however, it is still unclear as to the role CARD8 plays in negative regulation of caspase-1. Due to its similarity to NLRP1 it is not surprising that CARD8 undergoes a shared mechanism of activation through functional degradation. However, CARD8 does not contain the other N-terminal recognition domains of NLRP1, but instead contains a long, disordered N-terminal tail which is required for its function.[135] Like NLRP1, CARD8 can be activated through functional degradation of its N-terminal fragment which is independent of ubiquitylation.[135] As CARD8 is highly expressed in most tissues and cell types, including macrophages and T cells, it was of interest to identify T cell and macrophage tropic viruses that may contain proteases that could cleave CARD8, leading to its activation.[104,136,137] Indeed, we recently showed that HIV, one of the most important T cell and macrophage tropic viruses, is sensed by CARD8 leading to its activation.[97] The mechanism of HIV-mediated activation of CARD8 will be discussed in detail below. It has also been reported that Coxsackievirus B3 2Apro and 3Cpro trigger CARD8 inflammasome activation and pyroptosis of endothelial cells and cardiomyocytes.[138] This unique mechanism of sensing PAMPs distinguishes NLRP1 and CARD8 from the other inflammasome sensors as it senses pathogen protein enzymatic activity. It also relies upon the degradation of a portion of the inflammasome sensors representing a distinct activation pathway in comparison to other sensors.

Theoretically any pathogen-derived protease with a putative cleavage site on NLRP1 or CARD8 could potentially activate them. This opens a new field of research into identifying which proteases can activate these sensors and how this may change depending upon individual genetic variation in the recognition sites such as the N-terminal tail of CARD8.

1.2.3 Regulation of NLRP1 and CARD8 by DPP9

In 2004, a small molecule dipeptidyl peptidase inhibitor called Val-boroPro (VbP, talabostat, or PT-100) was found to possess antitumor effects on tumors from fibrosarcoma, lymphoma, melanoma, and mastocytoma cell lines.[139] However, its mechanism of action was largely unknown until work by Okondo and colleagues showed that VbP induced caspase-1-dependent pyroptosis in monocytes and macrophages including the monocytic cell line THP-1.[140,141] VbP is a potent inhibitor of post-proline cleaving serine proteases such as DPP4, 7, 8, 9, and FAP which cleave peptides containing Xaa-Pro sites (Xaa represents any amino acid).[142-144] Upon further investigation, knockout of DPP9, and not the other targets of VbP, was able to induce pyroptosis in THP-1 cells, indicating that DPP9 is the key target for VbP induction of pyroptosis.[140] However, VbP treatment of DPP9 knockout cells still induced low levels of cell death, suggesting the role of another target which was identified as DPP8.[140] DPP8 and DPP9 share many structural similarities and knocking out both targets was able to render THP-1 cells resistant to VbP-mediated cell death.[140] As VbP-induced pyroptosis was shown to be ASC independent, it was thought to induce inflammasome activation of a PRR that can directly interact with caspase-1.[140,145] The NLRP1 alleles present in mice and rats have this capability and were shown to render cells resistant to VbP upon knockout.[107-109,146] While this was the first time NLRP1 was associated with DPP9, human NLRP1 cannot directly interact with caspase-1. This led to the identification of CARD8 as the key mediator in VbP induced pyroptosis.[78,99,104,146]

Indeed, VbP was shown to induce caspase-1-dependent pyroptosis in acute myeloid leukemia (AML) cell lines which was abolished via knockout of CARD8 and not NLRP1.[104] While NLRP1 did not play a role in VbP mediated cell death in this model, it was later found to induce pyroptosis in keratinocytes.[147] As DPP8/9 inhibitors were found to selectively activate the NLRP1 and CARD8 inflammasomes, they could be used as tools to study mechanisms of NLRP1 and CARD8 activation, opening the door for future studies on these inflammasome sensors.

Most of the understanding surrounding NLRP1 and CARD8 inflammasome functions has centered around activation with VbP and has largely come about through a number of structural studies on DPP9 in complex with NLRP1 or CARD8.[105,148,149] DPP8 and DPP9 have been shown to form a distinct complex upon binding to the FIIND domains of NLRP1 and CARD8.[105,147-149] Both proteins form a complex consisting of one molecule of DPP9 and two of either NLRP1 or CARD8. DPP9 first binds to the Zu5 domain of full-length NLRP1 or CARD8. DPP9 then binds to a freed C-terminal fragment containing the UPA-CARD which is mediated by binding of the UPA domain with both DPP9 and the UPA domain of the full-length NLRP1 or CARD8.[105,148,149] This secondary binding of freed C-terminal fragments is thought to prevent auto-activation of the inflammasome and promote safe turnover of these molecules. The key difference between NLRP1 and CARD8 in binding to DPP9 presents unique mechanisms of regulation of these proteins and activation by VbP. The neo-N-terminus of the UPA-CARD of freed C-terminal NLRP1 binds to the active enzymatic site of DPP9; this binding is not dependent upon its enzymatic activity as catalytically dead S759A DPP9 is still able to bind NLRP1 and CARD8.[148,150] In contrast, neither molecule of CARD8 binds to the enzyme active site of DPP9.[149] This presents a unique mechanism of activation via VbP as it directly binds to

the enzyme active site of DPP8 and 9.[105,149] In the context of NLRP1, VbP directly displaces the C-terminal fragment and induces inflammasome activation, whereas VbP does not directly displace either fragment of CARD8.[105,149] Instead, VbP inhibits the C-terminal capture of CARD8.[149] This is further evidenced by the fact that VbP activation of NLRP1 is not dependent upon functional degradation as VbP treatment in the presence of proteasome inhibitors does not affect the activation of NLRP1, indicating that DPP9 inhibition is downstream of NLRP1 activation.[148] Conversely, proteasome inhibitors are able to completely block VbP activation of CARD8, suggesting DPP9 acts upstream of CARD8 activation.[134] Additionally, autoprocessing deficient CARD8 was found to bind equally well as its autoprocessed counterpart, but autoprocessing deficient NLRP1 has reduced binding to DPP9, indicating distinct mechanisms of binding that interact with separate binding sites.[105,147,149,151] This structural restriction of the C-terminal fragments of NLRP1 and CARD8 have been repeatedly shown to be integral to restraining inflammasome formation as this complex occludes the binding sites necessary for oligomerization and recruitment of ASC and caspase-1 for NLRP1 and caspase-1 only for CARD8. Additionally, expression of NLRP1 or CARD8 in DPP8 and DPP9 knockout cells induce spontaneous inflammasome formation. However, during activation of CARD8 or NLRP1 the balance of intracellular full-length protein to C-terminal protein is shifted in favor of C-terminal protein due to functional degradation of the full-length protein. This allows for the cell to overcome DPP9 inhibition that is specific to sensing of intracellular PAMPs while still maintaining a careful homeostasis under unstressed conditions.

The enzymatic activity of DPP9 is also thought to play a central role in the regulation of CARD8 and NLRP1. While both NLRP1 and CARD8 have potential proline residues that theoretically could be cleaved by DPP9, neither protein has been found to be directly cleaved by

DPP9.[105,147,150] Nonetheless, several studies have shown that DPP9, when treated with VbP, promotes indirect N-terminal degradation of full-length NLRP1 and CARD8 through an unidentified mechanism. Although both NLRP1 and CARD8 can bind to catalytically dead S759A DPP9, this only partially rescues spontaneous activation of NLRP1 and does not rescue CARD8 mediated cell death indicating an important bifurcation in DPP9's regulation of these sensors. Recently, Rao and colleagues reported that M24B aminopeptidase inhibitors were able activate the CARD8 inflammasome.[152] The M24B aminopeptidase inhibitor CQ31 inhibits prolidase (PEPD) and Xaa-Pro aminopeptidase 1 (XPNPEP1) which increase intracellular concentrations of Xaa-Pro dipeptides.[152] This increase of Xaa-Pro dipeptides results in inhibition of DPP9 and subsequent activation of the CARD8 inflammasome but not the NLRP1 inflammasome.[152] The introduction of exogenous Xaa-Pro peptides alone was sufficient to induce CARD8 inflammasome activation, reiterating the importance of DPP9 enzymatic function in regulating CARD8.[152] The role of DPP9's enzymatic activity in both inhibition and activation of CARD8 remains largely unknown. Regardless, it can still be concluded that both the occlusion of the C-terminal fragments through direct binding and the enzymatic activity of DPP9 are essential for inhibiting NLRP1 and CARD8 inflammasome activation. This can be reversed by DPP8 and 9 inhibitors, such as VbP or the more selective 8j and 1g244.[153,154] These inhibitors bind to the active site of these enzymes leading to indirect N-terminal degradation of the full-length fragments and either direct displacement of NLRP1 or inhibition of C-terminal sequestration of CARD8.

1.3 Activation of the CARD8 Inflammasome by the HIV Protease

1.3.1 Activation of CARD8 by HIV Protease

As previously mentioned, CARD8 is known to be highly expressed in hematopoietic cells including T cells, B cells, NK cells, and macrophages.[104,136,137] These cell types were shown to undergo CARD8-dependent pyroptosis upon treatment of VbP. As NLRP1 had been shown to be triggered by viral proteases, this raised the question if CARD8 could sense T-cell and monocyte/macrophage tropic viruses like HIV. Indeed, we recently reported that CARD8 could directly sense intracellular HIV protease activity through its unstructured N-terminal domain, representing the first known PAMP recognized by CARD8 **Figure 1.3**.[97] The overexpression of HIV in HEK293T cells leads to spontaneous dimerization of the Gag-Pol polyprotein, resulting in premature intracellular protease activity.[152] Thus, co-transfection of HEK293T cells with HIV-1 and CARD8 results in cleavage of the CARD8 N-terminus between the F59 and F60 residues of CARD8 thereby creating a neo-N-terminus.[97] This neo-N-terminus then undergoes proteasomal degradation and subsequent release of the CARD8-C-terminal fragment which can be blocked through the introduction of the HIV-1 PR cleavage site mutation F59A/F60A (FAFA). Co-transfection of HIV, CARD8, pro-caspase-1, and pro-IL-1β can induce caspase-1 activation as evidenced by the increase in P20 and P10 fragments and pro-IL-1β processing to IL-1β. IL-1β activation is reliant on HIV protease activity, as activation is blocked when HIV protease activity is inhibited, either with protease inhibitors (such as lopinavir) or through transfection with the proteolytically dead HIV protease D25A/H mutation. Furthermore, pro-caspase-1 and pro-IL-1β activation are blocked by the proteasome inhibitors Bortezomib and

MG132, which demonstrates that CARD8 sensing of HIV-1 PR relies upon functional degradation of CARD8 as was previously shown with NLRP1.[110,111,121,134] This is also supported by the introduction of the autoprocessing deficient mutant S297A CARD8 which is unable to induce pro-caspase-1 and pro-IL-1β processing.[97] In addition, lysed HIV virions incubated with CARD8 *in vitro* are sufficient for CARD8 cleavage, which suggests that no other protein partners are involved in direct sensing; however, the role of other proteins in localization and interaction of CARD8 and HIV are still unknown in cell-based systems.

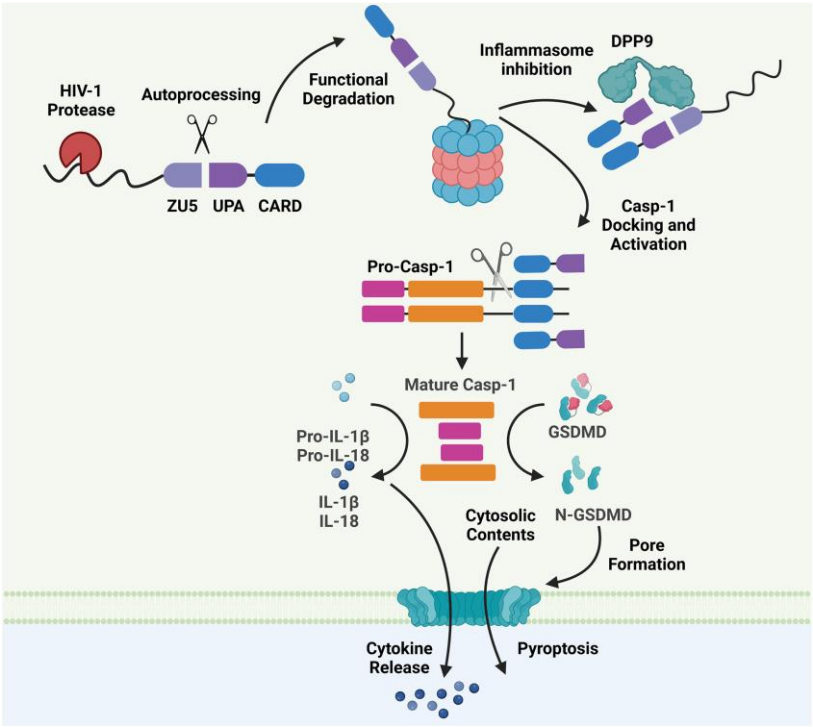

Figure 1.3: Mechanism of CARD8 Inflammasome Activation by HIV Protease.

HIV protease activation of the CARD8 inflammasome begins with cleavage of the N-terminal of autoprocessed CARD8. Cleavage leads to the formation of a neo-N-terminus that is targetted for functional degradation through the proteasome thereby releasing the bio-active C-terminus. This fragment can either be sequestered by DPP9 or go on to provide a docking platform for pro-Caspase-1 leading to it's activation and subsequent cleavage of Gasdermin D, Pro-IL-1β, and Pro-IL-18 for pyroptosis and cytokine release.

1.3.2 Non-Nucleoside Reverse Transcriptase Inhibitors (NNRTIs) Induce Pyroptosis of HIV-Infected Cells

In infected cells, HIV protease resides in an inactive state imbedded in the HIV Gag-Pol polyprotein.[156-159] The processing of the Gag-Pol polyprotein is dependent upon dimerization which leads to functional protease activation and subsequent cleavage of the individual subunits of Gag-pol, thereby releasing them into their active forms. This process is typically mediated through close interactions in the viral particle as the Gag-Pol density at budding HIV particles is much greater than its cytosolic concentrations.[160-162] This indicates that Gag-Pol protein density is necessary for processing and function of HIV protease, which can be overcome by overexpression in a transfection-based system.[155] Interestingly, a class of HIV antiretrovirals known as NNRTIs, which were initially developed to block HIV reverse transcriptase (RT) activity, were unexpectedly found to induce dimerization of HIV Gag-Pol and induce premature intracellular protease activity.[163]

The class of NNRTIs came to existence in 1989/1990 when the compounds HEPT (1-[(2-hydroxy-ethoxy) methyl]-6-phenylthiothymine) and TIBO (tetrahydro-imidazo[4,5,1-jk][l,4]-benzodiazepin-2(1H)-one and –thione) and their derivatives where first noted to demonstrate highly specific inhibition of HIV-1 replication *in vitro* without preventing dNTP interaction with the HIV-1 RT.[164,165] HIV-1 reverse transcriptase is a heterodimer composed of a p66 and p51 subunit and has ribonuclease activity as well as RNA and DNA primed polymerase activity. RNase H activity corresponds to the last 120aa of the p66 subunit and is the p15 fragment cleaved by the viral protease to yield the RT p51 subunit. The structure of the p66 subunit has often been compared to a hand where the fingers and thumb domains fold onto the palm domain which contains the polymerase activity. The RNase H activity domain is linked via a connection

domain. This same connection domain maintains interaction with the p51 subunit which contains no catalytic activity and maintains a rigid form, playing a more structural role in the heterodimer.[166] NNRTIs block reverse transcriptase activity by binding to an allosteric site on the RT enzyme now called the NNRTI binding pocket (NNIBP), which is located ~10Å from the catalytic site.[167] Here, they non-competitively inhibit binding of dNTPs to the HIV-1 RT. Binding of NNRTIs to the NNIBP sterically hinders motion of two key subunits of the p66 subunit of RT. While each of the NNRTIs function slightly differently, they all bind to the same pocket. Curiously, no other retroviruses, including HIV-2 and SIV, possess this additional pocket to accommodate this class of compounds, adding to the high specificity and selectivity index of NNRTIs.[168]

Following the discovery of TIBO and HEPT, extensive drug screens led to the production of the first generation of NNRTIs, nevirapine (NVP, 1996), delaviradine (DLV, 1997), and efavirenz (EFV, 1998). Of these, NVP and EFV are still widely used today. These compounds are structurally similar in that they both have a hydrophilic center and two hydrophobic ring structures in a butterfly like configuration.[169] Co-crystal structure of nevirapine with the HIV-1 RT helped elucidate the mechanism of inhibition of the first generation of NNRTIs.[167,170] Early clinical trials of NNRTI monotherapy or dual therapy combined with AZT showed rapid virologic failure and emergence of NNRTI resistance[171-174], largely due to a minimal fitness cost imposed by NNRTI resistance mutations.[175,176] To overcome this issue, the second generation of NNRTIs were developed and FDA-approved roughly a decade after the first: etravirine (ETR, 2008), rilpivirine (RPV, 2011) and doravarine (DOR, 2018). The less rigid structure of these compounds allows them to have torsional flexibility and reposition in the hydrophobic NNRTI binding pocket despite NNRTI resistance mutations. Therefore, they retain efficacy even in the

presence of mutations which confer resistance to EFV and NVP.[177-179] Use of NNRTIs remains part of first line therapy for treatment of HIV, though they have moved from preferred first line to alternate first line regimens since the 2018 treatment guidelines.[180]

The RT enzyme is directly downstream of protease and is integral in Gag-Pol dimerization for proper activation of the protease.[171-173] Interestingly, some of these NNRTIs, such as EFV and RPV, were found to potently induce premature Gag-Pol dimerization, mediated through RT, resulting in premature intracellular protease activity.[163] NNRTIs had been shown to induce HIV protease-dependent cell death in $CD4^+$ T cells, but the mechanism of cell death was unknown until our recent work on NNRTI-induced activation of the CARD8 inflammasome.[97,184,185] EFV or RPV treatment of HIV-infected primary monocyte derived macrophages (MDMs) and $CD4^+$ T cells induces rapid cell death, which is abrogated by protease inhibitors.[97] This phenotype is exclusive to NNRTIs that are known to induce dimerization, such as EFV, ETR, or RPV.[97,186] This cell death could also be blocked through treatment of proteasome inhibitors Bortezomib and MG132 as well as the pan-caspase inhibitor *Z*-VAD-FMK and caspase-1 inhibitor VX765.[97]

To decipher the mechanistic underpinning of NNRTI induction of pyroptosis, the monocytic cell line THP-1 was used for knockout of the relevant inflammasome genes. Upon knockout of CARD8 and caspase-1 NNRTI-induced pyroptosis was ablated whereas knockout of NLRP3 and ASC did not affect killing of HIV infected cells. This reinforces that pyroptosis of NNRTI treated cells infected with HIV is dependent upon the CARD8 inflammasome and that this inflammasome activation is ASC-independent. This also reiterated the mechanism of activation of CARD8 which can directly interact with and activate caspase-1 instead of through an intermediate adaptor like ASC. More importantly, NNRTIs induce pyroptosis in all subtypes of HIV-1 strains. Interestingly, while all HIV strains exhibited some level of NNRTI-dependent

cell death, the magnitude of this response varies across strains, which may be due to the intrinsic dimerization capacity, protease activity, or NNRTI-binding capacity. As the full mechanism of HIV protease interaction and subsequent cleavage of CARD8 is still unknown, it is possible that other host or viral components can affect the efficiency of this process.[97]

As previously mentioned, CARD8 activation is dependent upon the ratio of full-length CARD8 and freed C-terminal CARD8. Under homeostatic conditions, DPP9 is able to compensate for the levels of C-terminal CARD8 and prevent autoactivation of the inflammasome.[149] NNRTIs are one way to shift the balance toward the C-terminal CARD8 to overwhelm DPP9 and induce the CARD8 inflammasome. However, this is completely reliant upon intracellular concentrations of NNRTIs and their dimerization capacity. Since micromolar concentrations of NNRTIs are needed to induce sufficient CARD8 activation and cell death, it raises a distinct issue in their clinical implementation as NNRTI intracellular concentrations are likely insufficient to induce robust dimerization and CARD8 activation.[97,186] This is likely due to the high binding affinity that NNRTIs have for human serum proteins which reduce the intracellular concentrations of these drugs, which poses a significant hurdle in implementing this strategy for an HIV cure.[187] As a regulator of CARD8 function, DPP9 became the direct target for a way to tip this balance toward CARD8 activation. Inhibition of DPP9 function sensitizes cells to NNRTI-induced pyroptosis as it inhibits capture of C-terminal CARD8 and may induce degradation of full-length CARD8 further tipping the balance to freed C-terminal CARD8.[149,186]

1.3.3 Potential Impact of NNRTIs on HIV Reservoirs

The main barrier to an HIV cure is the seeding of the latent reservoir in $CD4^+$ T cells and potentially macrophages, as lifting antiretroviral therapy allows these latently infected cells to spontaneously reactivate and a rebound in viral load is seen.[20-22,188] An HIV cure, therefore,

requires the elimination of host cells with integrated virus. One method that is being studied to accomplish this is called the "shock and kill" method.[42] This method requires a "shock" which is induced by a latency reversal agent (LRA) whose role is to reactivate latent HIV transcription. As latency reversal is sporadic during pathogenesis, it is necessary to induce robust reactivation of the latent reservoir to reactivate gene transcription and viral protein expression to target with a "kill" strategy. Other kill strategies have relied upon recognition of highly mutable epitopes of the viral genome such as the HIV envelope protein.[43-45] As this protein can withstand a greater mutational burden, it is able to quickly evade strategies designed to eliminate HIV infected cells. Conversely, HIV proteins that rely upon recognition of highly conserved enzymatic functions have greater potential in being broadly applicable without the virus developing an escape mechanism.[46] We posit that one of these potential enzymatic targets could be HIV protease through sensing by CARD8 as it is highly conserved, and its function is necessary for viral replication. Previous studies showed that NNRTI treatment alone or in combination with DPP9 inhibitors is able to clear latently infected cells from PLWH upon reactivation.[97,186] However, whether NNRTIs affect latent HIV reservoirs *in vivo* is unclear.

The initial clinical trials comparing integrase strand transfer inhibitors (INSTIs) to NNRTIs showed no difference in outcomes or virological failure (VF), but improved tolerability compared to the first generation NNRTIs. The STARTMRK trial compared raltegravir to efavirenz on a background of tenofovir and emtricitabine and showed non-inferiority.[189] Similarly, the initial trial comparing elvitegravir/cobistat vs efavirenz on a tenofovir/emtricitabine background showed non-inferiority and no difference in virologic failure.[190] Similarly, comparison of dolutegravir vs efavirenz in SPRING-1 and SINGLE showed non-inferiority but improved tolerability.[191,192] The NNRTI class contributes to a substantial

number of the single pill once a day regimens, which make it convenient for patients to dose. These include Atripla (EFV/TDF/FTC), Complera (RPV/TDF/FTC), and its newer version Odefsey (RPV/TAF/FTC). Rilpivirine has additionally been approved as part of the complete two drug regimen, Juluca (DTG/RPV) for individuals who are well controlled on a three drug regimen. The SWORD-1 and SWORD-2 studies evaluating this found no loss in virologic control over 48 weeks.[193] Most recently, rilpivirine has been FDA approved as part of long-acting injectable therapy for treatment. The ATLAS and FLAIR studies showed no difference in virologic suppression between monthly injections of CAB/RVP when compared to an oral three drug regimen.[192,193] The POLAR study was again able to show that a slightly higher intra-muscular (IM) dose resulted in no higher virologic failure when dosed bimonthly.[194]

Starting in 2007, when raltegravir (the first available integrase inhibitor) received FDA approval, integrase inhibitors have replaced NNRTIs and protease inhibitors (PIs) as the ideal anchor drug to pair with a two nucleoside reverse transcriptase inhibitor (NRTI) backbone. Initial appeal of INSTIs came from fewer drug–drug interactions and fewer lipid abnormalities than PIs and a better tolerability profile compared to NNRTIs. In addition, before combination therapy became the standard of care, many patients developed resistance mutations to PIs and NNRTIs; for these treatment experienced individuals a novel class of effective therapeutics was necessary to achieve control over ongoing viral replication. All forms of currently available ART regimens prevent uninfected cells from becoming HIV infected but have no impact on already infected cells. The UK CHIC study performed an observation cohort study where 12,585 participants on INSTI, NNRTI or PI based regimens were compared for virologic failure. Virologic failure was defined as two consecutive VL > 50 at least 6 months post starting therapy. They found that NNRTI-based regimens were associated with the lowest risk of virologic failure, hazard ratio

(HR) for INSTI-based treatments was 1.52 (95% CI: 1.19–1.95) and HR for PI based regimens was 2.7 (95% CI: 2.27–3.21).[195] Subgroup analysis showed that the likelihood of virologic failure was lowest for efavirenz and rilpivirine treated participants. Future studies are warranted to understand whether NNRTIs activate the CARD8 inflammasome to reduce viral reservoirs *in vivo*.

1.4 SIV Pathogenesis

1.4.1 Overview of SIV in Non-Human Primates

Simian immunodeficiency virus (SIV) is a family of primate lentiviruses that gave rise to HIV-1 and HIV-2.[198] Nearly every species of African non-human primate has been found to harbor a strain of SIV constituting over 40 species with known SIV infection.[199-201] This ubiquitous dispersal – except for some chimpanzee subspecies, baboons and patas monkeys – indicates an ancient origin of the ancestor to the SIV strains seen today.[198,202,203] Strikingly, SIV infection has not been found in NHP species from other continents including the closely related Asian *Cercopithecidae* (old world monkey) species such as macaques or the Asian ape species such as orangutans and gibbons.[204,205] This evidence points to an age of SIV after the Asian migration of these species and estimates place the origin of SIV conservatively to be at least 32,000 years ago.[206] These hypotheses are also in concordance with the theory of an ancestral origin of all lentiviruses in Africa, as other lentiviruses have also been traced to an ancient African origin such as with Feline immunodeficiency virus (FIV).[207] Since its origin, SIV has adapted to the myriad NHP species extensively resulting in species typically only harboring one strain of SIV.[208] This species specificity represents monophyletic groups of viruses that have greatly

adapted to host entry receptors and to avoid host responses to infection such as tetherin, trim5α, and APOBEC family members.[209-212]

There are 8 distinct clades of SIV which cluster by closely related species: guenons, mandrills, great apes (with HIV-1), African Green Monkeys, Mangabeys (with HIV-2), L'hoest monkeys, sykes monkeys, and colobus monkeys.[208] These 8 clades can be further simplified based on the genome structure and more importantly the presence of key accessory proteins.[208] The accessory protein *vpu* is only present in HIV-1, SIVcpz, SIVgor, and SIVs from some *Cercopithecus* monkeys (guenons).[213] The clade of SIVs from mangabeys (SIVsmm, SIVrcm, and HIV-2) instead contain another protein called *vpx* which is thought to take on the roles that *vpr* and *vpu* play in HIV-1-like viruses.[214] All other clades contain neither *vpu* nor *vpx* and it is thought that their *nef* and *env* genes have evolved to take on these cellular tasks.[208,214]

In nearly all of these "naturally hosts"), SIV infection is generally thought to be non-pathogenic in nature. Although there is ecological evidence for this classification, only two species have been greatly studied for their status as non-pathogenic hosts: sooty mangabeys (*Cercocebus atys*) and African green monkeys (*Chlorocebus sabaeus*).[199,208] The hallmark of lentiviral disease progression is progressive $CD4^+$ T cell loss and, as such, presents logistical difficulties in longitudinal measurements of $CD4^+$ T cells.[199] This instead forces researchers to rely upon captive animals with the two main African non-human primate models displaying a lack of $CD4^+$ T cell progression and AIDS like pathology.[215-218] However, further work is still required for the rest of the African NHPs to be fully characterized as non-pathogenic. The phenotype of non-pathogenic hosts and its proposed explanations are discussed further below.

Although SIV is relatively species specific, cross species transmissions have been identified in a few notable cases often resulting in pathogenesis in the species to which the

spillover has occurred. The first notable case is that of SIV in chimpanzees (SIVcpz).[219-221] SIVcpz has been found only in two subspecies of the common chimpanzees: *Pan troglodytes troglodytes (P.t.t)* and *Pan troglodytes schweinfurthii* (*P.t.s*).[221-226] Alternatively, SIV has yet to be recovered from the other species of chimpanzee the bonobo (*Pan paniscus*) as well as the other *Pan troglodytes* subspecies *P.t. ellioti* and *P.t. verus*.[198] The absence of SIV in these groups suggests a much more recent spillover than that of the origins of SIV.[198,228] Instead, it is more consistent with the hypothesis that it arose in these subspecies since their genetic divergence 400-800 years ago.[229] Interestingly, SIVcpz shares similarity to two clades of SIV from the *Cercopithicedae* lineages: SIVrcm from red capped mangabeys and a clade including several guenons (*Cercopithecus nictitans, Cercopithecus cephus*, and *Cercopithecus mona*).[227] The 5' half of the SIVcpz genome, *nef*, and the 3' LTR are all most closely related to SIVrcm, whereas the accessory proteins and *env* share closer relatedness to the SIVs of the Cercopithecus monkeys.[227] This finding points to an origin most likely as a result of recombination between these viruses inside the host which can be pinpointed to a subsection of *P.t.t* chimpanzees which shares a geographical range with both groups of primates that serve as prey meat.[198,229] In both subspecies of chimpanzees, there is substantial evidence of pathogenesis and increased mortality.[198,230,226] However, it is still considered less pathogenic than HIV-1 in humans.[207,230] As they have not experienced SIV infection as long as *Cercopithecidae* primates, we hypothesize that chimpanzees have not had the sufficient evolutionary time to avoid $CD4^+$ T cell loss.

SIVcpz has since resulted in two other spillover events with the first resulting in infection of Western lowland gorillas (*gorilla gorilla gorilla)* resulting in SIVgor.[231,232] This cross-species transmission event probably occurred only once from SIVcpz from *P.t.t* chimpanzees as it clusters most closely with this strain in phylogenetic trees.[231,232] This event was only present in

the western lowland gorillas and not the eastern gorillas (*Gorilla beringei*) and is estimated to have occurred 100-200 years ago.[234,235] More importantly, the second instance of an SIVcpz spillover occurred at the beginning of the 20th century resulting in the HIV-1 pandemic.[221,224,234-237] This spillover was again caused twice by the *Pan troglodytes troglodytes* subspecies and can be pinpointed to likely spillovers in southeastern Cameroon.[221,224] These two spillover events comprise HIV-1 groups M and O, with M representing almost all HIV-1 cases worldwide and O representing less than 1% of cases.[238-240] The HIV-1 groups N and P cluster more closely to SIVgor but only represent a handful of cases.[198,241-243] The exact cause of this spillover to humans is unclear but is hypothesized to be a product of the exposure to blood or bodily fluids of chimpanzees infected with SIV during bushmeat hunting.[198,244] With the advent of guns for hunting, these human and ape encounters became more frequent and allowed the hunting of these species likely resulting in the pandemic we see today.[244]

In contrast to HIV-1, HIV-2 arose from a spillover event from a completely unrelated species: the sooty mangabey.[245-247] HIV-2 clusters more closely to SIVsmm than any other strain and contains the same *vpx* protein.[213] HIV-2 is responsible for far fewer cases, with cases diminishing, than its counterpart and is primarily localized to West Africa which is also the only known range of sooty mangabeys.[198,207,248,249] The virus has lower infectivity, viral set point, maternal transmission, and most importantly, a lower frequency of AIDS as many individuals do not develop $CD4^+$ T cell loss.[250,251] This difference in disease progression, however, is not surprising as these viruses are very distantly related.

Similar to the SIV spillover events to humans and gorillas, another important cross-species transmission event occurred in animals in captivity which gave rise to the current NHP models of pathogenic SIV disease progression.[252-254] This spillover likely happened in the 1970's

in primate centers in the US where SIVsmm was accidentally transmitted to Rhesus Macaques (*Macaca mulatta*) giving rise to SIVmac.[252-254] Interestingly, although SIVsmm did not cause pathogenesis in their natural host, SIVsmm infection in macaques recapitulated almost all aspects of disease progression in humans.[255,256] This important event gave rise to the usage of macaque species (*Macaca mulatta*, *Macaca fascicularis*, and *Macaca nemestrina*) as pathogenic models for studying disease progression, antiretroviral therapy, and cure strategies.[255,256] Regardless of the species-specific context, it appears that recent spillovers of SIV from natural hosts generally results in pathogenic SIV infection in non-adapted species, pointing to a host specific response being the cause of $CD4^+$ T cell depletion.

1.4.2 Pathogenesis of HIV and SIV

While HIV infection induces a well-defined cytopathic effect, $CD4^+$ T cell depletion is not confined to virus-infected cells, because only around 1 in 10^2[57] peripheral blood mononuclear cells (PBMCs) or up to 1% $CD4^+$ T cells are infected in untreated individuals.[257-261] Notably, only cells positive for HIV RNA, DNA, or protein were defined as infected cells in these studies, thus identifying cells in which the life cycle of productive HIV infection has reached at least the state of retro-transcription and, most likely, virus integration in the host genome. In fact, viral RNA was rarely observed in the dying $CD4^+$ T cells during HIV infection.[262] However, these cells likely experienced a co-receptor-mediated interaction with the virus, possibly resulting in virus entry but without engaging in productive infection, as suggested by the observation that $CD4^+$ T cell depletion requires HIV co-receptor expression.[263,264] These data gave rise to the theory of bystander $CD4^+$ T cell death where productive infection is not required and instead cells undergo rapid cell death in response to viral entry. This rapid response to the HIV viral

particle creates logistical difficulties in studying pathogenesis in cells that do not harbor large quantities of viral RNA or protein.

Other hallmarks of lentiviral disease progression in pathogenic hosts include progressive depletion of mucosal $CD4^+$ T Cells, mucosal barrier disruption, microbial translocation, chronic immune activation, and vertical transmission.[198] In the case of natural hosts none of these characteristics of disease progression are present despite high viral loads, viral cytopathicity, and a lack of adaptive immune control.[199,215-217,266-269] Many hypotheses have attempted to explain this difference in pathogenesis but have failed to identify a singular causative mechanism to support these claims. It is most likely that a combination of these mechanisms contributes to the pathogenic specificity of SIVs and this dissertation presents another hypothesis on this mechanism of action that likely acts in concert with these previous ideas on pathogenesis.

The first proposed hypothesis posited that there are intrinsic properties of the virus that are responsible for differences in species specific cytopathicity.[268-270] This hypothesis has been extensively studied and was found to not be supported as the infection of Rhesus macaques with SIVsmm results in progression to AIDS.[255,256] Additionally, the direct cytopathicity of productively infected cells *in vitro* is similar in both natural and non-natural hosts.[268-270] This again supports the idea of bystander $CD4^+$ T cell death being responsible for pathogenesis. Viral replication fitness also cannot fully explain differences in pathogenesis as viral titers in natural hosts are equivalent to their pathogenic counterparts and do not display defects in fitness when transferred from natural hosts to pathogenic hosts.[199,215-217] As different SIV accessory proteins have greatly evolved to combat their host-specific restriction factors it was also believed that this may contribute to these differences.[271,272] Some evidence supports these claims as these accessory proteins lose some of their antagonism of host-restriction factors in different hosts,

such as with *nef* which downmodulates CD3-TCR from $CD4^+$ T cells in natural hosts but not in chimpanzees or humans.[271,272] These accessory proteins may be involved in chronic immune activation, but substantial evidence for this claim is still lacking. However, in concordance with the above data on replication fitness this is unlikely to fully explain the differences in bystander $CD4^+$ T cell death.

The next central hypothesis focuses not on the intrinsic bystander cell death, but instead takes a systematic approach to disease progression through a key phenotype present in pathogenic hosts: chronic immune activation.[273-275] Chronic immune activation is seen in pathogenic hosts as displayed by chronic interferon response, increased activation markers on cells, T cell exhaustion, and increased B cell turnover.[273-275] This is thought to be a positive feedback loop where increased T cell activation allows for increased infection and cell death. It is still unclear, however, whether chronic immune activation is a cause of pathogenesis or a byproduct of it. During lentiviral infection gut associated lymphocytes are the initial targets for infection and are rapidly depleted as they are the largest reservoir of $CCR5^+$ $CD4^+$ T cells.[276,277] Specifically, TH17 $CD4^+$ T cells are integral maintaining gut barrier homeostasis through production of IL17 and IL22.[276,278,279] The rapid depletion of this subset results in a loss of gut barrier integrity resulting in microbial translocation.[276] This translocation can be seen in systemic LPS and scCD14 levels in the plasma of PLWH and SIV infected macaques, which can then cause chronic immune activation to begin the positive feedback loop.[276,277,281] TH17 cells are not depleted in non-pathogenic hosts and consequently chronic immune activation, gut barrier integrity, and microbial translocation are also not seen in these NHPs.[278-280] Further, studies on introduction of exogenous LPS and induction of chronic immune activation have not been able to recapitulate disease progression in natural hosts.[282] Taken together these data support the

hypothesis that while chronic immune activation is important for disease progression in pathogenic hosts, but it cannot fully explain the lack of pathogenicity in natural hosts.

The last key hypothesis on deducing the differences in pathogenicity revolves around the host cells targeted for infection in different hosts.[283-285] In HIV and pathogenic SIV infection, central memory $CD4^+$ T cells are one of the main targets of infection.[286-288] However, in sooty mangabeys central memory cells show low levels of coreceptor expression and are not infected at comparable levels to effector memory cells *in vivo* and *in vitro*.[286-288] This is also borne out in studies that show SIV replication in lymph nodes is lower in natural hosts compared to pathogenic hosts.[289,290] This cell type specificity may play a role in pathogenesis but likely cannot fully explain the lack of bystander cell death.

The usage of natural hosts for studying HIV and SIV pathogenesis has been a central topic in the field as these hosts have been able to adapt to a highly pathogenic virus. The theory of using these NHPs in research is to identify ways in which hosts have naturally adapted to these infections to recapitulate them in humans. In non-pathogenic hosts, the adaptive immune response is still unable to restrict infection which is likely due to the highly mutagenic nature of the SIV *env*. Despite ~32,000 years of adaptation the adaptive immune response is still insufficient for viral control and these hosts have instead developed a way to avoid the pathogenic effects of viral infection.[267-269] This finding can influence current cure strategies for HIV as strategies to improve the adaptive immune response will likely be insufficient for remission of infection. Instead, strategies that focus on avoidance of bystander cell death that recapitulate natural adaptation to SIV should be employed.

1.4.3 The Role of the Inflammasome in Lentiviral Pathogenesis

Bystander cell death caused by abortive infection has long been regarded as the causative mechanism for $CD4^+$ T cell depletion in both humans and pathogenic hosts of SIV.[261-263,291,292] While at first it was suspected to be caused by apoptotic pathways resulting in caspase 3 activation, more recent studies have shown that CASP1 activation accounts for ~95% of this cell death.[293-296] This can be seen in studies that show increased preferential activation of pyroptotic markers of cell death such as CASP1 in comparison to CASP3.[294-296] In humans, CASP1 activation and pyroptotic cell death were observed in bystander $CD4^+$ T cells from viremic individuals.[294] Recently, it was demonstrated *in vivo* in Rhesus macaques that pyroptotic cell death in the periphery and in tissues was the major driver of cell death.[296] These data support the hypothesis that while a small fraction of cells die due to apoptosis via viral mediated cytopathic effects, the vast majority of bystander cell death can be attributed to pyroptosis. While other studies have suggested a role of other inflammasome sensors such as IFI16 and NLRP3, our studies show that these PRRs contribute minimally to pyroptotic cell death.[294,296-298] Instead, we show that CARD8 is the main driver of $CD4^+$ loss during HIV infection. Below we describe our recent findings of CARD8-mediated depletion of $CD4^+$ T cells during HIV infection.

To determine how HIV induces rapid loss of $CD4^+$ T cells and whether CARD8 is involved, activated $CD4^+$ T cells pre-infected with HIV were co-cultured with autologous peripheral blood or tonsil mononuclear cells (PBMCs or ToMCs) in the presence of antiretroviral drugs (ARVs). The percentage of $CD4^+$ and $CD8^+$ T cells was measured by flow cytometry within six hours after co-culture, allowing us to examine cell death immediately after viral entry **(Figure 1.4A)**. The CD4 to CD8 ratio was reduced from 2.4 to 0.6 when co-cultured with $CD4^+$ T cells pre-infected with HIV_{NL4-3}. Inhibitors AMD3100 and T20 that block viral entry

completely abolished $CD4^+$ T-cell loss despite the presence of viral spreading cells, whereas blocking viral reverse transcription by tenofovir (TFV) or integration by raltegravir (RAL) did not prevent $CD4^+$ T-cell depletion **(Figures 1.4B-D)**. The extent of cell loss was determined by the ratio between infected and uninfected cells. These results suggested that cell death occurred post-viral entry but before reverse transcription. When $CD4^+$ T cells, pre-infected with the CCR5-tropic HIV_{BaL}, were used for the co-culture experiments, a rapid depletion of $CCR5^+$ $CD4^+$ T cells was observed **(Figures 1.4E** and **F)**, demonstrating that this effect was entry-dependent and was not limited to X4-tropic viruses.

To determine whether the rapid $CD4^+$ T-cell destruction post-viral entry was due to CARD8-mediated pyroptosis, we first confirmed that it was prevented by the CASP1-specific inhibitor VX765 and the proteasome inhibitor MG132 **(Figures 1.5A** and **B)**. Next, we modified the co-culture system to test Cas9-edited $CD4^+$ T cells **(Figure 1.5C).** We found that *CARD8*-, *CASP1*-, and *GSDMD*-KO $CD4^+$ T cells were resistant to HIV entry-mediated cell killing, whereas NLRP1 and other ASC-dependent inflammasomes were not involved in this process (**Figures 1.5D** and **1.5E**).

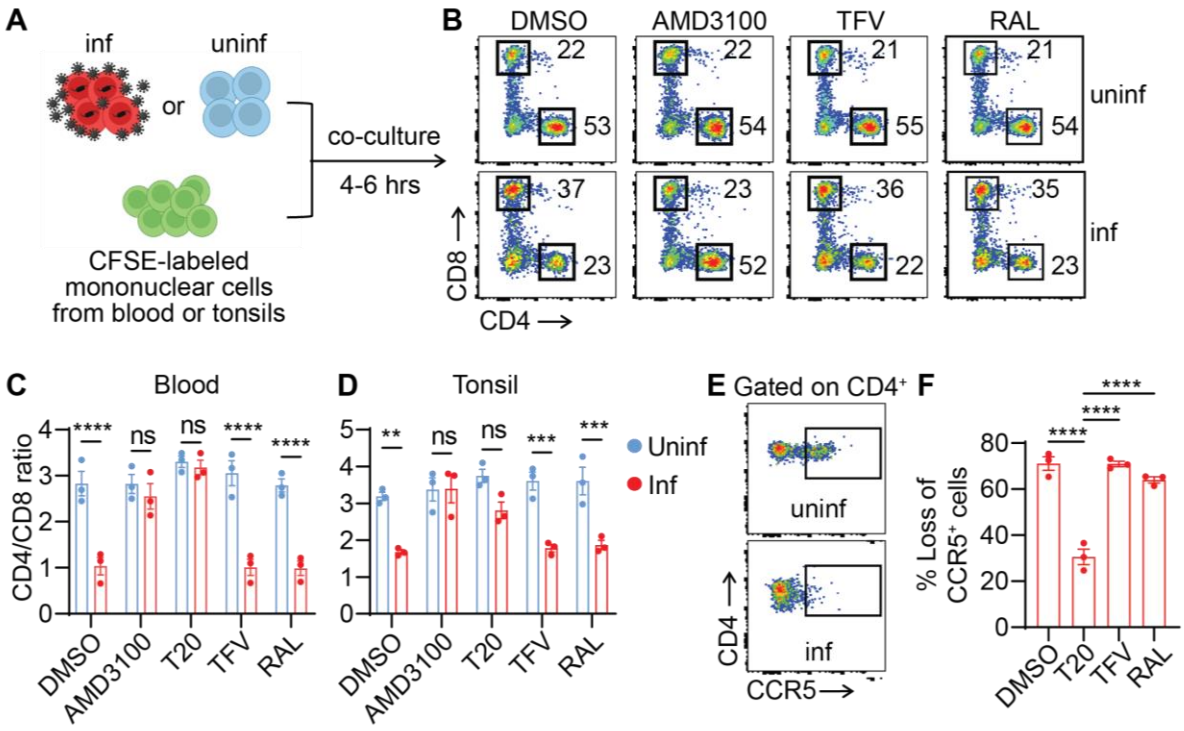

Figure 1.4: HIV Entry Triggers Rapid Loss of $CD4^+$ T Cells.

(a) The co-culture schemes. Activated blood or tonsillar $CD4^+$ T cells were infected with either HIV_{NL4-3} or HIV_{BaL} for three days. Virus-producing cells were then co-cultured at a 1:1 ratio with CFSE-labeled donor-matched unstimulated mononuclear cells from blood or tonsils for four to six hours with the presence of indicated ARVs. **(b)** Representative plots were shown from blood cells infected with HIV_{NL4-3}. **(c** and **d)** Rapid loss of blood and tonsillar $CD4^+$ T cells. Virus-producing cells were infected with HIV_{NL4-3}. Three blood samples and three tonsillar samples were used. **(e** and **f)** Rapid loss of $CCR5^+$ $CD4^+$ T cells. Virus-producing cells were infected with HIV_{BaL}. Three blood samples were used. In **c** and **d**, *p* values were calculated using the two-way ANOVA with Šidák's multiple comparison tests. In **f**, *p* values were calculated using the one-way ANOVA with Dunnett tests. ** $p < 0.01$. *** $p < 0.001$, **** $p < 0.0001$. Error bars show mean values with standard errors of the mean (SEM).

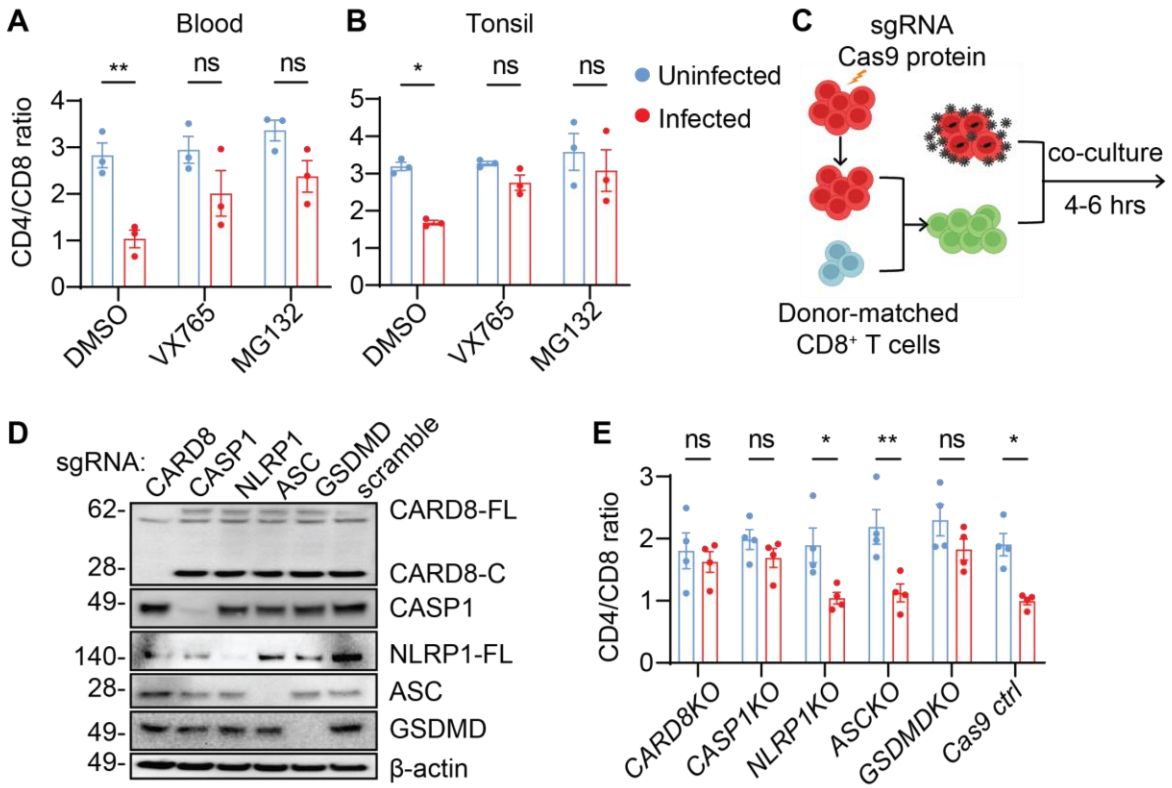

Figure 1.5: CD4⁺ T Cell Depletion by HIV is Mediated by the CARD8 Inflammasome.

(a and **b**) Rapid CD4⁺ T-cell death is proteasome- and CASP1-dependent. Unstimulated PBMCs (A) or ToMCs (B) were pretreated with VX765 (50 μM) or MG132 (10 μM) for 30 minutes and then co-cultured with donor-matched uninfected or HIV_{NL4-3}-producing CD4⁺ T cells for six hours before flow cytometry analyses. (**c**) The co-culture scheme of Cas9-edited unstimulated CD4⁺ T cells and HIV-infected autologous CD4⁺ T cells. Unstimulated CD4⁺ T cells electroporated with the indicated gene-specific sgRNA were cultured for three weeks and then mixed with donor-matched CD8⁺ T cells before co-culture with HIV-infected CD4⁺ T cells from the same donor. **(d** and **e**) The CARD8 inflammasome is required for the rapid loss of CD4⁺ T cells. Unstimulated CD4⁺ T cells with indicated knockouts were mixed with autologous CD8⁺ T cells at a 2:1 ratio before co-culture with HIV_{NL4-3}-producing cells. Cas9 editing efficiency was confirmed in D. The immunoblots represent four independent experiments. Four blood samples were used. *p* values were calculated using two-way ANOVA with Šidák's multiple comparison tests. * $p < 0.05$, ** $p < 0.01$, ns: not significant. Error bars show mean values with SEM from three or four independent blood donors.

Previous studies showed that cell-free viral particles triggered rapid cell death of $CD4^+$ T cells.[299] Since the multiplicity of infection by spin-inoculation is likely higher than natural infection, we aimed to determine whether abrogation of CARD8 function could protect $CD4^+$ T cells from pyroptosis despite exposure to a copious amount of HIV particles. We utilized the cell-free replication-defective HIV reporter virus NL4-3-Δ*Env*-EGFP pseudotyped with the NL4-3 envelope for primary $CD4^+$ T cells or VSV-G for THP-1 cells to study cell death post viral entry. Cell death after exposure to HIV particles was determined by quantitation of ATP and LDH release and staining of annexin V, propidium iodide (PI), Zombie live/dead, and active caspase-1, while productive infection was determined by GFP expression. Productive infection (GFP^+) in the DMSO group was measured 72 hours post exposure. Similar to the co-culture experiments, cell death was observed four hours post-exposure to cell-free HIV particles, which was completely blocked by a viral protease inhibitor lopinavir (LPV) regardless of viral doses (**Figure. 1.6A**). Cell death was also blocked by viral entry inhibitors T20 and AMD3100, whereas ARVs that did not block viral entry had no effect on cell death, except for LPV (**Figures 1.6B and C**). These results suggest that the rapid cell killing was due to release of the viral protease during or immediately after viral entry and that the viral protease was sufficient to drive $CD4^+$ T-cell death. Furthermore, deletion of *CARD8*, *CASP1*, and *GSDMD* in $CD4^+$ T cells completely abrogated early cell death induced by HIV entry, confirming that HIV infection induces rapid pyroptosis in $CD4^+$ T cells through the CARD8 inflammasome (**Figure 1.6D**).

Dipeptidyl peptidase 9 (DPP9) negatively regulates CARD8 activity by binding to and sequestering the bioactive CARD8 C-fragment.[149] Thus, abolishing CARD8 and DPP9 interaction sensitizes the CARD8 inflammasome in cells exposed to HIV particles.[186] While the DPP9 inhibitor 1G244 alone at ≤1μM did not drive cell death, it greatly enhanced HIV entry

triggered pyroptosis of $CD4^+$ T cells (**Figures 1.6E and F**), further demonstrating that CARD8 is the driver of the post-viral entry cell death.

Our previous study demonstrated that HIV protease cleaves CARD8 between F59 and F60, leading to the formation of an unstable neo-N-terminus for proteasome degradation and subsequent activation of the CARD8 inflammasome.[97] In this study, we sought to find direct evidence of CARD8 cleavage and activation by HIV particle-derived viral protease. We generated *CARD8*-KO THP-1 cells replete with wild-type (wt), cleavage-deficient (F59G-F60G), or autoprocessing-deficient (S297A) CARD8. Autoprocessing is required for HIV protease-induced CARD8 inflammasome activation, because only the autoprocessed CARD8 can release its bioactive C-terminus from the proteasome complex due to the non-covalent bond. HIV triggered LDH release and IL-1β secretion with the presence of the wtCARD8, whereas both wtCARD8 and the F59G-F60G mutant restored VbP-triggered cell death and IL-1β secretion in *CARD8*$^{-/-}$ THP-1 cells (**Figures 1.6G and H**). These results demonstrate that the HIV protease encapsulated in the incoming viral particles is required and sufficient to trigger CARD8-mediated pyroptosis immediately after viral entry.

Since CARD8 can be activated immediately after HIV entry, it may function as a host restriction factor to suppress HIV replication. To test this hypothesis, *CARD8*-KO or control $CD4^+$ T cells from blood and tonsils were infected with CXCR4- or CCR5-tropic HIV isolates to measure infection by intracellular p24 staining. Both HIV_{NL4-3} and HIV_{BaL} replicated more efficiently in *CARD8*-KO $CD4^+$ T cells (**Figures 1.6I and J**). In addition, sensitization of CARD8 by the DPP9 inhibitor 1G244 suppressed viral replication in *Cas9* control cells infected with either replication-competent HIV_{NL4-3} or a single-round HIV reporter virus, whereas

knockout of CARD8 abolished this effect (**Figure 1.6K**). Taken together these results suggest that the CARD8 inflammasome is responsible for CD4^{+} T cell depletion during HIV infection.

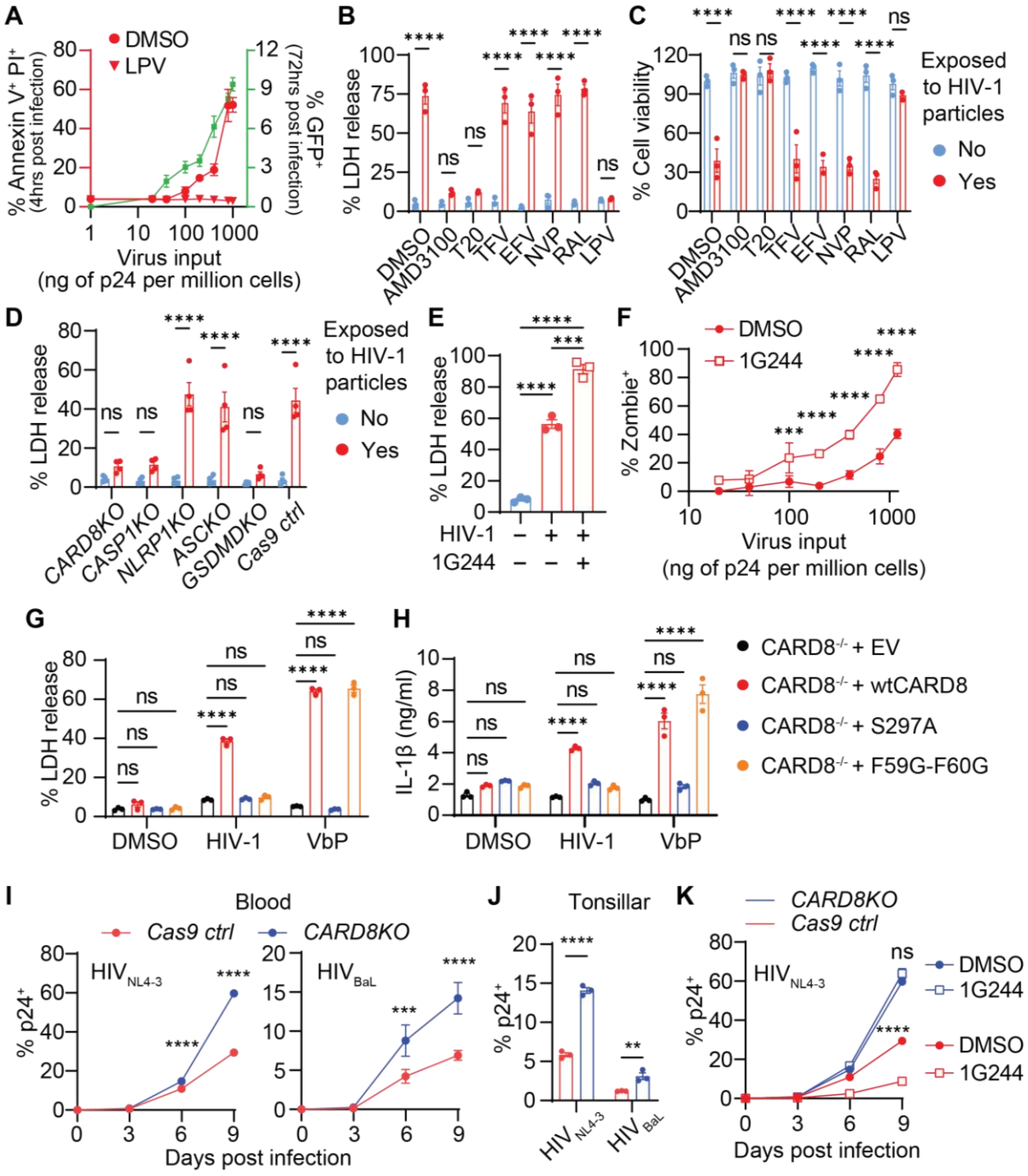

Figure 1.6: HIV Infection Induces CARD8 Inflammasome Activation by Virion-Packaged Protease

(a-c) Rapid loss of $CD4^+$ T cells induced by HIV protease encapsulated in the incoming viral particles. In **(a)**, unstimulated $CD4^+$ T cells were exposed to cell-free HIV reporter virus NL4-3-Δ*Env*-EGFP pseudotyped with the NL4-3 envelope. Cell death and productive infection (GFP^+) were measured four hours and three days post-infection, respectively. In (**b** and **c**), unstimulated $CD4^+$ T cells were treated with indicated antiretroviral drugs for 30 minutes before being exposed to HIV reporter viral particles. **(d)** Rapid loss of $CD4^+$ T cells is mediated by the CARD8 inflammasome. Cell death was determined in different knockout cells. (**e** and **f**) 1G244 enhances HIV entry-triggered pyroptosis of $CD4^+$ T cells. Unstimulated $CD4^+$ T cells were exposed to cell-free virions with or without 1G244 for four hours. **(g** and **h)** Activation of CARD8 inflammasome by HIV-1 in THP-1 cells. *CARD8*-KO THP-1 cells expressing wild-type or mutant CARD8 were exposed to HIV reporter virus NL4-3-Δ*Env*-EGFP pseudotyped with the VSVG envelope for six hours before LDH or IL-1β measurement. VbP (5 μM) was used as positive controls. **(i-k)** Loss of CARD8 leads to increased susceptibility to HIV infection in unstimulated $CD4^+$ T cells. *CARD8*-KO or *Cas9* ctrl unstimulated $CD4^+$ T cells from blood (**i**) or tonsil (**j**) were infected with HIV_{NL4-3} or HIV_{BaL} at 40 ng HIVp24 per million cells. Infection was measured by intracellular p24 staining. Tonsillar samples were analyzed on day six post-infection. In (**k**), *CARD8*-KO or *Cas9* ctrl unstimulated $CD4^+$ T cells were infected with HIV_{NL4-3} or HIV_{BaL} with or without 1G244 (500 nM). In (**e**), *p* values were calculated using the one-way ANOVA with Tukey's multiple comparisons tests. Other *p* values were calculated using the two-way ANOVA with Šidák's multiple comparison tests. * $p < 0.05$, ** $p < 0.01$, **** $p < 0.0001$. The data points are means with SEM and represent three or more independent experiments. N=3.

1.5 Thesis Rationale and Significance

The HIV pandemic has affected the lives of millions, especially LGBTQ+ individuals and communities of color. While antiretroviral therapy has allowed PLWH to live a full and healthy life, research has not been able to identify ways to eliminate the viral reservoir in a sustainable and equitable fashion. Our recent findings on the novel host restriction factor CARD8 have opened the door to new possibilities in the HIV cure field. Chapter 2 of this dissertation aims to begin bridging the gap between *in vitro* studies of CARD8 and clinical applications for an HIV cure. Key issues of intracellular NNRTI concentrations and NNRTI resistance necessitated the identification of alternative strategies to enhance NNRTI-mediated clearance of HIV reservoirs. In this chapter we show that inhibition of DPP9 can greatly enhance NNRTI efficacy in eliminating viral reservoirs *ex vivo* from PLWH in a shock and kill model as well as *in vivo* in a humanized mouse model. These studies prove the potential of leveraging the CARD8 inflammasome for an HIV cure. However, this is only the beginning, our work has laid the foundation for future studies in optimizing drug regimens to increase efficacy and reduce side effect potential. As the identification of CARD8 as an inflammasome sensor for HIV protease is still relatively new, myriad methodologies for improving this sensing can now be investigated for their potential in enhancing this sensing in latently infected $CD4^+$ T cells and macrophages.

CARD8's role in restricting HIV infection has led to further discoveries in its role in HIV-1 pathogenesis. The field has long grappled with identifying the key host restriction factor responsible for bystander $CD4^+$ T cell loss and subsequent progression to AIDS. We believe that CARD8 plays a central role in pyroptotic $CD4^+$ T cell death which is elicited immediately upon viral entry. As pyroptotic cell death has been shown the leading form of bystander cell death of

$CD4^+$ T cells in humans and rhesus macaques, we hypothesize that CARD8 inflammasome activation is the most probable cause of disease progression to AIDS. These studies have opened the door to further work on identifying ways to modulate the CARD8 inflammasome to improve clinical outcomes for HIV treatment. SIV disease progression in NHP's represents a heterogenous host response to infection in contrast to their human counterparts. African NHP species do not develop $CD4^+$ T cell depletion or AIDS like pathology representing an idealized model where the host has adapted to persistent lentiviral infections over millennia. These hosts have developed a way to live with SIV in an almost symbiotic fashion. While the molecular mechanism of this resistance has plagued researchers for decades, it has remained a central question in HIV cure research. If we can leverage this natural adaptation by NHPs to humans, we can help prevent HIV disease progression and move toward an HIV cure. In chapter 3 we present a new hypothesis for the molecular mechanism of $CD4^+$ T cell loss escape in non-pathogenic hosts. We show that CARD8 loss of function mutations, facilitated by the presence of a reverse tandem gene duplication, have allowed these natural hosts to avoid CARD8 sensing upon viral entry thereby escaping $CD4^+$ T cell loss and AIDS. This work in combination with our work on CARD8 and HIV disease progression solidifies the role of CARD8 in lentiviral pathogenesis. It also again stresses the importance of identifying ways to neutralize the CARD8 inflammasome sensing in humans to prevent further $CD4^+$ T cell loss upon initiation of antiretroviral therapy. Overall, this dissertation aims to increase the field's understanding of the CARD8 inflammasome's role and importance in HIV cure and pathogenesis research. We offer new insights into clinical strategies, drug targets, and disease progression that can move the field toward an HIV cure.

1.6 References

1. AIDS data, HIV data, Fact sheet - Latest global and regional statistics on the status of the AIDS epidemic. 2019. UNAIDS. https://www.unaids.org/en/resources/fact-sheet
2. CDC FACT SHEET: HIV Among Gay and Bisexual Men. 2016. CDC. https://www.cdc.gov/nchhstp/newsroom/docs/factsheets/cdc-msm-508.pdf
3. Peltzer, K. et al. Socioeconomic Factors in Adherence to HIV Therapy in Low- and Middle-income Countries. Journal of Health. *Population and Nutrition* **31**(2) (2013). doi:10.3329/jhpn.v31i2.16379
4. Govender, R. et al. Global Epidemiology of HIV/AIDS: A resurgence in North America and Europe. *J. Epidemiol Glob Health* **3**, 296-301 (2021). Doi: 10.2991/jegh.k.210621.001
5. Deeks, SG et al. International AIDS Society global scientific strategy: towards an HIV cure 2016. *Nature Medicine* **22**(8), 839–850 (2016). doi:10.1038/nm.4108
6. Ratner, L. et al. Complete nucleotide sequence of the AIDS virus. HTLV-III. *Nature* **313**(6000), 277-284 (1985).
7. Wright, E.R. et al. Electron cryotomography of immature HIV-1 virions reveals the structure of the CA and SP1 Gag shells. *EMBO* J **26**(8), 2218-2226 (2007). Doi: 10.1038/sj.emboj.7601664
8. Berger, E.A. et al. Chemokine receptors as HIV-1 coreceptors: roles in viral entry, tropism, and disease. *Annu. Rev. Immunol.* **17**, 657-700 (1999). doi: 10.1146/annurev.immunol.17.1.657
9. Klasse, P.J. The molecular basis of HIV entry. *Cell Microbiol.* **14**(8), 1183-1192 (2012). doi:10.1111/j.1462-5822.2012.01812.x
10. Doms, R.W. et al. HIV-1 membrane fusion. *J. Cell Biol.* **151**, F9-F14 (2000). Doi: 10.1083/jcb.151.2.f9
11. Muller, T.G. et al. Capsid Uncoating and Reverse Transcription of HIV-1. *Annual Review of Virology* **9**, 261-284 (2022). Doi: 10.1146/annurev-virology-020922-110929
12. Warrilow, D. et al. Maturation of the HIV reverse transcription complex: putting the jigsaw together. *Rev. Med. Virol.* **19**(6), 324-337 (2009). Doi: 10.1002/rmv.627
13. Krishnan, L. et al. Retroviral integrase proteins and HIV-1 DNA integration. *J. Biol. Chem.* **287**(49), 40858-40866 (2012). Doi: 10.1074/jbc.R112.39776
14. Ott, M. et al. The control of HIV transcription: keeping RNA polymerase II on track. *Cell Host Microbe* **10**(5), 426-453 (2011). Doi: 10.1016/j.chom.2011.11.002
15. Briggs, J.A. et al. The molecular architecture of HIV. *J. Mol. Biol.* **410**(4), 491-500 (2011). Doi: 10.1016/j.jmb.2011.04.021
16. Saad, J.S. et al. Structural basis for targeting HIV-1 Gag proteins to the plasma membrane for virus assembly. *Proc Natl Acad Sci USA* **103**(30), 11364-11369 (2006). Doi: 10.1073/pnas.0602818103
17. Fisher, R.J. et al. Sequence-specific binding of human immunodeficiency virus type 1 nucleocapsid protein to short oligonucleotides. *J. Virol.* **72**(3), 1902-1909 (1998).
18. Tang, C. et al. Visualizing transient events in amino-terminal autoprocessing of HIV-1 protease. *Nature* **455**(7213), 693-696 (2008). doi: 10.1038/nature07342

19. Konnyu, B. et al. Gag-pol processing during HIV-1 virion maturation: A systems biology approach. *PLoS Comp. Biol.* 9(6): e1003103 (2013). Doi: 10.1371/journal.pcbi.1003103
20. Finzi, D. et al. Identification of a reservoir for HIV-1 in patients on highly active antiretroviral therapy. *Science* **278**, 1295–1300 (1997).
21. Ganor, Y. et al. HIV-1 reservoirs in urethral macrophages of patients under suppressive antiretroviral therapy. *Nat. Microbiol.* **4**, 633–644 (2019).
22. Eisele, E. & Siliciano, R. F. Redefining the viral reservoirs that prevent HIV-1 eradication. *Immunity* **37**, 377–388 (2012).
23. Finzi, D. et al. Latent infection of CD4+ T cells provides a mechanism for lifelong persistence of HIV-1, even in patients on effective combination therapy. *Nat Med.* **5**(5), 512–7 (1999).
24. Pierson, T. et al. Reservoirs for HIV-1: mechanisms for viral persistence in the presence of antiviral immune responses and antiretroviral therapy. *Annu Rev Immunol.* **18**, 665–708 (2000).
25. Siliciano, J.D. et al. Long-term follow-up studies confirm the stability of the latent reservoir for HIV-1 in resting CD4+ T cells. *Nat Med.* **9**(6), 727–728 (2003).
26. Archin, N. M. et al. Eradicating HIV-1 infection: seeking to clear a persistent pathogen. *Nat. Rev. Microbiol.* **12**, 750–764 (2014).
27. Maina, E.K. et al. A review of current strategies towards the elimination of latent HIV-1 and subsequent HIV-1 Cure. Curr. *HIV Res* **19**(1), 14-26 (2021).
28. Hütter, G. et al. Long-term control of HIV by CCR5 Delta32/Delta32 stem-cell transplantation. *N. Engl. J. Med.* **360**, 692–698 (2009).
29. Gupta, R.K. et al. HIV-1 remission following CCR5Δ32/Δ32 haematopoietic stem-cell transplantation. *Nature* **568**, 244–248 (2019).
30. Jensen, B.-E.O. et al. In-depth virological and immunological characterization of HIV-1 cure after CCR5Δ32/Δ32 allogeneic hematopoietic stem cell transplantation. *Nat. Med.* **29**, 583-587 (2023).
31. Hsu, J. et al. HIV-1 remission and possible cure in a woman after haplo-cord blood transplant. *Cell* **186**, 1115-1126 (2023).
32. Samson, M. et al. Resistance to HIV-1 infection in Caucasian individuals bearing mutant alleles of the CCR-5 chemokine receptor gene. *Nature* **382**, 722-725 (1996).
33. Soppe, J. A. et al. Antiviral goes viral: harnessing CRISPR/Cas9 to combat viruses in humans. *Trends in Microbiology* **10**(25), 833–850 (2017).
34. Darcis, G. et al. The impact of HIV-1 genetic diversity on CRISPR-Cas9 antiviral activity and viral escape. *Viruses* **11**,255 (2019).
35. Fu, Y. et al. High-frequency off-target mutagenesis induced by CRISPR-Cas nucleases in human cells. *Nat. Biotechnol.* **31**, 822–826 (2013).
36. Anderson, K.R. et al. CRISPR off-target analysis in genetically engineered rats and mice. *Nat. Methods.* **15**, 512–514 (2018).
37. Kuscu, C. et al. Genome-wide analysis reveals characteristics of off-target sites bound by the Cas9 endonuclease. *Nat. Biotechnol.* **32**, 677–683 (2014).
38. Leibowitz, M.L. et al. Chromothripsis as an on-target consequence of CRISPR-Cas9 genome editing. *Nature Genetics* 2021; **53**, 895-905 (2021).
39. Pham, H. T. et al. The latest evidence for possible HIV-1 curative strategies. *Drugs in Context* **7**, 212522 (2018).

40. Deeks, S.G. et al. HIV: Shock and kill. *Nature* **487**(7408), 439–40 (2012).
41. Kim, Y., Anderson, J.L., & Lewin, S.R. Getting the "kill" into "shock and kill": strategies to eliminate latent HIV. *Cell Host Microbe* **23**(1), 14-26 (2018).
42. Phillips, R. E. et al. Human immunodeficiency virus genetic variation that can escape cytotoxic T-cell recognition. *Nature* **354**, 453–459 (1991).
43. Kwong, P. D. et al. HIV-1 evades antibody-mediated neutralization through conformational masking of receptor-binding sites. *Nature* **420**, 678–682 (2002).
44. Caskey, M. et al. Viraemia suppressed in HIV-1-infected humans by broadly neutralizing antibody 3BNC117. *Nature* **522**, 487–491 (2015).
45. Rhee, S. Y. et al. HIV-1 protease, reverse transcriptase and integrase variation. *J. Virol.* **90**, 6058–6070 (2016).
46. Martinon, F., Burns, K., & Tschopp, J. The inflammasome: A molecular platform triggering activation of inflammatory caspases and processing of pro IL-beta. *Molecular Cell* **10**, 417–426 (2002).
47. Crawford, E.D., & Wells, J.A. Caspase substrates and cellular remodeling. *Annual Review of Biochemistry* **80**, 1055–1087 (2011).
48. Julien, O., & Wells, J.A. Caspases and their substrates. *Cell Death and Differentiation* **24**, 1380–1389 (2017).
49. Lamkanfi, M., et al. Alice in caspase land. A phylogenetic analysis of caspases from worm to man. *Cell Death and Differentiation* **9**, 358–361 (2002).
50. Thornberry, N.A., & Lazebnik, Y. Caspases: Enemies within. *Science* **281**, 1312–1316 (1998).
51. Yuan, J., & Kroemer, G. Alternative cell death mechanisms in development and beyond. *Genes & Development* **24**, 2592–2602 (2010).
52. Yuan, J., et al. The C. elegans cell death gene ced-3 encodes a protein similar to mammalian interleukin-1 beta-converting enzyme. *Cell* **75**,641–652 (1993).
53. Alnemri, E.S., et al. Human ICE/CED-3 protease nomenclature. *Cell* **87**,171 (1996).
54. Salvesen, G.S., & Riedl, S.J. Caspase mechanisms. Advances in Experimental Medicine and Biology **615**, 13–23 (2008).
55. Stennicke, H.R., & Salvesen, G.S. Caspases—Controlling intracellular signals by protease zymogen activation. *Biochim. Biophys. Acta.* **1477**, 299–306 (2000).
56. Fuentes-Prior, P., & Salvesen, G.S. The protein structures that shape caspase activity, specificity, activation and inhibition. *The Biochemical Journal* **384**, 201–232 (2004).
57. Thornberry, N.A., et al. A novel heterodimeric cysteine protease is required for interleukin-1beta processing in monocytes. *Nature* **356**,768–774 (1992).
58. Riedl, S.J., & Shi, Y. Molecular mechanisms of caspase regulation during apoptosis. *Nature Reviews Molecular Cell Biology* **5**, 897–907 (2004).
59. Riedl, S.J., et al. Structural basis for the activation of human pro caspase-7. *Proc. Natl. Acad. Sci. USA* **98**, 14790–14795 (2001).
60. Riedl, S.J., & Salvesen, G.S. The apoptosome: signalling platform of cell death. *Nat. Rev. Mol. Cell Biol.* **8**, 405-413 (2007).
61. Renatus, M., et al. Dimer formation drives the activation of the cell death protease caspase 9. *Proc. Natl. Acad. Sci. USA* **98**, 14250-14255 (2001).
62. Boatright, K.M., *et al.* A unified model for apical caspase activation. *Mol. Cell* **11**, 529-541 (2003).

63. Kischkel, F.C., *et al.* Cytotoxicity-dependent APO-1 (Fas/CD95)-associated proteins form a death-inducing signaling complex (DISC) with the receptor. *EMBO J.* **14**, 5579-5588 (1995).
64. Nakagawa, T. *et al.* Caspase-12 mediates endoplasmic-reticulum-specific apoptosis and cytotoxicity by amyloid-beta. *Nature* **403**, 98-103 (2000).
65. Salvesen, G.S. & Ashkenazi, A. Snapshot: caspases. *Cell* **147**, 476-476.e471 (2011).
66. Schroder, K. & Tschopp, J. The inflammasomes. *Cell* **140**, 821-832 (2010).
67. Janeway, C.A. & Medzhitov, R. Innate immune recognition. *Annu. Rev. Immunol.* **20**, 197-216 (2002).
68. Li, D. & Wu, M. Pattern recognition receptors in health and diseases. *Signal Transduct Target Ther.* **6**, 291 (2021).
69. ShaoPing, H. et al. Research advancement of innate immunity and pattern recognition receptors. *Chinese Journal of Animal Nutrition* **29**(11)**,** 3844-3851 (2017).
70. Park, H.H. *et al.* The death domain superfamily in intracellular signaling of apoptosis and inflammation. *Annu. Rev. Immunol.* **25**, 561-586 (2007).
71. Park, H.H. Caspase recruitment domains for protein interactions in cellular signaling. *Int. J. Mol. Med.* **43**, 1119-1127 (2019).
72. Kwon, D. *et al.* A comprehensive manually curated protein-protein interaction database for the Death Domain superfamily. *Nucleic Acids Res.* **40**, D331-336 (2012).
73. Reed, J.C. et al. The domains of apoptosis: a genomics perspective. *Sci. STKE* **2004**(239) (2004).
74. Zheng, D., Liwinski, T., & Elinav, E. Inflammasome activation and regulation: toward a better understanding of complex mechanisms. *Cell Discov.* **6**, 36 (2020).
75. Liu, X. et al. Inflammasome-activated gasdermin D causes pyroptosis by forming membrane pores. *Nature* **535**, 153-158 (2016).
76. Shi, J., Gao, W., Shao, F. Pyroptosis: Gasdermin-Mediated Programmed Necrotic Cell Death. *Trends Biochem. Sci.* **42**, 245-254 (2017).
77. Li, Y. et al. Cryo-EM structures of ASC and NLRC4 CARD filaments reveal a unified mechanism of nucleation and activation of caspase-1. *Proc. Natl. Acad. Sci. USA* **115**, 10845-10852 (2018).
78. Ball, D.P. et al. Caspase-1 interdomain linker cleavage is required for pyroptosis. *Life. Sci. Alliance* **3** (2020).
79. Lu, A. et al. Unified polymerization mechanism for the assembly of ASC-dependent inflammasomes. *Cell* **156**, 1193-1206 (2014).
80. Morrone, S.R. et al. Cooperative assembly of IFI16 filaments on dsDNA provides insights into host defense strategy. *Proc. Natl. Acad. Sci. USA* **111**, E62-71 (2014).
81. Poeck, H. et al. Recognition of RNA virus by RIG-I results in activation of CARD9 and inflammasome signaling for interleukin 1 beta production. *Nat. Immunol.* **11**, 63-69 (2010).
82. Jin, T. et al. Structures of the HIN domain:DNA complexes reveal ligand binding and activation mechanisms of the AIM2 inflammasome and IFI16 receptor. *Immunity* **36**, 561-571 (2012).
83. Morrone, S.R. et al. Assembly-driven activation of the AIM2 foreign-dsDNA sensor provides a polymerization template for downstream ASC. *Nat. Commun.* **6**, 7827 (2015).

84. Jin, T. et al. Structure of the absent in melanoma 2 (AIM2) pyrin domain provides insights into the mechanisms of AIM2 autoinhibition and inflammasome assembly. *J. Biol. Chem.* **288**, 13225-13235 (2013).
85. Xu, H. et al. Innate immune sensing of bacterial modifications of Rho GTPases by the Pyrin inflammasome. *Nature* **513**, 237-241 (2014).
86. Ting, J.P. et al. The NLR gene family: a standard nomenclature. *Immunity* **28**, 285-287 (2008).
87. He, Y. et al. NEK7 is an essential mediator of NLRP3 activation downstream of potassium efflux. *Nature* **530**, 354-357 (2016).
88. Schmid-Burgk, J.L. et al. A Genome-wide CRISPR (Clustered Regularly Interspaced Short Palindromic Repeats) Screen Identifies NEK7 as an Essential Component of NLRP3 Inflammasome Activation. *J. Biol. Chem.* **291**, 103-109 (2016).
89. Sharif, H. et al. Structural mechanism for NEK7-licensed activation of NLRP3 inflammasome. *Nature* **570**, 338-343 (2019).
90. Shi, H. et al. NLRP3 activation and mitosis are mutually exclusive events coordinated by NEK7, a new inflammasome component. *Nat. Immunol.* **17**, 250-258 (2016).
91. Halff, E.F. et al. Formation and structure of a NAIP5-NLRC4 inflammasome induced by direct interactions with conserved N- and C-terminal regions of flagellin. *J. Biol. Chem.* **287**, 38460-38472 (2012).
92. Kofoed, E.M & Vance, R.E. Innate immune recognition of bacterial ligands by NAIPs determines inflammasome specificity. *Nature* **477**, 592-595 (2011).
93. Tenthorey, J.L. et al. Molecular basis for specific recognition of bacterial ligands by NAIP/NLRC4 inflammasomes. *Mol. Cell* **54**, 17-29 (2014).
94. Zhao, Y. et al. The NLRC4 inflammasome receptors for bacterial flagellin and type III secretion apparatus. *Nature* **477**, 596-600 (2011).
95. Kortmann, J., Brubaker, S.W., & Monack, D.M. Cutting Edge: Inflammasome Activation in Primary Human Macrophages Is Dependent on Flagellin. *J. Immunol.* **195**, 815-819 (2015).
96. Franchi, L. et al. Cytosolic flagellin requires Ipaf for activation of caspase-1 and interleukin 1beta in salmonella-infected macrophages. *Nat. Immunol.* **7**, 576-582 (2006).
97. Wang, Q. et al. CARD8 is an inflammasome sensor for HIV-1 protease activity. *Science* eabe1707 (2021).
98. Jones, J.D., Vance, R.E., Dangl, J.L. Intracellular innate immune surveillance devices in plants and animals. *Science* **354**, (2016).
99. Finger, J.N. et al. Autolytic proteolysis within the function to find domain (FIIND) is required for NLRP1 inflammasome activity. *J. Biol. Chem.* **287**, 25030-25037 (2012).
100. Zhong, F.L. et al. Germline NLRP1 Mutations Cause Skin Inflammatory and Cancer Susceptibility Syndromes via Inflammasome Activation. *Cell* **167**, 187-202.e117 (2016).
101. D'Osualdo, A. et al. CARD8 and NLRP1 undergo autoproteolytic processing through a ZU5-like domain. *PLoS One* **6**, e27396 (2011).
102. Pathan, N. et al. TUCAN, an antiapoptotic caspase-associated recruitment domain family protein overexpressed in cancer. *J. Biol. Chem.* **276**, 32220-32229 (2001).
103. Frew, B.C., Joag, V.R., Mogridge, J. Proteolytic processing of Nlrp1b is required for inflammasome activity. *PLoS Pathog.* **8**, e1002659 (2012).

104. Johnson, D.C. et al. DPP8/DPP9 inhibitor-induced pyroptosis for treatment of acute myeloid leukemia. *Nat. Med.* **24**, 1151-1156 (2018).
105. Hollingsworth, L.R. et al. DPP9 sequesters the C terminus of NLRP1 to repress inflammasome activation. *Nature* **592**, 778-783 (2021).
106. Gong, Q. et al. Structural basis for distinct inflammasome complex assembly by human NLRP1 and CARD8. *Nat. Commun.* **12**, 188 (2021).
107. Broz, P. et al. Differential requirement for Caspase-1 autoproteolysis in pathogen-induced cell death and cytokine processing. *Cell Host Microbe* **8**, 471-483 (2010).
108. Van Opdenbosch, N. et al. Activation of the NLRP1b inflammasome independently of ASC-mediated caspase-1 autoproteolysis and speck formation. *Nat. Commun.* **5**, 3209 (2014).
109. Masters, S.L. et al. NLRP1 inflammasome activation induces pyroptosis of hematopoietic progenitor cells. *Immunity* **37**, 1009-1023 (2012).
110. Chui, A.J. et al. N-terminal degradation activates the NLRP1B inflammasome. *Science* **364**, 82-85 (2019).
111. Sandstrom, A. et al. Functional degradation: A mechanism of NLRP1 inflammasome activation by diverse pathogen enzymes. *Science* **364**, (2019).
112. Tang, G. & Leppla, S.H. Proteasome activity is required for anthrax lethal toxin to kill macrophages. *Infect. Immun.* **67**, 3055-3060 (1999).
113. Wickliffe, K.E., Leppla, S.H., Moayeri, M. Killing of macrophages by anthrax lethal toxin: involvement of the N-end rule pathway. *Cell Microbiol.* **10**, 1352-1362 (2008).
114. Boyden, E.D. & Dietrich, W.F. Nalp1b controls mouse macrophage susceptibility to anthrax lethal toxin. *Nat. Genet.* **38**, 240-244 (2006).
115. Sastalla, I. et al. Transcriptional analysis of the three Nlrp1 paralogs in mice. *BMC Genomics* **14**, 188 (2013).
116. Moayeri, M. & Leppla, S.H. Cellular and systemic effects of anthrax lethal toxin and edema toxin. *Mol. Aspects Med.* **30**, 439-455 (2009).
117. Roberts, J.E. et al. Ltx1, a mouse locus that influences the susceptibility of macrophages to cytolysis caused by intoxication with Bacillus anthracis lethal factor, maps to chromosome 11. *Mol. Microbiol.* **29**, 581-591 (1998).
118. Moayeri, M. et al. Inflammasome sensor Nlrp1b-dependent resistance to anthrax is mediated by caspase-1, IL-1 signaling and neutrophil recruitment. *PLoS Pathog.* **6**, e1001222 (2010).
119. Greaney, A.J. et al. Frontline Science: Anthrax lethal toxin-induced, NLRP1-mediated IL-1β release is a neutrophil and PAD4-dependent event. *J. Leukoc. Biol.* **108**, 773-786 (2020).
120. Chavarría-Smith, J. & Vance, R.E. Direct proteolytic cleavage of NLRP1B is necessary and sufficient for inflammasome activation by anthrax lethal factor. *PLoS Pathog.* **9**, e1003452 (2013).
121. Xu, H. et al. The N-end rule ubiquitin ligase UBR2 mediates NLRP1B inflammasome activation by anthrax lethal toxin. *EMBO J.* **38**, e101996 (2019).
122. Chavarría-Smith, J. et al. Functional and Evolutionary Analyses Identify Proteolysis as a General Mechanism for NLRP1 Inflammasome Activation. *PLoS Pathog.* **12**, e1006052 (2016).

123. Neiman-Zenevich, J. et al. Listeria monocytogenes and Shigella flexneri Activate the NLRP1B Inflammasome. *Infect. Immun.* **85** (2017).
124. Lei, J. & Hilgenfeld, R. RNA-virus proteases counteracting host innate immunity. *FEBS Lett.* **591**, 3190-3210 (2017).
125. Tsu, B.V. et al. Diverse viral proteases activate the NLRP1 inflammasome. *Elife* **10** (2021).
126. Robinson, K.S. et al. Enteroviral 3C protease activates the human NLRP1 inflammasome in airway epithelia. *Science* **370** (2020).
127. Planès, R. et al. Human NLRP1 is a sensor of pathogenic coronavirus 3CL proteases in lung epithelial cells. *Mol. Cell.* **82**, 2385-2400.e2389 (2022).
128. Bauernfried, S. et al. Human NLRP1 is a sensor for double-stranded RNA. *Science* **371** (2021).
129. Liao, K.C. & Mogridge, J. Activation of the Nlrp1b inflammasome by reduction of cytosolic ATP. *Infect. Immun.* **81**, 570-579 (2013).
130. Faustin, B. & Reed, J.C. Sunburned skin activates inflammasomes. *Trends Cell. Biol.* **18**, 4-8 (2008).
131. Feldmeyer, L. et al. The inflammasome mediates UVB-induced activation and secretion of interleukin-1beta by keratinocytes. *Curr. Biol.* **17**, 1140-1145 (2007).
132. Robinson, K.S. et al. ZAKα-driven ribotoxic stress response activates the human NLRP1 inflammasome. *Science* **377**, 328-335 (2022).
133. Razmara, M. et al. CARD-8 protein, a new CARD family member that regulates caspase-1 activation and apoptosis. *J. Biol. Chem.* **277**, 13952-13958 (2002).
134. Chui, A.J. et al. Activation of the CARD8 Inflammasome Requires a Disordered Region. *Cell. Rep.* **33**, 108264 (2020).
135. Hsiao, J.C. et al. A ubiquitin-independent proteasome pathway controls activation of the CARD8 inflammasome. *J. Biol. Chem.* **298**, 102032 (2022).
136. Johnson, D.C. et al. DPP8/9 inhibitors activate the CARD8 inflammasome in resting lymphocytes. *Cell Death Dis.* **11**, 628 (2020).
137. Linder, A. et al. CARD8 inflammasome activation triggers pyroptosis in human T cells. *EMBO J.* **39**, e105071 (2020).
138. Nadkarni, R. et al. Viral proteases activate the CARD8 inflammasome in the human cardiovascular system. *J. Exp. Med.* **219** (2022).
139. Adams, S. et al. PT-100, a small molecule dipeptidyl peptidase inhibitor, has potent antitumor effects and augments antibody-mediated cytotoxicity via a novel immune mechanism. *Cancer Res.* **64**, 5471-5480 (2004).
140. Okondo, M.C. et al. DPP8 and DPP9 inhibition induces pro-caspase-1-dependent monocyte and macrophage pyroptosis. *Nat. Chem. Biol.* **13**, 46-53 (2017).
141. Taabazuing, C.Y., Okondo, M.C., & Bachovchin, D.A. Pyroptosis and Apoptosis Pathways Engage in Bidirectional Crosstalk in Monocytes and Macrophages. *Cell Chem. Biol.* **24**, 507-514.e504 (2017).
142. Geiss-Friedlander, R. et al. The cytoplasmic peptidase DPP9 is rate-limiting for degradation of proline-containing peptides. *J. Biol. Chem.* **284**, 27211-27219 (2009).
143. Taabazuing, C.Y., Griswold, A.R., & Bachovchin, D.A. The NLRP1 and CARD8 inflammasomes. *Immunol. Rev.* **297**, 13-25 (2020).

144. Bachovchin, D.A. et al. A high-throughput, multiplexed assay for superfamily-wide profiling of enzyme activity. *Nat. Chem. Biol.* **10**, 656-663 (2014).
145. Zhang, H. et al. Advances in understanding the expression and function of dipeptidyl peptidase 8 and 9. *Mol. Cancer Res.* **11**, 1487-1496 (2013).
146. Okondo, M.C. et al. Inhibition of Dpp8/9 Activates the Nlrp1b Inflammasome. *Cell Chem. Biol.* **25**, 262-267.e265 (2018).
147. Zhong, F.L. et al. Human DPP9 represses NLRP1 inflammasome and protects against autoinflammatory diseases via both peptidase activity and FIIND domain binding. *J. Biol. Chem.* **293**, 18864-18878 (2018).
148. Huang, M. et al. Structural and biochemical mechanisms of NLRP1 inhibition by DPP9. *Nature* **592**, 773-777 (2021).
149. Sharif, H. et al. Dipeptidyl peptidase 9 sets a threshold for CARD8 inflammasome formation by sequestering its active C-terminal fragment. *Immunity* **54**, 1392-1404.e1310 (2021).
150. Griswold, A.R. et al. A Chemical Strategy for Protease Substrate Profiling. *Cell Chem. Biol.* **26**, 901-907.e906 (2019).
151. Griswold, A.R. et al. DPP9's Enzymatic Activity and Not Its Binding to CARD8 Inhibits Inflammasome Activation. *ACS Chem. Biol.* **14**, 2424-2429 (2019).
152. Rao, S.D. et al. M24B aminopeptidase inhibitors selectively activate the CARD8 inflammasome. *Nat. Chem. Biol.* **18**, 565-574 (2022).
153. Van Goethem, S. et al. Inhibitors of dipeptidyl peptidase 8 and dipeptidyl peptidase 9. Part 2: isoindoline containing inhibitors. *Bioorg. Med. Chem. Lett.* **18**, 4159-4162 (2008).
154. Jiaang, W.T. et al. Novel isoindoline compounds for potent and selective inhibition of prolyl dipeptidase DPP8. *Bioorg. Med. Chem. Lett.* **15**, 687-691 (2005).
155. Park, J. & Morrow, C.D. Overexpression of the gag-pol precursor from human immunodeficiency virus type 1 proviral genomes results in efficient proteolytic processing in the absence of virion production. *J. Virol.* **65**, 5111-5117 (1991).
156. Kräusslich, H.G. Human immunodeficiency virus proteinase dimer as component of the viral polyprotein prevents particle assembly and viral infectivity. *Proc. Natl. Acad. Sci. USA* **88**, 3213-3217 (1991).
157. Murakami, T. et al. Regulation of human immunodeficiency virus type 1 Env-mediated membrane fusion by viral protease activity. *J. Virol.* **78**, 1026-1031 (2004).
158. Wyma, D.J. et al. Coupling of human immunodeficiency virus type 1 fusion to virion maturation: a novel role of the gp41 cytoplasmic tail. *J. Virol.* **78**, 3429-3435 (2004).
159. Louis, J.M., Clore, G.M., & Gronenborn, A.M. Autoprocessing of HIV-1 protease is tightly coupled to protein folding. *Nat. Struct. Biol.* **6**, 868-875 (1999).
160. Huang, Y. et al. Effect of mutations in the nucleocapsid protein (NCp7) upon Pr160(gag-pol) and tRNA(Lys) incorporation into human immunodeficiency virus type 1. *J. Virol.* **71**, 4378-4384 (1997).
161. Khorchid, A. et al. Role of RNA in facilitating Gag/Gag-Pol interaction. *J. Virol.* **76**, 4131-4137 (2002).
162. Benner, B.E. et al. Perturbing HIV-1 Ribosomal Frameshifting Frequency Reveals a. *J. Virol.* **96**, e0134921 (2022).
163. Figueiredo, A. et al. Potent nonnucleoside reverse transcriptase inhibitors target HIV-1 Gag-Pol. *PLoS Pathog.* **2**, e119 (2006).

164. Baba, M. et al. Highly specific inhibition of human immunodeficiency virus type 1 by a novel 6-substituted acyclouridine derivative. *Biochem. Biophys. Res. Commun.* **165**, 1375-1381 (1989).
165. Pauwels, R. et al. Potent and selective inhibition of HIV-1 replication in vitro by a novel series of TIBO derivatives. *Nature* **343**, 470-474 (1990).
166. Ivetac, A. & McCammon, J.A. Elucidating the inhibition mechanism of HIV-1 non-nucleoside reverse transcriptase inhibitors through multicopy molecular dynamics simulations. *J. Mol. Biol.* **388**, 644-658 (2009).
167. Kohlstaedt, L.A. et al. Crystal structure at 3.5 A resolution of HIV-1 reverse transcriptase complexed with an inhibitor. *Science* **256**, 1783-1790 (1992).
168. Goff, S.P. Retroviral reverse transcriptase: synthesis, structure, and function. *J. Acquir. Immune Defic. Syndr. (1988)* **3**, 817-831 (1990).
169. De Clercq, E. Antiviral drug discovery and development: where chemistry meets with biomedicine. *Antiviral Res.* **67**, 56-75 (2005).
170. Smerdon, S.J. et al. Structure of the binding site for nonnucleoside inhibitors of the reverse transcriptase of human immunodeficiency virus type 1. *Proc. Natl. Acad. Sci. USA* **91**, 3911-3915 (1994).
171. Havlir, D. et al. High-dose nevirapine: safety, pharmacokinetics, and antiviral effect in patients with human immunodeficiency virus infection. *J. Infect. Dis.* **171**, 537-545 (1995).
172. Cheeseman, S.H. et al. Phase I/II evaluation of nevirapine alone and in combination with zidovudine for infection with human immunodeficiency virus. *J. Acquir. Immune Defic. Syndr. Hum. Retrovirol.* **8**, 141-151 (1995).
173. de Jong, M.D. et al. Alternating nevirapine and zidovudine treatment of human immunodeficiency virus type 1-infected persons does not prolong nevirapine activity. *J. Infect. Dis.* **169**, 1346-1350 (1994).
174. McClung, R.P. et al. Transmitted Drug Resistance Among Human Immunodeficiency Virus (HIV)-1 Diagnoses in the United States, 2014-2018. *Clin. Infect. Dis.* **74**, 1055-1062 (2022).
175. Joly, V. et al. Evolution of human immunodeficiency virus type 1 (HIV-1) resistance mutations in nonnucleoside reverse transcriptase inhibitors (NNRTIs) in HIV-1-infected patients switched to antiretroviral therapy without NNRTIs. *Antimicrob. Agents Chemother.* **48**, 172-175 (2004).
176. Little, S.J. et al. Persistence of transmitted drug resistance among subjects with primary human immunodeficiency virus infection. *J. Virol.* **82**, 5510-5518 (2008).
177. Das, K. et al. Roles of conformational and positional adaptability in structure-based design of TMC125-R165335 (etravirine) and related non-nucleoside reverse transcriptase inhibitors that are highly potent and effective against wild-type and drug-resistant HIV-1 variants. *J. Med. Chem.* **47**, 2550-2560 (2004).
178. Das, K. et al. High-resolution structures of HIV-1 reverse transcriptase/TMC278 complexes: strategic flexibility explains potency against resistance mutations. *Proc. Natl. Acad. Sci. USA* **105**, 1466-1471 (2008).
179. Ludovici, D.W. et al. Evolution of anti-HIV drug candidates. Part 3: Diarylpyrimidine (DAPY) analogues. *Bioorg. Med. Chem. Lett.* **11**, 2235-2239 (2001).

180. Saag, M.S. et al. Antiretroviral Drugs for Treatment and Prevention of HIV Infection in Adults: 2018 Recommendations of the International Antiviral Society-USA Panel. *JAMA* **320**, 379-396 (2018).
181. Tachedjian, G., Aronson, H.E., & Goff, S.P. Analysis of mutations and suppressors affecting interactions between the subunits of the HIV type 1 reverse transcriptase. *Proc. Natl. Acad. Sci. USA* **97**, 6334-6339 (2000).
182. Tachedjian, G. et al. Role of residues in the tryptophan repeat motif for HIV-1 reverse transcriptase dimerization. *J. Mol. Biol.* **326**, 381-396 (2003).
183. Ghosh, M. et al. Alterations to the primer grip of p66 HIV-1 reverse transcriptase and their consequences for template-primer utilization. *Biochemistry* **35**, 8553-8562 (1996).
184. Jochmans, D. et al. Selective killing of human immunodeficiency virus infected cells by non-nucleoside reverse transcriptase inhibitor-induced activation of HIV protease. *Retrovirology* **7**, 89 (2010).
185. Zerbato, J.M Tachedjian, G. & Sluis-Cremer, N. Nonnucleoside Reverse Transcriptase Inhibitors Reduce HIV-1 Production from Latently Infected Resting CD4. *Antimicrob. Agents Chemother.* **61**, (2017).
186. Clark, K. et al. CARD8 Inflammasome Sensitization through Chemical Inhibition of DPP9 Promotes Clearance of HIV-1-infected Cells. *Nat. Chem. Biol.* **19**(4), 431-439 (2023).
187. Almond, L.M. et al. Intracellular and plasma pharmacokinetics of efavirenz in HIV-infected individuals. *J. Antimicrob. Chemother.* **56**, 738-744 (2005).
188. Castro-Gonzalez, S., Colomer-Lluch, M. & Serra-Moreno, R. Barriers for HIV Cure: The Latent Reservoir. *AIDS Res. Hum. Retroviruses* **34**, 739-759 (2018).
189. Lennox, J.L. et al. Raltegravir versus Efavirenz regimens in treatment-naive HIV-1-infected patients: 96-week efficacy, durability, subgroup, safety, and metabolic analyses. *J Acquir Immune Defic. Syndr.* **55**, 39-48 (2010).
190. Zolopa, A. et al. A randomized double-blind comparison of coformulated elvitegravir/cobicistat/emtricitabine/tenofovir disoproxil fumarate versus efavirenz/emtricitabine/tenofovir disoproxil fumarate for initial treatment of HIV-1 infection: analysis of week 96 results. *J. Acquir. Immune Defic. Syndr.* **63**, 96-100 (2013).
191. Stellbrink, H.J. et al. Dolutegravir in antiretroviral-naive adults with HIV-1: 96-week results from a randomized dose-ranging study. *AIDS* **27**, 1771-1778 (2013).
192. Walmsley, S.L. et al. Dolutegravir plus abacavir-lamivudine for the treatment of HIV-1 infection. *N. Engl. J. Med.* **369**, 1807-1818 (2013).
193. Llibre, J.M. et al. Efficacy, safety, and tolerability of dolutegravir-rilpivirine for the maintenance of virological suppression in adults with HIV-1: phase 3, randomised, non-inferiority SWORD-1 and SWORD-2 studies. *Lancet* **391**, 839-849 (2018).
194. Swindells, S. et al. Long-Acting Cabotegravir and Rilpivirine for Maintenance of HIV-1 Suppression. *N. Engl. J. Med.* **382**, 1112-1123 (2020).
195. Orkin, C. et al. Long-Acting Cabotegravir and Rilpivirine after Oral Induction for HIV-1 Infection. *N. Engl. J. Med.* **382**, 1124-1135 (2020).
196. Mills, A. et al. Long-acting cabotegravir and rilpivirine for HIV-1 suppression: switch to 2-monthly dosing after 5 years of daily oral therapy. *AIDS* **36**, 195-203 (2022).
197. El Bouzidi, K. et al. First-line HIV treatment outcomes following the introduction of integrase inhibitors in UK guidelines. *AIDS* **34**, 1823-1831 (2020).

198. Sharp, P.M. & Hahn, B.H. Origins of HIV and the AIDS pandemic. *Cold Spring Harb. Perspect. Med.* **1**: a006841 (2011).
199. Chahroudi, A. et al. Natural SIV hosts: showing AIDS the door. *Science* **335** 1188–93 (2012).
200. Apetrei, C., Robertson, D.L., & Marx, P.A. The history of SIVS and AIDS: epidemiology, phylogeny and biology of isolates from naturally SIV infected non-human primates (NHP) in Africa. *Front Biosci.* **9**, 225–54 (2004).
201. Bibollet-Ruche, F. et al. New simian immunodeficiency virus infecting de brazza's monkeys (Cercopithecus neglectus): evidence for a cercopithecus monkey virus clade. *J. Virol.* **78**, 7748–62 (2004).
202. Jin, M.J. et al. Infection of a yellow baboon with simian immunodeficiency virus from African green monkeys: Evidence for cross-species transmission in the wild. *J. Virol.* 68, 8454–8460 (1994).
203. Bibollet-Ruche, F. et al. Simian immunodeficiency virus infection in a patas monkey (*Erythrocebus patas*): Evidence for cross-species transmission from African green monkeys (*Cercopithecus aethiops sabaeus*) in the wild. *J. Gen. Virol.* **77**, 773–781 (1996).
204. Fabre, P.H., Rodrigues, A., & Douzery, E.J. Patterns of macroevolution among primates inferred from a supermatrix of mitochondrial and nuclear DNA. *Mol. Phylogenet. Evol.* **53**, 808–825 (2009).
205. Ylinen, L.M. et al. Conformational adaptation of Asian macaque TRIMCyp directs lineage specific antiviral activity. *PLoS Pathog.* **6**, e1001062 (2010).
206. Worobey, M. et al. Island biogeography reveals the deep history of SIV. *Science* **329**, 1487 (2010).
207. Pecon-Slattery, J. et al. Evolution of Feline immunodeficiency virus in Felidae: Implications for human health and wildlife ecology. *Vet. Immunol Immunopathol.* **123**(1-2), 32-44 (2008).
208. Klatt, N.R., Silvestri, G., & Hirsch, V. Nonpathogenic Simian Immunodeficiency Virus Infection. *Cold Spring Harb. Perspect. Med.* a007153 (2012).
209. Huot, N. et al. Innate immune cell responses in non pathogenic versus pathogenic SIV infections. *Current Opinion in Virology* **19**, 37-44 (2016).
210. Sheehy, A.M. et al. Isolation of a human gene that inhibits HIV-1 infection and is suppressed by the viral Vif protein. *Nature* **418**, 646–650 (2002).
211. Stremlau, M. et al. The cytoplasmic body component TRIM5α restricts HIV-1 infection in Old World monkeys. *Nature* **427**, 848–853 (2004).
212. Neil, S.J., Zang, T., & Bieniasz, P.D. Tetherin inhibits retrovirus release and is antagonized by HIV-1 Vpu. *Nature* **451**, 425–430 (2008).
213. Courgnaud, V. et al. Identification of a new simian immunodeficiency virus lineage with a *vpu* gene present among different *Cercopithecus* monkeys (*C. mona, C. cephus,* and *C. nictitans*) from Cameroon. *J. Virol.* **77**, 12523–12534 (2003).
214. Sauter, D. et al. Tetherin-driven adaptation of Vpu and Nef function and the evolution of pandemic and nonpandemic HIV-1 strains. *Cell Host Microbe* **6**, 409–421 (2009).
215. Silvestri, G. Nonpathogenic SIV infection of sooty mangabeys is characterized by limited bystander immunopathology despite chronic high-level viremia. *Immunity* **18**, 441 (2003).

216. Goldstein, S. et al. Comparison of simian immunodeficiency virus SIVagmVer replication and CD4+ T-cell dynamics in vervet and sabaeus African green monkeys. *J. Virol.* **80**, 4868 (2006).
217. Pandrea, I. et al. Simian immunodeficiency viruses replication dynamics in African non-human primate hosts: common patterns and species-specific differences. *J. Med. Primatol.* **35**, 194 (2006).
218. Rey-Cuille, M.A. et al. Simian immunodeficiency virus replicates to high levels in sooty mangabeys without inducing disease. *J. Virol.* **72**, 3872 (1998).
219. Sharp, P.M., Shaw, G.M., & Hahn, B.H. Simian immunodeficiency virus infection of chimpanzees. *J. Virol.* **79**, 3891–3902 (2005).
220. Santiago, M.L. et al. Foci of endemic simian immunodeficiency virus infection in wild-living eastern chimpanzees (*Pan troglodytes schweinfurthii*). *J. Virol.* **77**, 7545–7562 (2003).
221. Keele, B.F. et al. Chimpanzee reservoirs of pandemic and nonpandemic HIV-1. *Science* **313**, 523–526 (2006).
222. Santiago, M.L. et al. SIVcpz in wild chimpanzees. *Science* **295**, 465 (2002).
223. Worobey, M. et al. Origin of AIDS: Contaminated polio vaccine theory refuted. *Nature* **428**, 820 (2004).
224. Van Heuverswyn, F. et al. Genetic diversity and phylogeographic clustering of SIVcpz*Ptt* in wild chimpanzees in Cameroon. *Virology* **368**, 155–171 (2007).
225. Li, Y. et al. Molecular epidemiology of simian immunodeficiency virus in eastern chimpanzees and gorillas. In 17th Conference on Retroviruses and Opportunistic Infections (2010).
226. Rudicell, R.S. et al. Impact of simian immunodeficiency virus infection on chimpanzee population dynamics. *PLoS Pathog.* **6**, e1001116 (2010).
227. Bailes, E. et al. Hybrid origin of SIV in chimpanzees. *Science* **300**, 1713 (2003).
228. Wetheim, J.O. & Worobey, M. Dating the Age of the SIV Lineages that gave rise to HIV-1 and HIV-2 *PLoS Comput. Biol.* **5**(5), e1000377 (2009).
229. Goodall, J. *The Chimpanzees of Gombe: Patterns of behavior*. *Belknap Press, Cambridge, UK* (1986).
230. Keele, B.F. et al. Increased mortality and AIDS-like immunopathology in wild chimpanzees infected with SIVcpz. *Nature* **460**, 515–519 (2009).
231. Van Heuverswyn, F. et al. Human immunodeficiency viruses: SIV infection in wild gorillas. *Nature* 444, 164 (2006).
232. Takehisa, J. et al. Origin and biology of simian immunodeficiency virus in wild-living western gorillas. *J. Virol.* **83**, 1635–1648 (2009).
233. Neel, C. et al. Molecular epidemiology of simian immunodeficiency virus infection in wild-living gorillas. *J. Virol.* **84**, 1464–1476 (2010).
234. Gao, F. et al. Origin of HIV-1 in the chimpanzee *Pan troglodytes troglodytes*. *Nature* **397**, 436–441 (1999).
235. Korber, B. et al. Timing the ancestor of the HIV-1 pandemic strains. *Science* **288**, 1789–1796 (2000).
236. Lemey, P. et al. The molecular population genetics of HIV-1 group O. *Genetics* **167**, 1059–1068 (2004).

237. Worobey ,M. et al. Direct evidence of extensive diversity of HIV-1 in Kinshasa by 1960. *Nature* **455**, 661–664 (2008).
238. De Leys, R. et al. Isolation and partial characterization of an unusual human immunodeficiency retrovirus from two persons of west-central African origin. *J. Virol.* **64**, 1207–1216 (1990).
239. Gurtler, L.G. et al. A new subtype of human immunodeficiency virus type 1 (MVP-5180) from Cameroon. *J. Virol.* **68**, 1581–1585 (1994).
240. Mauclere, P. et al. Serological and virological characterization of HIV-1 group O infection in Cameroon. *AIDS* **11**, 445–453 (1997).
241. Vallari, A. et al. Four new HIV-1 group N isolates from Cameroon: Prevalence continues to be low. *AIDS Res. Hum. Retroviruses* **26**, 109–115 (2010).
242. Plantier, J.C. et al. A new human immunodeficiency virus derived from gorillas. *Nature Med.* **15**, 871–872 (2009).
243. Vallari, A. et al. Confirmation of putative HIV-1 group P in Cameroon. *J. Virol.* **85**, 1403–1407 (2011).
244. Peeters, M. et al. Risk to human health from a plethora of simian immunodeficiency viruses in primate bushmeat. *Emerg. Infect. Dis.* **8**, 451–457 (2002).
245. Hirsch, V.M. et al. An African primate lentivirus (SIVsm) closely related to HIV-2. *Nature* **339**, 389–392 (1989).
246. Gao, F. et al. Human infection by genetically diverse SIVsm-related HIV-2 in west Africa. *Nature* **358**, 495–499 (1992).
247. Chen, Z. et al. Genetic characterization of new West African simian immunodeficiency virus SIVsm: Geographic clustering of household-derived SIV strains with human immunodeficiency virus type 2 subtypes and genetically diverse viruses from a single feral sooty mangabey troop. *J. Virol.* **70**, 3617–3627 (1996).
248. van der Loeff, M.F. et al. Sixteen years of HIV surveillance in a West African research clinic reveals divergent epidemic trends of HIV-1 and HIV-2. *Int. J. Epidemiol.* **35**, 1322–1328 (2006)
249. Hamel, D.J. et al. Twenty years of prospective molecular epidemiology in Senegal: Changes in HIV diversity. *AIDS Res. Hum. Retroviruses* **23**, 1189–1196 (2007).
250. Popper, S.J. et al. Low plasma human immunodeficiency virus type 2 viral load is independent of proviral load: Low virus production in vivo. *J. Virol.* **74**, 1554–1557 (2000).
251. Berry, N. et al. Low level viremia and high CD4% predict normal survival in a cohort of HIV type-2-infected villagers. *AIDS Res. Hum. Retroviruses* **18**, 1167–1173 (2002).
252. Apetrei, C. et al. Molecular epidemiology of simian immunodeficiency virus SIVsm in U.S. primate centers unravels the origin of SIVmac and SIVstm. *J. Virol.* **79**, 8991–9005 (2005).
253. Apetrei, C. et al. Kuru experiments triggered the emergence of pathogenic SIVmac. *AIDS* **20**, 317–321 (2006).
254. Murphey-Corb, M. et al. Isolation of an HTLV-III-related retrovirus from macaques with simian AIDS and its possible origin in asymptomatic mangabeys. *Nature* **321**, 435–437 (1986).
255. Johnson, P.R. & Hirsch, V.M. SIV infection of macaques as a model for AIDS pathogenesis. *Int. Rev. Immunol.* **8**, 55–63 (1992).

256. Haigwood, N.L. Update on animal models for HIV research. *Eur. J. Immunol.* **39**, 1994–1999 (2009).
257. Schnittman, S.M. et al. Increasing viral burden in CD4+ T cells from patients with human immunodeficiency virus (HIV) infection reflects rapidly progressive immunosuppression and clinical disease. *Ann. Intern. Med.* **113**, 438-443 (1990).
258. Brinchmann, J.E., Albert, J., & Vartdal, F. Few infected CD4+ T cells but a high proportion of replication-competent provirus copies in asymptomatic human immunodeficiency virus type 1 infection. *J. Virol.* **65**, 2019-2023 (1991).
259. Hsia, K., & Spector, S.A. Human immunodeficiency virus DNA is present in a high percentage of CD4+ lymphocytes of seropositive individuals. *J. Infect. Dis.* **164**, 470-475 (1991).
260. Psallidopoulos, M.C. et al. Integrated proviral human immunodeficiency virus type 1 is present in CD4+ peripheral blood lymphocytes in healthy seropositive individuals. *J. Virol.* **63**, 4626-4631 (1989).
261. Simmonds, P. et al. Human immunodeficiency virus-infected individuals contain provirus in small numbers of peripheral mononuclear cells and at low copy numbers. *J. Virol.* **64**, 864-872 (1990).
262. Finkel, T.H. et al. Apoptosis occurs predominantly in bystander cells and not in productively infected cells of HIV- and SIV-infected lymph nodes. *Nat. Med.* **1**, 129-134 (1995).
263. Brenchley, J.M. et al. CD4+ T cell depletion during all stages of HIV disease occurs predominantly in the gastrointestinal tract. *J. Exp.Med.* **200**, 749-759 (2004).
264. Grivel, J.C. et al. Human immunodeficiency virus type 1 coreceptor preferences determine target T-cell depletion and cellular tropism in human lymphoid tissue. *J. Virol.* **74**, 5347-5351 (2000).
265. Dunham, R. et al. The AIDS resistance of naturally SIV-infected sooty mangabeys is independent of cellular immunity to the virus. *Blood* **1**, 108-209(2006).
266. Wang, Z. et al. Th-1-type cytotoxic CD8+ T-lymphocyte responses to simian immunodeficiency virus (SIV) are a consistent feature of natural SIV infection in sooty mangabeys. *J. Virol.* **80**, 2771 (2006).
267. Li, B. et al. Nonpathogenic simian immunodeficiency virus infection of sooty mangabeys is not associated with high levels of autologous neutralizing antibodies. *J. Virol.* **84**, 6248 (2010).
268. Gordon, S.N. et al. Short-lived infected cells support virus replication in sooty mangabeys naturally infected with simian immunodeficiency virus: implications for AIDS pathogenesis. *J. Virol.* **82**, 3725 (2008).
269. Pandrea, I. et al. Simian immunodeficiency virus SIVagm dynamics in African green monkeys. *J. Virol.* **82**, 3713 (2008).
270. VandeWoude, S. & Apetrei, C. Going wild: lessons from naturally occurring Tlymphotropic lentiviruses. *Clinical Microbiology Reviews.* **19**, 728 (2006).
271. Zeng, M. et al. Cumulative mechanisms of lymphoid tissue fibrosis and T cell depletion in HIV-1 and SIV infections. *J. Clin. Invest.* **121**, 998 (2011).
272. Riddick, N.E. et al. A novel CCR5 mutation common in sooty mangabeys reveals SIVsmm infection of CCR5-null natural hosts and efficient alternative coreceptor use in vivo. *PLoS Pathog.* **6**, e1001064 (2010).

273. Sedaghat, A.R. et al. Chronic CD4+ T-cell activation and depletion in human immunodeficiency virus type 1 infection: Type I interferon-mediated disruption of T-cell dynamics. *J. Virol.* **82**, 1870 (2008).
274. Hyrcza, M.D. et al. Distinct transcriptional profiles in ex vivo CD4+ and CD8+ T cells are established early in human immunodeficiency virus type 1 infection and are characterized by a chronic interferon response as well as extensive transcriptional changes in CD8+ T cells. *J. Virol.* **81**, 3477 (2007).
275. Joas, S. et al. Species-specific host factors rather than virus-intrinsic virulence determine primate lentiviral pathogenicity. *Nat. Commun.* **9**, 1371 (2018).
276. Klatt, N.R., Funderburg, N.T., & Brenchley, J.M. Microbial translocation, immune activation, and HIV disease. *Trends in Microbiology* **21**(1), 6–13 (2013).
277. Brenchley, J.M. et al. Microbial translocation is a cause of systemic immune activation in chronic HIV infection. *Nat. Med.* **12**, 1365 (2006).
278. Brenchley, J.M. et al. Differential Th17 CD4 T-cell depletion in pathogenic and nonpathogenic lentiviral infections. *Blood* **1**(112), 2826 (2008).
279. Favre, D. et al. Critical loss of the balance between Th17 and T regulatory cell populations in pathogenic SIV infection. *PLoS Pathog.* **5**, e1000295 (2009).
280. Estes, J.D. et al. Damaged intestinal epithelial integrity linked to microbial translocation in pathogenic simian immunodeficiency virus infections. *PLoS Pathog.* **6**, e1001052 (2010).
281. Dinh, D.M. et al. Intestinal Microbiota, Microbial Translocation, and Systemic Inflammation in Chronic HIV Infection. *Journal of Infectious Diseases* **211**(1), 19–27 (2014).
282. Pandrea, I. et al. Cutting edge: Experimentally induced immune activation in natural hosts of simian immunodeficiency virus induces significant increases in viral replication and CD4+ T cell depletion. *J. Immunol.* **181**, 6687 (2008).
283. Paiardini, M. et al. Low levels of SIV infection in sooty mangabey central memory CD T cells are associated with limited CCR5 expression. *Nat. Med.* **17**, 830 (2011).
284. Pandrea, I. et al. Paucity of CD4+CCR5+ T cells is a typical feature of natural SIV hosts. *Blood* **109**, 1069 (2007).
285. Beaumier, C.M. et al. CD4 downregulation by memory CD4+ T cells in vivo renders African green monkeys resistant to progressive SIVagm infection. *Nat. Med.* **15**, 879 (2009).
286. Okoye, A. et al. Progressive CD4+ central memory T cell decline results in CD4+ effector memory insufficiency and overt disease in chronic SIV infection. *J. Exp. Med.* **204**, 2171 (2007).
287. Letvin, N.L.et al. Preserved CD4+ central memory T cells and survival in vaccinated SIV-challenged monkeys. *Science* **312**, 1530 (2006).
288. Brenchley, J.M. et al. T-cell subsets that harbor human immunodeficiency virus (HIV) in vivo: Implications for HIV pathogenesis. *J. Virol.* **78**, 1160 (2004).
289. Meythaler, M. et al. Early induction of polyfunctional simian immunodeficiency virus (SIV)-specific T lymphocytes and rapid disappearance of SIV from lymph nodes of sooty mangabeys during primary infection. *J. Immunol.* **186**, 5151 (2011).
290. Heeney, J.L. AIDS: A disease of impaired Th-cell renewal? *Immunol. Today* **16**, 515 (1995).

291. Gougeon, M. & Montagnier, L. Apoptosis in AIDS. *Science* **260**, 1269–1270 (1993).
292 . Garg, H. & Blumenthal, R. Role of HIV Gp41 mediated fusion/hemifusion in bystander apoptosis. *Cell. Mol. Life Sci.* **65**, 3134–3144 (2008).
293. Garg, H. Host and Viral Factors in HIV-Mediated Bystander Apoptosis. *Viruses* **9**(8), 237 (2017).
294. Doitsh, G. et al. Cell death by pyroptosis drives CD4 T-cell depletion in HIV-1 infection. *Nature* **505**, 509–514 (2014).
295. Galloway, N.L. et al. Cell-to-cell transmission of HIV-1 is required to trigger pyroptotic death of lymphoid-tissue-derived CD4 T cells. *Cell Rep.* **12**, 1555–1563 (2015).
296. He, X. Rapid loss of cd4 T cells by pyroptosis during acute siv infection in rhesus macaques. *J. Virol.* 2022.
297. Bandera, A. et al. The NLRP3 inflammasome is upregulated in HIV-infected antiretroviraltherapy-treated individuals with defective immune recovery. *Frontiers in Immunology* **9**, 214 (2018).
298. Chivero, E.T. et al. HIV-1tatprimesandactivatesmicroglialNLRP3 inflammasome-mediatedneuroinflammation.*The Journal of Neuroscience* **37**, 3599–3609 (2017).
299. Zhou, Y. et al. Preferential cytolysis of peripheral memory CD4+ T cells by in vitro X4-tropic human immunodeficiency virus type 1 infection before the completion of reverse transcription. *J. Virol.* **82**, 9154-9163 (2008).

Chapter 2: Chemical inhibition of DPP9 sensitizes the CARD8 inflammasome in HIV-1-infected cells

This chapter has been reproduced and adapted from the following publication:

Clark KM, Kim JG, Wang Q, Gao H, Presti RM, Shan L. CARD8 Inflammasome Sensitization through Chemical Inhibition of DPP9 Promotes Clearance of HIV-1-infected Cells. *Nature Chemical Biology* (Oct. 2022). DOI: 10.1038/s41589-022-01182-5

2.1 Abstract

Non-nucleoside reverse transcriptase inhibitors (NNRTIs) induce pyroptosis of HIV-1 infected $CD4^+$ T cells through induction of intracellular HIV-1 protease activity, which activates the CARD8 inflammasome. Due to high concentrations of NNRTIs being required for efficient elimination of HIV-1-infected cells, it is important to elucidate ways to sensitize the CARD8 inflammasome to NNRTI-induced activation. We show that this sensitization can be achieved through chemical inhibition of the CARD8 negative regulator DPP9. The DPP9 inhibitor Val-boroPro (VbP) can kill HIV-1 infected cells without the presence of NNRTIs and act synergistically with NNRTIs to promote clearance of HIV-1-infected cells *in vitro*, and in humanized mice. More importantly, VbP is able to enhance clearance of residual HIV-1 in $CD4^+$ T cells isolated from people living with HIV (PLWH). We also show that VbP can partially overcome NNRTI resistance. This offers a promising strategy for enhancing NNRTI efficacy in elimination of HIV-1 reservoirs in PLWH.

2.2 Introduction

Despite the enhancement of antiretroviral therapy (ART) that allows people living with HIV (PLWH) to have an undetectable viral load, there have only been a few documented cases of complete remission from HIV infection[1,2]. This clearly indicates the need for novel therapeutics for HIV cure strategies. The primary hurdle in eradicating HIV-1 is the seeding of the latent reservoir which occurs quickly after infection[3] primarily in activated $CD4^+$ T cells that transition to resting memory cells[4] and possibly in tissue macrophages[5]. These cells can self-replenish and evade all immune responses due to HIV transcriptional inactivity[6]. However, in these latently infected cells, the integrated provirus is still able to reactivate upon stimulation and spread infection[6]. This poses a significant barrier to HIV-1 eradication as current antiretroviral therapies prevent viral replication but do not remove the latent reservoir. One of the main strategies to eliminate the HIV-1 reservoir is through the "shock and kill" approach. This strategy utilizes latency reversal agents (LRAs) to reactivate the latent reservoir (shock) and then induce targeted cell death of infected cells (kill)[7]. Optimal efficiency is needed for both steps of this strategy, but we recently reported that the inflammasome sensor caspase recruitment domain[8] (CARD8) senses intracellular HIV-1 protease activity and induces targeted cell killing of HIV-1 infected cells providing a potential kill strategy[8].

The inflammasome is a multi-protein complex that is assembled upon sensing of its cognate ligand. Caspase-1 (CASP1) is the key effector for the canonical inflammasome, and its active form can cleave gasdermin D leading to pyroptosis[9,10]. Recent studies demonstrated that CARD8 triggered CASP1 activation and pyroptosis in human $CD4^+$ T cells when treated with Val-boroPro (VbP), the inhibitor of the known CARD8 negative regulator Dipeptidyl Peptidase

9 (DPP9)[11,12]. Although VbP can also disrupt the NLRP1-DPP9 interaction[13], it does not lead to NLRP1 activation in macrophages and primary $CD4^+$ T cells[11,12]. Recently, we showed that CARD8 senses intracellular HIV-1 protease activity leading to pyroptosis of infected cells[8]. The CARD8 C-terminus (CARD8C) contains two key domains: the function-to-find domain (FIIND) and a CARD domain. Full-length CARD8 undergoes autoprocessing at the FIIND domain leaving two non-covalently associated subunits14. HIV-1 protease was found to cleave CARD8 on the N-terminal subunit which allows proteasomal degradation of the N-terminal fragment thereby freeing the C-terminal fragment. While recent work has shown that CARD8 activation and proteasomal degradation occurs through a ubiquitin independent pathway, more studies are needed to understand if HIV-1 activation of CARD8 also follows this ubiquitin independent pathway[15]. The C-terminal fragment, in high enough concentrations, can then activate CASP1 and induce pyroptosis. However, freed C-terminal fragments may also be sequestered by the CARD8 negative regulator DPP9 which can inhibit pyroptosis[16].

HIV-1 protease has limited intracellular activity before budding and must be activated by other methods to be properly sensed by the CARD8 inflammasome. Premature intracellular protease activity can either be achieved through overexpression of HIV-1 or through the usage of non-nucleoside reverse transcriptase inhibitors (NNRTIs)[17]. This strategy offers benefits over other immune-based kill strategies that often rely upon recognition of highly variable HIV-1 epitopes[18-20] as a result of HIV-1 protease being less tolerant to mutation[21]. This is due to the critical need of the virus to maintain its enzymatic activities. Several reports have shown that NNRTIs such as Efavirenz (EFV) and Rilpivirine (RPV) can induce HIV-1 protease-dependent killing of infected $CD4^+$ T cells[8, 22, 23] which is attributed to CARD8 inflammasome activation[8]. However, the efficacy of an NNRTI-based strategy to activate the CARD8 inflammasome for

HIV-1 reservoir clearance may be suboptimal because EFV and RPV at micromolar concentrations are required to drive CARD8 activation and cell death. Strategies for NNRTI-independent killing of HIV-1-infected cells or for enhancement of NNRTI potency are needed for efficient clearance of viral reservoirs *in vivo*. In this study, we aimed to identify the hurdles for clinical use of NNRTIs and how to overcome them by sensitizing the CARD8 inflammasome through inhibiting its negative regulator DPP9.

2.3 Results

2.3.1 NNRTIs induce dose-dependent death of HIV-1 infected cells

While NNRTI pharmacodynamics have been heavily studied for their ability to inhibit HIV-1 reverse transcription, they have yet to be studied in the context of their ability to activate the CARD8 inflammasome. To determine the *in vitro* pharmacodynamics of NNRTIs in $CD4^+$ T cells, an HIV-1 reporter virus pNL4-3-pol was used to infect primary blood $CD4^+$ T cells isolated from three independent healthy donors. Infected cells were treated with efavirenz (EFV), rilpivirine (RPV), etravirine (ETR), doravirine (DOR), or nevirapine (NVP) in serial three-fold dilutions to assess the EC_{50} of killing for each NNRTI. The measurement of killing of HIV-1-infected cells is described in **Figure S2.1a and b**. EFV, RPV, and ETR were able to induce robust cell killing at triple-digit nanomolar to low micromolar concentrations, whereas Doravirine and Nevirapine were ineffective at inducing cell death (**Figure 2.1a and 1b**). We also demonstrate a similar dose-dependent relationship in THP-1 cells, as macrophages are also key cellular targets for HIV-1, and were shown to have a functional CARD8 inflammasome[8,24] (**Figure 2.1c)**. This relationship is dependent on CARD8 inflammasome activation as no cell killing was observed in *CARD8*-KO or *CASP1*-KO THP-1 cells (**Figure 2.1d and e**). Killing of

HIV-1-infected cells was determined by the reduction of GFP^+ cells because we used GFP reporter viruses in which *egfp* was inserted into *env*. Percent killing plateaued at 75% to 80% based on GFP detection. Since CARD8-based killing is dependent upon Gag-Pol expression, we re-measured cell killing based on p24 detection and found that the clearance of $p24^+$ cells by EFV at 3.3 µM was around 90% and was close to 95% with more potent treatment (**Figure S2.1c and d**). It is possible that the reporter viruses had unusual transcriptional or splicing patterns that led to the discordance between GFP and Gag-Pol expression. Nonetheless, we chose the more convenient and reproducible GFP-based analysis, although it may underestimate overall killing.

The translatability of an NNRTI-based strategy for killing of HIV-1-infected cells is met with several barriers that can potentially reduce NNRTI efficacy *in vivo*. One key barrier to implementation is NNRTIs' high affinity for binding human serum proteins *in vivo*[25]. To assess this effect, we cultured $CD4^+$ T cells in the presence of 50% human serum and observed stark increases in the EC_{50} values for EFV, RPV, and ETR (**Figure S2.1e).** In the presence of human serum, the dose response curves for RPV and ETR are shifted out of clinical concentration recommendations whereas EFV is less affected by the presence of human serum as evidenced by a smaller log fold change in the EC_{50} (**Figure 2.1f-h**). These data suggest that EFV offers a distinct benefit over other NNRTIs for use in shock and kill strategies due to higher plasma concentration tolerance and greater bioavailability in the presence of human serum[26-27]. However, the efficacy of EFV is reduced with the presence of human serum which calls for the elucidation of strategies that could either increase intracellular NNRTI concentrations or sensitize the CARD8 inflammasome to NNRTI-based killing.

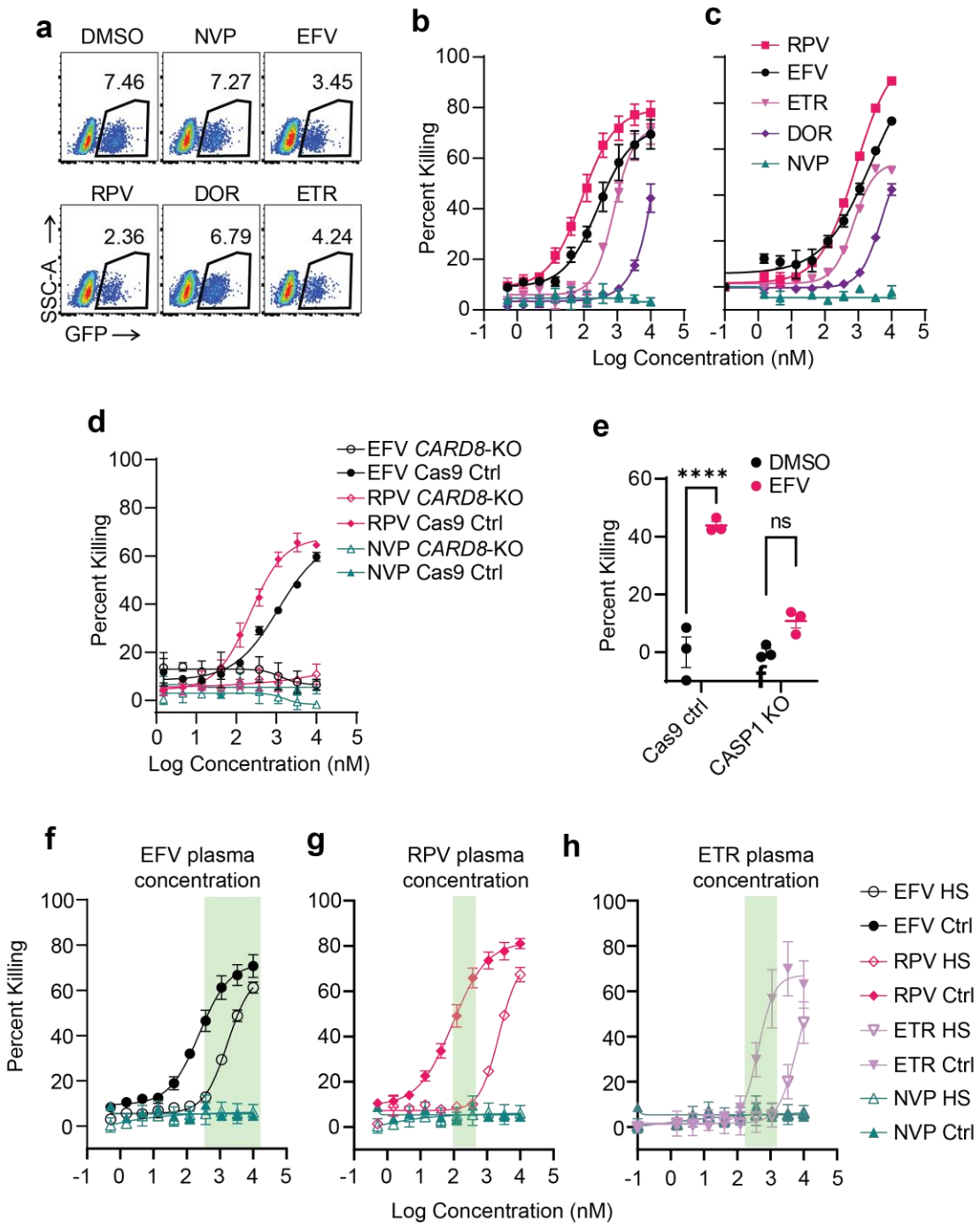

Figure 2.1: NNRTIs Induce Dose-Dependent Death of HIV-1-Infected Cells.

a, Representative flow cytometry plots of primary $CD4^+$ T cells treated with 1.11 μM of various NNRTIs. **b**, Cell-killing dose–response curves for NNRTIs in successive threefold dilutions in HIV-1-infected primary $CD4^+$ T cells. Three healthy donor $CD4^+$ T cells isolated from PBMCs

were included. EC_{50} values for EFV, RPV and ETR, are as follows: 266.1 nM, 87.8 nM and 786.6 nM, respectively. NVP and DOR did not provide sufficient killing for EC_{50} calculation. **c**, Cell-killing dose–response curves for HIV-1-infected THP-1 cells treated with NNRTIs, as in **b**. EC_{50} values for EFV, ETR and RPV are as follows: 787.4 nM, 657.3 nM and 443.1 nM. **d**, Cell-killing dose–response curves for HIV-1-infected *CARD8*-KO or *Cas9* control THP-1 cells. **e**, Killing of HIV-1-infected *CASP1*-KO THP-1 cells. ****$P < 0.0001$; NS, not significant. Two-way ANOVA with Sidak's multiple comparison test. **f**–**h**, Dose–response curves of EFV (**f**), RPV (**g**) and ETR (**h**) treatment with or without 50% human serum (HS). The green shaded area denotes the NNRTI plasma concentration range. EFV, 500–12,000 nM; RPV, 100–500 nM; ETR, 200–1,200 nM. Zero drug concentration values for dose–response curves were plotted at 0.1 nM to allow log-transformation. Data are presented as mean values and s.e.m. ($n = 3$).

2.3.2 DPP9 inhibition sensitizes the CARD8 inflammasome to HIV-1

DPP9 can bind to CARD8 first as a heterodimer with one copy of the full length CARD8 protein, then as a heterotrimer by catching a freed CARD8 C-terminal fragment (CARD8C)[16]. As the C-terminal fragment is responsible for inflammasome activation, DPP9's ability to catch CARD8C inhibits CARD8-induced pyroptosis. Overcoming DPP9 inhibition therefore should increase the rate of CARD8 inflammasome activation and sensitize the inflammasome to sensing HIV-1 protease activity. As expected, knock-down of DPP9 enhanced killing of HIV-1 infected cells by NNRTIs (**Figure S2.2a and b).** It was recently reported that VbP can bind to the DPP9-CARD8 heterodimer and prevent heterotrimer formation hence increasing intracellular CARD8C concentrations[16]. Additionally, VbP has another mechanism of action whereby it can induce N-terminal degradation of CARD8 which may activate the inflammasome, although the direct mechanism of action has yet to be elucidated[16, 28]. We therefore posited that VbP's ability to inhibit DPP9 may act synergistically with NNRTI-induced activation of HIV-1 protease by

lowering the threshold of protease activity needed to activate CARD8 in HIV-1 infected cells. Interestingly, VbP alone was able to clear up to 30% of HIV-1-infected cells (**Figure 2.2a**), suggesting that boosting CARD8 activity by DPP9 inhibition enabled it to sense the low levels of Gag-Pol dimerization and HIV-1 protease activity in naturally infected cells even without the presence of NNRTIs. We hypothesize that this may be due to low levels of spontaneous intracellular dimerization of Gag-Pol, sufficient to drive inflammasome activation upon sensitization by VbP. Next, we showed that NNRTI-induced killing of HIV-1 infected $CD4^+$ T cells was enhanced upon treatment with VbP or 1g244, another inhibitor with more specificity for DPP8/9 (**Figure 2.2b and S2.2c**) [29–30]. This enhancement of NNRTIs was shown to be dose-dependent. Upon addition of VbP, the EC_{50} had log fold change shifts up to -1.1 for both EFV and RPV (**Figure S2.2d)**. Due to VbP's ability to inhibit the capture of CARD8C by DPP9, we hypothesized that this relationship would be synergistic in nature. To further understand this complex relationship, we used SynergyFinder2.0 to identify whether this relationship was additive or synergistic[31]. As expected, combination treatment of VbP with EFV or RPV was found to be synergistic by Loewe's analysis[32] (**Figure S2.2e**).

HIV-1 protease-mediated activation of the CARD8 inflammasome is dependent upon both the levels of Gag-Pol expression and dimerization. We show that the cells that are not killed upon NNRTI treatment have a lower mean fluorescent intensity of GFP indicative of more efficient killing of cells with higher levels of HIV-1 expression (**Figure S2.3a and b**). The addition of VbP to NNRTI-based treatment is able to further reduce the MFI thereby lowering the level of Gag-Pol expression needed for NNRTI-mediated clearance. We also note that this reduction in GFP MFI is not due to drug treatment as no changes in MFI were observed in *CARD8-KO* THP-1 cells (**Figure S2.3b**). We also show that the frequency of HIV-1 DNA^+ cells,

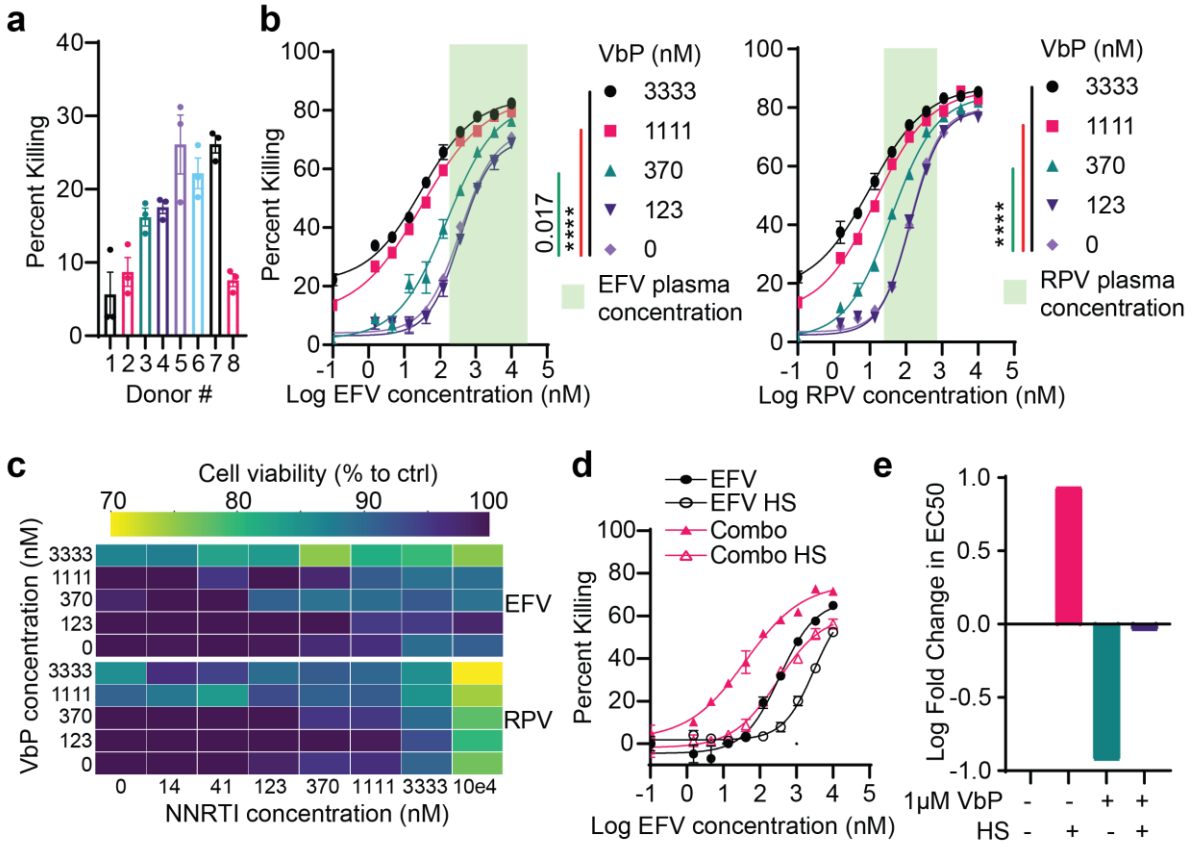

Figure 2.2: DPP9 Inhibition Sensitizes the CARD8 Inflammasome to HIV-1.

a, Killing of HIV-1-infected $CD4^+$ T cells by VbP (1 μM). $CD4^+$ T cells from eight healthy donors were infected with HIV-1 reporter viruses for three days before VbP treatment for two days. **b**, Dose–response curves for three donors of $CD4^+$ T cells treated with EFV or RPV in combination with VbP. The green shaded area denotes the NNRTI plasma concentration range. EFV, 500–12,000 nM; RPV, 100–500 nM. Extra sum-of-squares F-test. **c**, Drug toxicity. MTS assays were performed to determine the viability of primary $CD4^+$ T cells at the indicated drug concentrations. Results were from three donors of $CD4^+$ T cells. **d**, EFV dose–response curves for $CD4^+$ T cells cultured in the presence of human serum (HS) with or without 1 μM VbP. **e**, Respective log fold changes in the EC_{50} values from **d** in comparison to EFV alone. Zero drug concentration values for dose–response curves were plotted at 0.1 nM to allow log-transformation. In **a**, **b** and **d**, data are plotted as mean values and s.e.m. ($n = 3$). ****$P < 0.0001$.

as measured by qPCR is reduced in EFV- or combo-treated THP-1 cells as an additional measurement of cell death. This reduction in HIV-1 DNA is CARD8 inflammasome dependent as *CARD8-KO* THP-1 did not display the same phenotype (**Figure S2.3c**).

High concentrations of VbP (>2μM) can activate the CARD8 inflammasome in $CD4^+$ T cells and THP-1 cells[11, 12] but has no toxicity at concentrations up to 10μM in *CARD8*-KO cells (**Figure S2.4a and b)**. As shown in **Figure 2.2c**, the drug concentrations used in our study had no toxicity via MTS assay. Next, we show that this cell death is specific for HIV infected cells upon live dead staining of sorted GFP^+ and GFP^- $CD4^+$ T cells post infection and treatment of our combination strategy (**Figure S2.4c and d**). We also tested cytotoxicity of uninfected $CD4^+$ T cells across time with live dead staining and no cytotoxicity at the timepoints and concentrations used in this study (1-2 days) was observed (**Figure S2.4e and f**). We also showed that the addition of 1μM VbP overcomes the EC_{50} shift due to the presence of human serum for EFV (**Figure 2.2d and e**) – and partially for RPV (**Figure S2.5a)** – demonstrating that DPP9 inhibition is essential for efficient CARD8 inflammasome activation by NNRTIs at clinically relevant conditions.

2.3.3 VbP enhancement is CARD8 and HIV-1 protease dependent

To understand the dynamics of VbP enhancement of NNRTI-induced cell killing, we analyzed killing in $CD4^+$ T cells upon combination or single treatment across time. Upon treatment with EFV at a physiologically relevant concentration, the killing of HIV-1-infected cells became more rapid and robust with the presence of VbP (**Figure S2.5b**). It was previously shown that inhibition of the CARD8C capture by DPP9 was a rapid response, which we hypothesize is the main contributor to rapid enhancement of NNRTI induced cell killing14.

There is a second phase of cell killing between 6 and 24 hours before the maximal killing plateaus for both EFV and combination treatments. When looking at the cellular killing by combination treatment in comparison to EFV alone, the fold change enhancement remains relatively consistent indicating a rapid but uniform enhancement across time (**Figure S2.5c**). In the VbP monotreatment group, killing was not observed until 48 hours post treatment. This slow killing could either be due to the levels of CARD8C generated by inefficient and spontaneous Gag-Pol dimerization now being sufficient with DPP9 inhibition, or N-terminal degradation of CARD8 directly induced by VbP adding to the pool of HIV-1 PR-cleaved CARD8 fragments thereby inducing the inflammasome. This experiment was repeated for THP-1 cells and demonstrated similar results to $CD4^+$ T cells (**Figure S2.5d and e**). In $CD4^+$ T cells infected with NL4-3-Pol containing the protease inactivating mutant D25A, no killing was observed after treatment indicating that VbP-based killing is dependent upon HIV-1 protease (**Figure 2.3a**). Additionally, co-treatment with the protease inhibitor lopinavir (LPV) was also able to block VbP killing and enhancement in THP-1 cells (**Figure S2.6a**). Cleavage of CARD8 by HIV-1 protease was enhanced by EFV since it promotes dimerization of HIV-1 Gag-Pol to increase the viral protease activity. By contrast, VbP did not have a direct role in the cleavage at the CARD8 N-terminus because inhibition of HIV-1 protease by LPV completely blocked the generation of the neo-C-terminus (**Figure S2.6b**). These results were also confirmed in HIV-1 infected MT4 cells stably transduced with WT but not HIV-1 protease cleavage site mutant (F59A/F60A or FAFA) CARD8 (**Figure S2.6c**). This provides evidence of HIV cleavage of CARD8 in naturally infected cells and confirms that VbP is not directly increasing HIV-1 cleavage efficiency but rather acts downstream of HIV-1 cleavage.

To eliminate the possibility that VbP-based enhancement of NNRTIs is due to an unknown mechanism of cell death, we used *CARD8*-KO and *CASP1*-KO THP-1 cells and tested combination treatment in comparison to *Cas9* control cells. *CARD8*-KO conferred complete protection against cell killing by EFV or combination treatment (**Figure 2.3b**). This clearly shows that any additional killing by the incorporation of VbP to NNRTI treatment is dependent upon CARD8 for its mechanism of action. Next, we show that HIV-1 cleavage of CARD8 is necessary for VbP killing and enhancement. Repleting *CARD8*-KO THP-1 cells with cleavage site mutant FAFA CARD8 did not restore killing (**Figure 2.3c and S2.6d**). After HIV-1 cleavage, the N-terminal fragment of CARD8 undergoes proteasomal degradation. Enhancement and killing by VbP were also shown to be dependent upon proteasomal degradation (**Figure 2.3d**), a key process to generate the bioactive CARD8C. Caspase 8 has also been shown to be cleaved by HIV-1 protease33. Knocking out CASP8 did not diminish killing or enhancement after NNRTI and VbP treatment (**Figure S2.7**), suggesting that CASP8 was not involved NNRTI-mediated cell killing.

We next investigated whether combination treatment could enhance downstream activation of the CARD8 inflammasome components such as CASP1 and IL-1β. To test enhancement of CASP1 activation, we infected primary $CD4^+$ T cells and treated the cells concurrently with a dye that specifically stains the active form of CASP1. As seen in Figure 3e, addition of VbP to EFV resulted in increased CASP1 activation in HIV-1-infected $CD4^+$ T cells which was not observed in uninfected cells. VbP alone also showed significant CASP1 activation specifically in HIV-1-infected cells but not control cells, suggesting that VbP alone can induce HIV-1-dependent CARD8 inflammasome activation. Notably, VbP at 10 μM triggered CASP1 activation regardless of HIV-1 infection. This underscores that while higher concentrations of

VbP can activate the CARD8 inflammasome without HIV-1 and lead to general cytotoxicity, lower concentrations of VbP specifically kill HIV-1-infected cells and enhance NNRTI-mediated pyroptosis. We also tested IL-1β processing in HIV-1-infected THP-1 cells and found that VbP treatment alone led to release of IL-1β and it also enhanced IL-1β release in EFV-treated cells (Figure 3f). IL-1β release was blocked by LPV reiterating that VbP enhancement and killing is HIV-1 dependent.

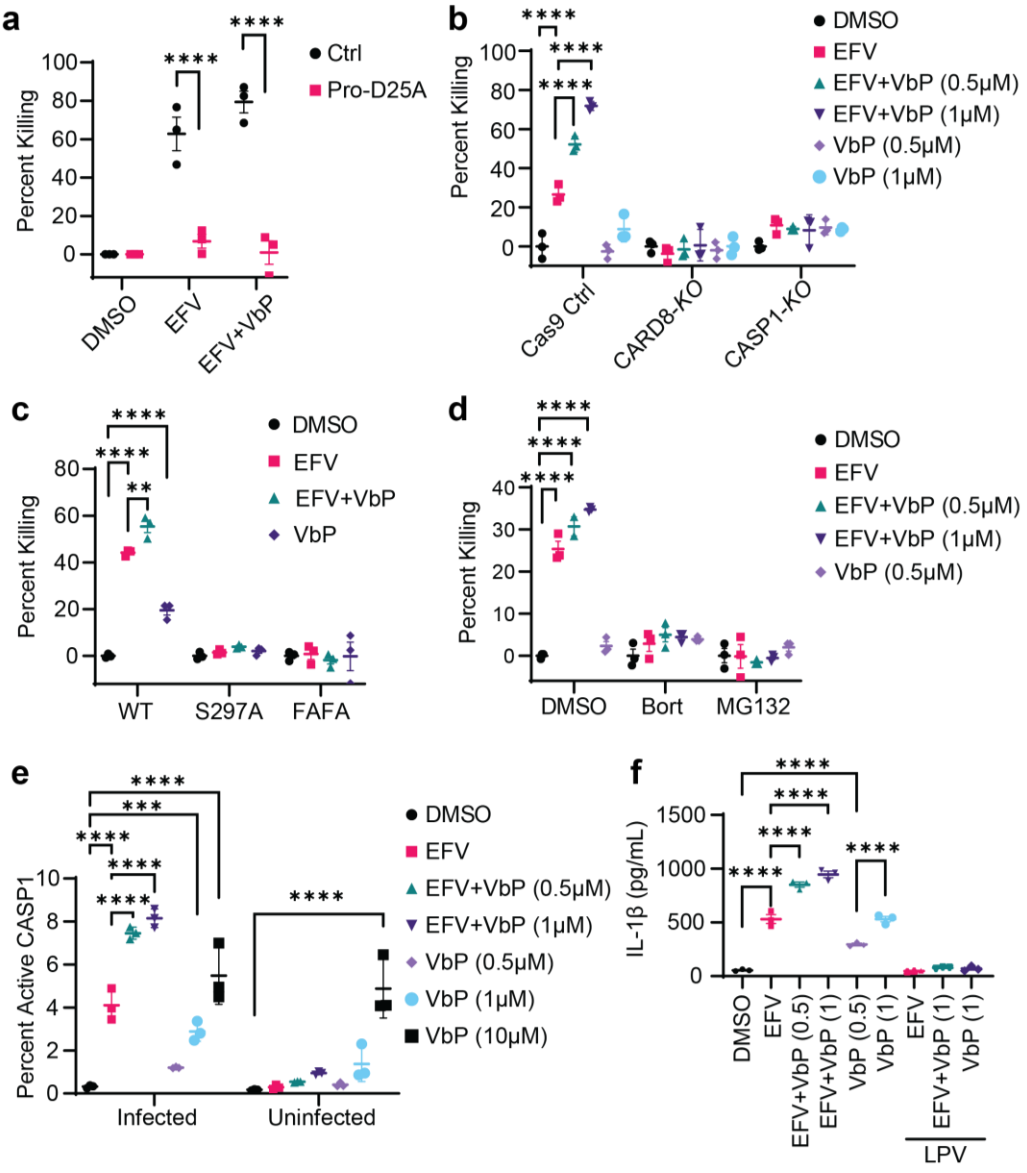

Figure 2.3: VbP Enhancement is CARD8- and HIV-1 Protease Dependent.

a, VbP enhancement and killing is HIV-1 protease-dependent. Primary $CD4^+$ T cells infected with NL4-3-Pol with or without the Pro-D25A mutation were treated with DMSO, EFV (3 μM) or combination (EFV (3 μM) + VbP (0.5 μM)). **b**, NNRTI-based killing and VbP enhancement is specific to the CARD8 inflammasome. *CARD8*-KO, *CASP1*-KO and *Cas9* control THP-1 cells were infected with HIV-1 before treatment for two days with DMSO, EFV (3 μM), VbP or combination. Cell killing was determined 48 h post drug treatment. **c**, VbP enhancement and killing is dependent on HIV-1 protease cleavage of CARD8. *CARD8*-KO cells replete with doxycycline-inducible constructs for WT CARD8, S297A or FAFA were infected and treated with doxycycline for one day before treatment with DMSO, EFV (3 μM), VbP (0.5 μM) or combination for one day. **d**, Proteasomal degradation is required for cell killing by NNRTIs and enhancement by VbP. Cells were treated with the proteasome inhibitors bortezomib (5 μM) or MG132 (10 μM), together with DMSO, EFV (3 μM), VbP or combination. Cell killing was determined 6 h post treatment. **e**, CASP1 activation by NNRTIs and VbP. One donor of primary $CD4^+$ T cells was infected and simultaneously treated with EFV (3 μM) ± VbP and stained with CASP1 staining dye for 6 h. **f**, IL-1β secretion. HIV-1-infected THP-1 cells were stimulated with lipopolysaccharide (LPS) (20 ng μl^{-1}) for 3 h before treatment with DMSO, EFV (3 μM), VbP or combination for 24 h. LPV (1 μM) was included in some groups to block HIV-1 protease activity. Two-way ANOVA with Sidak's multiple comparison test (**a**) or Tukey's multiple comparison test (**b**–**f**). Data are presented as mean values and s.e.m. ($n = 3$).$^{**}P < 0.01$, $^{****}P < 0.0001$.

2.3.4 CARD8 inflammasome sensitization overcomes NNRTI resistance

As HIV-1 has a high mutation rate, the circulating pool of HIV-1 strains shows distinct genetic variation across clades[34] which can lead to the rise of variants that confer resistance to NNRTIs. This poses a major concern for implementation of NNRTIs in a "shock and kill" approach as NNRTI resistance-associated mutations (RAMs) cause significant shifts in the EC_{50} values for blocking reverse transcriptase activity. Therefore, we examined if these RAMs also

conferred resistance to NNRTI-induced CARD8 inflammasome activation[35-38]. RAMs were introduced into our HIV-1 reporter virus (pNL4-3-pol) via site-directed mutagenesis. RAMs were chosen for key regions on HIV reverse transcriptase which can be seen in **Figure 2.4a**. These RAMs were treated with serial three-fold dilutions of EFV – with or without VbP – to determine the level of resistance to killing and VbP's ability to rescue killing efficacy**.**

As previously documented for blocking reverse transcriptase activity, NNRTI RAMs differ in the level of resistance that they confer. Strong NNRTI RAMs may confer complete resistance to NNRTI-mediated killing whereas others may simply show reduced efficacy (**Figure 2.4b**). This may help in the classification of viral strains that may respond to NNRTI treatment alone versus those that require VbP enhancement for their function. Indeed, we see two classes of NNRTI RAMs when comparing the fold change in EFV alone EC_{50} of mutant viruses in comparison to controls: those with reduced efficacy (E138G, Y181C, H221Y, F227L, and M230L) and those with near complete resistance (K103N and Y188L) (**Figure 2.4b and c**). All RAMs tested showed increased rates of killing upon combination treatment and most showed significant shifts in the EC_{50} of killing (**Figure 2.4d**). Since cell killing by VbP alone relies on low levels of naturally occurring intracellular Gag-Pol dimerization, it was not surprising that we observed around 20% killing of all RAMs treated with VbP alone, except Y181C (**Figure 2.4b and S2.8**). The increased killing of Y181C may be attributed to enhanced spontaneous intracellular Gag-Pol dimerization. This also highlights the promise of using DPP9 inhibitors for treating individuals with viruses containing NNRTI RAMs as it is NNRTI independent and unaffected by resistance.

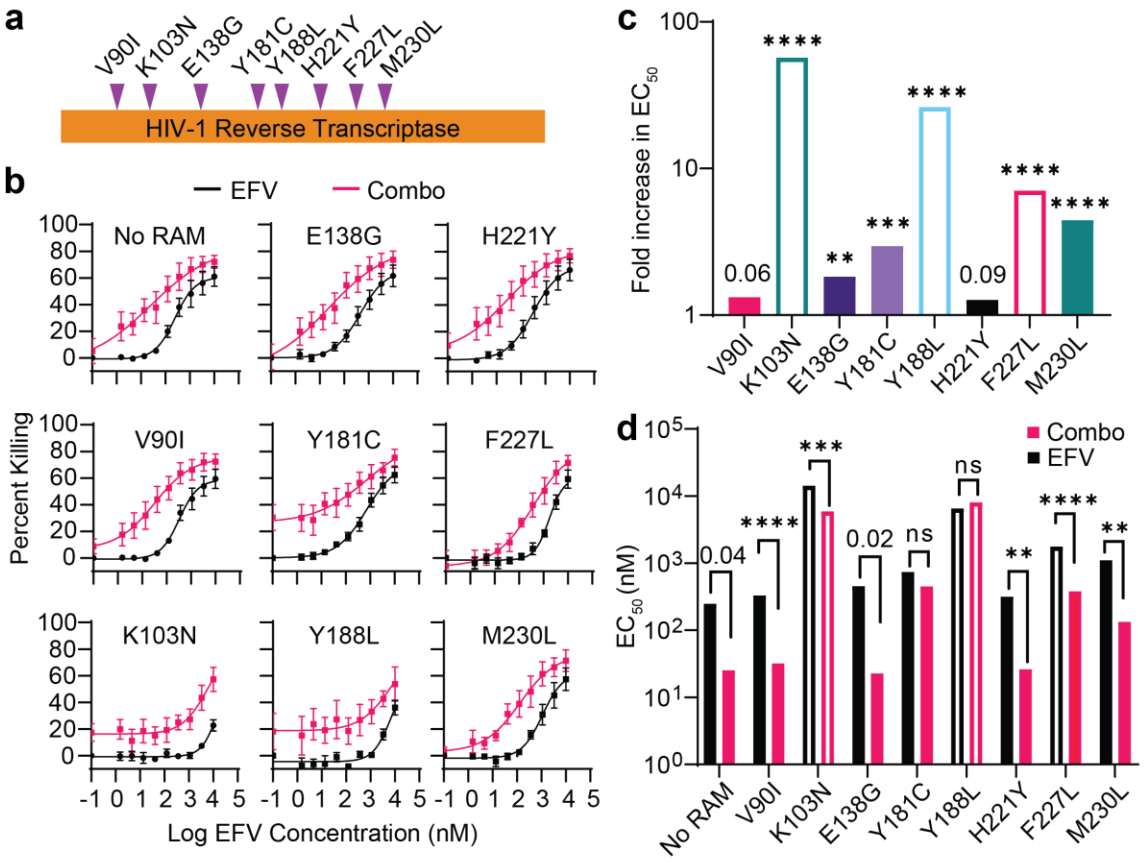

Figure 2.4: CARD8 Inflammasome Sensitization Overcomes NNRTI Resistance.

a, Graphical depiction of the location of NNRTI RAMS. **b**, Dose–response curves for the selected NNRTI RAMs in three donors of $CD4^+$ T cells treated with serial threefold EFV dilutions with (red) or without (black) the presence of 1 μM of VbP. Zero drug concentration values were plotted at 0.1 nM to allow log-transformation. Data are presented as mean values and s.e.m. ($n = 3$). **c**, Fold change in EC_{50} values of mutant viruses in comparison to non-mutant control. **d**, EC_{50} values are shown for all viruses with or without the presence of VbP. In **c** and **d**, open bars indicate EC_{50} values that were extrapolated due to inefficient killing by these mutants that led to a lack of an EC_{max} value. Significance was calculated using the extra sum-of-squares F-test. $*P < 0.05$, $**P < 0.01$, $***P < 0.001$, $****P < 0.0001$; NS, not significant.

2.3.5 VbP enhances clearance of HIV-1 infected cells in mice

Humanized mice were used to test the ability of NNRTIs to induce pyroptosis of HIV-1-infected $CD4^+$ T cells *in vivo*. The MISTRG-6-15 mouse was developed through knock-ins of human cytokine coding genes including *m-csf, il-3, gm-csf, sirp-α, thpo, il-6* and *il-15*[39-40]. Primary $CD4^+$ T cells infected with pNL4-3-pol were transfused into mice. IP injection of EFV alone at 20mg/kg (0.5mg per mouse) had modest but significant effects at killing HIV infected cells at 6 and 24 hours post treatment (**Figure 2.5a**). Since the dose we used here was comparable to the 600mg dose for patients, it clearly indicates the need for an enhancement strategy, such as with VbP, for NNRTI efficacy *in vivo*. Therefore, we repeated this experiment with groups treated either with 60µg VbP/mouse, 0.5mg EFV/mouse, or combination. VbP treatment alone showed comparable efficacy in killing HIV-1-infected cells as EFV alone which was greatly enhanced when the two treatments were combined as evidenced by reductions in infected cells in blood (**Figure 2.5b**). This phenotype held in lung tissue $CD4^+$ T cells (**Figure 2.5c and d**). This experiment was repeated in four independent mouse cohorts infused with $CD4^+$ T cells from different donors and the therapeutic effects of EFV, VbP, and combo were consistent across all cohorts (**Figure 2.5e**).

To test if this strategy could further clear HIV-1-infected cells *in vivo,* we tested a multi-dose regimen in comparison to a single combination dose. As can be seen in **Figure 2.5f**, there was a significant increase in killing efficiency in the blood of the multi-dose group in comparison to single dose with near significant improvement ($p=0.08$) in the lungs (**Figure 2.5g**). We tested our single combination strategy in four separate cohorts with similar results, indicating that this is a highly reproducible phenotype with significant enhancement in the presence of VbP. We also tested a separate cohort using IV injection and showed that there was

no significant difference between modes of injection at 6 or 24 hours (**Figure S2.9a-f**). Additionally, we note that there were no reductions in human $CD4^+$ T cell counts in comparison to control, indicating that there was no significant *in vivo* human $CD4^+$ T cell cytotoxicity due to treatment with EFV or VbP (**Figure S2.9g and h**). Taken together, these results prove the ability of this combination strategy to clear HIV-1-infected cells *in vivo* despite barriers such as low intracellular NNRTI concentrations. Since the cells in our animal studies carried transcriptionally active HIV-1, future studies using ART-treated humanized mice to test the "shock and kill" strategy by NNRTI and VbP will provide more insights on viral reservoir clearance.

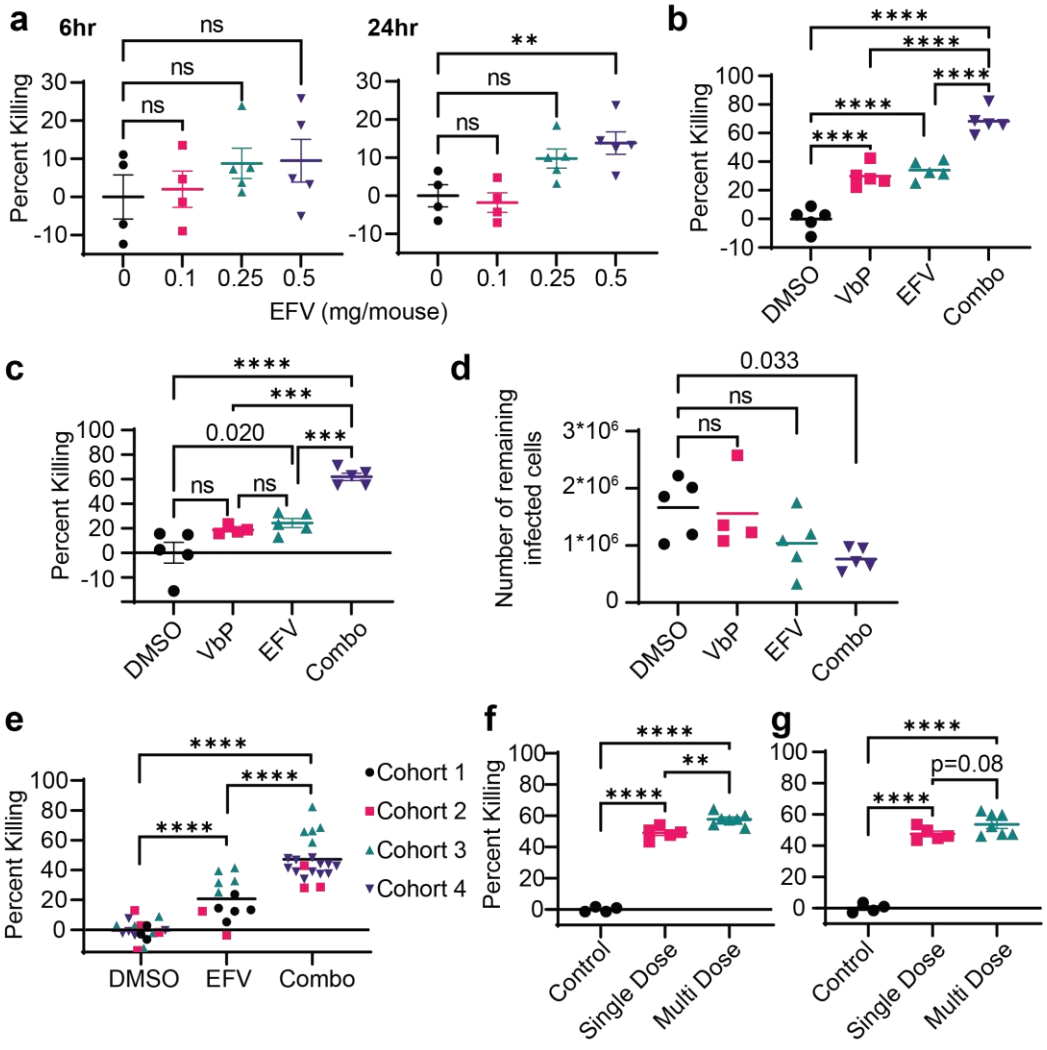

Figure 2.5: VbP Enhances Clearance of HIV-1-Infected Cells in Mice.

Primary $CD4^+$ T cells were infected with NL4-3-Pol. Three days post infection, these cells were transfused into mice (5–10 million cells per mouse). EFV and VbP were provided by i.p. and i.v. injection, respectively. **a**, Killing of HIV-1-infected human $CD4^+$ T cells from blood of transfused mice at 6 h and 24 h post treatment with EFV. Mice were either treated with DMSO ($n = 4$ mice) or varying doses of EFV (0.1 mg, $n = 4$; 0.25 mg, $n = 5$; 0.5 mg, $n = 5$). **b**–**d**, Killing of infected human $CD4^+$ T cells in blood (**b**) and lung tissues (**c**,**d**) at 24 h post treatment with DMSO, 0.5 mg EFV, 60 µg VbP or combination. Four or five mice were used per treatment condition. **e**, Cross-cohort comparison of blood from four independent cohorts of mice treated with DMSO, EFV or combination as described above. $CD4^+$ T cells from four separate donors were used. **f**,**g**, Killing of infected human $CD4^+$ T cells in blood (**f**) or lung (**g**) with DMSO control ($n = 4$) and single-dose ($n = 5$) or multi-dose ($n = 7$) combination treatment regimens. The multi-dose regimen group received 0.5-mg EFV injections on days 0, 1 and 2 and 60-µg VbP injections on days 0 and 2. The single-dose regimen received both EFV and VbP only on day 0. Data are presented as mean values with s.e.m. One-way ANOVA with Dunnett's multiple comparison test (**a**,**d**), Tukey's multiple comparison test (**b**,**c**,**e**,**f**) or Holm–Šídák's multiple comparisons test (**g**). $*P < 0.05$, $**P < 0.01$, $***P < 0.001$, $****P < 0.0001$; NS, not significant.

2.3.6 VbP enhances clearance of latent HIV-1

As our prior assays were performed with GFP-reporter viruses, we tested if VbP enhancement and killing was conserved in replication-competent viruses. We infected $CD4^+$ T cells with clinical strains for 4-6 days prior to treatment with EFV, VbP, or combination. T-20 and raltegravir were added to the media at the time of treatment to halt further rounds of infection, which had no effect on killing or cytotoxicity as previously described[8,41]. As expected, VbP was able to enhance EFV-mediated clearance of HIV infected cells and demonstrated significant killing alone (**Figure 2.6a-j**). Interestingly, VbP alone killing also varied widely by virus strain, indicating intrinsic differences in natural Gag-Pol dimerization. Many strains had a

significantly greater level of VbP based killing than our reporter viruses (~50% for LAI) which may be explained by multiple rounds of infection of the same cell leading to greater intrinsic Gag-Pol expression and dimerization. We also note that like our measurements with GFP, the remaining cells unaffected by NNRTI treatment demonstrated a lower p24 MFI reinforcing Gag-Pol expression and dimerization as the limiting factors for this strategy (**Figure S2.10a and b**). The MFI was further reduced upon VbP addition to EFV again demonstrating that DPP9 inhibition lowers the threshold of Gag-Pol expression required for NNRTI-mediated clearance. We also note that this phenotype is not specific to VbP and was reproduced with 1g244 (**Figure S2.10c**). To test whether this strategy could enhance clearance of latent HIV-1, we isolated $CD4^+$ T cells from PLWH under suppressive ART for measurement of viral reservoir size. To simulate a "shock and kill" strategy cells were co-stimulated with αCD3/CD28 antibodies ("shock") in the presence of T-20 and Raltegravir to prevent further spread during treatment. Cells were then treated with clinically relevant concentrations of NVP, EFV, or EFV and VbP for days 1-3 of stimulation ("kill"). The median infectious units per million cells were 7.55 (NVP), 3.747 (EFV), and 1.886 (combination) indicating a rapid clearance of 50.4% and 75.0% of latent HIV reservoirs from EFV and combination respectively (**Figure 2.6k**). As previously described, this two-day treatment may not catch residual viruses in the treatment groups that had delayed reactivation from latency.

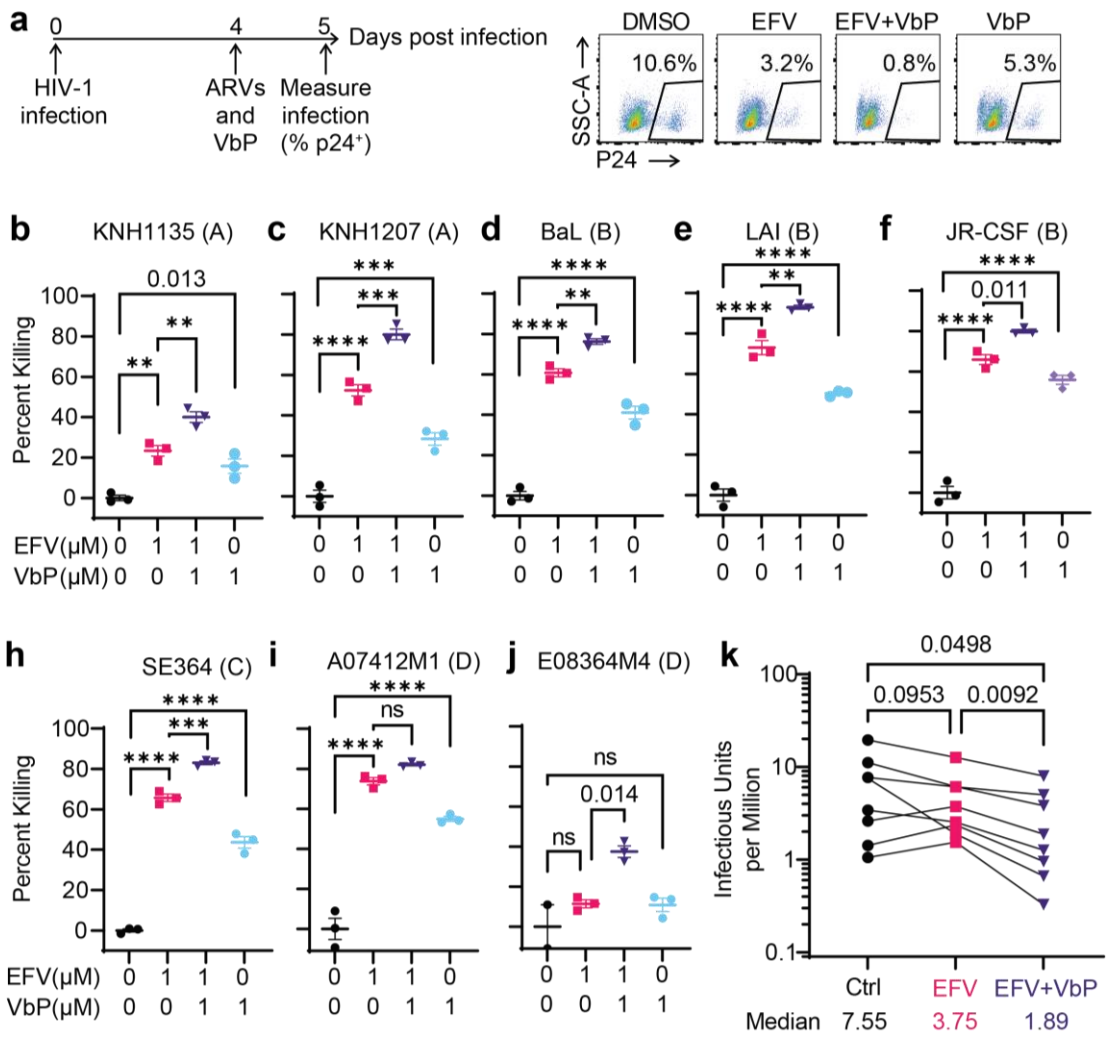

Figure 2.6: VbP Enhances Clearance of Latent HIV-1.

a, Scheme of the killing assays (left). Primary $CD4^+$ T cells were infected with clinical isolates for 4–6 days until a sufficient infection rate was obtained (p24 > 2%). Infected cells were then treated for one day with DMSO, EFV (1 μM), VbP (1 μM) or combo. Representative flow cytometry plots of $CD4^+$ T cells HIV-LAI-infected (right). **b**–**i**, Killing of primary $CD4^+$ T cells infected with various HIV-1 clinical isolates: KNH1135 (A) (**b**); KNH1207 (A) (**c**); BaL (B) (**d**); LAI (B) (**e**); JR-CSF (B) (**f**); SE364 (C) (**g**); A07412M1 (D) (**h**); E08364M4 (D) (**i**). Treatment is described in **a**. One-way ANOVA with Tukey's multiple comparison test. **j**, Clearance of latent HIV-1. The frequency of latent HIV-1 was determined by quantitative viral outgrowth assay. One-way ANOVA with Holm–Šídák's multiple comparisons test. Data in **b**–**i** presented as mean values with s.e.m. ($n = 3$). *$P < 0.05$, **$P < 0.01$, ***$P < 0.001$, ****$P < 0.0001$.

2.4 Discussion

Since NNRTIs offer a promising strategy for eradication of HIV-1 latent reservoirs, improving their *in vivo* cell killing potency is essential to treatment efficacy. This study proves that sensitization of the CARD8 inflammasome through DPP9 inhibition can reduce the threshold of CARD8 activation and provide more effective clearance of HIV infected cells for clinically relevant scenarios. We also show that DPP9 inhibition may reduce the level of Gag-Pol expression needed for CARD8 activation indicating that a lower level of latency reversal may be needed for "shock and kill", which is the key hurdle in implementing this strategy. Additionally, we show that DPP9 inhibition through chemical means such as with VbP can induce targeted cell killing even without NNRTIs, which varies across $CD4^+$ T cell donors and viral strains as demonstrated by NNRTI RAMs and clinical strains. We therefore posit that there may be varying levels of intrinsic Gag-Pol dimerization of these strains which can be sensed by CARD8 upon treatment with VbP, offering an NNRTI independent treatment possibility. This suggests that viral strains that confer near-complete resistance to NNRTIs may still be sensitive to targeted killing. Taken together, these data demonstrate that although NNRTI resistance may prove to be a significant barrier in implementation of NNRTIs for a shock and kill approach, they are not insurmountable when the CARD8 inflammasome is sensitized through DPP9 inhibition.

The major hurdle for implementation of VbP as a combination therapy is its cytotoxicity at high concentrations. This is likely in large part due to a lack of specificity for inhibiting the DPP9 and CARD8 interaction. With the advent of our previous work on CARD8 sensing of HIV-1 protease activity and this work on enhancement of sensing through DPP9 inhibition, there

is sufficient rationale for the development of new DPP9 inhibitors. As prior screens for DPP9 inhibitors had to rely upon CARD8 inflammasome activation, they had great potential for identifying compounds with greater toxicity and less specificity. Further work will be done to screen for chemical inhibitors that can specifically prevent CARD8C capture rather than binding to the enzyme active site on DPP9. This should sensitize the CARD8 inflammasome to biological activators like HIV-1 rather than directly induce non-specific N-terminal degradation and CARD8 activation. Through this there should be increased potency and specificity for enhancement of NNRTI-based strategies and potentially lead to NNRTI-independent treatment regimens that can sensitize the CARD8 inflammasome enough to be robustly activated by the lower level of intrinsic Gag-Pol expression and dimerization. Recent work has also shown that M24B aminopeptidase inhibitors were able to selectively activate the CARD8 inflammasome which is mediated through DPP9 providing another potential target for drug development and sensitization of the CARD8 inflammasome to HIV-1 protease sensing[42]. Additionally, while our study shows that VbP alone and the combination strategy can eliminate HIV-1-infected $CD4^+$ T cells in a transfusion model, further work will utilize an *in vivo* infection model to verify the ability to eliminate HIV reservoirs *in vivo*. While the exact mechanism of VbP induction of the CARD8 inflammasome and enhancement of HIV-1 sensing is still not fully understood, this work provides a promising new angle for a “shock and kill” strategy.

2.5 Materials and Methods

2.5.1 Human subjects

People living with HIV were recruited at the Infectious Diseases Clinic at Barnes-Jewish Hospital. Both males and females were included. All study participants were on ART and had undetectable plasma HIV-1 RNA (< 20 copies per ml) for at least six months. Study participants were provided with written informed consent. De-identified peripheral blood samples were acquired from the Mississippi Valley Regional Blood Center. This study was approved by the Washington University School of Medicine Internal Review Board (approval number: 201709175).

2.5.2 Plasmids

To generate plasmids for HIV-1 reporter viruses, mutations were introduced into the pNL4-3-GFP vector (AIDS Reagent Program #111100), which contains an enhanced green fluorescent protein (EGFP) inserted into *env*. pNL4-3-pol contained stop codon mutations or truncations in all genes except pol, tat, and rev8. Stop codon mutations were introduced into *vif* and *vpr* of the pNL4-3-GFP to generate pNL4-3-Δ*vif*-*vpr*. L40C-CRISPR.EFS.PAC (Addgene #89393) vector was used for sgRNA delivery via lentivirus. CRISPR/Cas9 guide RNAs were selected using the CCTop selection tool v1.1.0. pLKO.1puro (Addgene #8453) was used for gene knockdown via lentivirus vector. Doxycycline-inducible lentiviral construct pCW-hygro was generated by replacing the Cas9-puro to hygromycin gene from pCW-Cas9 (Addgene #50661). Site-directed mutagenesis to obtain NNRTI RAMs or protease D25A mutation was done using PCR primers on the NL4-3-Pol plasmid and were confirmed by sequencing; primers can be found in Supplementary Table 1.

2.5.3 Chemicals and antibodies

Antiretrovirals (ARVs) were obtained from the NIH AIDS Research and Reference Reagent Program: rilpivirine (RPV), efavirenz (EFV), etravirine (ETR), nevirapine (NVP), T-20, and raltegravir (RAL). Doravirine (DOR), Val-boroPro (VbP), along with additional EFV and RPV, were obtained from Selleck chem (#S6492, #S8455, #S4685, and # S7303). EFV for mouse studies (HY-10572) and 1g244 (HY-116304) were obtained from MedChemExpress. HIV-p24 staining was performed using the Cytofix/CytopermTM kit (BD #554714) using anti-HIV-1 p24-PE antibody (#6604667, 1:1000 dilution) purchased from Beckman Coulter. Proteasome inhibitors MG132 (#10012628) and Bortezomib (#10008822) were purchased from Cayman Chemical. The FLICA660 Caspase1 staining reagents were purchased from ImmunoChemistry Technologies (#9122). The following antibodies were used in this study: Anti-CD3 (Biolegend #300333, clone: HIT3a, 1mg/mL), anti-CD28 (Biolegend #302943, clone: CD28.2, 1mg/mL), anti-HIV p24PE (Beckman Coulter #6604667, Clone: KC57, 1:1000 dilution), anti-CD3PE (Biolegend #317308, clone: OKT3, 1:200 dilution), anti-CD3APC (Biolegend #317318, clone: OKT3, 1:100 dilution), anti-mouse CD45 APC (Biolegend #103112, clone: 30-f11, 1:200 dilution), anti-mouse CD45 PE (Biolegend #103106, clone: 30-f11, 1:200 dilution), anti-HIV p24 (NIH AIDS Reagent program #530, clone: 71-31, 1:1000 dilution), anti-beta-actin (Invitrogen #MA1-140, clone: 15G5A11/E2, 1:2000 dilution), HRP-conjugated goat anti-mouse IgG (Invitrogen #31439, clone: polyclonal, 1:10000 dilution), HRP-conjugated goat anti-rabbit IgG (Sigma Aldrich #12-348, clone: polyclonal, 1:10000 dilution), anti-Caspase-8 (Cell Signaling #9746S, clone: 1C12 , 1:500 dilution), anti-C-terminal CARD8 (Abcam #ab24186, clone: polyclonal, 1:500 dilution), anti-DPP9 (Abcam #ab42080, clone: polyclonal, 1:500 dilution), and anti-HA (Biolegend #901502, clone: HA.11, 1:500 dilution). Validation of

antibodies was performed by the manufacturer and were evaluated via the following methods: Western Blot (anti-HA, anti-DPP9, Caspase 8, anti-HIVp24, anti-beta-actin, goat-anti-mouse IgG, goat-anti-rabbit IgG, anti-C-terminal CARD8), flow cytometry (anti-HA, Anti-CD3, Anti-CD28, anti-HIVp24PE, anti-CD3PE, anti-CD3APC, anti-mouseCD45PE, anti-mouseCD45APC), immunocytochemistry (anti-HA, anti-DPP9, anti-beta-actin, goat-anti-mouse IgG, anti-C-terminal CARD8), immunoprecipitation (anti-HA, anti-Caspase 8, anti-beta-actin, goat-anti-mouse IgG), immunohistochemistry (anti-DPP9, anti-beta-actin, goat-anti-mouse IgG, goat-anti-rabbit IgG), and ELISA (anti-HIVp24, goat-anti-mouse IgG, goat-anti-rabbit IgG).

2.5.4 Cell culture

HEK293T (CRL-3216) and THP-1 cells (TIB-202) were ordered from ATCC and cultured in DMEM or RPMI 1640 medium respectively with 10% heat-inactivated fetal bovine serum (FBS), 1 U/mL penicillin, and 100 mg/mL streptomycin (Gibco). MT4 cells were obtained from the NIH AIDS reagent program (#120) and were cultured in RPMI 1640 medium with 10% FBS, 1U/Ml penicillin, and 100mg/mL streptomycin. $CD4^+$ T cells from blood were isolated from healthy donor peripheral blood mononuclear cells (PBMCs) using the BioLegend human $CD4^+$ T cell isolation kit (BioLegend #480010). Purified $CD4^+$ T cells were co-stimulated with plate-bound CD3 antibody (Biolegend #300333) with media containing soluble CD28 (Biolegend #302943) antibody and 20 ng/ml IL-2 (Biolegend #589106) for 3 days. Human serum containing media comprised 50% human serum obtained from Gemini Bio (#100-110) with 10% FBS, 1U/mL penicillin, 100mg/mL streptomycin, and 40% RPMI 1640 medium. For MTS assays the CellTiter 96® Aqueous One Solution Cell Proliferation Assay (MTS) from Promega was used (Promega #G3580). Uninfected $CD4^+$ T cells or THP-1 cells were treated with EFV,

RPV, VbP, or DMSO for two days prior to addition of MTS reagent, MTS reading was done following manufacturer's protocol. For live-dead staining, stimulated $CD4^+$ T cells were treated with DMSO, EFV, VBP, or combo along a time course with live-dead staining using the Zombie UV™ fixable viability kit (Biolegend #423107) according to the manufacturer's protocol.

2.5.5 Preparation of HIV-1 and lentiviruses

HIV-1 reporter viruses were packaged by co-transfecting HEK293T cells with viral vectors, packaging vector pC-Help (44), and pVSV-G (Addgene #8454). Lentiviruses carrying shRNA, CARD8 constructs, or Cas9 and sgRNA were also packaged in HEK293T cells by co-transfecting pVSV-G, psPAX2 (Addgene #12260) using Lipofectamine 2000 (Thermo Fisher Scientific # 11668019). Lenti-X Concentrator (TaKaRa #631232) was used to concentrate supernatant containing virus. For HIV-1 clinical isolates (AIDS reagent program #11412), CD8-depleted PHA-stimulated PBMCs were infected with isolate stocks and supernatant was collected and filtered 6-9 days post infection.

2.5.6 Generation of THP-1 cells with gene knockout or knockdown

The sgRNA and shRNA sequences can be found in Supplementary Table 2 and were verified by sequencing. THP-1 cells were transduced with sgRNA or shRNA lentiviruses via spin inoculation for 2 hours at 1200g at 25°C. Cells were then selected with puromycin or hygromycin (1 μg/ml) for 5-7 days or neomycin (200μg/mL) for two weeks prior to infection with HIV-1 reporter virus NL4-3-Δ*vif-vpr*. The controls for knockout cells were transduced with a Cas9-expressing lentiviral vector without sgRNA. Immunoblotting was performed to confirm knockout or knockdown efficiency.

2.5.7 Transfection and immunoblotting

For CARD8 cleavage of transfected HEK293T cells, 4x105 cells were seeded onto 12-well plates and cultured overnight. Cells were transfected with the CARD8 encoding plasmid (200ng) along with HIV-1 (1µg) using Lipofectamine 2000. Cells were treated for 24 hours prior to collection for western blotting.

1x106 HEK293T cells or MT4 cells for CARD8 cleavage or 5x106 THP-1 cells for knockdown verification were washed twice with PBS prior to resuspension in RIPA buffer (Cell Signaling Technology #9806) containing protease inhibitor cocktail (Thermo Scientific #78430). The BCA protein assay kit (Thermo Scientific #A53225) was used to determine protein concentration for equal loading on SDS-PAGE (Invitrogen #NW04125BOX) which was then immunoblotted and imaged using the ChemiDoc Imaging System (Bio-Rad).

2.5.8 HIV-1 infection, cell killing measurement, and dose response

HIV-1 p24 ELISA was used to verify viral stock concentration (XpressBio #XB-1000). HIV-1 reporter virus infection was performed at a multiplicity of infection (MOI) of 10. Infection was performed by spin inoculation (1,200g) for 2 hours at 25 °C. NNRTIs alone or in combination with VbP were added to HIV-1-infected cells 3-4 days post infection. The NL4-3-pol reporter virus or clinical HIV-1 isolates were used for all $CD4^+$ T cell experiments. The NL4-3-Δ*vif-vpr* virus was used for all THP-1 and MT4 experiments. For dose response curves NNRTI's were serially diluted 3-fold prior to addition to infected cells. Clinical HIV-1 isolate infection rate was determined by intracellular HIV-p24 staining with the Cytofix/Cytoperm^{TM} kit (BD #554714). Percent infection (GFP^+ or $p24^+$) was determined by flow cytometry (BD LSRFortessa, BD FACSCanto, BD LSRFortessa X-20, or BD accuri c6 plus). Purification of

HIV-1-infected cells (GFP^+) was performed using BD FACSAria II. For detection of IL-1β in the culture supernatant, THP-1 cells were LPS stimulated (50ng/mL) for three hours, washed twice with PBS, treated for 6-24 hours and culture supernatant was used for IL-1β ELISA (BioLegend #437004). Flow cytometry data were analyzed using Flowjo (v.10.8.1). Extrapolation of EC_{50} values for incomplete dose response curves was conducted in Prism 8 (GraphPad) using non-mutant EC_{max} values. Percent killing, log fold change in EC_{50}, and fold change of enhancement were calculated as follows:

$$Log\ Fold\ Change\ of\ Human\ Serum = log\left(\frac{EC_{50} Human\ Serum}{EC_{50} No\ Human\ Serum}\right) \quad (2.1)$$

$$Fold\ Change\ Enhancement = \left(\frac{Percent\ infection\ of\ EFV + VBP}{Percent\ infection\ of\ EFV}\right) \quad (2.2)$$

$$Fold\ Change\ in\ EC_{50}\ to\ No\ RAMS = \left(\frac{EC_{50} RAM}{EC_{50}\ No\ RAM}\right) \quad (2.3)$$

Dose response curve fits were performed in graphpad using inhibitor vs. response with variable slope (four parameters). Zero NNRTI concentrations were assigned the lowest concentration to allow log transformation but were not included in EC_{50} calculations. To assess differences in EC_{50} shifts due to the presence of VbP or NNRTI RAM's, the extra sum-of-squares F test was used with EFV only treatment or no mutation EC_{50} as the expected values for hypothesis testing. One- and two-way ANOVA tests relied upon assumptions of normality, homoscedasticity, and sample independence.

2.5.9 HIV DNA measurement

The frequency of HIV DNA^+ cells in HIV-infected *CARD8-KO* or *Cas9* control THP-1 cells was measured by qPCR. Cells were washed three times with PBS post infection to remove

any residual plasmid DNA. Three days later, cells were treated with DMSO, EFV, VbP or combination for two days. Total cellular DNA was extracted by the Quick-DNA Miniprep Kit (Zymo Research #D3025). Real-time PCR was performed using the Luna Universal Probe qPCR Master Mix (#M3004E). Quantity of HIV-1 viral DNA was measured using primers and probe specific to HIV-1 gag. The copies of host genome were determined using primers and probe specific to POLR2A (TaqMan assay #Hs05645071_s1). HIV-1 gag DNA was normalized to POLR2A levels to determine the frequency of HIV DNA^+ cells.

2.5.10 Humanized mice

The generation of knock-in mice encoding human *MCSF*, *GMCSF*, *IL3*, *SIRPA*, *THPO*, *IL6*, and *IL15* in a 129xBALB/c (N3) genetic background was performed using Velocigene technology by Regeneron Pharmaceuticals. Mice were bred to a $Rag2^{-/-}$ $IL2rg^{-/-}$ background with homozygous knockin to generate the MISTRG-6-15 mouse colony $MCSF^{h/h}$ $IL3^{h/h}$ $SIRPA^{h/h}$ $THPO^{h/h}$ $IL6^{h/h}$ $IL15^{h/h}$ $RAG^{-/-}$ $IL2rg^{null}$. All animal experiments were approved by the Institutional Animal Care and Use Committee of Washington University School of Medicine.

Transfusion experiments were conducted using primary $CD4^+$ T cells isolated from healthy donors as previously described that were infected with pNL4-3-pol prior to IV transfusion of 5-10 million cells per mouse. VbP was injected via IV injection and 60µg/mouse doses were diluted in DMSO. Figure 5a IP injections of EFV and Figure S9a and b were also diluted in DMSO prior to injection. All other cohorts received an IP injection of EFV diluted in vehicle (0% DMSO, 40% PEG300, 5% Tween-80, and 45% saline). Controls received the respective EFV diluent from the same cohort. Blood was collected at 6 and 24 hours (24 and 72 for multi-dose cohort) and lung tissues were collected at 24 hours post-treatment. $CD4^+$ T cells

were collected from lung tissues that were homogenized to achieve single cell suspension and analyzed via flow cytometry.

2.5.11 Quantitative Viral Outgrowth Assay (QVOA)

QVOA assay was modified from previously described methods[8,40]. Purified $CD4^+$ T cells from people living with HIV were plated on αCD3 coated plates in RPMI media containing αCD28, IL-2 (20ng/mL), T-20 (1μM) and RAL(1μM) at concentrations of $1x10^6$, $0.2x10^6$, and $0.08x10^6$ per well. One day post-stimulation cells were treated with NVP as a control (1μM), EFV (1μM), or EFV plus VbP (both 1μM). Cells were treated for an additional two days of stimulation before being washed four times with PBS to remove any residual drugs. Cells were then co-cultured with CD8-depleted PHA-stimulated PBMCs from HIV negative individuals. Two rounds of feeder cells were added on d3 and d10, and culture supernatants were collected between day 16 and 21 for HIV-1 p24 ELISA (XpressBio #XB-10000). The frequency of HIV-1 p24 positive wells was used to calculate the infectious units per million (IUPM) using IUPMStats v1.0 (https://silicianolab.johnshopkins.edu/)[43]. Samples with a control IUPM value less than one were excluded from analysis.

2.5.12 Statistical Analysis

All dose response measurements were performed in triplicate for THP-1 cells or using $CD4^+$ T cells from at least three separate healthy donors unless otherwise noted. Statistical analyses were performed using Prism 8 (GraphPad). The methods for statistical analysis were included in the figure legends. Error bars show mean values with SEM. The web application for SynergyFinder2.0 was used to calculate synergy and the output graphs were used. Heatmaps

were generated using Python (v.3.7.3) with the Seaborn (v.0.10.0) and Matplotlib (v.3.1.3) packages.

2.6 Contributions

Kolin Clark, Liang Shan, and Qiankun Wang designed the study. Liang Shan and Kolin Clark analyzed the data and wrote the manuscript. Josh Kim edited the manuscript, performed experiments using dox-inducible CARD8 constructs, and assisted in mouse and IUPM experiments. Qiankun Wang conducted DPP9 knockdown experiments, provided CARD8- and *Caspase 1*-KO cell lines, and generated dox-inducible CARD8 cell lines. Hongbo Gao conducted experiments of live/dead staining of GFP sorted THP-1 cells. Kolin Clark conducted all other experiments. Rachel Presti supervised the studies using clinical samples.

2.7 Acknowledgements

We thank the volunteers who participated in this study; L. Kessels, M. Klebert, A. Haile, T. Spitz, and T. Minor for study subject recruitment. We thank Regeneron Pharmaceuticals and the Richard Flavell laboratory at Yale University for generating the human cytokine knock-in mice. The following reagents were obtained through the AIDS Research and Reference Reagent Program, Division of AIDS, NIAID, NIH: rilpivirine, efavirenz, lopinavir, etravirine, nevirapine, maraviroc, T-20, tenofovir, raltegravir, pNL4-3-GFP, international HIV-1 isolates, and HIV-1 p24 antibodies. Funding: This work was supported by NIH grants R01AI162203 and R01AI155162 (LS), and by F31AI165251 (KC). The organizations that supplied these funds had no part in the planning or execution of the work presented in this study.

2.8 Supplementary Figures and Tables

Primer Name	Sequence (5'-3')
Fragment_1_F	GACATAGCAGGAACTACTAGTACCCTTCAGGAACAAATAGG
Fragment_2_R	AATACACTCCATGTACCGGTTCTTTTAGAATCTCCCTG
V90I_1_R	TAATTGAATTTCCCAGAAATCTTGAGTTCTCTT
V90I_2_F	TGGGAAATTCAATTAGGAATACCACATCCTGCA
K103N_1_R	GATTTGTTCTGTTTTAACCCTGCAGGATGTGG
K103N_2_F	AAAACAGAACAAATCAGTAACAGTACTGGATGTGG
E138G_1_R	CCCTGGTGTCCCATTGTTTATACTAGGTATGGT
E138G_2_F	CCTAGTATAAACAATGGGACACCAGGGATTAGA
Y181C_1_R	CATGTATTGACAGATGACTATGTCTGGATTTTGTTT
Y181C_2_F	ATAGTCATCTGTCAATACATGGATGATTTGTATGTA
Y188L_1_R	AGATCCTACAAGCAAATCATCCATGTATTGATAGAT
Y188L_2_F	GATGATTTGCTTGTAGGATCTGACTTAGAAATAGGG
H221Y_1_R	TTCTTTCTGATATTTTTTGTCTGGTGTGGTAAA
H221Y_2_F	ACACCAGACAAAAAATATCAGAAAGAACCTCCA
F227L_1_R	ATAACCCATCCAAAGGAGTGGAGGTTCTTTCTG
F227L_2_F	CCTCCACTCCTTTGGATGGGTTATGAACTCCAT
M230L_1_R	ATAACCCAGCCAAAGGAATGGAGGTTCTTTCTG
M230L_2_F	CCTCCATTCCTTTGGCTGGGTTATGAACTCCAT
Pr_D25A_1_R	ATCTGCTCCTGTAGCTAATAGAGCTTC
Pr_D25A_2_F	GAAGCTCTATTAGCTACAGGAGCAGAT

Supplementary Table 2.1: Primers for the generation of NL4-3-Pol Mutants

Table of the primers used to conduct site-directed mutagenesis of the NL4-3-Pol-GFP reporter virus.

sgRNA/shRNA	Sequence (5’-3’)
CARD8 sgRNA	TGAGGCCTTGCTGAGCATGG
CASP1 sgRNA1	TTTATCCGTTCCATGGGTGA
sgCASP8-1F	TCTAGATGTTATTCCAGAGACTCC
sgCASP8-1R	AAACGGAGTCTCTGGAATAACATC
sgCASP8-2F	TCTAGATGGGTTCTTGCTTCCTTTG
sgCASP8-2R	AAACCAAAGGAAGCAAGAACCCATC
shScramble	CCTAAGGTTAGTCGCCCTCG
DPP9 shRNA1	GCTGGTGAATAACTCCTTCAA
DPP9 shRNA2	GCTGCACTTTCTACAGGAATA

Supplementary Table 2.2: sgRNA and shRNA Sequences

Sequences of sgRNA guides used for knockout via CRISPR/Cas9 or shRNA for knockdown.

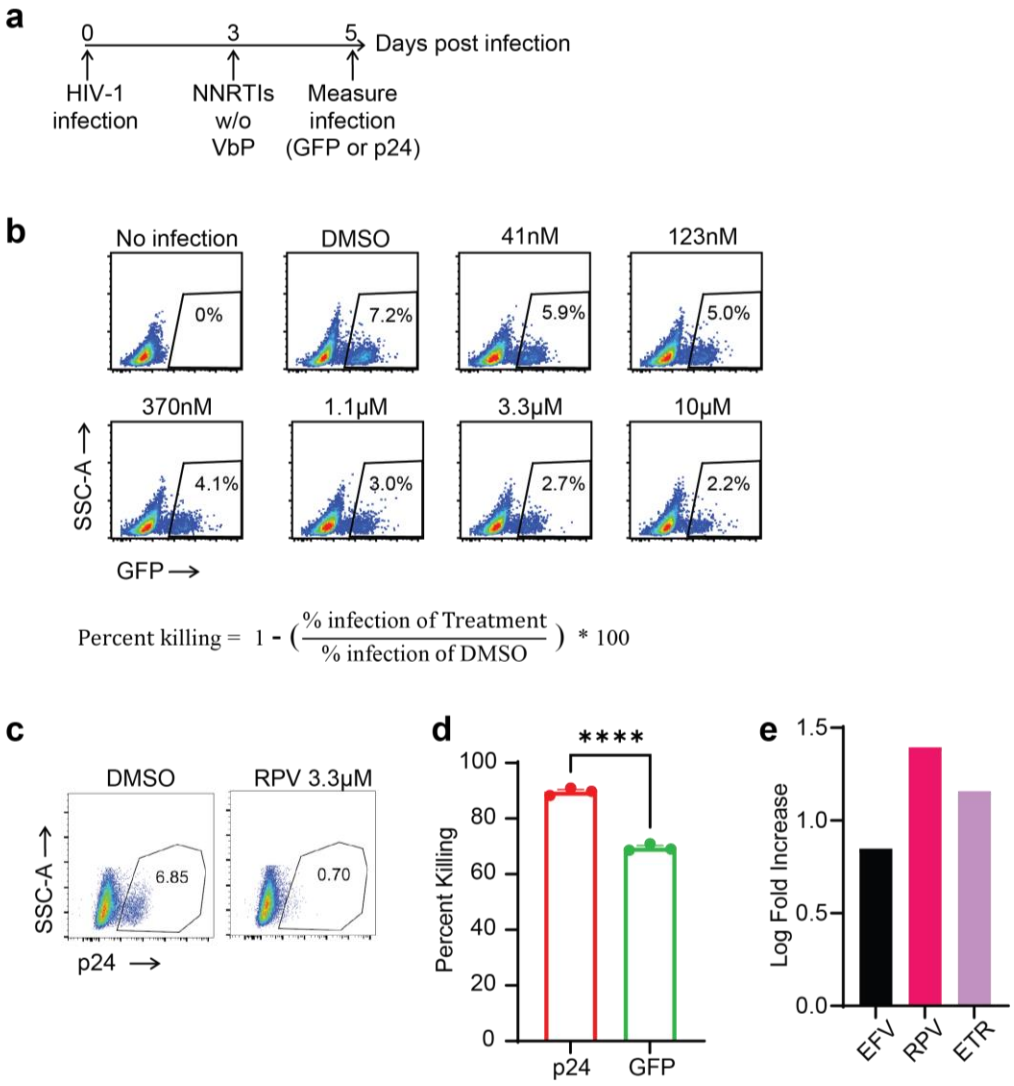

Supplementary Figure 2.1: Cell Killing Measurement.

a, Scheme of the killing assays for single-round HIV-1 reporter viruses. Primary $CD4^+$ T cells were infected with HIV-1 reporter viruses for 3 days before NNRTI treatment for 2 days. **b, c**, Representative flow cytometry plots are shown for one replicate of one donor. Percent killing is calculated as the percent infection of the treatment condition divided by the percent infection of DMSO control. Percent infection was determined by GFP (**b**) or intracellular p24 (**c**). **d**, Percent killing calculated from **c**. Unpaired two-sided t test. **** $p < 0.0001$. Error bars show mean values with SEM (n = 3). **e**, The log fold increase in EC_{50} calculated from the treatment of three donors of $CD4^+$ T cells with EFV, RPV and ETR with or without the presence of 50% human serum (HS) in the culture media. Data from Fig. 1f–h were used.

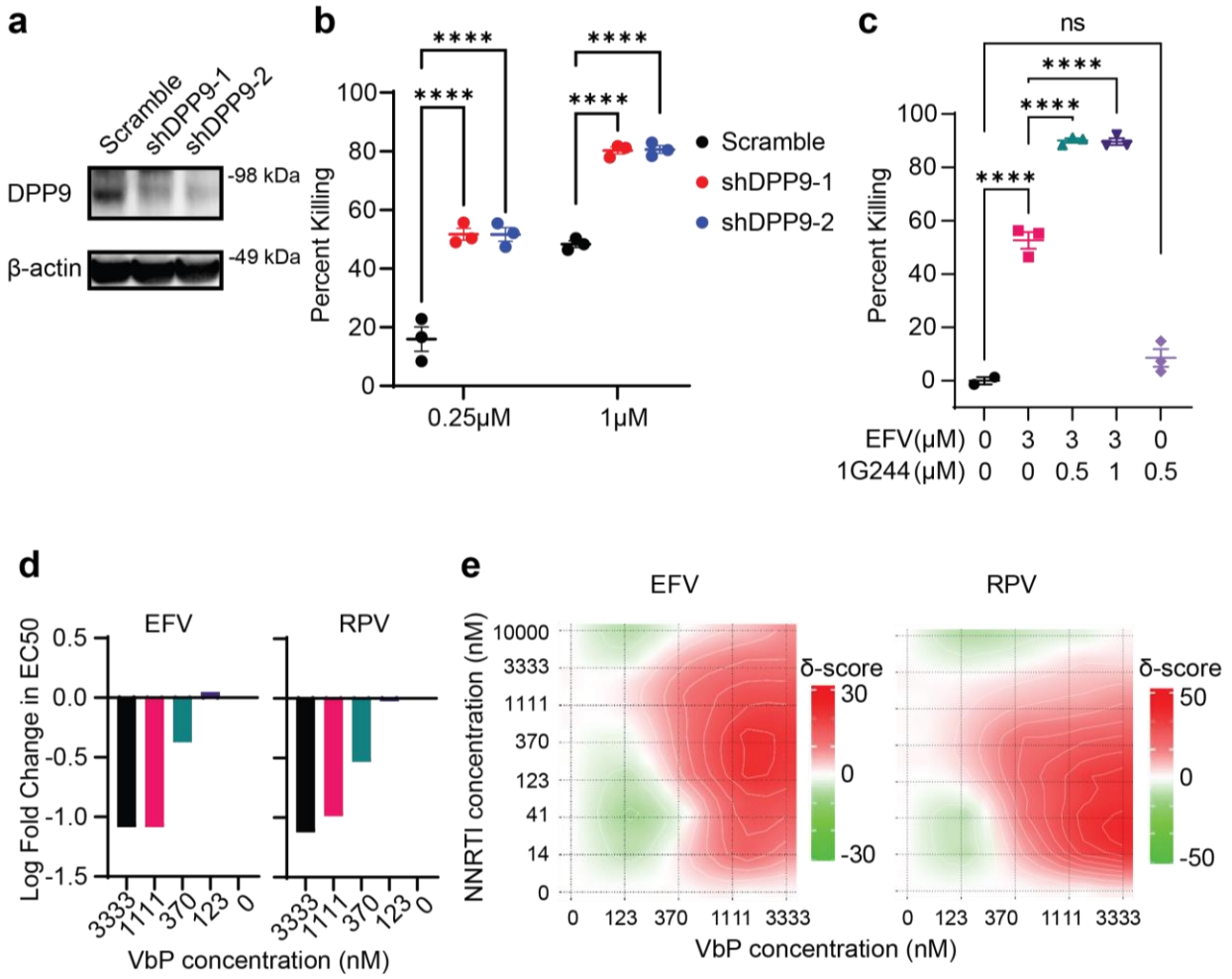

Supplementary Figure 2.2: DPP9 Inhibition Enhances NNRTI-Mediated Killing in THP⁻1. **a**, Two shRNA constructs delivered by lentiviral vectors for knockdown of DPP9 are confirmed by immunoblotting (experiment repeated three times with similar results). **b**, Killing of HIV-1-infected THP⁻1 cells by RPV. THP-1 cells were transduced with lentiviruses carrying DPP9-specific or scramble shRNA. Two-way ANOVA with Dunnett's multiple comparison test (n = 3). **c**, Killing of HIV infected THP-1 cells treated for two days with DMSO, EFV, 1g244, or combination (n = 3). One-way ANOVA with Tukey's multiple comparison test. * $p < 0.05$ and **** $p < 0.0001$. Error bars show mean values with SEM. **d**, Log fold changes in EC_{50} due to VbP. **e**, Combination treatment denotes a synergistic relationship as evidenced by Loewe's additivity model calculated with SynergyFinder2.0. Areas in red denote increased synergy. In **(d, e)**, data from Fig. 2b were used for the analysis.

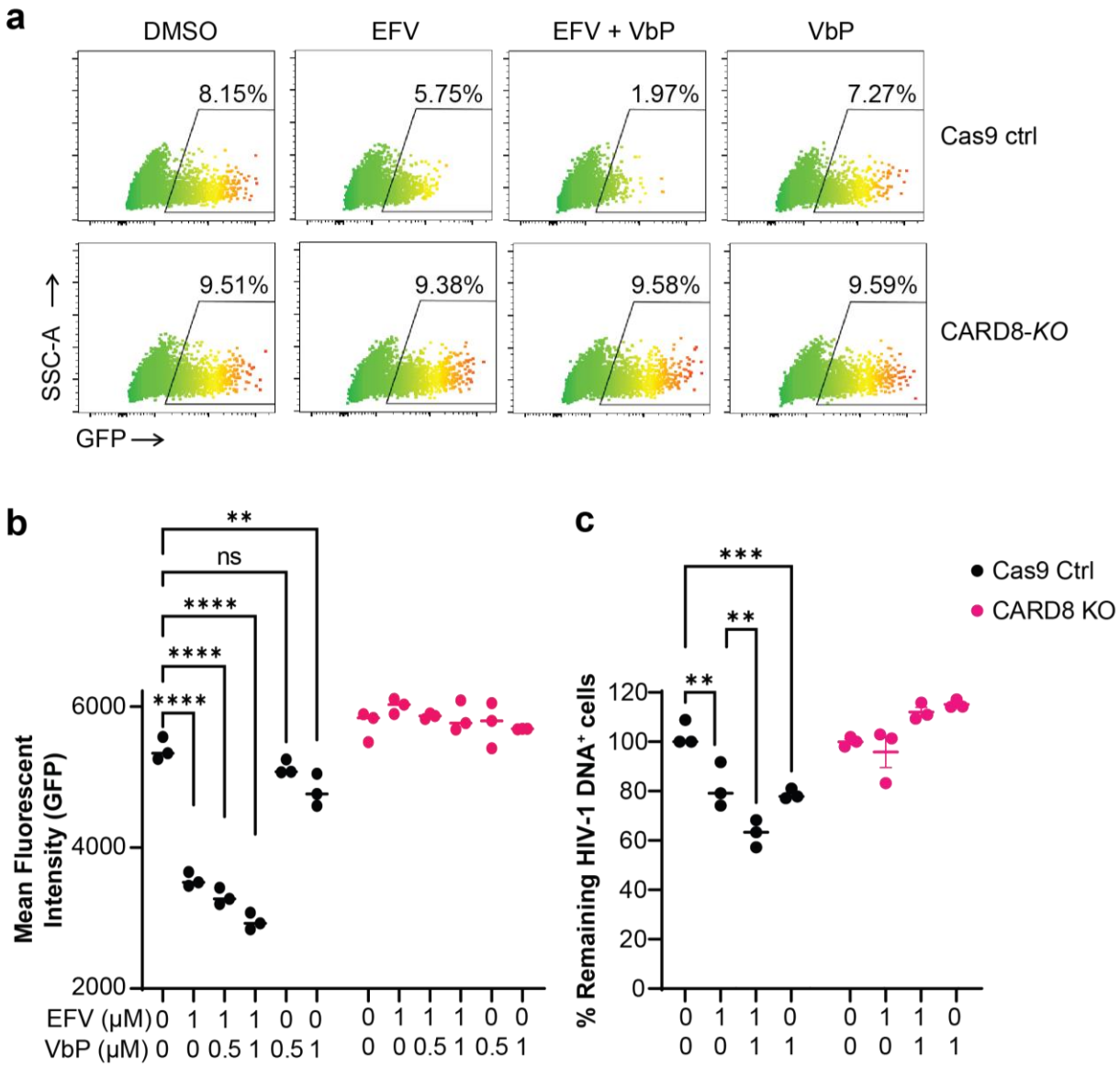
a
DMSO
EFV
EFV + VbP
VbP
8.15%
5.75%
1.97%
7.27%
Cas9 ctrl
9.51%
9.38%
9.58%
9.59%
CARD8-KO
SSC-A
GFP
b
Mean Fluorescent Intensity (GFP)
6000
4000
2000
**
ns
****
****
****
EFV (μM) 0 1 1 1 0 0 0 1 1 1 0 0
VbP (μM) 0 0 0.5 1 0.5 1 0 0 0.5 1 0.5 1
c
% Remaining HIV-1 DNA+ cells
120
100
80
60
40
20
0
***
**
**
Cas9 Ctrl
CARD8 KO
0 1 1 0 0 1 1 0
0 0 1 1 0 0 1 1

Supplementary Figure 2.3: CARD8 Inflammasome Activation is Dependent on Gag-Pol Expression.

a, Representative flow cytometry plots of *CARD8*-KO or *Cas9* control THP-1 cells treated with DMSO, EFV (3 μM), VbP (1 μM), or combination. Heatmap plots are colored according to mean fluorescent intensity (MFI) of GFP with higher MFI colored in red and lower MFI in green. **b**, Mean fluorescent intensity of three replicates from **(a)**. Two-way ANOVA with Dunnett's multiple comparison test. **c**, Frequency of HIV-1 DNA^+ cells measured by qPCR. *CARD8*-KO or *Cas9* control THP-1 cells were infected with HIV-1 for 3 days and treated with DMSO, EFV (3 μM), VbP (1 μM), or combination for 2 days. HIV-1 gag levels were normalized to POLR2A to determine the frequency of HIV-1 DNA^+ cells. The frequency in the treatment groups was measured as the percent of the DMSO control (n = 3). Two-way ANOVA with Tukey's multiple comparison test. * $p < 0.05$, ** $p < 0.01$ and **** $p < 0.0001$. Error bars show mean values with SEM.

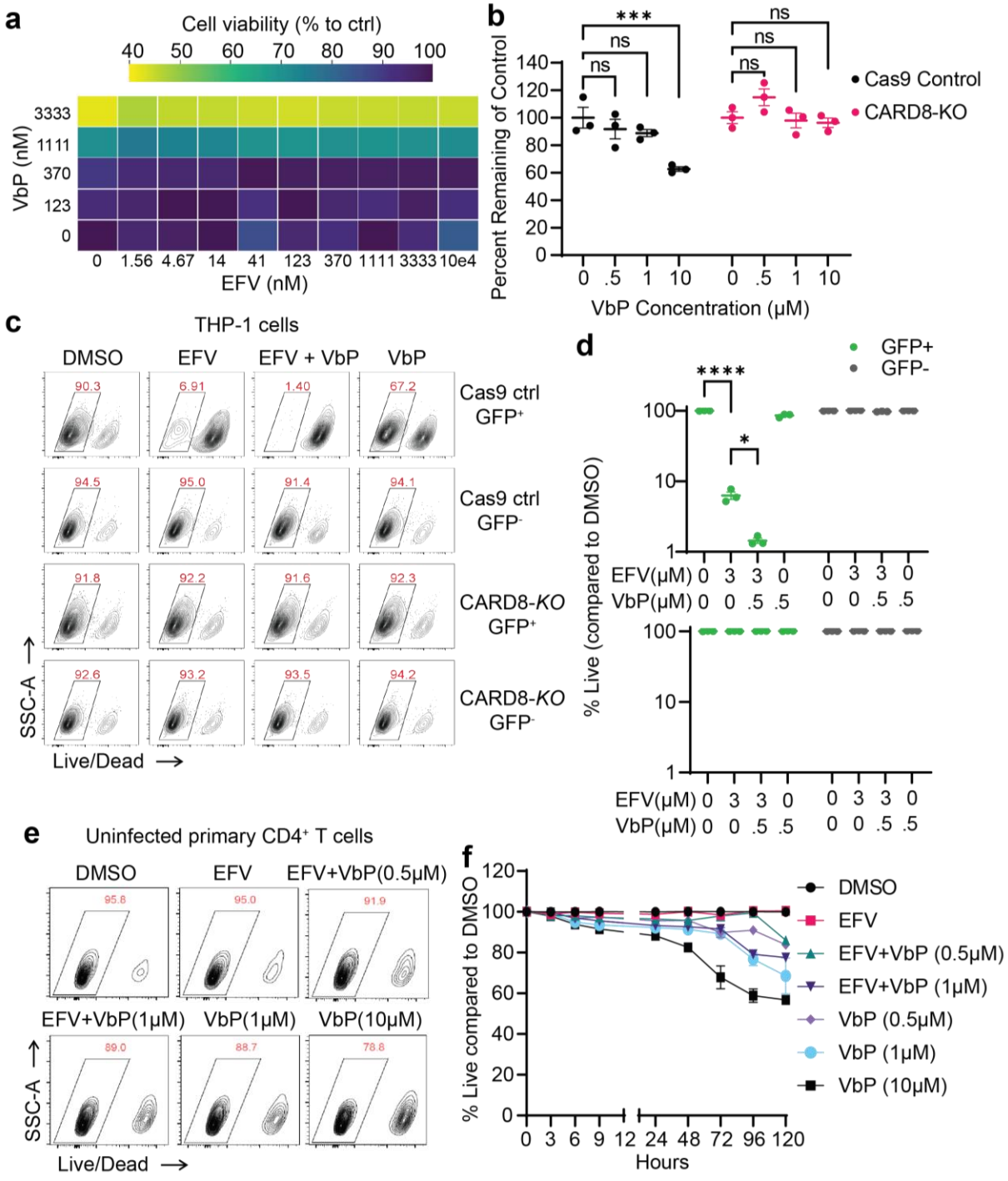
a
Cell viability (% to ctrl)
40 50 60 70 80 90 100
VbP (nM)
3333
1111
370
123
0
0 1.56 4.67 14 41 123 370 1111 3333 10e4
EFV (nM)
b
Percent Remaining of Control
***
ns
ns
ns
ns
ns
Cas9 Control
CARD8-KO
0 .5 1 10 0 .5 1 10
VbP Concentration (μM)
c
THP-1 cells
DMSO
EFV
EFV + VbP
VbP
90.3
6.91
1.40
67.2
Cas9 ctrl GFP+
94.5
95.0
91.4
94.1
Cas9 ctrl GFP-
91.8
92.2
91.6
92.3
CARD8-KO GFP+
92.6
93.2
93.5
94.2
CARD8-KO GFP-
SSC-A
Live/Dead
d
GFP+
GFP-
****
*
% Live (compared to DMSO)
EFV(μM) 0 3 3 0 0 3 3 0
VbP(μM) 0 0 .5 .5 0 0 .5 .5
e
Uninfected primary CD4+ T cells
DMSO
EFV
EFV+VbP(0.5μM)
95.8
95.0
91.9
EFV+VbP(1μM)
VbP(1μM)
VbP(10μM)
89.0
88.7
78.8
SSC-A
Live/Dead
f
% Live compared to DMSO
DMSO
EFV
EFV+VbP (0.5μM)
EFV+VbP (1μM)
VbP (0.5μM)
VbP (1μM)
VbP (10μM)
0 3 6 9 12 24 48 72 96 120
Hours

Supplementary Figure 2.4: VbP Cytotoxicity is CARD8 and HIV-1 Specific.

a, VbP cytotoxicity. THP-1 cells were treated for two days with EFV with or without VbP. Cell viability was determined by the MTS assay denoted by the heatmap. **b**, VbP toxicity is CARD8 dependent. *CARD8*-KO and *Cas9* control THP-1 cells were treated with VbP for 4 days. Cell viability was determined by the MTS assay. Two-way ANOVA with Dunnett's multiple comparison test. **c, d**, VbP killing of THP-1 cells is HIV-1 and CARD8 dependent. *CARD8*-KO or *Cas9* control THP-1 cells were infected with HIV-1 reporter viruses. On day 3 post infection, GFP^+ and GFP^- cells were purified by sorting before treatment with DMSO, EFV (3 μM), VbP (1 μM), or combination for 2 days. In **c**, representative flow cytometry plots of live dead staining. In **(d)**, percent live cells normalized to DMSO control for *Cas9* control (top) and *CARD8*-KO (bottom). One-way ANOVA with Tukey's multiple comparison test. **e, f**, Time course of live/dead staining of $CD4^+$ T cells treated with DMSO, EFV (3 μM), VbP, or combinations. Primary $CD4^+$ T cells were co-stimulated with CD3 and CD28 antibodies for 3 days before EFV and VbP treatment. Percent live were normalized to DMSO control. In **(e)**, representative FACS plots for the 48 hr time point. Error bars show mean values with SEM (n = 3). * $p < 0.05$, *** $p < 0.001$ and **** $p < 0.0001$.

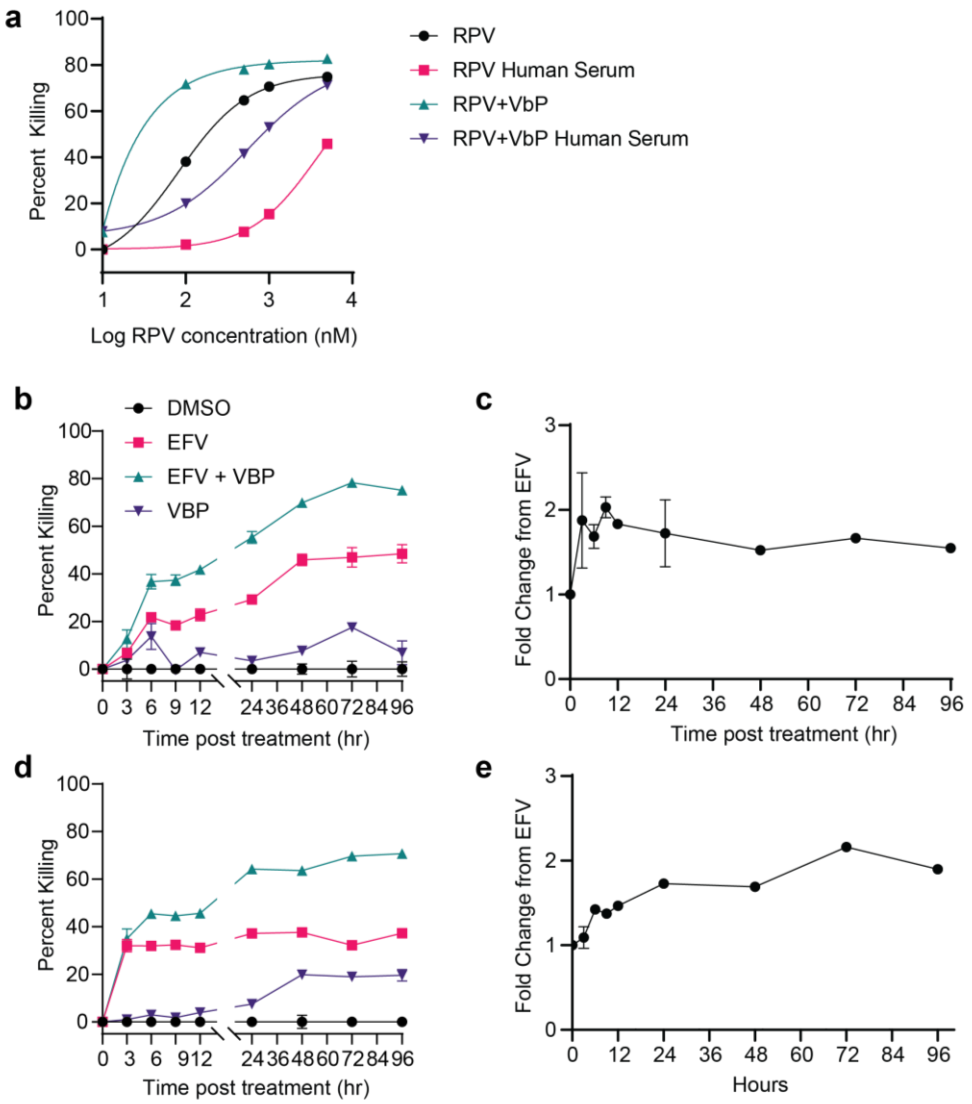

Supplementary Figure 2.5: VbP Sensitizes the CARD8 Inflammasome to HIV-1.

a, VbP overcomes reduced RPV killing efficacy by human serum. Dose response curves for killing of HIV-1-infected $CD4^+$ T cells treated with RPV or combo (VbP 1 μM) with or without the presence of 50% human serum. Zero values of RPV were plotted at 0.1 nM to allow for log transformation. Error bars show mean values with SEM (n = 3). **b**–**e**, Time course treatment of three donors of HIV-1 infected primary $CD4^+$ T cells **(b, c)** or THP-1 cells **(d, e)**. Cells were treated with DMSO, EFV (0.5 μM), VbP (1 μM), or combo. Fold change enhancement of combination treatment in comparison to EFV alone treatment was shown in **(c)** and **(e)**.

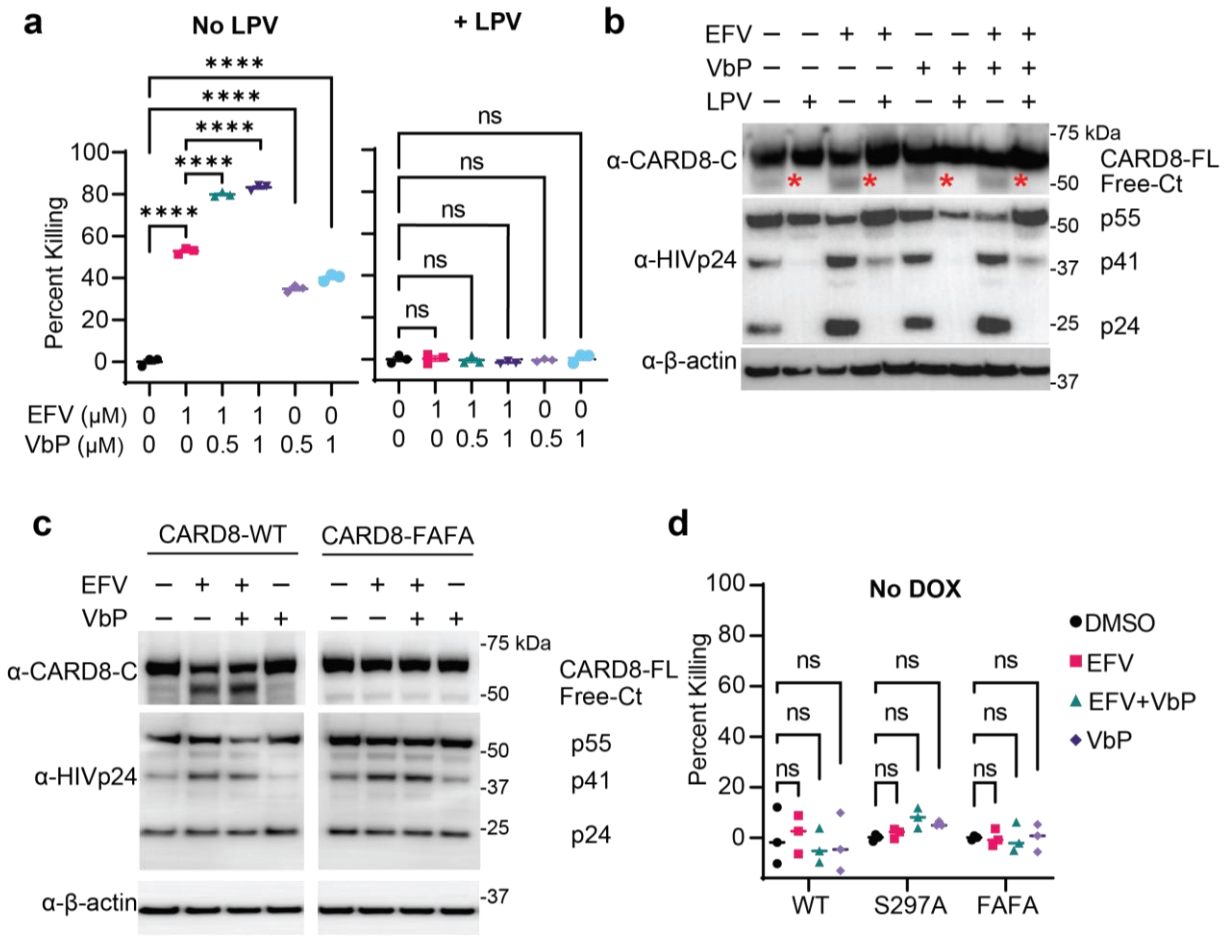
a
No LPV
+ LPV
Percent Killing
EFV (μM)
VbP (μM)
b
EFV
VbP
LPV
α-CARD8-C
α-HIVp24
α-β-actin
CARD8-FL
Free-Ct
p55
p41
p24
75 kDa
c
CARD8-WT
CARD8-FAFA
d
No DOX
DMSO
EFV
EFV+VbP
VbP
WT
S297A
FAFA

Supplementary Figure 2.6: Characterization of VbP enhancement of CARD8 activation.

a, VbP enhancement and killing is HIV-1 protease dependent. Percent killing of HIV-1-infected THP-1 cells treated for two days with DMSO, EFV, VbP, or combination with or without protease inhibitor LPV (1 μM). One-way ANOVA with Tukey's multiple comparison test. Error bars show mean values with SEM (n = 3). **b**, CARD8 cleavage in transfected HEK293T cells. HEK293T cells were co-transfected with a CARD8-expressing plasmid and the HIV-1 plasmid pNL4-3-GFP with the presence of indicated drugs. EFV: 3 μM. VbP: 1 μM. LPV: 1 μM. Cell lysates were collected 24hrs post transfection for western blot analysis. This experiment was repeated an additional two times and provided similar results. **c**, CARD8 cleavage in HIV-1-infected MT4 cells. MT4 cells were stably transduced with lentiviral vectors expressing WT or FAFA CARD8. Cells were infected for three days prior to treatment with DMSO, EFV (3 μM), VbP (1 μM), or EFV and VbP combination in the presence of a proteasome inhibitor MG132 (5 μM) to block degradation of the neo-C-fragment. Cell lysates were collected six hours post treatment for western blot analysis. This experiment was repeated an additional two times and provided similar results. **d**, Percent killing of *CARD8*-KO THP-1 cells replete with Dox-inducible CARD8 constructs for WT, S297A, or FAFA. Conditions shown were treated as in Fig. 3E but were not dox induced. One-way ANOVA with Dunnett's multiple comparison test. **** $p < 0.0001$.

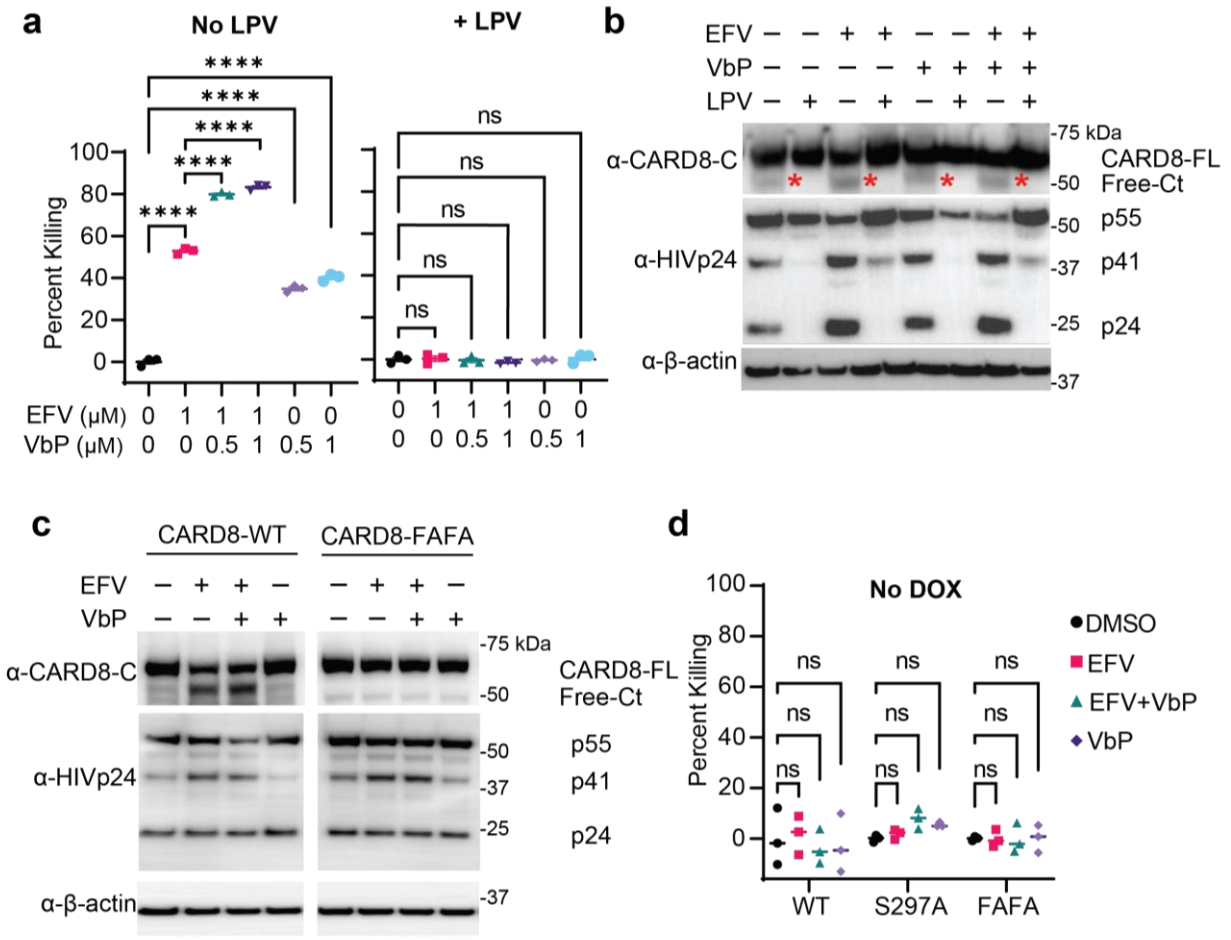

Supplementary Figure 2.7: VbP Enhancement and Killing is Caspase 8 Independent.

a, Two sgRNA constructs for knockout of *Caspase 8* are confirmed by immunoblotting (experiment repeated three times with similar results). **b**, Percent killing of *Cas9* Control, *Casp8*-KO, or *CARD8*-KO THP-1 cells infected with HIV-1 reporter viruses. Infected cells were treated with EFV (3 μM) with or without VbP for two days. Two-way ANOVA with Dunnett's multiple comparison test. Error bars show mean values with SEM (n = 3). **** $p < 0.0001$.

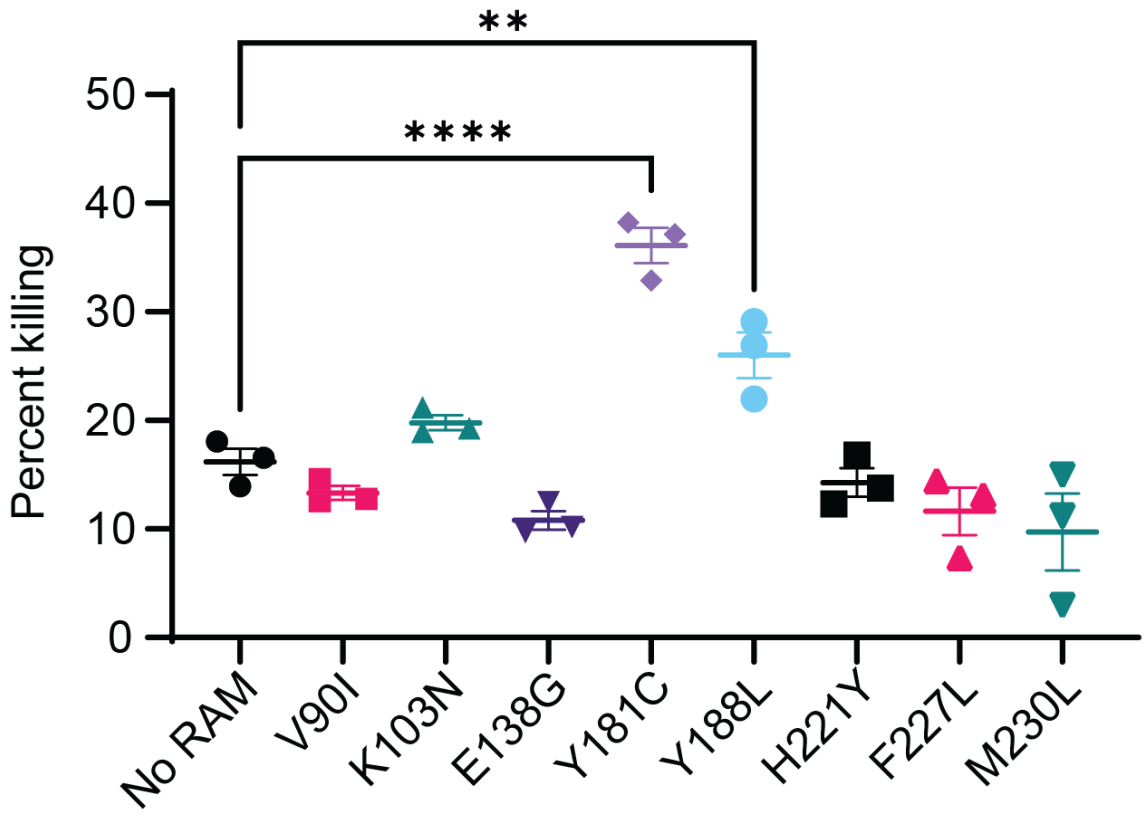

Supplementary Figure 2.8: Killing of Cells Infected with NNRTI RAMs by VbP.

Primary $CD4^+$ T cells were infected with HIV-1 reporter viruses carrying various NNRTI RAMs for 3 days before treatment with 1 μM VbP for two days. Error bars show mean values with SEM (n = 3). One-way ANOVA with Dunnett's multiple comparison test. ** $p < 0.01$ and **** $p < 0.0001$.

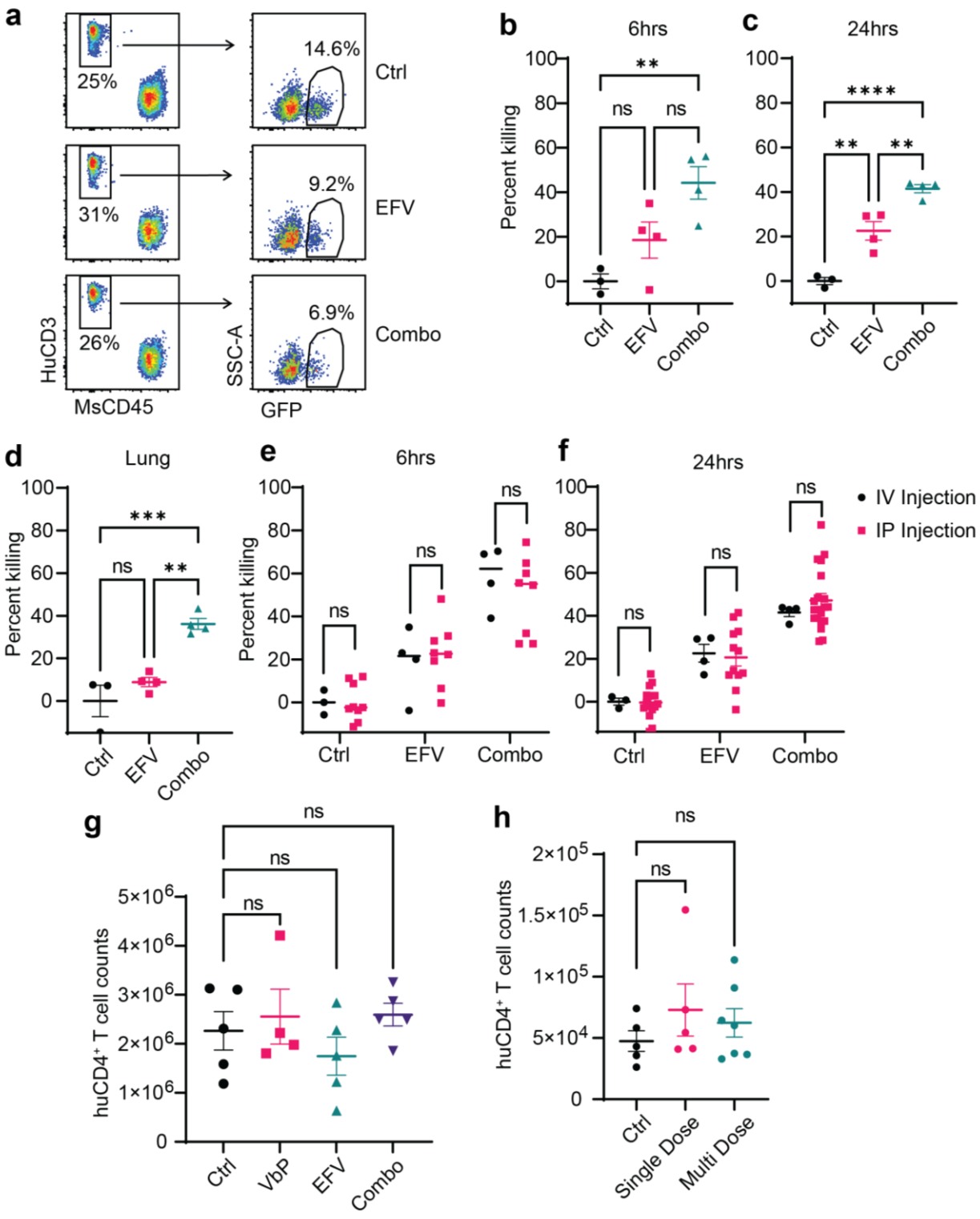
a
25%
14.6%
Ctrl
31%
9.2%
EFV
26%
6.9%
Combo
HuCD3
MsCD45
SSC-A
GFP
b
6hrs
Percent killing
**
ns
ns
Ctrl
EFV
Combo
c
24hrs
****
**
**
d
Lung
***
ns
**
e
6hrs
f
24hrs
IV Injection
IP Injection
g
huCD4⁺ T cell counts
VbP
h
Single Dose
Multi Dose

Supplementary Figure 2.9: Combination Treatment Effects *in vivo*.

Primary $CD4^+$ T cells were infected with the HIV-1 reporter virus NL4-3-Pol. Three days post infection, these cells were transfused into mice (5–10 million cells per mouse). EFV and VbP were provided by IV injection immediately after cell infusion. Remaining infected cells were measured by flow cytometry. **a**, Representative flow cytometry plots measuring remaining infected $CD4^+$ T cells in blood 6hrs post treatment. **b, c**, blood samples were collected 6hrs and 24 hr post EFV and VbP treatment (n = 4) or control (n = 3). **d**, Lung tissues were collected 24 hrs post EFV and VbP treatment. Two-way ANOVA with Sidak's multiple hypothesis test. **e, f**, Comparison of killing between IV and IP injection of EFV and VbP. Blood samples were collected 6hrs and 24 hr post EFV and VbP treatment. Two-way ANOVA with Sidak's multiple hypothesis test. (IV sample sizes are the same as **b-d**, IP samples sizes are as follows: DMSO = 17, EFV = 12, combination = 20. **g**, $CD4^+$ T cell counts from lung tissues of mice treated with control (n = 5), EFV (n = 4), VbP (n = 5), or combination (n = 5) after 24 hours. Two-way ANOVA with Dunnett's multiple hypothesis test. **h**, $CD4^+$ T cell counts from lung tissues from mice with control (n = 5), single-dose (n = 5), or multi-dose (n = 7) combination treatment regimens. Two-way ANOVA with Dunnett's multiple hypothesis test. Error bars show mean values with SEM. ** $p < 0.01$, **** $p < 0.0001$.

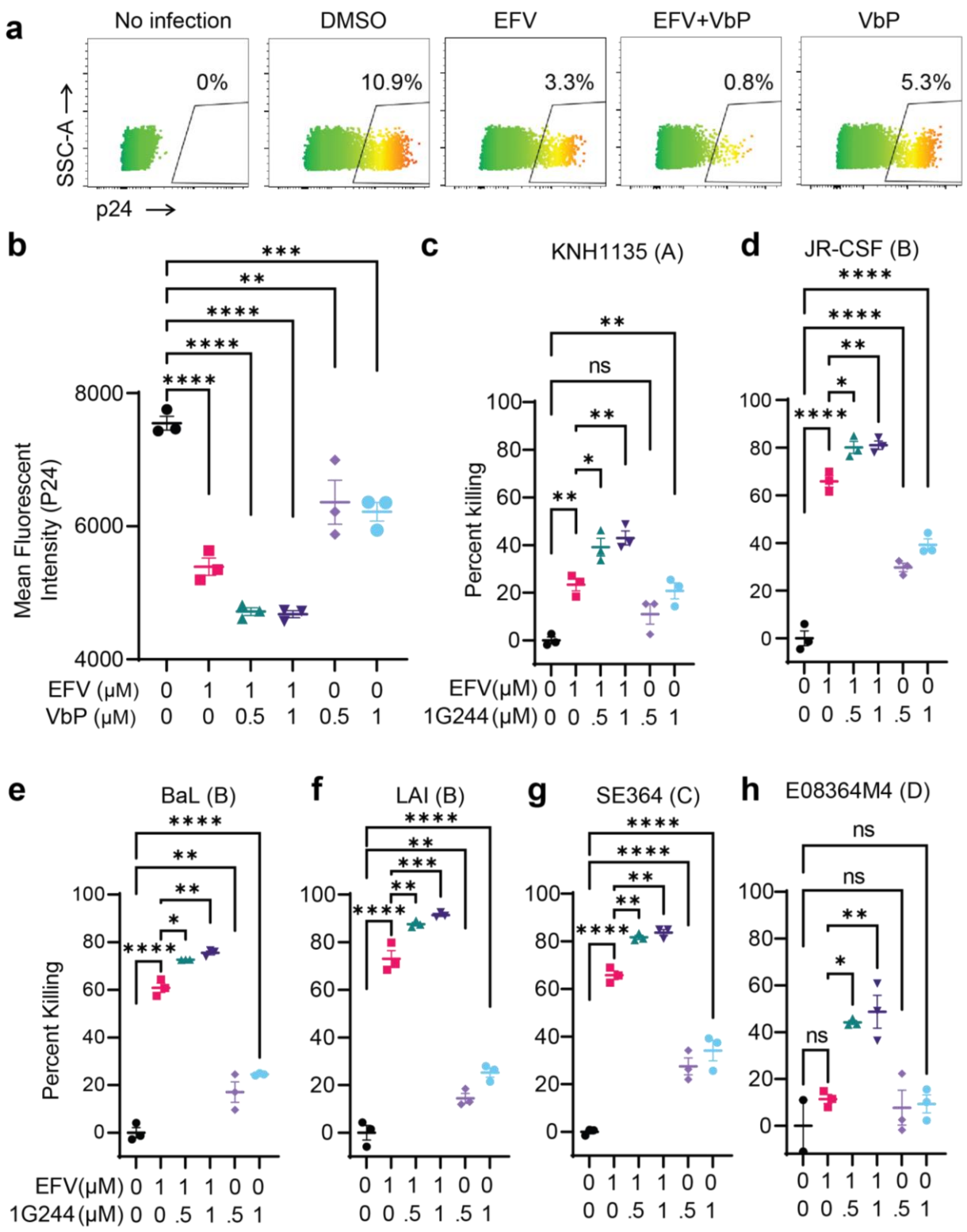
a
No infection
DMSO
EFV
EFV+VbP
VbP
0%
10.9%
3.3%
0.8%
5.3%
SSC-A
p24
b
Mean Fluorescent Intensity (P24)
EFV (μM) 0 1 1 1 0 0
VbP (μM) 0 0 0.5 1 0.5 1
c
KNH1135 (A)
Percent killing
EFV(μM) 0 1 1 1 0 0
1G244 (μM) 0 0 .5 1 .5 1
d
JR-CSF (B)
e
BaL (B)
Percent Killing
f
LAI (B)
g
SE364 (C)
h
E08364M4 (D)
ns

Supplementary Figure 2.10: DPP9 Inhibition Enhances Clearance of HIV-1 Clinical Isolates.

a, b, $CD4^+$ T cells were infected with HIV-LAI for four days and treated for one day with DMSO, EFV (1 μM), VbP (1 μM), or combination. In **(a)**, representative flow cytometry plots. Heatmap plots are colored according to mean fluorescent intensity (MFI) of intracellular HIV-p24 (PE) with higher MFI colored in red and lower MFI in green. In **(b)**, Mean fluorescent intensity of three replicates from **(a)**. One-way ANOVA with Dunnett's multiple hypothesis test. **c**–**h**, 1G244 enhances killing of primary $CD4^+$ T cells infected with various HIV-1 clinical isolates. Cells were infected for 4–6 days before treated with DMSO, EFV, 1g244, or combination for one day prior to intracellular HIV-p24 staining. One-way ANOVA with Tukey's multiple comparisons test. Error bars show mean values with SEM (n = 3). * $p < 0.05$, ** $p < 0.01$, ** $p < 0.001$ and **** $p < 0.0001$.

2.9 References

1. Gupta, R.K. et al. HIV-1 remission following CCR5Δ32/Δ32 haematopoietic stem-cell transplantation. *Nature* **568**, 244-248 (2019).
2. Hütter, G. et al. Long-term control of HIV by CCR5 Delta32/Delta32 stem-cell transplantation. *N. Engl. J. Med.* **360**, 692-698 (2009).
3. Castro-Gonzalez, S., Colomer-Lluch, M. & Serra-Moreno, R. Barriers for HIV Cure: The Latent Reservoir. *AIDS Res. Hum. Retroviruses* **34**, 739-759 (2018).
4. Finzi, D. et al. Identification of a reservoir for HIV-1 in patients on highly active antiretroviral therapy. *Science* **278**, 1295-1300 (1997).
5. Ganor, Y. et al. HIV-1 reservoirs in urethral macrophages of patients under suppressive antiretroviral therapy. *Nat. Microbiol.* **4**, 633-644 (2019).
6. Eisele, E. & Siliciano, R.F. Redefining the viral reservoirs that prevent HIV-1 eradication. *Immunity* **37**, 377-388 (2012).
7. Kim, Y., Anderson, J.L., & Lewin, S.R. Getting the "Kill" into "Shock and Kill": Strategies to Eliminate Latent HIV. *Cell Host Microbe* **23**, 14-26 (2018).
8. Wang, Q. et al. CARD8 is an inflammasome sensor for HIV-1 protease activity. *Science* **371**, 6535 (2021).
9. Broz, P. & Dixit, V.M. Inflammasomes: mechanism of assembly, regulation and signaling. *Nat. Rev. Immunol.* **16**, 407-420 (2016).
10. Gross, O., Thomas, C.J., Guarda, G. & Tschopp, J. The inflammasome: an integrated view. *Immunol. Rev.* **243**, 136-151 (2011).
11. Johnson, D.C. et al. DPP8/9 inhibitors activate the CARD8 inflammasome in resting lymphocytes. *Cell Death Dis.* **11**, 628 (2020).
12. Linder, A. et al. CARD8 inflammasome activation triggers pyroptosis in human T cells. *EMBO J.* **39**, e105071 (2020).
13. Hollingsworth, L.R. et al. DPP9 sequesters the C terminus of NLRP1 to repress inflammasome activation. *Nature* **592**(7856):778-783 (2021)**.**
14. D'Osualdo, A. et al. CARD8 and NLRP1 undergo autoproteolytic processing through a ZU5-like domain. *PLoS One* **6**, e27396 (2011).
15. Hsiao, J.C. et al. A ubiquitin-independent proteasome pathway controls activation of the CARD8 inflammasome. *J. Biol. Chem.* **298**(7), 102032 (2022).
16. Sharif, H. et al. Dipeptidyl peptidase 9 sets a threshold for CARD8 inflammasome formation by sequestering its active C-terminal fragment. *Immunity* **54**, 7 (2021).
17. Figueiredo, A. et al. Potent nonnucleoside reverse transcriptase inhibitors target HIV-1 Gag-Pol. *PLoS Pathog.* **2**, e119 (2006).
18. Phillips, R.E. et al. Human immunodeficiency virus genetic variation that can escape cytotoxic T cell recognition. *Nature* **354**, 453-459 (1991).
19. Kwong, P.D. et al. HIV-1 evades antibody-mediated neutralization through conformational masking of receptor-binding sites. *Nature* **420**, 678-682 (2002).
20. Caskey, M. et al. Viraemia suppressed in HIV-1-infected humans by broadly neutralizing antibody 3BNC117. *Nature* **522**, 487-491 (2015).
21. Rhee, S.Y. et al. HIV-1 Protease, Reverse Transcriptase, and Integrase Variation. *J. Virol.* **90**, 6058-6070 (2016).

22. Jochmans, D. et al. Selective killing of human immunodeficiency virus infected cells by non-nucleoside reverse transcriptase inhibitor-induced activation of HIV protease. *Retrovirology* **7**, 89 (2010).
23. Zerbato, J.M., Tachedjian, G., & Sluis-Cremer, N. Nonnucleoside Reverse Transcriptase Inhibitors Reduce HIV-1 Production from Latently Infected Resting CD4. *Antimicrob. Agents Chemother*. **61** (2017).
24. Boffito, M. et al. Protein Binding in Antiretroviral Therapies. *AIDS Research and Human Retroviruses* **19**, 825–835 (2003).
25. Almond, L.M. et al. Intracellular and plasma pharmacokinetics of efavirenz in HIV-infected individuals *J. Antimicrob. Chemother*. **56**(4), 738-44 (2005).
26. Rotger, M. et al. Swiss HIV Cohort Study. Influence of CYP2B6 polymorphism on plasma and intracellular concentrations and toxicity of efavirenz and nevirapine in HIV-infected patients. *Pharmacogenet Genomics* **15**(1), 1-5 (2005).
27. Tanaka, R. et al. Intracellular Efavirenz Levels in Peripheral Blood Mononuclear Cells from Human Immunodeficiency Virus-Infected Individuals. *Antimicrob. Agents Chemother*. **52**(2), 782-5 (2008).
28. Griswold, A. et al. DPP9's Enzymatic Activity and Not Its Binding to CARD8 Inhibits Inflammasome Activation. *ACS Chemical Biology* **14**(11), 2424-2429 (2019).
29. Wu. J.J. *et al.* Biochemistry, pharmacokinetics, and toxicology of a potent and selective DPP8/9 inhibitor. *Biochemical Pharmacology* **78**(2), 203-210 (2009).
30. Lankas, G.R. et al. Dipeptidyl peptidase IV inhibition for the treatment of type 2 diabetes: potential importance of selectivity over dipeptidyl peptidases 8 and 9. *Diabetes* **54**, 2988–2994 (2005).
31. Ianevski, A., Giri, A., & Aittokallio, T. SynergyFinder 2.0: visual analytics of multi-drug combination strategies. *Nucleic Acids Research* **48**(W1), W488-W493 (2020).
32. Loewe, S. The problem of synergism and antagonism of combined drugs. *ArzneimiettelForschung* **3**, 286–290 (1953).
33. Nie, Z. et al. HIV-1 protease processes procaspase 8 to cause mitochondrial release of cytochrome c, caspase cleavage and nuclear fragmentation. *Cell Death Differ*. **9**(11), 1172-84 (2002).
34. Preston, B.D. & Dougherty, J.P. Mechanisms of retroviral mutation. *Trends Microbiol*. **4,** 16-21 (1996).
35. Azijn, H. et al. TMC278, a next-generation nonnucleoside reverse transcriptase inhibitor (NNRTI), active against wild-type and NNRTI-resistant HIV-1. *Antimicrob. Agents Chemother*. **54**, 718-727 (2010).
36. Waters, J.M. et al. Mutations in the thumb-connection and RNase H domain of HIV type-1 reverse transcriptase of antiretroviral treatment-experienced patients. *Antivir. Ther.* **14**, 231-239 (2009).
37. King, R.W. et al. Potency of nonnucleoside reverse transcriptase inhibitors (NNRTIs) used in combination with other human immunodeficiency virus NNRTIs, NRTIs, or protease inhibitors. *Antimicrob. Agents Chemother.* **46**, 1640-1646 (2002).
38. Basson, A.E. et al. Impact of drug resistance-associated amino acid changes in HIV-1 subtype C on susceptibility to newer nonnucleoside reverse transcriptase inhibitors. *Antimicrob. Agents Chemother*. **59**, 960-971 (2015).

39. Rongvaux, A. et al. Development and function of human innate immune cells in a humanized mouse model. *Nat. Biotechnol.* **32**(4), 364-72 (2014).
40. Herndler-Brandstetter, D. et al. Humanized mouse model supports development, function, and tissue residency of human natural killer cells. *PNAS* **114**(45), E9626-E9634 (2017).
41. Siliciano, J.D. et al. Enhanced culture assay for detection and quantitation of latently infected, resting CD4+ T-cells carrying replication-competent virus in HIV-1 infected individuals. *Methods Mol. Biol.* **304**, 3-15 (2005).
42. Rao, S.D. et al. M24B aminopeptidase inhibitors selectively activate the CARD8 inflammasome. *Nat. Chem. Biol.* **18**, 565–574 (2022).
43. Laird, G. M. et al. Measuring the frequency of latent HIV-1 in resting CD4+ T cells using a limiting dilution coculture assay. *Methods Mol. Biol*. **1354**, 239–253 (2016).

Chapter 3: The CARD8 Inflammasome Dictates SIV Pathogenesis and Disease Progression

This chapter has been reproduced and adapted from the following unpublished manuscript:

Wang*, Q., Clark*, K.M., Tiwari, R., Burdo, T.H., Silvestri, G., Shan, L. The CARD8 Inflammasome Dictates HIV/SIV Pathogenesis and Disease Progression.

* These authors contributed equally.

The work on $CD4^+$ T Cell depletion due to HIV is discussed in chapter 1.4.3 and was conducted by Qiankun Wang. The work on pathogenesis in SIV infection was completed by Kolin Clark and is discussed in this chapter.

3.1 Abstract

While $CD4^+$ T-cell depletion is key to disease progression in HIV-infected individuals and SIV-infected macaques, the mechanisms underlying this depletion remains incompletely understood, with most cell death involving uninfected cells. In contrast, SIV infection of "natural" hosts such as sooty mangabeys do not cause $CD4^+$ depletion and AIDS despite high-level viremia. Here, we report that the CARD8 inflammasome is activated immediately after HIV entry by the viral protease encapsulated in incoming virions. Sensing of HIV protease activity by CARD8 leads to rapid pyroptosis of quiescent cells without productive infection, while T-cell activation abolishes CARD8 function and increases permissiveness to infection. Finally, we discovered loss-of-function mutations in the CARD8-coding gene from "natural hosts", which may explain the

peculiarly non-pathogenic nature of these infections. Our study suggests that the CARD8 inflammasome drives $CD4^+$ T cell depletion during pathogenic HIV/SIV infections.

3.2 Introduction

The hallmark of human immunodeficiency virus (HIV) pathogenesis is a progressive depletion of $CD4^+$ T-cell populations, which represents the main pathogenic mechanism responsible for the increased susceptibility to opportunistic infections and progression to acquired immunodeficiency syndrome (AIDS). The mechanism through which HIV depletes $CD4^+$ T cells in humans has been the subject of intense research for decades. Our recent work, presented in section 1.4.3, suggests that the CARD8 inflammasome is the main driver of $CD4^+$ T cell depletion during HIV-1 infection. We found that HIV entry induces rapid $CD4^+$ T cell loss through the CARD8 inflammasome. Rapid cell death of $CD4^+$ T cells co-cultured with viral producing cells or using cell free virus was rapidly induced upon exposure to viral particles. This rapid cell death could be abrogated by inhibitors AMD3100 and T20 that block viral attachment and fusion indicating viral attachment is required. Conversely, antiretrovirals that block reverse transcription or integration had no effect on cell death indicating an initiation of cell death prior to the subsequent steps of the viral life cycle. In concordance with previous literature, we also saw that this rapid cell death was isolated to $CCR5^+$ $CD4^+$ T cells when using a CCR5 tropic virus.

We next set out to determine this rapid cell death's dependence upon the CARD8 inflammasome. Caspase-1 inhibitors and proteasome inhibitors, which are key downstream components of the CARD8 inflammasome, were able to block this rapid cell death indicating the role of the inflammasome. Upon knockout of CARD8, CASP1, and GSDMD we also saw a lack

of cell death whereas knocking out NLRP1 or ASC, which mediates all other inflammaosmes besides NLRC4, did not have any effect on cell death, further solidifying the reliance upon the CARD8 inflammasome for this phenotype. To confirm that CARD8 was sensing viral protease activity, we treated cells with the protease inhibitor LPV which was able to block cell death. Additionally, *CARD8*-KO cells replete with wtCARD8 was able to restore this phenotype whereas the HIV protease cleavage site mutant F59A/F60A was not able to restore cell death. Lastly, we showed that CARD8 acts as a restriction factor for HIV infection by treating cells with the DPP9 inhibitor 1g244 or by knocking out CARD8 and measuring infection and cell death. Indeed, when the cells are sensitized by 1g24 greater rates of cell death and IL-1β release were seen along with reductions in viral infection. In the *CARD8*-KO cells we were able to show increased viral infectivity as there is no longer any bystander cell death to inhibit viral spread. These data confidently support the hypothesis that upon attachment and fusion of the viral particle, HIV-1 protease is released which can cleave CARD8 and induce pyroptosis prior to productive infection. We also highlight that further sensitization by DPP9 inhibitors can greatly enhance $CD4^+$ T cell loss and solidify CARD8 as a critical host restriction factor for HIV infection. While this work greatly supports the role of CARD8 in HIV pathogenesis, it was still unclear how it contributed to SIV pathogenesis.

Pathogenic simian immunodeficiency virus (SIV) infections in rhesus macaques (*Macaca mulatta, RM*) is also associated with high viremia, rapid depletion of non-productively infected CCR5-expressing $CD4^+$ T cells, and progression to simian AIDS.[1-3] In SIV-infected RMs, rapid inflammasome activation was observed both at the site of SIV inoculation and the sites of distal virus spread.[4] In this model, caspase-1(CASP1)-dependent pyroptosis has been described as the dominant mechanism responsible for the rapid CD4 depletion by SIV, whereas other

programmed cell death mechanisms contribute minimally.[5] These studies are in concordance with the phenotype seen in humans where CASP1 activation and pyroptotic cell death were observed in bystander $CD4^+$ T cells from viremic individuals.[6]

Naturally occurring SIV infections have been identified in over 40 different African NHP species. Interestingly, natural SIV infections of the African *Cercopithicenae* species sooty mangabeys (*Cercocebus atys*) and African green monkeys (*Chlorocebus sabaeus*) do not lead to systemic $CD4^+$ T-cell loss and progression to AIDS, even though the virus is equally cytopathic in productively infected $CD4^+$ T cells and plasma viral loads are comparable to untreated HIV infections and SIV-infected RMs.[7] Chimpanzees (*Pan troglodytes*) acquired SIV by transmission and recombination of SIVs infecting primate species on which they prey[8], and SIVcpz infection of chimpanzees resulted in increased mortality and development of AIDS-related symptoms.[9-11] Of note, studies using chimeric SIVs suggested that pathogenicity is determined by specific aspects of the host-pathogen interaction, as opposed to intrinsic differences in the viral genomes, thus indicating that the immune response to the virus during pathogenic infections likely contributes to the observed $CD4^+$ T cell depletion.[12] In natural SIV hosts, the resistance to disease progression has been attributed to several non-mutually exclusive factors, including the absence of chronic immune activation[7,13,14], the low levels of microbial translocation from the gut [15,16] and subsequent systemic immune activation[17], and the limited level of infection of specific $CD4^+$ T cells subsets including central memory cells, stem-cell memory cells, and follicular helper cells.[18-20] Since one of the hallmarks of non-pathogenic SIV infection is the lack of bystander $CD4^+$ T cell death,[14] it is important to understand whether $CD4^+$ T cells from the natural hosts are inherently resistant to SIV-induced bystander cell death.

Taken together, the vast majority of available observations are compatible with the hypothesis that direct, virus-mediated cytopathic effect in productively infected cells is not the major driver of $CD4^+$ T-cell depletion during pathogenic HV/SIV infection of humans and RMs. However, the mechanisms by which SIV trigger cell death in bystander $CD4^+$ T cells remains poorly understood, including the role of inflammasome activation. In this regard, it should be noted that most aspects of inflammasome function and biology have been identified and characterized in myeloid cells, and that their roles in human $CD4^+$ T cells are not well defined. In this study, we aimed to determine whether CARD8 is responsible for SIV-induced CD4 depletion, and if so, how CARD8 is activated during the natural course of viral infection to drive rapid $CD4^+$ T-cell loss. Additionally, we aimed to investigate the genetic differences in the NHP CARD8, which may help explain the differences seen in SIV pathogenesis across NHP species.

3.3 Results

3.3.1 The NHP CARD8 coding gene in non-pathogenic hosts of SIV contains loss-of-function mutations

To first understand the conservation of the CARD8 gene, CARD8 protein sequences from a majority of the mammalian orders were aligned and used to construct a maximum likelihood gene tree (**Figure 3.1**). CARD8 can be found in most extant mammalian species that have been sequenced, with distinct variation seen in the mammalian superorder *Laurasiatheria*. The Carnivora order clustered more closely with the superorders of *Xenartha*, *Afrotheria*, and *Euarchontoglires* instead of with the other more closely related members of *Laurasiatheria* indicating a potentially distinct diversification of the CARD8 gene in this order which more closely resembles that of the members of the *Xenartha, Afrotheria,* and *Euarchontoglires*.

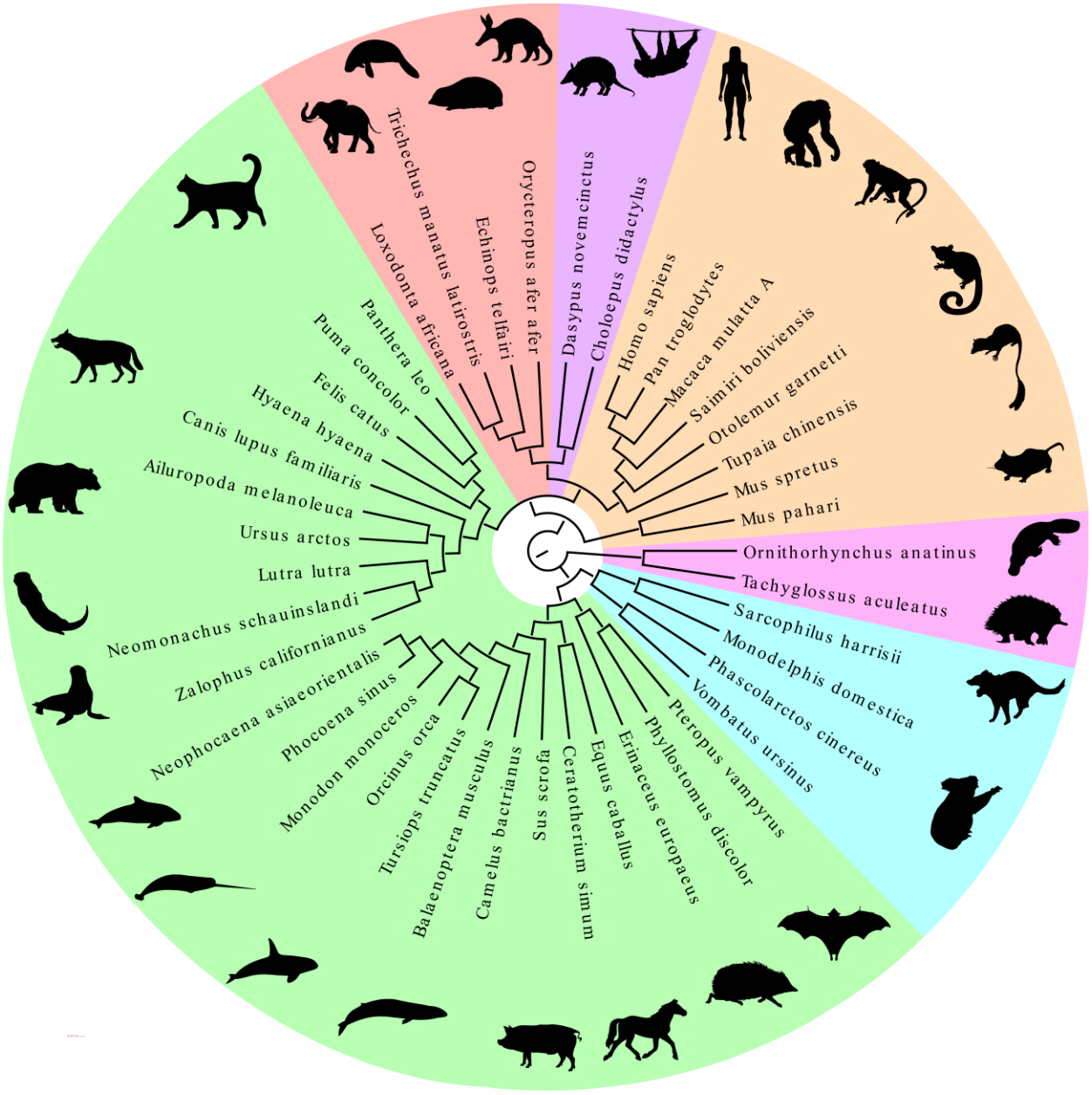

Figure 3.1: Phylogenetic Analysis of Mammalian CARD8

The protein sequences of the longest isoform for each CARD8 gene from each species were aligned and used to construct the maximum likelihood tree shown. CARD8 is present in every superorder (pink: *Monotremata*, blue: *Marsupiala*, purple: *Xenartha*, red: *Afrotheria*, green: *Laurasiatheria*, and orange: *Euarchontoglires)*. *Laurasiatheria* is polyphyletic, *Euarchontoglires* is paraphyletic, and all other superorders are monophyletic. The sequences used to generate this tree may be found in **Table S3.1**.

We also note that the *Euarchontoglires* does not represent a monophyletic group due to diversification of the CARD8 gene in rodents. As CARD8 is present in most mammalian species, with large genetic variations seen, we next sought to understand how genetic variation has impacted CARD8's evolution in NHPs. We identified CARD8 sequences from 25 different NHPs, and surprisingly we found that all *Cercopithecoidae* have evidence of a reverse tandem gene duplication of CARD8 (**Figure S3.1a**). Of note, one of these copies – hereby termed CARD8B – has a truncated N-terminal region due to genomic loss of these exons, which is the critical region for viral protease recognition. In contrast, the other copy– hereby termed CARD8A – maintained an intact N-terminus. As this version of the gene is the most likely functional copy for lentiviral recognition, we next aligned CARD8A of *Cercopithecoidae* with the only copy of CARD8 for the other NHPs (**Figure 3.2a**). Interestingly, the CARD8A of the non-pathogenic SIV hosts *Chlorocebus sabaeus* and *Cercocebus atys* have truncations in the CARD domain (**Figure 3.2b and S3.1b)**, which may impact its interaction with CASP1. The *Chlorocebus* CARD8A completely lost the CARD domain exons and the *Cercocebus* gene contained several small deletions resulting in frameshifts giving rise to large variations in the domain and a five amino acid deletion. However, the CARD domain of rhesus macaques and chimpanzees remain intact and share homology with the human sequence (**Figure 3.2b)**. Next, a species tree of the expected evolutionary relationships of non-human primates and their close relatives of the *Scandentia* order was created using the NCBI taxonomy browser and adjusted to account for updated relationships identified from recently published findings from whole genome phylogenomics of more than 200 primate species[21-23] (**Figure 3.3a)**. This phylogenetic tree shows large differences in comparison to the one based on evolutionary relationships of

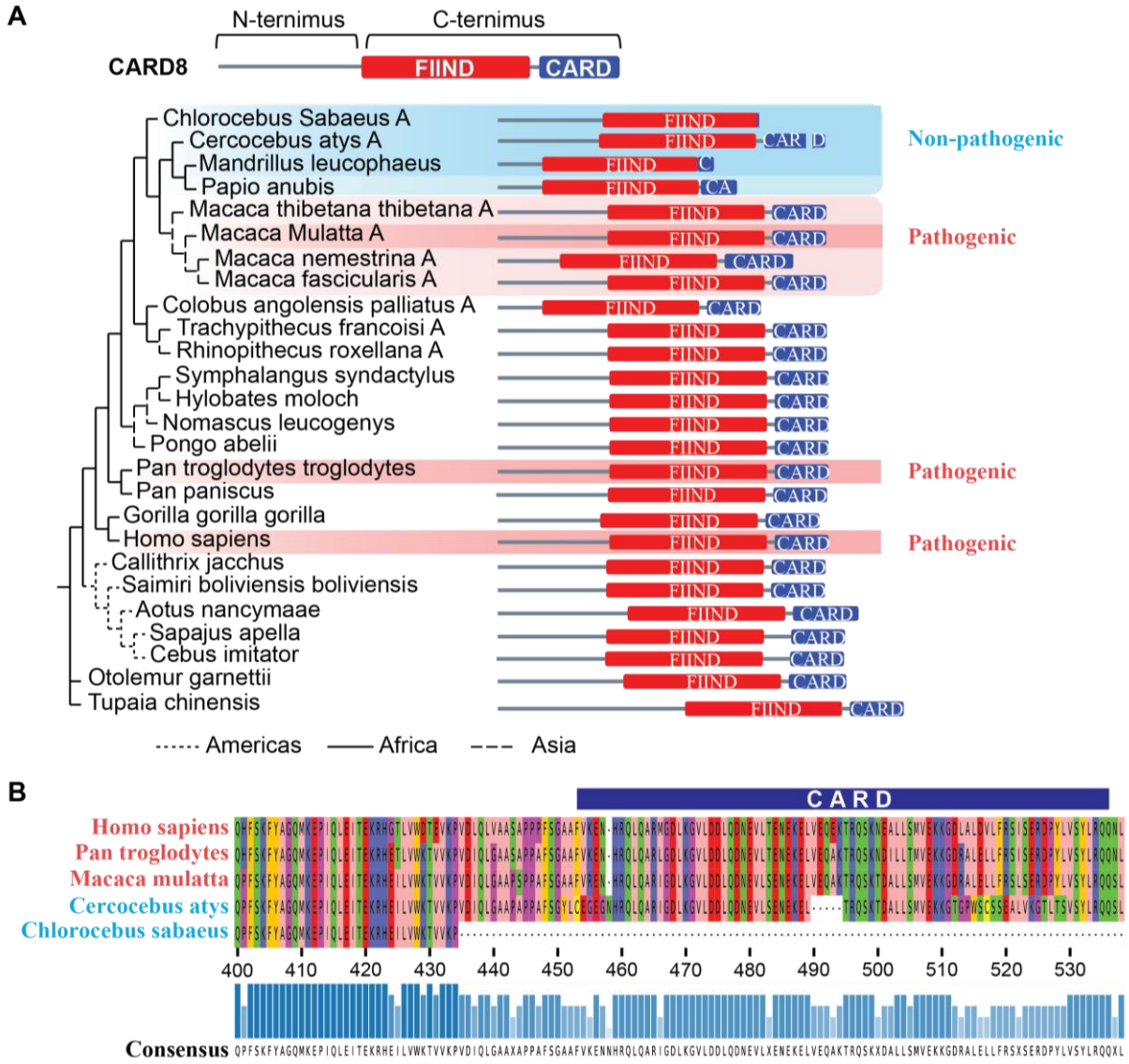

Figure 3.2: Genetic Analysis of the NHP CARD8 Inflammasome Reveals Functional Defects in Non-Pathogenic Hosts of SIV Infection

(a) Maximum likelihood gene tree of CARD8 or CARD8A from the selected NHP species. Dark red shading indicates known pathogenic HIV/SIV hosts, dark blue depicts known non-pathogenic hosts, and light blue the suspected non-pathogenic hosts. The protein schemes on the right depict the predicted domain architecture based on the alignment to the known domain structure of the human protein. **(b)** Protein alignment of the CARD domains and part of the FIIND domains of the species of known pathogenicity status.

NHP CARD8A, indicating substantial evolution of CARD8 in comparison to the whole genome. We believe this may be assisted by the presence of the gene duplication events in the *Cercopithecoidae* species, as gene duplication allows for greater mutational rates. This is in stark contrast to other inflammasome sensors reported to play a role in $CD4^+$ T cell bystander cell death such as with interferon gamma inducible protein 16 (IFI16). The gene tree developed for IFI16 more closely resembles that of the expected evolutionary relationships of NHP species (**Figure S3.2b**). IFI16 proteins between pathogenic and non-pathogenic hosts share 98% and 97% homology in contrast to 89% and 73% for CARD8 (**Figure S3.1b and S3.2c)**. We therefore theorize that the genetic differences in CARD8 may be better suited to explain the differential response to SIV infection in non-pathogenic and pathogenic hosts of SIV infection.

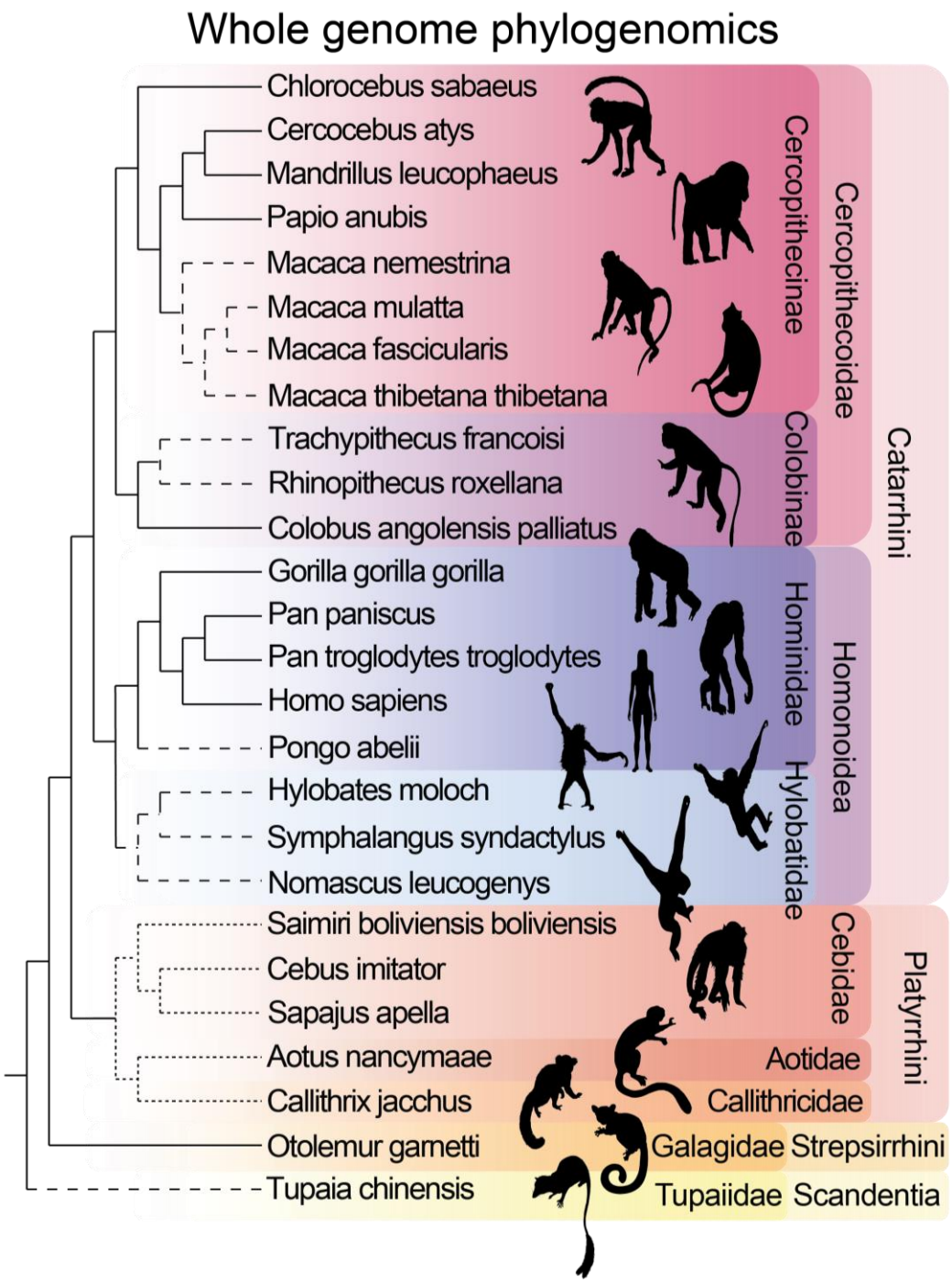

Figure 3.3: Expected Non-Human Primate Phylogeny from Whole Genome Phylogenomics

(a) Expected evolutionary relationships of primate species based on the NCBI taxonomy browser and recent analyses of whole genome phylogenomics[22,23]. Geographic locations of each species are indicated by dashed lines.

3.3.2 The CARD8 inflammasome is defective in non-pathogenic hosts of SIV

To further assess whether the CARD8 inflammasome can explain differences in pathogenicity of NHPs, we cloned the NHP CARD8 coding genes including *card8* from chimpanzee (CPZ), and *card8a* and *card8b* from rhesus macaque (RM), sooty mangabey (SM), and African green monkey (AGM). Human CARD8 and the autoprocessing-deficient S297A mutant were included as controls. Expression of these human and NHP CARD8 proteins in human or NHP cell lines demonstrates that CARD8B from all three *Cercopithecinae* species (in purple) do not autoprocess (**Figure 3.4a** and **S3.3a),** likely due to the common CARD8B N-terminal truncation in *Cercopithecinae* species. Based on genomic analyses, CARD8A from sooty mangabeys and African green monkeys have deletions in the CARD domain, thus they are smaller than the CARD8 from the pathogenic hosts (**Figure 3.4a)**. To further understand whether the N-terminal truncation affected the autoprocessing in the FIIND-CARD domain, we swapped the N- and C-terminus of RM-CARD8A and AGM-CARD8B. The intact CARD8A N-terminus was able to restore autoprocessing in the CARD8B FIIND-CARD domain (**Figure 3.4b**). By contrast, the CARD8B N-terminal region was able to abolish autoproteolytic activity of the FIIND-CARD of CARD8A. We next generated *CARD8-KO* THP-1 cells that stably express different NHP CARD8 to test the capacity of these proteins to respond to VbP, a known activator of the human CARD8 inflammasome. We found that CARD8 proteins from the pathogenic hosts were able to respond to VbP treatment (**Figure 3.4c**). As VbP is a non-specific activator of the CARD8 inflammasome independent upon PR recognition, we next tested whether NHP CARD8 senses SIV PR by an *in vitro* cleavage assay using purified PR and CARD8 proteins. HIV and SIV were able to cleave CARD8 from their respective hosts, which is blocked by the putative cleavage site mutations (**Figure 3.4d**). Interestingly, PR from SIV_{RM} and SIV_{CPZ} had strong cross species

activities, whereas HIV PR cleaved RM CARD8 less efficiently (**Figure 3.4e**). To test whether this cleavage could result in functional inflammasome activation, we transfected *CARD8*-KO HEK293T cells with human pro-CASP1, pro-IL-1β, and the NHP CARD8 along with HIV or SIV reporter plasmids.

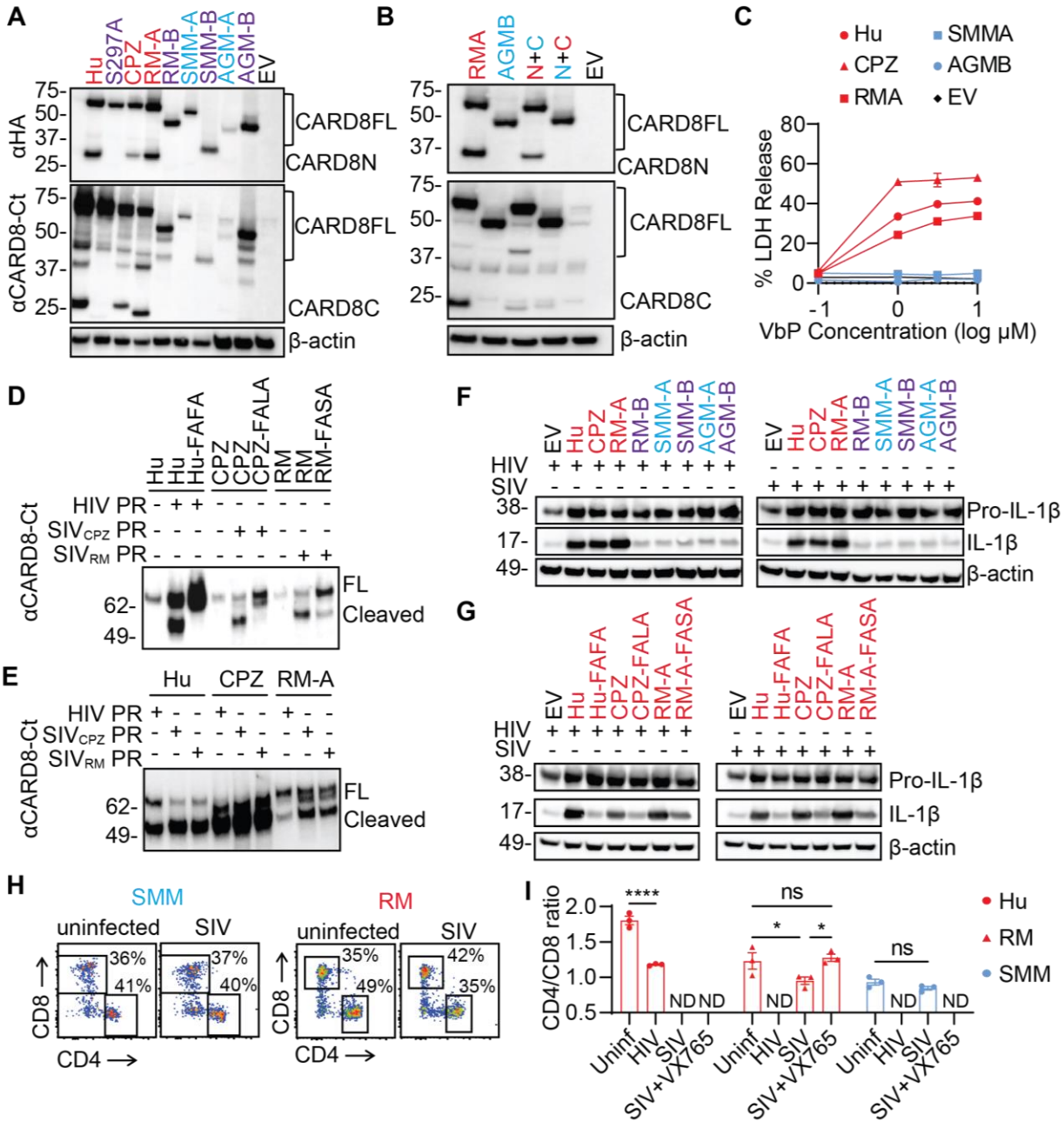

Figure 3.4: The CARD8 Inflammasome is Functional in Pathogenic Hosts and Defective in Non-Pathogenic Hosts of SIV Infection

(a) Autoprocessing of NHP CARD8. HEK293T cells were transfected with plasmids expressing HA-tagged CARD8 from Hu and CPZ, and CARD8A and CARD8B from RM, SMM, and AGM. **(b)** CARD8 N-terminal truncation inhibits its C-terminal autoprocessing. The two chimeric CARD8 (N+C) were RMA N-terminus (red) plus AGMB C-terminus (cyan) and AGMB N-terminus (cyan) plus RMA C-terminus (red). **(c)** Validation of NHP CARD8 functions. *CARD8*-KO THP-1 cells replete with indicated NHP CARD8 were treated with VbP (5 μM) for four hours before cell death measurement by the LDH release assay. **(d** and **e)** *In vitro* cleavage of human and NHP CARD8 by HIV and SIV protease. Purified CARD8 proteins and SIV or HIV protease were incubated for one hour before immunoblotting. CARD8 cleavage site mutants included Hu-FAFA, CPZ-FALA, and RM-FASA. **(f** and **g)** Activation of human and NHP CARD8 inflammasome by HIV and SIV. *CARD8*-KO HEK293T cells were co-transfected with plasmids encoding CASP1, pro–IL-1β, and human or NHP CARD8 with or without cleavage site mutations, together with HIV or SIV plasmids. **(h** and **i)** Rapid loss of $CD4^+$ T cells. Co-culture of human, RM, and SMM PBMCs with SIVmac251-infected CEM-174 cells. CD4/CD8 ratio was measured 16 hours post co-culture. Two-way ANOVA with Šídák's multiple comparisons test.

Co-transfection with HIV and SIV led to cleavage of pro-IL-1β to its active form (**Figure 3.4f**), which was blocked after the introduction of cleavage mutations (**Figure 3.4g**). Finally, we conducted co-culture experiments using RM and SMM PBMCs alongside human PBMC controls. CEM-174 cells were used as the viral producing cells for SIVmac 251 and were co-cultured with unstimulated NHP PBMCs (**Figure S3.3b**). Only the PBMCs from RMs had rapid $CD4^+$ T cell depletion as evidenced by the reduction in the CD4:CD8 ratio in PBMCs from five different animals, which was blocked by VX765 (**Figures 3.4h** and **i**, and **S3.3c**). In contrast, $CD4^+$ T cell loss was not observed in SMM PBMCs. Taken together, these data suggest that

CARD8 in natural hosts of SIV is functional defective and cannot trigger pyroptosis upon SIV entry. In summary, proto-OWMs underwent a CARD8 gene duplication which resulted in a functional CARD8A and a dysfunctional CARD8 carrying a truncated N-terminus (**Figure 3.5**). OWM species remained in Africa further acquired loss-of-function truncations or mutations in the CARD domain, rendering these species resistant to SIV PR-mediated $CD4^+$ T cell pyroptosis.

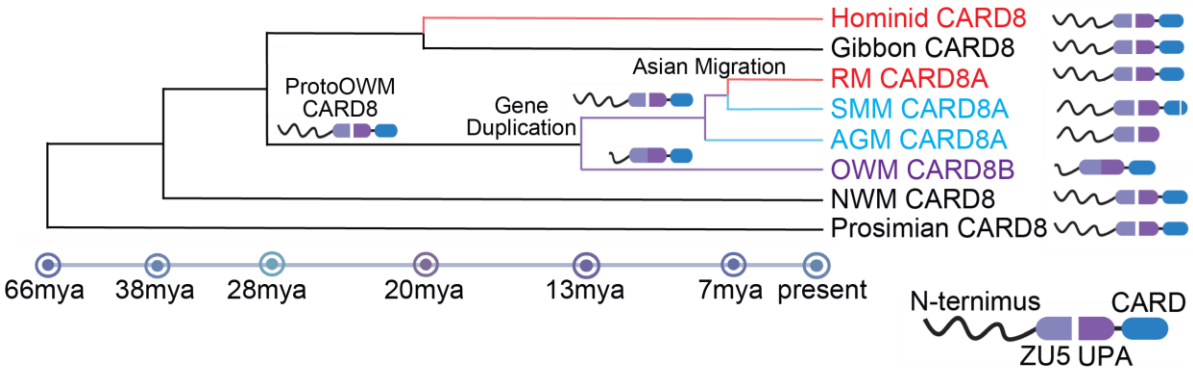

Figure 3.5: Theory of CARD8 Evolution in NHPs

The evolution of non-human primate CARD8 depicting key events in its evolution. CARD8 underwent a reverse tandem gene duplication in the ancestor to old world monkeys (OWM) giving rise to a non-functional CARD8B and a functional CARD8A. The CARD8A of non-pathogenic hosts in Africa underwent further selection leading to non-functionalization of the protein whereas the Asian migration of macaques allowed for escape from this selective pressure. Speciation dates are estimated based on recently published findings.[36] NWM – new world monkeys.

3.4 Discussion

Pathogenic HIV infection of humans and SIVmac infection of rhesus macaques (RMSs) are characterized by progressive $CD4^+$ T cell depletion even though productive viral infection is largely confined to activated $CD4^+$ T cells, the majority of which are already destined to die rapidly regardless of infection.[24] In contrast, non-pathogenic SIV infection of natural SIV hosts,

such as sooty mangabyes (SM) and African green monkeys (AGMs) is associated with normal or near normal $CD4^+$ T cell counts despite chronic high levels of virus replication. These observations prompted a series of investigations aimed clarifying the mechanisms responsible for the death of non-productively infected $CD4^+$ T cells during pathogenic HIV and SIV infections (or, conversely, the mechanisms allowing the survival of these cells during non-pathogenic SIV infection of SMs and AGMs). Of note, during pathogenic SIV infection of RMs, the rapid depletion of $CD4^+$ T cells by CCR5- or CXCR4-tropic chimeric simian–human immunodeficiency virus (SHIV) involves predominantly $CCR5^+$ memory cells or $CXCR4^+$ cells, respectively, strongly suggesting that the mechanism for $CD4^+$ T-cell depletion involves viral entry or at least co-receptor engagement by the *env* glycoprotein.[7] In addition, the observation that the vast majority of $CD4^+$ T cells die of pyroptosis during pathogenic SIV infection in RMs[9,10] raised the question of what molecular mechanism(s) triggers inflammasome activation in $CD4^+$ T cells after the HIV/SIV envelope protein engages the co-receptor, and if that phenomenon requires virus entry.

In the current study, we provide for the first time substantial experimental evidence indicating that the $CD4^+$ T cell depletion associated with pathogenic primate lentiviral infections is caused by an aberrant activation of the CARD8 inflammasome pathway. In addition, we posit that those primate species that have evolved to be natural hosts for non-pathogenic SIV infections (i.e., SMs and AGMs) have developed truncations in the CARD domain of the CARD8 locus that could have been expedited by the presence of CARD8B. While the molecular dynamics of both copies of CARD8 (i.e., “A” and “B”) are not fully understood, we believe that CARD8B may retain additional yet unknown functions of CARD8 that allowed, in evolutionary terms, for the ablation of its inflammasome activity in response to persistent SIV infection.

While in this study we offer a snapshot of the predicted splicing patterns of these CARD8 genes in various NHP species, future work will focus on a comparative *in vivo* functional analysis of the CARD8 inflammasome system in these species. Future work will also investigate whether the two copies of CARD8 gene could be working in concert via subfunctionalization to retain a low level of inflammasome activity.

While the function of various components of inflammasomes has been studied in T cells, the CARD8 inflammasome is best characterized to trigger pyroptosis in human lymphocytes.[25] In this regard, our work emphasizes the need for further investigation into CARD8 functionality in NHPs *in vivo*, as the paucity of available *in vivo* experimental systems and reagent limitations have hindered a more thorough investigation of this molecular pathway in these highly relevant models of HIV/AIDS pathogenesis. Of note, SIV can activate the CARD8 inflammasome of RMs and chimpanzee *in vitro*, thus laying the ground for future studies of the role of CARD8 in SIV pathogenesis, for instance by assessing the impact of CARD8 blockade and/or inhibition and/or gene targeting in RMs.

In conclusion, the current study defines a novel paradigm to explain the marked differences observed in the clinical outcomes of primate lentiviral infections between pathogenic, experimental hosts, such as humans and RMs, versus non-pathogenic, natural hosts, such as SMs and AGMs. According to this paradigm, the progressive $CD4^+$ T cell depletion that characterizes pathogenic infections and involves predominantly cells that are not experiencing productive viral infection, is due to the activation of the CARD8 inflammasome which follows virus entry into $CD4^+$ T-cells. The contribution of this novel mechanism of $CD4^+$ T cell depletion to the progressive immune deficiency which characterizes pathogenic lentiviral infections remains to

be determined, as well as its relationship with previously described, non-mutually exclusive mechanisms of disease progression.

3.5 Materials and Methods

3.5.1 Non-Human Primate Samples

For the *in vitro* studies involving non-human primate samples, we used cryopreserved peripheral blood mononuclear cells (PBMCs) that had been isolated from 30 ml blood collections obtained by standard venipuncture from Indian origin rhesus macaques (RMs) (Macaca mulatta) and sooty mangabeys (SMs) (Cercocebus atys) housed at the Emory National Primate Research Center (ENPRC) of Emory University, which is one of the seven centers belonging to the NIH-sponsored National Primate Research Center Program (NPRCP). All animals were housed according to the Institutional Animal Care and Use Committee (IACUC) rules and regulations, and all blood collections were approved by existing IACUC protocols.

3.5.2 Cell Lines

HEK 293T cells, Vero-E6 cells, CEM-174 cells, and ACH-2 cells were cultured in DMEM or RPMI containing 10% heat-inactivated fetal bovine serum (FBS), 1 U/ml penicillin, and 100 mg/ml streptomycin. THP-1 cells, carrying doxycycline-inducible CARD8 expression cassettes were described previously,[39] were cultured in RPMI 1640 medium supplemented with 10% FBS, 1 U/ml penicillin, and 100 mg/ml streptomycin. Blood or tonsil $CD4^+$ T cells were isolated using a human CD4+ T cell isolation kit. Purified $CD4^+$ T cells were used without stimulation or co-stimulated with plate-bound CD3 and soluble CD28 antibodies in the presence of 20 ng/ml IL-2 for three days. Human $CD34^+$ cells were isolated from cord blood using

EasySep™ human cord blood CD34 positive selection kit, which was then cryopreserved in Iscove's Modified Dulbecco's Medium (IMDM) containing 7.5% DMSO. The cryopreserved $CD34^+$ cells were thawed and cultured in IMDM supplemented with 50 ng/ml SCF, 50 ng/ml Flt3L, and 50 ng/ml TPO for 12 hours before electroporation.

3.5.2 Phylogenetic Analysis

The NHP species tree was generated from the NCBI taxonomy browser and adjusted for recently published data which has provided whole genome phylogenomic relationships of these species.[22,23] For the CARD8 gene trees, the NCBI and ensemble databases were used to collect the protein sequence of the longest isoform for each gene.[26] Each sequence entry can be found in **Table S3-5**. Sequences were aligned via ClustalW in MEGA11.[27] MEGA11's "Find Best DNA/Protein Models (ML)" tool was used to identify the most appropriate phylogenetic tree method. For all cases, the best model was the Jones-Taylor-Thornton (JTT) model with Gamma distribution. The Maximum likelihood trees were generated in MEGA11 with the JTT+G model with default settings. For primate phylogenies, Tupaia chinensis was selected for rooting and for the mammal phylogeny the monotremes were selected as the root. Newick trees were exported from MEGA11 and imported into python v3.8.5 and the ETE3 v3.1.3 toolkit was used to generate the phylogenetic trees.[28] Domain architecture was added via the ETE3 toolkit and was identified via the multiple sequence alignment of the sequences to the human reference. The corresponding locations were used as the predicted domain constraints. Trees were exported to adobe illustrator for cosmetic changes, branch distances were left untouched, and the addition of the species specific silhouettes were obtained from PhlyoPic and the attribution and license information can be found at the following permalink:

https://www.phylopic.org/permalinks/4e99be51d1c165798c1fea2747e55e9b95afb0b21c3248bea30cb0b757878ae8.

For the multiple sequence alignment visualizations, a subset of the CARD8 or IFI16 sequences was used for alignment as described above. The resulting alignments were visualized using the pymsaviz package v0.4.0 in python. Homology of IFI16 was assessed using NCBI BLASTP. The graphical overview of NHP CARD8 was created using BioRender and the speciation dates were calculated using previously published estimates.

3.5.4 Plasmids and Viruses

To prepare replication-defective HIV reporter viruses, HEK 293T cells were transfected with pNL4-3-Δ*Env*-EGFP (NIH HIV Reagent Program #11100), pNL4-3-Δ*Env*-EGFP-RT-D110A-D185A or pNL4-3-Δ*Env*-EGFP-IN-D116A, and the NL4-3 envelope expressing plasmid or pVSV-G. The replication-competent HIV_{NL4-3} was prepared by transfecting HEK293T with pNL4-3. The replication-competent HIV_{BaL} was produced by infecting CD8-depleted PHA-stimulated PBMCs. The culture supernatant was collected six to nine days post-infection. The lentiviruses were also produced in HEK 293T cells by co-transfecting pLKO.1puro, psPAX2, and NL4-3 envelope expressing plasmid. Viral stocks were concentrated with the Lenti-X Concentrator. SIVagm Tan-1 GFP was described previously.[29] SIVmac 251 (NIH HIV Reagent Program #253) was used to infect CEM-174 cells for expansion, infected CEM-174 cells were replenished with uninfected CEM-174 cells every 2-3 days and the supernatant was collected and concentrated via the Lenti-X concentrator.

3.5.5 NHP Construct Generation

The longest isoform for each gene of CARD8 from each NHP species was synthesized using IDT or Genscript gene synthesis, the protein sequences can be found in **Table S4**. These constructs were ligated into the pcdna 3.1 vector for mammalian expression as previously published. The N-terminal HA-FLAG tags were replaced by 3xHA tags to improve pull down and western blotting efficiency when the genes were synthesized. To generate dox-inducible CARD8 constructs for expression in *CARD8-KO* THP-1 cells, primers were used to alter the CARD8 sgRNA target site and placed into the doxycycline inducible vector as previously published. N-terminal CARD8 swapping was conducted via PCR to add on the N-terminal to the start of the FIIND domain to the other species FIIND-CARD for rhesus macaque and African green monkey CARD8.

3.5.6 Immunoblotting and ELISA

For GSDMD cleavage detection, the unstimulated $CD4^+$ T cells were spinoculated with X4-NL4-3-Δ*Env*-EGFP reporter virus for two hours and incubated for another hour. For IL-1β cleavage assay, *CARD8*-KO HEK293T cells (4×10^5) were seeded in 12-well plates and cultured overnight before transfection. Each well was co-transfected with plasmids encoding CASP1 (2 ng), pro-IL-1β (200 ng), and WT or mutant CARD8 (5 ng), together with HIV-1 or SIV_{agm}Tan1-GFP (1μg). Cells were harvested 24 hours post-transfection. For autoprocessing westerns of NHP CARD8, HEK293T or Vero-E6 cells were transfected with NHP CARD8 (1μg) as above and protein was collected 24 hours post-transfection. For doxycycline-inducible expression $CARD8^{WT}$, $CARD8^{S297A}$, and $CARD8^{F59GF60G}$ in *CARD8*-KO THP-1 cells, cells were pre-treated with doxycycline (1 μg/ml) for two days and then treated with DMSO or indicated inhibitors for

30 minutes. The treated cells were then infected with VSVG pseudotyped NL4-3-Δ*Env*-EGFP viruses for three hours. Doxycycline-treated THP-1 cells were stimulated with lipopolysaccharide (50 ng/ml) for three hours, washed twice with PBS, and infected with VSVG pseudotyped NL4-3-Δ*Env*-EGFP viruses for six hours. The culture supernatant was used for IL-1β ELISA. To test VbP activation of dox-inducible NHP CARD8, cells were treated with doxycycline as above for two days prior to treatment with VbP for six hours.

3.5.7 Cell Viability and LDH Release Assays

For the assessment of the cell viability, cells were washed with PBS and incubated with Zombie Violet for 30 minutes in accordance with the manufacturer's instructions. Cell viability measurement is based on the detection of ATP by the CellTiter-Glo® Luminescent Cell Viability Kit, or from the CyQUANT LDH Cytotoxicity Assay kit. For the Annexin V and Propidium Iodide staining, cells were washed with PBS and then incubated with Annexin V and Propidium Iodide (PI) in Annexin V Binding Buffer for 15 min at room temperature. Adding Annexin V Binding Buffer and the cells were analyzed by flow cytometry. The supernatants were collected after infection to determine the activity of LDH, and the LDH assay was performed according to the manufacturer's instructions.

3.5.8 In vitro Assessment of CARD8 Cleavage by HIV and SIV Protease

We obtained purified human and NHP CARD8 and HIV and SIV protease to assess cleavage *in vitro*. To express and purify HIV and SIV protease, HIV or SIV codon-optimized protease was cloned into pST50Trc (Addgene, # 64000) by using BamHI and EcoRI restriction sites. Protease expression and purification were performed as previously described for HIV-1 protease.[30,31] Freshly purified protease was used for CARD8 cleavage. To purify CARD8 proteins, HEK293T

cells were transfected with 10 μg of plasmids encoding the HA-tagged CARD8 in 10-cm dishes. Two days after transfection, cells were collected and lysed in 1x RIPA lysis buffer supplemented with 0.5 mM DTT and complete EDTA-free protease inhibitor cocktail (Roche). CARD8 was immunoprecipitated using 40 μL of Protein G Dynabeads® (Life Technologies) conjugated with a mouse anti-HA antibody (Biolegend, #901515). After immunoprecipitation, beads were washed three times with 1x RIPA buffer and once with protease cleavage buffer (50 mM sodium acetate, 50 mM Na-MES, 100 mM Tris, 2 mM beta-mercaptoethanol, pH 6.5). Beads were then resuspended in 200 μL of protease cleavage buffer for the cleavage assay. To perform cleavage, 10 μL viral protease was added on top of the beads bearing immunoprecipitated CARD8 and incubated at 30°C for 30 minutes on a thermal mixer set at 1200rpm. The eluate from the beads were analyzed by immunoblotting.

3.5.9 Co-Culture for $CD4^+$ T Cell Depletion in NHP PBMCs

CEM-174 cells were infected with $SIV_{mac}251$ or HIV_{NL4-3} for 6-9 days. Additional uninfected CEM-174 cells were added to the infected culture every 2-3 days depending on cell viability to allow for expansion of the viruses. Human and NHP PBMCs were cultured in RPMI 1640 medium supplemented with 10% FBS, 1 U/ml penicillin, and 100 mg/ml streptomycin in the presence of IL-7 and IL-15. For co-culture, 10^5 PBMC were labelled with CFSE and treated with 50 μM VX765 and co-cultured with 5×10^5 SIV- or HIV_{NL4-3}-infected CEM-174 cells for 16 hours. Flow cytometry analysis was conducted as with the human co-culture experiments.

3.5.10 Statistical Analysis

The statistical analysis was conducted using Prism 9. Phylogenetic statistics and analysis were performed as above. The methods for statistical analysis are described in the figure legends. The error bars indicate the standard error of the mean.

3.6 Contributions

L.S., Q.W., and K.M.C. designed the study and analyzed the data. Q.W. performed all human related experiments and analysis. K.C. performed the phylogenetic analysis and performed most NHP experiments. Q.W. conducted the NHP IL-1β cleavage experiments, R.T. performed the *in vitro* cleavage of NHP CARD8. G.S., and T.H.B. provided NHP samples. G.S. assisted in the design of the NHP experiments. L.S., Q.W., K.C., and G.S. wrote the manuscript.

3.7 Acknowledgements

The following reagents were obtained through the AIDS Research and Reference Reagent Program, Division of AIDS, NIAID, NIH: NIH: CEM-174 cell line, ACH-2 cell line, $SIV_{mac}251$, lopinavir, T20, tenofovir, raltegravir, efavirenz, nevirapine, pNL4-3, pNL4-3-GFP. This work was supported by NIH grants R01AI162203 and R01AI155162 to LS, F31AI165251 to KMC, and supported in part by the CRISPR for Cure Martin Delaney Collaboratory for HIV cure UM1AI164568 cofunded by NIAID, NIMH, NIDA, NINDS, NIDDK, and NHLB.

3.8 Supplementary Figures and Tables

Species name	Common name	Superorder	Protein Accession	Protein Length
Echinops telfairi	Small Madagascar Hedgehog	Afrotheria	XP_024610730.1	373
Neophocaena asiaeorientalis asiaeorientalis	Yangtze Finless Porpoise	Laurasiatheria	XP_049566240.1	625
Orcinus orca	Killer Whale	Laurasiatheria	XP_028925829.1	638
Tursiops truncatus	Common Bottlenose Dolphin	Laurasiatheria	XP_007941216.2	497
Phocoena sinus	Vaquita	Laurasiatheria	XP_042775368.1	625
Monodon monoceros	Narwhal	Laurasiatheria	XP_020844513.1	625
Balaenoptera musculus	Blue Whale	Laurasiatheria	XP_032485278.1	513
Canis lupus familiaris	Dog	Laurasiatheria	XP_028361024.1	534
Puma concolor	Cougar	Laurasiatheria	XP_023380256.1	554
Felis catus	Domestic Cat	Laurasiatheria	XP_025770087.1	555
Lutra lutra	Eurasian River Otter	Laurasiatheria	XP_031813451.1	545
Hyaena hyaena	Striped Hyena	Laurasiatheria	XP_020925386.1	554
Ursus arctos	Brown Bear	Laurasiatheria	XP_038602695.1	529
Ailuropoda melanoleuca	Giant Panda	Laurasiatheria	XP_023591965.1	541
Zalophus californianus	California Sea Lion	Laurasiatheria	XP_019801795.1	554
Neomonachus schauinslandi	Hawaiian Monk Seal	Laurasiatheria	XP_026337717.1	496
Pteropus vampyrus	Large Flying Fox	Laurasiatheria	XP_027731972.1	518
Phyllostomus discolor	Pale Spear-Nosed Bat	Laurasiatheria	XP_027475648.1	508
Dasypus novemcinctus	Nine-Banded Armadillo	Xenartha	XP_024610730.1	609
Sarcophilus harrisii	Tasmanian Devil	Marsupiala	XP_049566240.1	549
Monodelphis domestica	Gray Short-Tailed Opossum	Marsupiala	XP_028925829.1	521
Phascolarctos cinereus	Koala	Marsupiala	XP_007941216.2	524

Vombatus ursinus	Common Wombat	Marsupiala	XP_042775368.1	524
Erinaceus europaeus	Western European Hedgehog	Laurasiatheria	XP_020844513.1	513
Ornithorhynchus anatinus	Platypus	Monotremata	XP_032485278.1	508
Tachyglossus aculeatus	Australian Echidna	Monotremata	XP_028361024.1	509
Equus caballus	Horse	Laurasiatheria	XP_023380256.1	580
Choloepus didactylus	Southern Two-Toed Sloth	Laurasiatheria	XP_025770087.1	536
Loxodonta africana	African Savanna Elephant	Afrotheria	XP_031813451.1	531
Trichechus manatus latirostris	Florida Manatee	Afrotheria	XP_020925386.1	409
Orycteropus afer afer	Aardvark	Afrotheria	XP_038602695.1	387
Panthera leo	Lion	Laurasiatheria	XP_023591965.1	577
Mus spretus	Algerian Mouse	Euarchontoglires	XP_019801795.1	578
Mus pahari	Shrew Mouse	Euarchontoglires	XP_026337717.1	504
Camelus bactrianus	Bactrian Camel	Laurasiatheria	XP_027731972.1	567
Ceratotherium simum simum	Rhinoceros	Laurasiatheria	XP_027475648.1	516
Sus scrofa	Pig	Laurasiatheria	XP_024610730.1	535

Supplementary Table 3.1: Mammalian CARD8 Sequences

CARD8 sequences for the mammals used to create Figure 3.4 and their classification.

Species name	Common Name	Protein Accession	Protein Length	Database
Aotus nancymaae	Nancy Ma's Night Monkey	XP_021524182.1	586	NCBI
Callithrix jacchus	Common Marmoset	XP_008986567.3	532	NCBI
Cebus imitator	Panamanian White-Faced Capuchin	XP_017355929.1	564	NCBI
Cercocebus atys A	Sooty Mangabey	ENSCATT00000020868	515	Ensembl
Cercocebus atys B	Sooty Mangabey	ENSCATT00000039130	349	Ensembl
Chlorocebus sabaeus A	African Green Monkey	ENSCSAT00000000907	423	Ensembl
Chlorocebus sabaeus B	African Green Monkey	ENSCSAT00000000918	444	Ensembl
Colobus angolensis palliates A	Angolan Colobus	XP_011801862.1	426	NCBI
Colobus angolensis palliates B	Angolan Colobus	XP_011801863.1	426	NCBI
Gorilla gorilla gorilla	Western Lowland Gorilla	ENSGGOT00000000261	522	Ensembl
Homo sapiens	Humans	NP_001171829.1	537	NCBI
Hylobates moloch	Silvery Gibbon	XP_032025189.1	537	NCBI
Macaca fascicularis A	Crab-Eating Macaque	XP_045236815.1	533	NCBI
Macaca fascicularis B	Crab-Eating Macaque	XP_045236836.1	444	NCBI
Macaca mulatta A	Rhesus Macaque	XP_028694412.1	533	NCBI
Macaca mulatta B	Rhesus Macaque	XP_014979939.2	444	NCBI
Macaca nemestrina A	Pigtail Macaque	ENSMNET00000062826	479	Ensembl
Macaca nemestrina B	Pigtail Macaque	XP_024647661.1	426	NCBI
Macaca thibetana thibetana A	Thibetan Macaque	XP_050628397.1	533	NCBI
Macaca thibetana thibetana B	Thibetan Macaque	XP_050628495.1	444	NCBI
Mandrillus leucophaeus	Drill	ENSMLET00000002967	349	Ensembl
Nomascus leucogenys	Northern White-Cheeked Gibbon	XP_030676824.1	537	NCBI
Otolemur garnetti	Northern Greater Galago	XP_023363700.1	566	NCBI
Pan paniscus	Bonobo	XP_003814147.2	537	NCBI
Pan troglodytes	Chimpanzee	ENSPTRT00000087479	537	ensembl
Papio anubis	Olive Babboon	ENSPANT00000008509	387	Ensembl
Pongo abelii	Sumatran Orangutan	ENSPPYT00000051462	537	Ensembl

Rhinopithecus roxellana A	Golden Snub-Nosed Monkey	XP_030798493.1	534	NCBI
Rhinopithecus roxellana B	Golden Snub-Nosed Monkey	XP_010375680.2	444	NCBI
Saimiri boliviensis	Black-Capped Squirrel Monkey	XP_003940505.2	531	NCBI
Sapajus apella	Tufted Capuchin	XP_032126901.1	564	NCBI
Symphalangus syndactylus	Siamang	XP_055091816.1	537	NCBI
Trachypithecus francoisi A	François' Leaf Monkey	XP_033079745.1	534	NCBI
Trachypithecus francoisi B	François' Leaf Monkey	XP_033079745.1	534	NCBI
Tupaia chinensis	Chinese Tree Shrew	XP_006142263.2	660	NCBI

Supplementary Table 3.2: Non-Human Primate Sequences

Table of CARD8 sequences from the non-human primate species used in the phylogenetic analysis.

Species Name	Common Name	Protein Accession	Protein Length	Database
Aotus nancymae	Nancy Ma's Night Monkey	XP_021523053.1	593	NCBI
Callithrix jacchus	Common Marmoset	XP_008982935.1	524	NCBI
Cebus imitator	Panamanian White-Faced Capuchin	XP_017359172.1	520	NCBI
Cercocebus atys	Sooty Mangabey	XP_011948694.1	729	NCBI
Chlorocebus sabaeus	African Green Monkey	XP_007974780.2	728	NCBI
Colobus angolensis palliatus	Angolan Colobus	XP_011812558.1	733	NCBI
Gorilla gorilla gorilla	Western Lowland Gorilla	XP_018880631.2	733	NCBI
Homo sapiens	Humans	NP_001363517.1	729	NCBI
Hylobates moloch	Silvery Gibbon	XP_032009943.1	727	NCBI
Macaca fascicularis	Crab-Eating Macaque	XP_005541376.2	729	NCBI
Macaca mulatta	Rhesus Macaque	NP_001248590.1	729	NCBI
Macaca nemestrina	Pigtail Macaque	XP_011768309.1	729	NCBI
Macaca thibetana thibetana	Thibetan Macaque	XP_050613781.1	727	NCBI
Mandrillus leucophaeus	Drill	XP_011834012.1	729	NCBI
Nomascus leucogenys	Northern White-Cheeked Gibbon	XP_003258725.1	727	NCBI
Otolemur garnettii	Northern Greater Galago	XP_023372191.1	711	NCBI
Pan paniscus	Bonobo	XP_008972711.3	733	NCBI
Pan troglodytes	Chimpanzee	XP_009433469.1	733	NCBI
Papio anubis	Olive Babboon	XP_003892929.2	725	NCBI
Pongo abelii	Sumatran Orangutan	ENSPPYT00000061469	729	Ensembl
Rhinopithecus roxellana	Golden Snub-Nosed Monkey	ENSRROT00000040470	729	Ensembl
Saimiri boliviensis boliviensis	Black-Capped Squirrel Monkey	XP_039316010.1	524	NCBI
Sapajus apella	Tufted Capuchin	XP_032116655.1	520	NCBI
Trachypithecus francoisi	François' Leaf Monkey	XP_033052769.1	729	NCBI
Tupaia chinensis	Chinese Tree Shrew	XP_014447307.1	869	NCBI

Supplementary Table 3.3: Non-Human Primate IFI16 Sequences

Table of non-human primate IFI16 sequences used in phylogenetic analysis.

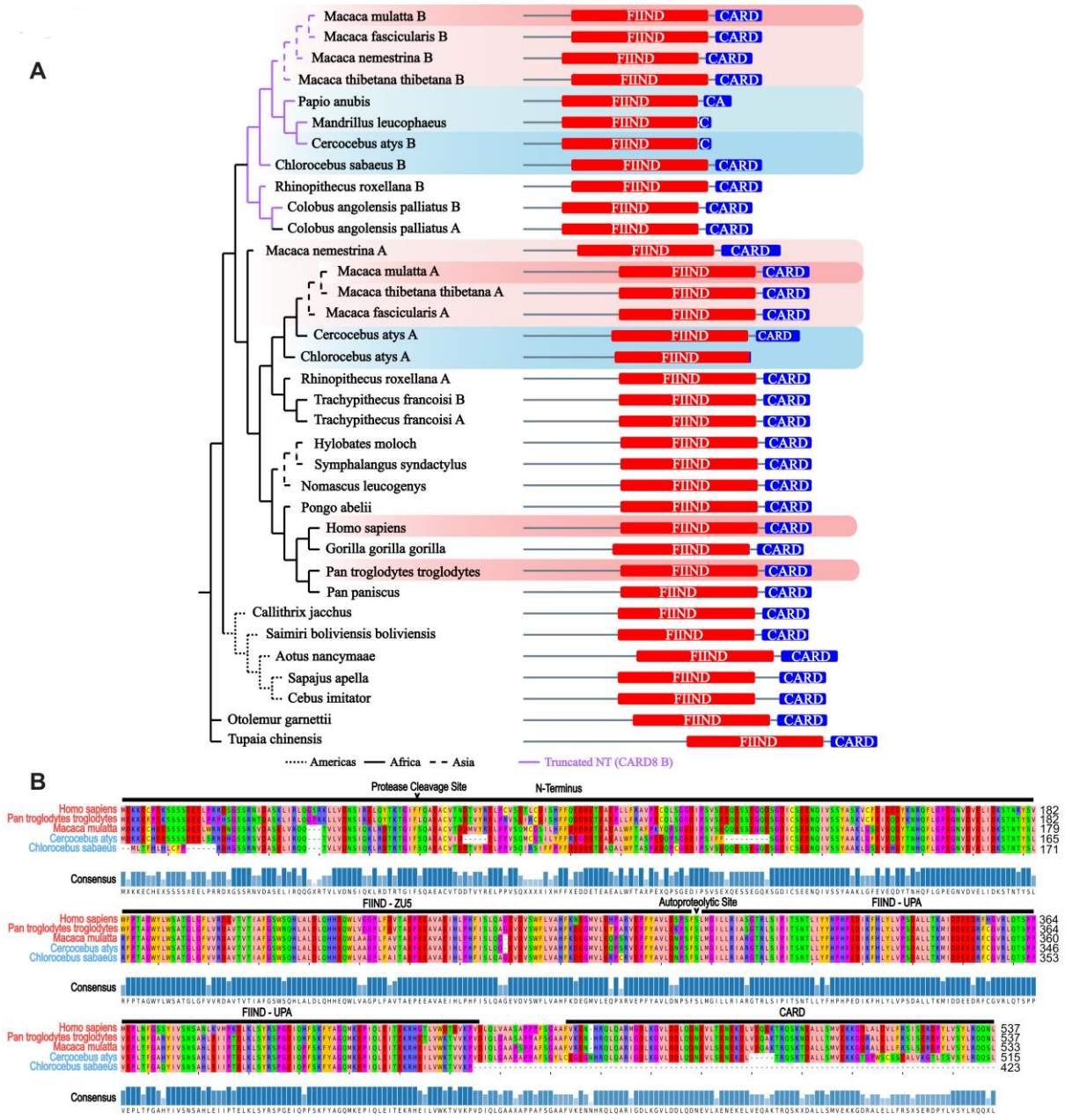

Supplementary Figure 3.1: Phylogenetic Analysis of CARD8A and B from Non-Human Primates

(a) Maximum likelihood tree of the CARD8 protein sequences from the longest isoform of each gene present in non-human primates. The predicted protein domain architecture to the right is based on alignment to the known domain constraints for human CARD8. Purple lines indicate the shared ancestry of CARD8B in *Cercopithecoidae* species which shows a severe truncation of the N-terminal region. Dashed lines indicate the geographic location of the indicated species.

Dark red shading highlights the known pathogenic hosts for SIV infection, whereas the light red indicates suspected pathogenic hosts. Dark blue shading denotes known non-pathogenic hosts of SIV infection and light blue indicates suspected non-pathogenic hosts. While *Papio anubis* and *Mandrillus leucophaeus* do not have a CARD8A there is evidence of pseudogenization of this gene for these species leaving them with only their CARD8B. The sequences used to construct this tree may be found in **Table S2**. **(b)** Multiple sequence alignment of CARD8(A) from primate species with known pathogenicity status of SIV/HIV infection. Key domains and sites are indicated above the alignment. Non-pathogenic hosts (blue) have truncations in the CARD domain rendering them non-functional whereas pathogenic hosts (red) maintain an intact CARD domain. Rhesus macaques share 89.33% and 72.80% identity with the *Cercocebus atys* and *Chlorocebus sabaeus* CARD8A sequences respectively via NCBI BLASTP.

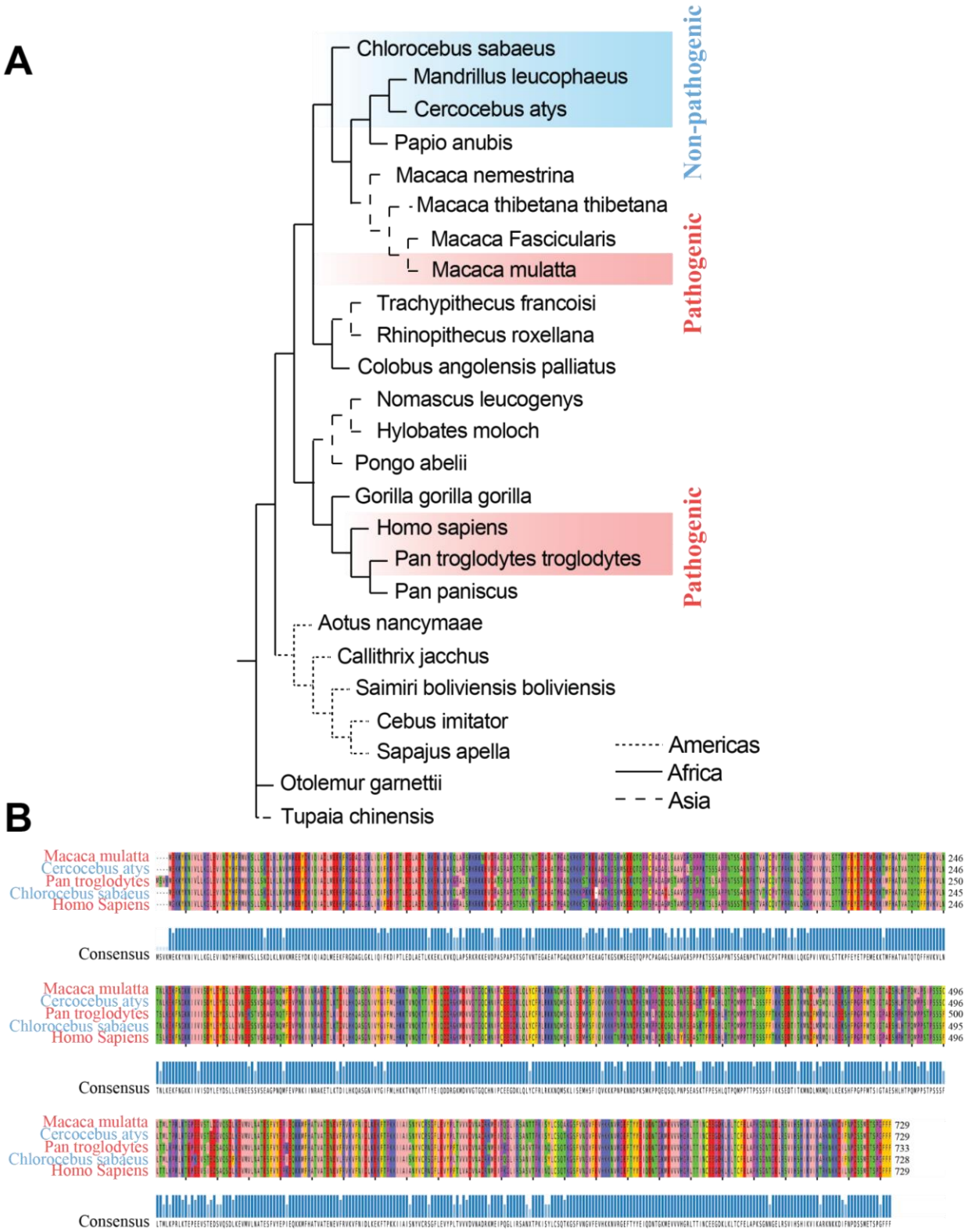
A
Chlorocebus sabaeus
Mandrillus leucophaeus
Cercocebus atys
Papio anubis
Macaca nemestrina
Macaca thibetana thibetana
Macaca Fascicularis
Macaca mulatta
Trachypithecus francoisi
Rhinopithecus roxellana
Colobus angolensis palliatus
Nomascus leucogenys
Hylobates moloch
Pongo abelii
Gorilla gorilla gorilla
Homo sapiens
Pan troglodytes troglodytes
Pan paniscus
Aotus nancymaae
Callithrix jacchus
Saimiri boliviensis boliviensis
Cebus imitator
Sapajus apella
Otolemur garnettii
Tupaia chinensis
Non-pathogenic
Pathogenic
Pathogenic
Americas
Africa
Asia
B
Macaca mulatta
Cercocebus atys
Pan troglodytes
Chlorocebus sabaeus
Homo Sapiens
Consensus
246
246
250
245
246
496
496
500
495
496
729
729
733
728
729

Supplementary Figure 3.2: IFI16 Follows the Predicted Evolutionary Relationships of NHPs

(a) Maximum likelihood phylogenetic tree for the multiple sequence alignments of non-human primate IFI16 protein sequences. Known pathogenic hosts are highlighted in red and known non-pathogenic hosts are highlighted in blue. This tree shows very few differences from the expected evolutionary relationships seen in a) and indicates far less genetic variation than the phylogenetic trees for CARD8. The sequences used to construct this tree may be found in **Table S3**. **(b)** Multiple sequence alignment of IFI16 from primate species with known pathogenicity status of SIV/HIV infection. There is far less variation between pathogenic and non-pathogenic hosts in comparison to the CARD8 alignment in **Figure S1b**. Rhesus macaques share 98.22% and 96.84% identity with the *Cercocebus atys* and *Chlorocebus sabaeus* IFI16 sequences respectively via NCBI BLASTP.

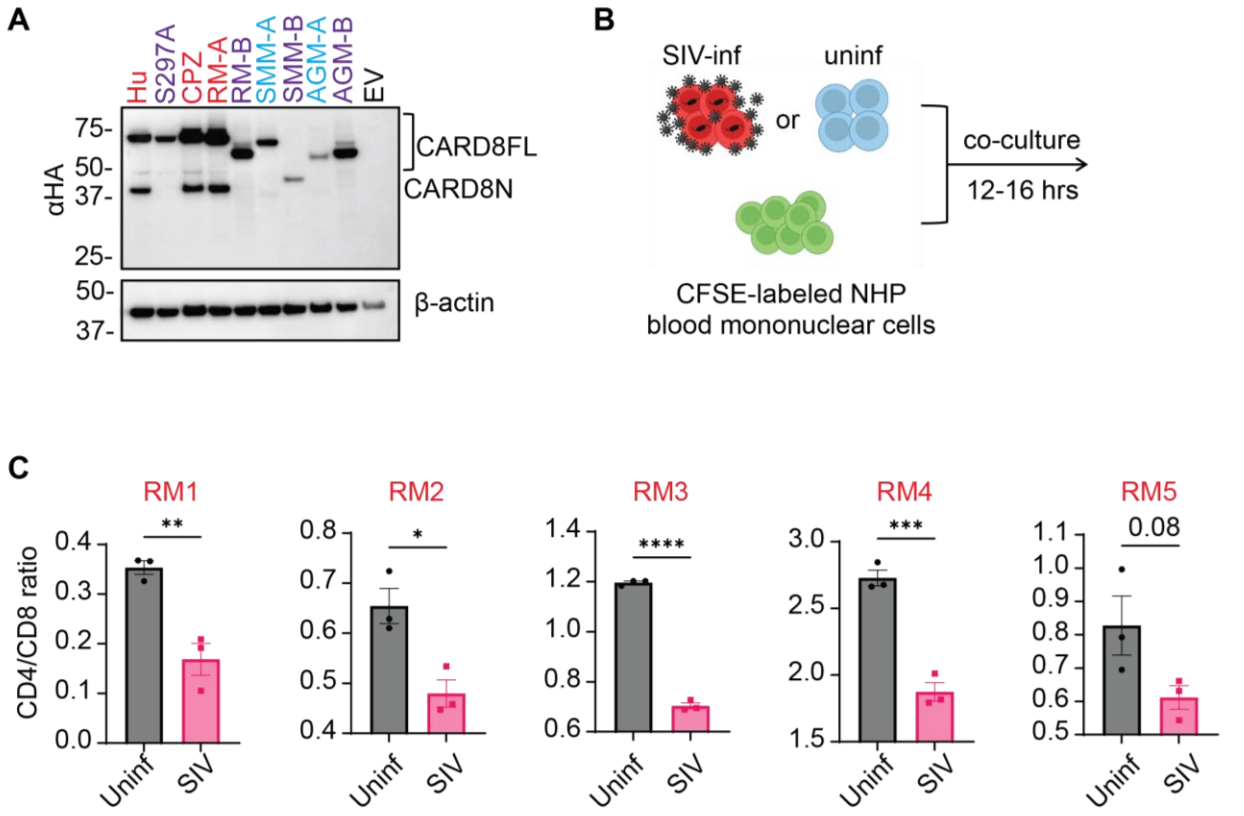

Supplementary Figure 3.3: CARD8 Functions in NHPS.

(**a**) Autoprocessing of NHP CARD8. Vero cells were transfected with plasmids expressing HA-tagged CARD8 from Hu and CPZ, and CARD8A and CARD8B from RM, SMM, and AGM. (**b**) The co-culture schemes. CEM-174 cells were infected with either HIV_{NL4-3} or SIV_{mac251} for six days. Virus-producing cells were then co-cultured at a 5:1 ratio with CFSE-labeled human or RM PBMCs. (**c**) Rapid loss of RM $CD4^+$ T cells. Co-culture of PBMCs from five RMs with SIVmac251-infected CEM-174 cells. CD4/CD8 ratio was measured 12-16 hours post co-culture. *p* values were calculated using an unpaired two-tailed t-test. * $p < 0.05$, ** $p < 0.01$, ***$p < 0.001$, and **** $p < 0.0001$. Error bars show mean values with SEM.

3.9 References

1. Finkel, T.H. et al. Apoptosis occurs predominantly in bystander cells and not in productively infected cells of HIV- and SIV-infected lymph nodes. *Nat. Med.* **1**, 129-134 (1995).
2. Harouse, J.M. et al. Distinct pathogenic sequela in rhesus macaques infected with CCR5 or CXCR4 utilizing SHIVs. *Science* **284**, 816-819 (1999).
3. Picker, L.J. et al. Insufficient production and tissue delivery of CD4+ memory T cells in rapidly progressive simian immunodeficiency virus infection. *J. Exp. Med.* **200**, 1299-1314 (2004).
4. Barouch, D.H. et al. Rapid Inflammasome Activation following Mucosal SIV Infection of Rhesus Monkeys. *Cell* **165**, 656-667 (2016).
5. He, X. et al. Rapid Loss of CD4 T Cells by Pyroptosis during Acute SIV Infection in Rhesus Macaques. *J. Virol.* **96**, e0080822 (2022).
6. Doitsh, G. et al. Cell death by pyroptosis drives CD4 T-cell depletion in HIV-1 infection. *Nature* **505**, 509-514 (2014).
7. Chahroudi, A. et al.Natural SIV hosts: showing AIDS the door. *Science* **335**, 1188-1193 (2012).
8. Bailes, E. et al. Hybrid origin of SIV in chimpanzees. *Science* **300**, 1713 (2013).
9. Barbian, H.J., Jackson-Jewett, R., Brown, C.S., Bibollet-Ruche, F., Learn, G.H., Decker, T., Kreider, E.F. et al.Effective treatment of SIVcpz-induced immunodeficiency in a captive western chimpanzee. *Retrovirology* **14**, 35 (2017).
10. Etienne, L. et al. Nerrienet, E., LeBreton, M., Bibila, G.T., Foupouapouognigni, Y., Rousset, D., Nana, A. et al. Characterization of a new simian immunodeficiency virus strain in a naturally infected Pan troglodytes troglodytes chimpanzee with AIDS related symptoms. *Retrovirology* **8**, 4 (2011).
11. Keele, B.F. et al. Increased mortality and AIDS-like immunopathology in wild chimpanzees infected with SIVcpz. *Nature* **460**, 515-519 (2009).
12. Joas, S. et al.Species-specific host factors rather than virus-intrinsic virulence determine primate lentiviral pathogenicity. *Nat. Commun.* **9**, 1371 (2018).
13. Pandrea, I., Silvestri, G., & Apetrei, C. AIDS in african nonhuman primate hosts of SIVs: a new paradigm of SIV infection. *Curr. HIV Res.* **7**, 57-72 (2009).
14. Silvestri, G. et al. Nonpathogenic SIV infection of sooty mangabeys is characterized by limited bystander immunopathology despite chronic high-level viremia. *Immunity* **18**, 441-452 (2003).
15. Brenchley, J.M. et al. Microbial translocation is a cause of systemic immune activation in chronic HIV infection. *Nat. Med.* **12**, 1365-1371 (2006).
16. Klatt, N.R. et al. Availability of activated CD4+ T cells dictates the level of viremia in naturally SIV-infected sooty mangabeys. *J. Clin. Invest.* **118**, 2039-2049 (2008).
17. Palesch, D. et al. Sooty mangabey genome sequence provides insight into AIDS resistance in a natural SIV host. *Nature* **553**, 77-81 (2018).
18. Brenchley, J.M. et al.Differential infection patterns of CD4+ T cells and lymphoid tissue viral burden distinguish progressive and nonprogressive lentiviral infections. *Blood* **120**, 4172-4181 (2012).

19. Cartwright, E.K. et al. Divergent CD4+ T memory stem cell dynamics in pathogenic and nonpathogenic simian immunodeficiency virus infections. *J. Immunol.* **192**, 4666-4673 (2014).
20. Paiardini, M. et al. Low levels of SIV infection in sooty mangabey central memory CD(4)(+) T cells are associated with limited CCR5 expression. *Nat. Med.* **17**, 830-836 (2011).
21. Kuderna, L.F.K. et al. A global catalog of whole-genome diversity from 233 primate species. *Science* **380**, 906-913 (2023).
22. Schoch, C.L. et al. NCBI Taxonomy: a comprehensive update on curation, resources and tools. *Database (Oxford)* (2020*)*.
23. Shao, Y. et al. Phylogenomic analyses provide insights into primate evolution. *Science* **380**, 913-924 (2023).
24. Douek, D.C., Picker, L.J., & Koup, R.A. T cell dynamics in HIV-1 infection. *Annu. Rev. Immunol.* **21**, 265-304 (2003).
25. Linder, A., & Hornung, V. Inflammasomes in T cells. *J. Mol. Biol.* **434**, 167275 (2022).
26. Cunningham, F. et al. Ensembl 2022. *Nucleic Acids Res*. **50**, D988-D995 (2022).
27. Tamura, K., Stecher, G., & Kumar, S MEGA11: Molecular Evolutionary Genetics Analysis Version 11. *Mol. Biol. Evol.* **38**, 3022-3027 (2021).
28. Huerta-Cepas, J., Serra, F., & Bork, P. ETE 3: Reconstruction, Analysis, and Visualization of Phylogenomic Data. *Mol. Biol. Evol.* **33**, 1635-1638 (2016).
29. Hatziioannou, T. et al. Restriction of multiple divergent retroviruses by Lv1 and Ref1. *EMBO J.* **22**, 385-394 (2003).
30. Mildner, A.M. et al. The HIV-1 protease as enzyme and substrate: mutagenesis of autolysis sites and generation of a stable mutant with retained kinetic properties. *Biochemistry* **33**, 9405-9413 (1994).
31. Ozen, A. et al. Structural basis and distal effects of Gag substrate coevolution in drug resistance to HIV-1 protease. *Proc. Natl. Acad. Sci. USA* **111**, 15993-15998 (2014).

Chapter 4: Conclusions and Future Directions

At the onset of this dissertation work, I set out to identify ways in which we could further progress on an HIV cure. As current methodologies are insufficient or unsustainable for achieving complete remission from HIV infection, it was critical to identify other approaches that could improve upon the "Shock and Kill" strategy that would be equitable in their implementation and not solely focus on strategies that could benefit the global north. Upon our lab's discovery of the CARD8 inflammasome a new direction became available for targeting HIV for elimination of the latent reservoir. In Chapter 2 I took on the task of identifying the clinical translatability of using NNRTIs for targeting the reservoir and found that alone they would be insufficient to achieve efficient clearance of HIV-1 infected cells. One of the main barriers to their implementation is NNRTIs high binding affinity for human serum proteins that results in lower intracellular concentrations in comparison to plasma concentrations. This causes ineffective activation of gag-pol dimerization and CARD8 inflammasome-mediated pyroptosis. Additionally, HIV-1 can develop NNRTI resistance mutations faster than most other antiretrovirals, which could potentially be caused by the selective pressure by the CARD8 inflammasome. These barriers highlighted the need for a way to sensitize the CARD8 inflammasome to NNRTI-mediated activation. We found that inhibiting DPP9, the negative regulator of CARD8, via small molecule inhibitors such as VbP and 1g244 could substantially sensitize the inflammasome to HIV-1 protease sensing. This sensitization completely ameliorated issues of human serum binding *in vitro* and *in vivo* thereby restoring the *in vivo* efficacy to predicted in *vitro* levels as measured by EC_{50}. We found the relationship between

DPP9 inhibitors and NNRTIs to be synergistic in nature and completely dependent upon HIV-1 protease activity and the CARD8 inflammasome. This reliance and specificity of HIV-1 protease sensing of the CARD8 inflammasome greatly reduces the potential for off-target effects of uninfected $CD4^+$ T cells in comparison to other "Shock and Kill" strategies such as those that utilize pro-apoptotic compounds.

Strikingly we also discovered that VbP was able to elicit cell death of HIV-1 infected cells on their own without the presence of NNRTIs. This finding gives rise to a new class of drugs that could be developed for targeting latent reservoirs. Our central hypothesis of this mechanism of action is that there is low levels of gag-pol dimerization that can elicit intracellular protease activity inside the cell. However, this low level of activity and cleavage of CARD8 can be overcome by DPP9 to block pyroptosis, and inhibition of this negative regulation therein allows for CARD8 activation in these cells. We also found that this relationship varied greatly by donor and viral strain used. Donor variation in VbP response leads to important questions on genetic heterogeneity in the CARD8 inflammasome pathway that can lead to differences in levels of CARD8 activity, DPP9 activity, or VbP binding affinity. These are central questions that should be investigated to understand which populations would benefit the most from this strategy and could potentially enhance our understanding of the relationship between CARD8 and DPP9. Viral based variation was also seen across a panel of HIV-1 clinical strains and in NNRTI resistance mutations. We showed that VbP can help reduce the EC_{50}'s of NNRTI RAM containing viruses, sometimes to comparable levels of Wt controls. We also noted that there were baseline differences in VbP-based killing that we hypothesize are due to differences in intrinsic gag-pol dimerization levels intracellularly. We believe this to also be true in our panel of clinical strains which we also saw increased levels of VbP activity in comparison to

replication defective viruses. This finding in conjunction with other data that showed *CARD8*-KO cells exhibited higher infection rates compared to controls gave rise to our hypothesis that CARD8 inflammasome activation may be triggered upon viral entry and is not exclusive to post-integrated viral protein production.

Future work on the topic of DPP9 inhibition will focus on identifying new compounds that are more specific for their inhibition of DPP9. VbP was originally developed as a DPP4 inhibitor and displays functionality in inhibiting DPP4, DPP8, DPP9, and FAP greatly reducing the potential specificity for DPP9. All other DPP9 inhibitors have been screened for their ability to either inhibit DPP9 enzymatic activity or their ability to activate the CARD8 inflammasome. However, these screening methods do not focus on DPP9's function as a CARD8 repressor and are not specific to enhancement of HIV-1 protease sensing. In contrast to NLRP1, CARD8 is thought to not require DPP9 enzymatic activity and relies upon conformational changes upon binding of inhibitors that negate it from catching freed C-terminal CARD8. Future screening methods should instead focus on DPP9 and CARD8 protein-protein interactions rather than enzymatic function such as screens utilizing fluorescent complementation such as Bi-FC. This could greatly increase the potency and specificity of DPP9 inhibitors to only be necessary when there is an activating signal of CARD8 such as that of HIV-1 protease cleavage of its N-terminus. Additionally, further screens should be conducted to identify more potent gag-pol dimerization inducing compounds that do not rely upon their ability to inhibit reverse transcriptase activity such as those screens conducted by Balibar and colleagues. This could again increase specificity for a "Shock and Kill" strategy and could potentially avoid issues of serum protein binding that plague the current NNRTI drug classes.

As previously mentioned, through our studies of CARD8 and DPP9 we realized that CARD8 may be activated immediately upon viral entry and does not rely upon post-integration gag-pol production. The incoming viral particle contains mature HIV protease that is released into the cytosol upon fusion of the viral particle to the host cell. We found that this was sufficient to trigger $CD4^+$ T cell loss in unstimulated $CD4^+$ T cells which are though to be a major contributor to the population susceptible to bystander cell death and overall $CD4^+$ T cell depletion. This is a landmark finding in the field as the host factor responsible for bystander cell death has eluded researchers for decades. We found this rapid cell death to be dependent upon the CARD8 inflammasome and HIV-1 protease activity *in vitro* and in humanized mice, further solidifying CARD8's role in HIV pathogenesis. Future work can now be conducted to identify CARD8's role in $CD4^+$ T cell depletion in humans and could lay the foundation for identifying inhibitors of CARD8 to prevent $CD4^+$ T cell loss in PLWH to enhance CD4 recovery and prevent disease progression.

This novel finding of CARD8's role in HIV pathogenesis led me to investigate if its role was conserved across NHP species that are susceptible to SIV infection. We initially sought to develop a NHP model for CARD8 inflammasome activation which gave rise to my investigation of CARD8 genetic heterogeneity in Chapter 3. I found that CARD8 has been present in almost all gnathostome species emphasizing its critical role throughout evolutionary history. However, stark genetic variation can be seen in many mammalian orders such as in *Carnivora* and *Rodentia* that raise questions about CARD8's evolution and selection in these species. Specifically, in the *Carnivora* order is the *Felidae* that also has an endemic lentivirus called feline immunodeficiency virus (FIV) that affects both wild large feline species such as lions, cougars, and domestic cats that lead to AIDS like symptoms in certain species. Future work will

be conducted to identify the role of feline CARD8's ability to sense FIV protease activity to see if this mechanism is conserved across mammalian species that naturally encounter lentiviral infections. These studies have the potential for great impacts in conservation biology as very little is known about FIV pathogenesis in wild species and could potentially identify susceptible species that have yet to experience spillover events. This can help to target conservation efforts to safeguard them from potential spillover events in the future.

The most striking finding in this phylogenetic analysis, however, was the identification of a reverse tandem duplication in the *Cercopithecoidae* lineage of non-human primates. We conducted an in-depth analysis of CARD8 genetic heterogeneity in NHP species and noticed that this reverse tandem duplication was present in all *Cercopithecoidae* species with annotated genomes. As the majority of species with naturally occurring SIV infections are found in members of the Cercopithecoidae lineage we hypothesize that this duplication event may have played a role in selection for avoiding SIV-mediated $CD4^+$ T cell depletion in "natural hosts". As gene duplication events allow for greater mutational rates, we posit that the enhanced variation allowed for more swift and efficient selection against disease progression in SIV affected NHPs. Importantly, when looking at the CARD8 sequences of these species we noticed that one copy of the CARD8 gene, CARD8b, had a truncation in the N-terminus of CARD8 that led to an alternative alpha-helix formation proximal to the FIIND domain that precludes CARD8 from autoprocessing. As autoprocessing is essential to CARD8's function, those proteins that lack this ability are rendered non-functional in their ability to sense viral protease activity but may maintain other unknown functions of CARD8. The other copy of CARD8, CARD8a, in these species was found to be intact in the macaque lineages but were found to have loss-of-function mutations in non-pathogenic hosts such as in *Cercocebus atys* and *Chlorocebus sabaeus*. These

species were found to have critical mutations in their CARD domains that render them incapable of activating CASP1 and inducing pyroptosis. Our central hypothesis is that these species, which have encountered SIV infection in the wild for millennia, have positively selected for mutations in the CARD domains of their CARD8a copy due to the selective pressure by SIV. This selection was mostly likely fast-tracked due to the gene duplication event allowing for greater genetic variation in the CARD8 gene. In contrast, the pathogenic hosts of infection such as in macaques have not experienced SIV infection in the wild as it is isolated to Africa and have thereby not had sufficient time for selection against CARD8 function. In the case of chimpanzees, there was a more recent spillover event and they do not have a second CARD8 copy and therefore have also not had sufficient time to develop resistance to SIV sensing by CARD8. Taken together we have developed a new hypothesis on the differences between pathogenicity of non-pathogenic and pathogenic hosts which could greatly enhance our understanding of disease progression in these animal models of SIV/HIV infection.

Further work on this topic should be conducted to understand the species level heterogeneity of CARD8 among wild populations of non-pathogenic and pathogenic hosts. Other species that have not been as well studied for SIV pathogenesis should also be undertaken as over 40 species of NHPs have been found to harbor SIV. This could help expedite our understanding of pathogenesis in these species as well as predict whether naïve species will be susceptible to SIV spillover events again contributing to conservation efforts of endangered species. Additionally, investigation into the nature of CARD8 copy number variation in non-human primates and other species which have varying levels of CNVs should be undertaken to understand the evolutionary and genetic changes CARD8 has undergone potentially in conjunction with pathogens to understand how host innate immune responses adapt to their

environments. Finally, the evolutionary and genetic relationship between CARD8 and NLRP1 are still not understood. As these are the only two proteins that contain a FIIND-CARD structure and are both regulated by DPP9, it is intuitive to hypothesize that they share a common origin or evolutionary pattern. We hypothesize that CARD8 gave rise to NLRP1 via a recombination of CARD8 with an ancestral NLRP protein. While both of these proteins are prone to CNVs and varying levels of CNVs exist across mammalian populations it will be interesting to identify the host cellular balance of CNVs of NLRP1 to CARD8 and how the host compensates for these variations such as through changes in DPP8/9.

Taken together this thesis which sets out to identify new strategies for an HIV cure has resulted in myriad avenues of investigation into pharmacology, lentiviral pathogenesis, evolution, genetics, and inflammasome biology. We found a new class of drugs for targeting the HIV-1 latent reservoir and made groundbreaking discoveries on SIV pathogenesis that can inform the field on HIV pathogenesis and ways in which natural hosts have been able to escape AIDS symptoms. Hopefully, a way can be devised to utilize the CARD8 inflammasome for clearing the latent reservoir or to develop a way to avoid disease progression.

Appendix 1: CARD8 Inflammasome Activation by HIV-1 Protease

This appendix has been reproduced and adapted from the following publication:
Kolin Clark, Qiankun Wang, and Liang Shan. CARD8 Inflammasome Activation by HIV-1 Protease. *Methods in Molecular Biology*. 2641:67-79 (Apr 2023) DOI:

A.1.1 Abstract:

The pattern recognition receptor CARD8 is an inflammasome sensor for intracellular HIV-1 protease activity. Previously, the only method for studying the CARD8 inflammasome has been through utilizing DPP8/DPP9 inhibitors including Val-boroPro (VbP) to modestly and nonspecifically activate the CARD8 inflammasome. The identification of HIV-1 protease as a target for sensing by CARD8 has opened the door for a new method of studying the underlying mechanism of CARD8 inflammasome activation. Additionally, triggering the CARD8 inflammasome offers a promising strategy for reducing HIV-1 latent reservoirs. Here we describe the methods to study CARD8 sensing of HIV-1 protease activity through non-nucleoside reverse transcriptase inhibitor (NNRTI)-mediated pyroptosis of HIV-1-infected immune cells and through an HIV and CARD8 co-transfection model.

A.1.2 Introduction:

The inflammasome is a multi-protein complex that is present in both immune and non-immune cells that, upon sensing of their cognate ligands, initiates a signaling cascade resulting in the activation of inflammatory caspases such as caspase-1 (CASP1)[1]. Inflammasome activation is initiated through sensing of a danger signal, such as pathogen-associated protease activity, by

unique pattern recognition receptors (PRRs). These PRRs are characterized as having either a caspase recruitment domain (CARD) or a pyrin domain (PYD) which can oligomerize with CASP1 leading to cleavage of pro-CASP1 to form active CASP1. Activation of CASP1 can further lead to cleavage of pro-interleukin (IL)-1β and gasdermin D (GSDMD) to induce IL-1β release and pyroptosis, respectively[2,3]. One such PRR, caspase recruitment domain 8 (CARD8), has been shown to trigger CASP1 activation in human $CD4^+$ T cells and macrophages when treated with Val-boroPro (VbP), a known inhibitor of dipeptidyl peptidase 9 (DPP9)[4-6].

CARD8 is characterized as having an unstructured N-terminal region and two key C-terminal domains: the function-to-find domain (FIIND) and a CARD domain. Full-length CARD8 undergoes autoproteolytic cleavage of the FIIND domain resulting in two non-covalently associated subunits, hereby termed the N- and C-terminal domains. The N-terminal domain contains the unstructured N-terminal region and a portion of the FIIND called the ZU5 domain. The C-terminal domain contains the remaining FIIND domain (UPA) and the CARD domain. The key sensing mechanism of CARD8 lies in its unstructured N-terminal domain which, upon cleavage or degradation, results in N-terminal subunit degradation by the proteasome. This N-terminal degradation allows for release of the non-covalently attached C-terminal fragment which can then oligomerize with CASP1, through its CARD domain, and activate the inflammasome[7-9].

Initial findings on the CARD8 inflammasome showed that VbP is able to induce N-terminal degradation of CARD8 through inhibiting its negative regulator DPP9[4-6,9]. More recently, CARD8 was shown to sense intracellular HIV-1 protease activity. HIV-1 protease can cleave CARD8 at the 59–60aa position which also leads to N-terminal subunit degradation by the proteasome and pyroptosis of HIV-1-infected cells[8]. While HIV-1 protease has limited

intracellular activity, this can be offset by either overexpression of HIV-1 or through the usage of non-nucleoside reverse transcriptase inhibitors (NNRTIs)[10]. Briefly, NNRTIs lead to intracellular HIV Gag-Pol dimerization resulting in premature HIV-1 protease activity. This premature protease activity has been shown to induce killing of HIV-1-infected $CD4^+$ T cells and macrophages through CARD8 inflammasome activation[8,10-12].

Here we describe the method to study CARD8 inflammasome activation through sensing of HIV-1 protease. We specifically highlight the methods to induce $CD4^+$ T cell and macrophage pyroptosis through the induction of premature intracellular protease activity using NNRTIs. We also describe the methods for studying HIV-1-dependent cleavage and inflammasome activation in HEK293T cells through overexpression of HIV Gag-Pol polyprotein which is independent of NNRTIs. As HIV-1 poses a major global disease burden, understanding restriction factors such as CARD8 can be pivotal to understanding HIV disease pathogenesis and offers a potential strategy for an HIV cure. Additionally, HIV-induced CARD8 inflammasome activation offers an invaluable tool for studying the CARD8 inflammasome and does not rely upon indirect mechanisms of activation such as through DPP9 inhibition.

A.1.3 Materials:

A.1.3.1 Cell Isolation and Culture Conditions

1. Whole blood from individuals without HIV.
2. Ficoll-Paque PLUS.
3. 50 mL conical tube.
4. PBMC wash buffer: Dulbecco's phosphate-buffered saline (PBS) with 2% fetal bovine serum and 1 mM EDTA.

5. Freezing media: 90% heat-inactivated fetal bovine serum (FBS) and 10% DMSO.
6. Human CD4 T-cell negative selection kit (BioLegend, #480130 or equivalent).
7. Human CD14 positive selection kit (BioLegend, #480094 or equivalent).
8. Cell culture medium for immune cells: RPMI 1640 supplemented with FBS (10% total volume) and penicillin/streptomycin (1% total volume).
9. Purified anti-human CD3 antibody (BioLegend, #300333).
10. Purified anti-human CD28 antibody (BioLegend, #302943).
11. Recombinant human IL-2.
12. PBS.
13. Recombinant human GM-CSF.
14. Recombinant human M-CSF.
15. Accutase cell detachment solution.
16. Cell lines: THP-1 cells (ATCC TIB-202), HEK293T (ATCC ACS-4500).

A1.3.2 Virus Preparation and Infection

1. HEK293T cells.
2. HEK293T medium: Dulbecco's modified eagle medium (DMEM) supplemented with FBS (10% total volume) and penicillin/streptomycin (1% total volume).
3. Polyethylenimine (PEI) (Polysciences, #24765–100).
4. Opti-MEM Reduced Serum Medium (Thermo Fisher Scientific, #31985070).
5. HIV reporter virus plasmid.
6. Lenti-X concentrator (Takara, #631232).
7. PBS.
8. Human CD8 depletion kit (BioLegend, #480108 or equivalent).

9. Phytohemagglutinin (PHA).

A1.3.3 Drug Treatments

1. 4% paraformaldehyde solution.
2. Intracellular staining kit (such as BD CytoFixation/CytoPermeabilization Kit, BD, #554714 or equivalent).
3. α-HIV-p24 antibody conjugated with a fluorophore such as PE (Beckman Coulter, clone KC57-RD1 #6604667 or equivalent).

A.1.3.4 HEK293T Cell Transfection

1. HEK293T cells.
2. HEK293T medium: DMEM supplemented with FBS (10% total volume) and penicillin/streptomycin (1% total volume).
3. Mammalian expression vectors containing human CARD8, pro-CASP1, and pro-IL1β.
4. 10x RIPA buffer.
5. 100X protease inhibitor cocktail.
6. BCA protein quantification kit.
7. SDS-PAGE gel.
8. SDS-PAGE running buffer diluted to 1x in ultrapure water.
9. PVDF membrane.
10. Methanol.
11. Transfer buffer diluted to 1x in ultrapure water with 20% methanol.
12. Tris-buffered saline with Tween (TBST) diluted to 1x in ultrapure water.
13. Blocking buffer: 5% blotting grade non-fat dry milk dissolved in 1x TBST.

A.1.4 Methods:

All steps are conducted at room temperature unless otherwise specified. All cell incubations occur at 37 ° C with 5% CO2.

A.1.4.1 Isolation of PBMC by Density Centrifugation

1. Collect whole blood from individuals without HIV, and layer slowly on top of a layer of Ficoll-Paque PLUS in a 50 mL conical tube in a ratio of 2:1 (blood to Ficoll).
2. Centrifuge at 300 × *g* for 30 minutes with acceleration 1 and deceleration 0.
3. Collect the buffy coat, and dispense into one 50 mL conical vial for 50 mL worth of whole blood (two conicals for 100 mL).
4. Top off each conical to 50 mL with PBMC wash buffer, centrifuge at 500 × *g* for 10 minutes, and remove supernatant. Repeat above wash for a total of two washes.
5. The remaining cells should contain PBMC and will be used for further isolation of $CD4^+$ T cells and monocyte-derived macrophages (MDMs). Alternatively, cells can be frozen down using freezing media.

A.1.4.2 Isolation of $CD4^+$ T Cells from PBMC

1. Pellet PBMC at 400 × *g* for 5 min at 4 ° C. Resuspend cells in cold PBMC wash buffer at a concentration of 10^8 cells per 1 mL.
2. Using a negative selection $CD4^+$ T cell isolation kit, add 100 µL of antibody cocktail per 10^8 cells, and incubate on ice for 15 min. Then add 100 µL of nanobeads per 10^8 cells and again incubate on ice for 15 min.
3. Top off cells with wash buffer to 2.5 mL, and place tube onto magnet for 5 min. Decant supernatant into a new tube. This supernatant contains the $CD4^+$ T cells; do not discard.

4. Repeat step 3 for a total of two collections.
5. Centrifuge $CD4^+$ T cells at 400 × g for 5 min at 4 ° C. Resuspend cells in RPMI media containing 5–20 ng/mL IL-2 and 1 μg/mL anti-CD28 antibody at a concentration of 10^6 cells per 1 mL of media.
6. Add cells to anti-CD3 antibody-coated plates. For coating plates, add 10 μg/mL anti-CD3 antibody in PBS for 2 hours, and incubate at 37 ° C with 5% CO_2. Wash twice with ice-cold PBS and add cells from above.
7. Incubate cells with co-stimulation for 3 days prior to infection (*see* **Note 1**). After 3 days of co-stimulation, culture $CD4^+$ T cells in RPMI with 5–20 ng/mL IL-2.

A.1.4.3 Isolation of Monocytes from PBMC and in Vitro Differentiation

1. Pellet PBMC at 400 × *g* for 5 min at 4 ° C. Resuspend cells in cold PBMC wash buffer at a concentration of 10^8 cells per 1 mL.
2. Using a monocyte-positive selection kit, add 50 μL of the provided Fc receptor blocking solution per 10^8 cells, and incubate at room temperature for 10 min. Add 100 μL of antibody nanobeads, and incubate on ice for 15 min. Top off cells to 4 mL with PBMC wash buffer, and centrifuge at 300 × *g* for 5 min. Resuspend cells in 2.5 mL of PBMC wash buffer.
3. Place tube with cells on magnet for 5 min. Decant and discard the supernatant; cells will be attached to the beads. Take cells off the magnet and resuspend in an additional 2.5 mL of PBMC wash buffer, and repeat the above for a total of three washes.
4. Take the cells off the magnet, and resuspend in 2 mL of PBMC wash buffer to collect monocytes attached to the beads. Centrifuge at 400 × *g* for 5 min. Resuspend in RPMI

with 50 ng/mL M-CSF and 50 ng/mL GM-CSF at a cell density of 10^6 cells per 1 mL in a 6-well plate.

5. Culture cells for 3 days, and wash plate with PBS twice without disturbing attached cells using 2 mL per well of the 6-well plate. Add media with 50 ng/mL M-CSF and 50 ng/mL GM-CSF, and incubate for another 3 days prior to infection.
6. To collect adherent MDMs, remove media and add a sufficient volume of Accutase to cover the cells. Incubate at room temperature for 5 to 10 minutes, checking periodically for cell detachment, and collect cells. Resuspend MDMs in media with 50 ng/mL M-CSF and 50 ng/mL GM-CSF.

A.1.4.4 Virus Preparation and Infection Using HIV-1 Reporter Viruses

1. Seed HEK293T cells at a density of 4×10^5 for 12-well plates in 1 mL of DMEM media, and incubate overnight until 60–80% confluent.
2. Transfect HEK293T cells by adding 440 ng of an HIV-1 reporter virus plasmid (*see* **Note 2)**, 220 ng VSV-G plasmid, and 440 ng packaging plasmid[13] to a tube with 50uL of Opti-MEM media. Add 3.5 μL of PEI to another tube containing 50 μL of Opti-MEM, and combine with contents of the first tube. Incubate at room temperature for 5 min, and remove 400 μL of media from one 12 well prior to adding the transfection mixture onto cells. Four to six hours after transfection, change media and incubate for 2 days.
3. Collect supernatant containing packaged virus, and concentrate virus using the Lenti-X concentrator (*see* **Note 3**). Filter supernatant with a .45 μm filter, and add concentrator reagent at a 3:1 ratio (supernatant to concentrator). Incubate at 4 ° C for at least 30 min or

overnight. Centrifuge virus at 1500 × *g* at 4 ° C for 45 min. Remove supernatant and add PBS to pellet containing virus at 1/100th volume of original media.

4. Infect cells at a density of 10^6 cells per mL of culture media, and add enough virus to attain 10–20% infection, determined empirically. Centrifuge plates containing infected cells at 1200 × *g* for 2 hours at 30 ° C.
5. Remove plates from centrifuge and incubate for 3 days. One day after infection, double the volume of culture medium. Assay cells for infection rate using flow cytometry prior to addition of drugs to study CARD8 inflammasome activation.

A.1.4.5 Virus Preparation and Infection Using Clinical Isolates of HIV-1

1. Expand clinical isolates using stimulated $CD4^+$ T cells or $CD8^+$ T-cell-depleted PBMC. For CD8 depletion, resuspend PBMC in cold PBMC wash buffer at a concentration of 10^8 cells per 1 mL. Add 75 μL of CD8 nanobeads per 10^8 cells, and incubate on ice for 15 min. Add PBMC wash buffer to 4 mL and centrifuge at 300 × *g* for 5 min.
2. Remove supernatant and add 2.5 mL of cold PBMC wash buffer, and place on magnet for 5 min. Decant supernatant into new tube (do not discard supernatant), and resuspend beads in 2.5 mL of PBMC wash buffer. Repeat process for a total of three collections. Centrifuge cells at 400 × *g* for 5 min, remove supernatant, and resuspend cells at $3x10^6$ cells per 1 mL of RPMI with 5–20 ng/mL IL-2 and 500 ng/mL PHA for stimulation of immune cells.
3. Incubate cells with PHA stimulation for 2–3 days and centrifuge cells at 400 × *g* for 5 min. Remove supernatant and resuspend cells in RPMI with 5–20 ng/mL IL-2.

4. Add clinical isolates to either stimulated $CD4^+$ T cells or CD8-depleted PBMC, and incubate for 5 days. Collect supernatant and filter with a .45 μm filter. Concentration of clinical isolates (see step 3 in Sect. 3.4) is not necessary but can be done if desired.
5. Infect $CD4^+$ T cells or MDMs using clinical isolates as above (see step 4 in Sect. 3.4). Incubate cells for 4–6 days after infection until 10–20% infection is reached, doubling the media on days 1 and 3 post-infection if needed.

A.1.4.6 HIV-1 Infection with NNRTIs

1. Centrifuge infected cells and add NNRTI of choice (see **Table A.1** for effective concentration ranges) or DMSO for as little as 6 hours and up to 2 days (*see* **Note 4**). For 96-well plates, seed 50–100 thousand cells per well (*see* **Note 5**).
2. Fix cells by adding 4% paraformaldehyde in a 1:1 ratio for a final concentration of 2% PFA for 10 minutes at room temperature. Centrifuge cells at 400 × *g* for 5 min and remove media with PFA. Wash once with PBS, and repeat centrifugation before final resuspension in PBS for flow cytometry.
3. Reporter virus infection rate can be assayed by measuring the percentage of GFP-positive cells in the sample (**Figure A.1**). Percent killing can be calculated as follows:

$$\text{Percent Killing} = \left(1 - \frac{Percent\ infection\ of\ treatment}{Percent\ infection\ DMSO}\right) * 100 \quad \text{(A.1.1)}$$

4. For addition of NNRTIs to clinical HIV-1 isolates, NNRTIs should be added as above but should also include 1 μM of the entry inhibitor T-20 and integrase inhibitor raltegravir to prevent further infection. Infection rate should be assayed 6 hours to 2 days post-addition.
5. To assay infection rate of clinical HIV-1 isolates, conduct intracellular HIV-p24 staining using an intracellular staining kit and PE-conjugated α-HIV-p24 antibody. For

intracellular staining, fix cells with fixation buffer provided in the intracellular staining kit at 4 °C for 20 min, and wash once with PBS.

6. Wash a second time with 1X fixation/permeabilization buffer provided in the intracellular staining kit.
7. Resuspend cells in α-HIV-p24 antibody diluted 1:1000 in fixation/permeabilization buffer, and incubate for 20 min at room temperature.
8. Wash twice with fixation/permeabilization buffer, and resuspend in PBS for flow cytometry. Percent killing is calculated as above using PE in place of GFP.

Drug	In vitro working concentrations
NNRTIs	
Efavirenz	500 nM–10 μM
Rilpivirine	500 nM–10 μM
Etravirine	500 nM–10 μM
Doravirine	>3.3 μM
Nevirapine	No evidence of CARD8 activation
Other antiretroviral drugs	
Lopinavir (protease inhibitor)	1–5 μM
T-20 (entry inhibitor)	1–5 μM
Raltegravir (integrase inhibitor)	1–5 μM
Proteasome inhibitors	
Bortezomib	5 μM
MG132	10 μM
Bestatin methyl ester (Me-Bs)	20 μM
Caspase inhibitors	
VX765	100 μM
Z-VAD-FMK	100 μM
DPP9 inhibitors	
Val-boroPro (VbP)/Talabostat	300 nM–3 μM

Table A.1: Drugs Used in This Method

Drugs used to study CARD8 inflammasome activation by HIV-1 protease

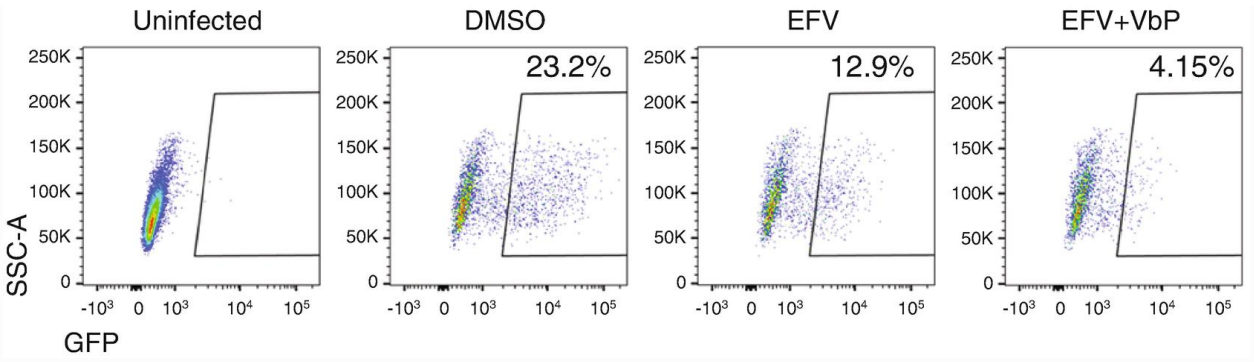

Figure A.1: Measurement of Killing HIV-1 Infected THP-1 cells

Representative gating of THP-1 cells infected with HIV-Δ*env*-eGFP for 3 days and treatment with EFV 3 μM with or without VbP 1 μM or DMSO control. Uninfected cells are used for gating purposes, FITC-positive (GFP-positive) cells are those infected with HIV, and the loss of infection rate is the rate of killing by CARD8 inflammasome activation. For example, the percent infection due to EFV can be calculated as (1−.129/.232)∗100 = 44.40%killing.

A.1.4.7 HIV-1 Infection with Inhibitors

1. Add proteasome inhibitors (see **Table A.1**) at the same time as NNRTIs to demonstrate inhibition of CARD8 inflammasome activation. Cells should be fixed and assayed for infection rate via flow cytometry 6 hours post-addition.
2. Protease inhibitors (see **Table A.1**) should be added at the same time as NNRTIs. Cells can be assayed for infection rate as soon as 6 hours and up to 2 days post-treatment.
3. Pan-caspase or caspase-1 inhibitors should be added 3 hours prior to addition of NNRTIs. Infection rate should be assayed 12 hours post-treatment (after this caspase-1 inhibitors will not be effective).
4. Assay synergy of DPP9 inhibitors (see **Table A.1**) with NNRTIs by adding inhibitors at the same time as NNRTIs, and/or treat HIV-1-infected cells with DPP9 inhibitors alone. Cells should be treated for at least 2 days to attain optimal synergy and killing by DPP9 inhibitors alone.

A1.4.8 HEK293T Cell Transfection

1. Seed HEK293T cells at a density of 4×10^5 cells in 12-well plates in 1 mL of DMEM media, and incubate overnight until 60–80% confluent.
2. For CARD8 cleavage, co-transfect CARD8 (200 ng) and HIV (1 μg) as previously described in Sect. 3.4 (*see* **Note 6)**.
3. For IL-1β cleavage, co-transfect pro-caspase-1 (2 ng), pro-IL-1β (200 ng), and HIV (1 μg) as previously described in Sect. 3.4.
4. Six hours after transfection, change medium to normal DMEM media or media supplemented with drugs (*see* **Note 7**).
5. One day after media change, remove media and remove cells using 1 mL of PBS. Centrifuge cells at 400 × *g* for 5 min at 4 °C and remove PBS. Wash cells again with 1 mL of PBS, and remove wash.
6. Resuspend cells in 50 μL of 1X RIPA buffer with 1X protease inhibitor. Leave on ice for 10 min, and centrifuge cells at 14,000 × *g* for 10 min at 4 °C. Remove supernatant, and measure protein concentration using a BCA protein kit or preferred method of protein quantification.
7. Load 30 μg of protein per sample mixed with loading buffer on an SDS-PAGE gel, and separate proteins by electrophoresis.
8. Transfer proteins to a PVDF membrane after soaking the membrane in 100% methanol for 30 seconds. After the transfer is completed, wash the membrane with TBST once, and block for 1 hour in blocking buffer with gentle shaking/rotation.
9. Incubate membrane with antibody of choice (*see* **Note 8** and **Table A.2**) diluted in blocking buffer for 1 hour with gentle shaking. Wash twice with TBST for 5 min with

heavy shaking. Incubate membrane with appropriate secondary antibody diluted in blocking buffer for 1 hour with gentle shaking. Antibody concentration should be determined empirically by each user. Wash thrice with TBST for 5 min with heavy shaking. Develop using an appropriate method for the secondary antibody used. CARD8 cleavage and IL-1β processing are shown in **Figure A.2**.

Antibody	Dilution	Manufacturer
CARD8 cleavage antibodies		
α CARD8 N-terminus	1:500	Abcam (#ab194585)
α CARD8 C-terminus	1:500	Abcam (#ab24186)
IL-1β cleavage antibodies		
α Pro-IL-1β	1:1000	Cell Signalling Technologies (#12703)
α cleaved-IL-1β	1:1000	Cell Signalling Technologies (#83186)
Antibodies used in both blots		
α HIV-1 p24	1:2000	NIH AIDS Reagent Program (#530)
α β-actin	1:2000	Invitrogen (#MA1-140)

Table A.2: Antibodies for Transfection Experiments

Antibodies used for western blotting and their working concentrations.

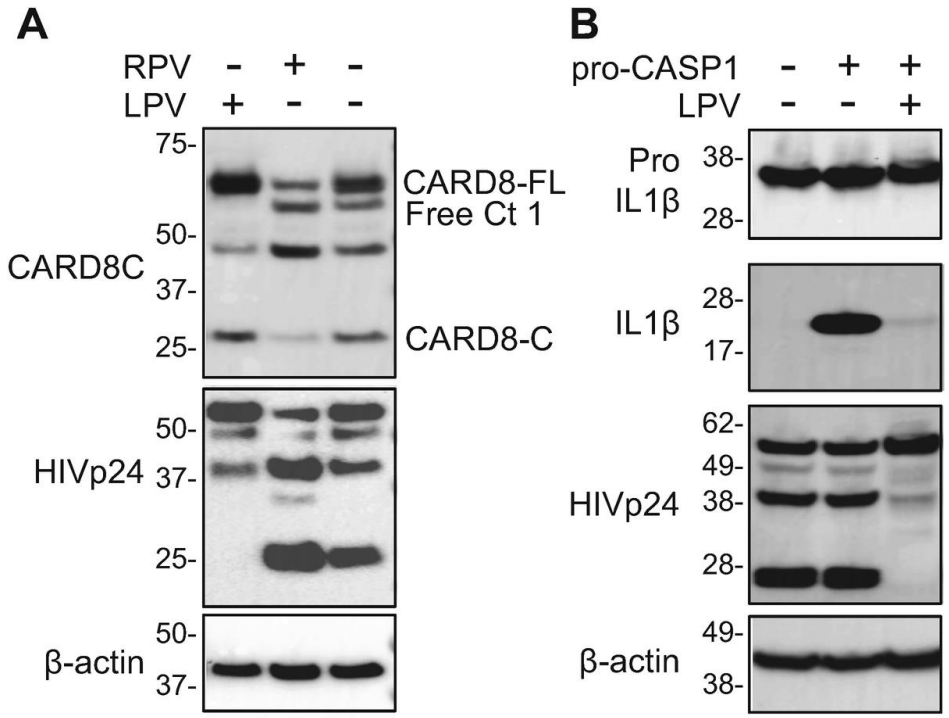

Figure A.2: Western Blotting to Study CARD8 Inflammasome Activation

CARD8 cleavage and IL1β processing in transfected HEK293T cells. (**a**) HEK293T cells were co-transfected with a CARD8-expressing plasmid together with the HIV reporter plasmid pNL4–3-Δ*env*-EGFP. (**b**) HEK293T cells were co-transfected with plasmids encoding CASP1, pro-IL-1β, and pNL4–3-GFP. RPV and LPV were added immediately after transfection. Transfected cells were collected 24 hours after transfection. In A, anti-CARD8-C, anti-HIVp24, and anti-β-actin antibodies were used sequentially on the same blot. In B, anti-pro-IL-1β, anti-IL-1β, anti-HIVp24, and anti-β-actin antibodies were used sequentially on the same blot. CARD8-FL, full-length CARD8; CARD8-C, C-terminal CARD8; Free Ct, freed C terminus.

A.1.5 Notes:

1. Cells can alternatively be cultured in RPMI with IL-2 (5–20 ng/mL) for 2 days prior to infection to expand cells, if needed.
2. HIV reporter viruses should include fluorophore of choice, e.g., NL4–3-Δ*env*-EGFP. Mutant viruses can be used to study CARD8 cleavage and NNRTI efficacy through use of NNRTI resistance mutants such as K103N or protease inactive mutants such as D25A.
3. Unconcentrated virus may be used, but the media should be changed to RPMI media during the transfection media change, and more supernatant will be needed to attain proper infection rates.
4. NNRTI-dependent killing can be seen as early as 6 hours but peaks around 48 hours.
5. For addition of NNRTIs or other drugs, it is easier to prepare a 96-well plate with media containing drugs of choice first, prior to addition of cells. For instance, drugs can be added in 2x final concentration in 50 μL of appropriate media. Cells can then be pelleted and resuspended in 50 μL of media per 50–100 thousand infected cells and added to the wells in the plate containing the drugs to achieve a final 1x concentration. If many conditions are being used, a multichannel pipette is preferred for consistency. Water or PBS should be added to the edges of the plate to prevent evaporation which may affect drug concentrations.
6. Mutant CARD8 plasmids can be used to study CARD8 activation such as HIV-1 cleavage site mutants F59G and F60G or autoprocessing-deficient mutant S297A.
7. CARD8 cleavage can be seen through HIV transfection alone and is enhanced by the addition of NNRTIs and blocked by protease inhibitors. IL-1β cleavage can be enhanced through addition of NNRTIs and blocked by protease and proteasome inhibitors.

8. For CARD8 cleavage Western blot, antibodies against CARD8 C-terminal and either N-terminal or HA (if the CARD8 construct has an HA tag) should be used. For IL-1β cleavage, antibodies against pro-IL-1β and cleaved-IL-1β should be used. For both blots, an antibody against a housekeeping gene like β-actin or GAPDH should be used as a loading control, and an HIV antibody such as HIV-p24 should be used to ensure protease activity through Gag-Pol processing.

A.1.6 References

1. Martinon F, Burns K, Tschopp J (2002) The inflammasome: a molecular platform triggering activation of inflammatory caspases and processing of proIL-1β. Mol Cell 10:417–426.
2. Broz P, Dixit VM (2016) Inflammasomes: mechanism of assembly, regulation and signaling. Nat Rev Immunol 16:407–420.
3. Gross O, Thomas CJ, Guarda G, Tschopp J (2011) The inflammasome: an integrated view. Immunol Rev 243:136–151.
4. Johnson DC, Okondo MC, Orth EL, Rao SD, Huang HC, Ball DP, Bachovchin DA (2020) DPP8/9 inhibitors activate the CARD8 inflammasome in resting lymphocytes. Cell Death Dis 11(628):628.
5. Linder A, Bauernfried S, Cheng Y, Albanese M, Jung C, Keppler OT, Hornung V (2020) CARD8 inflammasome activation triggers pyroptosis in human T cells. EMBO J 39(19):e105071.
6. Okondo MC, Johnson DC, Sridharan R, Bin Go E, Chui AJ, Wang MS, Poplawski SE, Wu Y, Liu Y, Lai JH, Sanford DG, Arciprete MO, Golub TR, Bachovchin WW, Bachovchin DA (2017) DPP8/9 inhibition induces pro-caspase-1-dependent monocyte and macrophage pyroptosis. Nat Chem Biol 13(1):46–53.
7. D'Osualdo A, Weichenberger CX, Wagner RN, Godzik A, Wooley J, Reed JC (2011) CARD8 and NLRP1 undergo autoproteolytic processing through a ZU5-like domain. PLoS One 6(11):e27396.
8. Wang Q, Gao H, Clark KM, Shema Mugisha C, Davis K, Tang JP, Harlan GH, DeSelm CJ, Presti RM, Kutluay SB, Shan L (2021) CARD8 is an inflammasome sensor for HIV-1 protease activity. Science 371(6535):eabe1707.
9. Sharif H, Hollingsworth LR, Griswold AR, Hsiao JC, Wang Q, Bachovchin DA, Wu H (2021) Dipeptidyl peptidase 9 sets a threshold for CARD8 inflammasome formation by sequestering its active C-terminal fragment. Immunity 54(7):1392–1404.
10. Figueiredo A, Moore KL, Mak J, Sluis-Cremer N, de Bethune MP, Tachedjian G (2006) Potent nonnucleoside reverse transcriptase inhibitors target HIV-1 gag-pol. PLoS Pathog 2(11):e119.
11. Jochmans D, Anders M, Keuleers I, Smeulders L, Kräusslich HG, Kraus G, Müller B (2010) Selective killing of human immunodeficiency virus infected cells by non-nucleoside reverse transcriptase inhibitor-induced activation of HIV protease. Retrovirology 7:89.
12. Zerbato JM, Tachedjian G, Sluis-Cremer N (2017) Nonnucleoside reverse transcriptase inhibitors reduce HIV-1 production from latently infected resting CD4. Antimicrob Agents Chemother 61(3):e01736.
13. Mochizuki H, Schwartz JP, Tanaka K, Brady RO, Reiser J (1998) High-titer human immunodeficiency virus type 1-based vector systems for gene delivery into nondividing cells. J Virol 72(11):8873.

Appendix 2: Data for Retention: Addressing under-representation of LGBT+ minorities in STEM

The following report has been reproduced and adapted from the Wilton Park Report available at the following link: https://www.wiltonpark.org.uk/app/uploads/2023/02/WP3105-Report-140823.pdf

In association with: the UK Science and Innovation Network (SIN)

A.2.1 Introduction:

LGBT+ minorities are under-represented in STEM disciplines in both the US and the UK. In both countries, however, policymakers are struggling to design evidence-based interventions to address this problem. Often, this is because there is very little data collected on this minority population, which prevents policymakers from targeting interventions. Policymakers cannot focus efforts on a particular discipline (e.g., the problem might be worse in Chemistry than in Physics) or on a particular timepoint in a research career trajectory (e.g., LGBT+ scientists might be dropping out in graduate school or at post-doctoral level) or even once they become established in their own labs.

Some consider this to be a 'leaky pipeline' problem, with insufficient information on where, when and why the 'leaks' occur. Others note that this does not fully highlight the problem, as active discrimination can also push people out of the system. In the absence of data to characterise the problem writ-large, there is obviously a limit to the efficacy of interventions.

In 2021, the UK Science and Innovation Network (SIN) established a partnership with the National Science Policy Network (NSPN) on a project to address LGBT+ attrition in STEM fields. To date, outputs from this project include the first bilateral report on the issue based on discussions with universities, NGOs, researchers, and funders in both the UK and the US.

The conference aims to build on work undertaken to date, in order to further understand and address under-representation of LGBT+ people in STEM. Discussion will explore what data is currently collected, gaps in existing data and ways in which to overcome barriers to future data collection.

The conference represented a key milestone toward collaboration on data sharing and the establishment of a US-UK repository of datasets. In particular, it aimed to progress the following objectives:

- **Establish a UK-US community** of experts working together on DEI in STEM from government, NGOs, university administrations, researchers, and funders.
- **Create the world's first repository of datasets** for researcher access.
- **Draft a UK-US open-source policy guide for universities** to reference in designing evidence-based interventions to stop the attrition of LGBT+ minorities in STEM.

The conference also supported the launch of new bilateral funding for research into LGBT+ attrition and retention in STEM.

A.2.2 Executive Summary

The problem: A growing body of evidence shows that LGBT+ people are underrepresented in STEM fields and face high rates of exclusion, harassment, and career limitations. However, due to a dearth of data collected on these populations, policymakers in the UK and the US have

struggled to design evidence-based policies which support retention of LGBT+ minorities in STEM. For example, policymakers don't know when attrition is likely to occur in the career trajectory of these scientists, nor which disciplines, geographies or identities are most likely to be affected. For a host of complex reasons, LGBT+ identities have not been tracked as broadly and consistently as other demographics and this results in policy interventions that are well-intentioned, but speculative.

The solution: In order to make the STEM ecosystem inclusive, attractive and welcoming for all, scientific communities in both the UK and the US are embarking on the enormous challenge of collection, collation and study of sexual orientation and gender identity (SOGI) data in STEM. Not only is this data critical to our understanding of the current status, but it will also be the foundation on which we must design policies to stem the attrition of LGBT+ and other minorities. We must do this if we want to create environments in which all talented individuals who want to pursue scientific careers can flourish.

The collaboration: Despite different legal structures, organisation of agencies, and extents of SOGI data collection in the two nations, the UK and the US share similar goals and have been having similar conversations separately. In fact, because they collect different types of data, it is clear that by working together the UK and the US can enrich each other's understanding of this complex issue. The meeting provided a unique opportunity to learn across sectors and from different perspectives, seeking to improve collaboration and information exchange.

The event: This meeting at Wilton Park brought together over 40 professionals from government agencies, funding bodies, university leadership, academia, and nongovernmental organisations in the United Kingdom and United States. Outcomes included:

1. Fostering bilateral collaboration on the topic of data for LGBT+ retention in STEM

2. Developing a set of recommendations on data collection
3. Compiling a list of existing datasets and literature
4. Announcing new funding mechanisms to promote research on improving STEM for LGBT+ communities.

Recurring themes of discussion included:

- We cannot change what we can't measure – data is key: Participants agreed that rich, reliable data is a crucial foundation for social change, and for policy progress. They gave deep consideration to the myriad of complex challenges facing institutions collecting SOGI data. These included issues spanning legality, privacy, trust, longevity, reliability and the need to appropriately balance data quality, respondent burden, confidentiality, and data user needs.
- Passion, power, and possibilities: The group aimed to inspire and imagine a world where LGBT+ people can thrive in the scientific milieu. The group carried this powerful vision to their deep consideration of the data questions at hand.
- Tackling multiple barriers: The LGBT+ community encompasses all other demographic categories, and efforts to understand and serve the community should give a voice to the most marginalised (particularly communities of colour or those tackling multiple barriers) a particular challenge when the data is limited given the small numbers.
- Collaboration is key - UK and the US synergies abound: The group relied on three questions to compare and contrast the UK and the US data infrastructure, asking: What data do we have? What data do we need? What are the barriers to collating this data? The answers to these core questions reveal complementary (rather than duplicative) data sets and myriad opportunities for collaboration.

A.2.3Terminology and Scope

- **"LGBT+"** is the official terminology used by the UK Foreign, Commonwealth & Development Office and is not meant to be an exhaustive representation of the community.
- **"SOGI data"** refers to demographic information about sexual orientation and gender identity. SOGI data are valid demographic data that should be handled similarly to other more commonly collected demographic items such as race, ethnicity, socioeconomic status, and ability. Collection of this data requires careful consideration of privacy, sensitivity, and mixed methods of analysis, especially in cases of disaggregation or small sample sizes.
- **"STEM"** refers broadly to the fields of science, technology, engineering, and mathematics, which may also include education, medicine, social sciences, or research and innovation generally, depending on context. For the purposes of this discussion, its scope has not been restricted.
- **"Retention"** in this report refers to individuals being able to stay in the STEM enterprise if they want to do so. Relatedly, we use the term "STEM pathways" as a framework for considering free movement within and in/out of STEM, rather than emphasising a single strict career pipeline which requires holding onto people who would otherwise leak out.
- **"Harmonisation"** refers to the creation of data standards that allow for semantic interoperability. Harmonised standards create a flexible but shared language of survey items that enables efficient processing and analysis across institutions so that they may share data effectively. Data harmonisation, in contrast to standardisation, does not intend

to create a rigid question format, but instead focuses on a shared methodology to improve interoperability.

A.2.4 Key issues and recommendations

Participants agreed on four key areas of future collaboration:

1. **Sharing best practices on SOGI data collation at the institutional level**

   Participants considered prior work which demonstrates that higher education institutions in both the UK and the US face challenges which have deterred them from collecting SOGI data. These challenges include sensitivity of data, safety concerns, political sensitivities, and uncertainty of how to ask questions. However, because these challenges also exist to varying extents for other demographic categories, participants agreed that they can be overcome through thoughtful design. Participants heard from speakers who covered their experiences in these methodologies. Like all data collection, SOGI data collection at institutions should involve:

   a) Purposeful design
   b) Rigorous methodologies
   c) Self-education on the issues in advance
   d) An internal audit of available resources
   e) Involvement of communities throughout the process
   f) Attention to privacy and security
   g) Inclusive and flexible language in survey items

   Data collection must also be accompanied by careful data analysis and data-informed interventions, though these topics generally fell outside the scope of this discussion.

2. **Sharing research datasets**

   Participants agreed that much can be learned from working with datasets already collated by colleagues, especially given the scant availability of SOGI data, and the survey burden on relatively small groups. Participants discussed safe, ethical ways in which data sharing might be possible. Participants also agreed about the utility of a high-level repository of datasets which would not allow access to individual data, rather would illuminate what data exists.

3. **Supporting social science and anthropology research which studies the mechanics of attrition and retention for SOGI communities**

   Participants agreed on the need for deep social science research into data for retention, including the study of survey design alongside experts, for example census professionals. The Royal Society of Chemistry will take this forward as part of a new funding mechanism for UK-US collaboration on Data for LGBT+ Retention in STEM, with the first cohort set to be announced by the Society in August 2023.

4. **Enriching the data that exists by supporting new work to study LGBT+ communities in STEM**

   Participants were unanimous in their call for more data, and their desire to support policymakers, institutions and researchers who are painstakingly working to collate it.

A.2.5 Background: The nature of SOGI data

Quantitative and qualitative data are essential for identifying LGBT+ representation and understanding the community's experience in STEM. Large population-based demographics rely upon quantitative demographic collection which is necessary for benchmarking LGBT+

population sizes in the broader population and in STEM to accurately assess the amount of underrepresentation in STEM. However, even without representation data, there is a growing body of evidence that demonstrates that LGBT+ people face harassment, discrimination, and exclusion in STEM (e.g. Cech et al., 2021 – see Bibliography). To further identify the specific experiences of the community, qualitative data can offer insight into the underlying culture in STEM that leads to poor outcomes for LGBT+ people (e.g. Bilimoria & Stewart 2009; Formby 2017). The user of demographic data collection should assess whether quantitative or qualitative methods best suit the needs of the organisation and the questions that are being asked. Importantly, disaggregation of qualitative data, when safely possible, offers the most power in addressing the needs of the most marginalised members of the community that may be overlooked due to insufficient numbers for statistical analysis in traditional quantitative methods.

Demographic data can be used as evidence for diagnosing a problem, but in itself is only one piece of the puzzle in addressing LGBT+ retention in STEM. Interlocutors were clear that more data is needed. Not only is it crucial in diagnosing the mechanics of the problem and informing policy interventions, but can also, in some cases, even be the determinant for whether or not a minority is legally considered as such. Interlocutors noted that in some ways, the act of collecting data in and of itself increases visibility for an often invisible population in the STEM enterprise. However, participants cautioned against survey fatigue among the relevant populations. To avoid this, they advised institutions to articulate what demographic data collection will do prior to implementing an extensive (and expensive) collation effort; institutions should make clear that they are not just collecting data, but willing to use it toward policies to improve STEM environments.

The fluid and complex nature of demographic data often creates complexities with statistical analysis. These are surmountable, even given perceived complexities of SOGI data in particular.

An example subset discussed at Wilton Park includes:

- **SOGI data as relational.** Individuals have a deep and sometimes complicated relationship with their own identities that can change depending upon the context of the survey and their current personal circumstances. Clear understanding by those filling out the surveys of how SOGI data will be used, the purpose of its incorporation, and the safety of this data can help mitigate issues of data inaccuracies when filling out SOGI items.
- **SOGI data as temporal.** There is fluidity and change in how individuals may identify, and identities change over time. This can constitute analytical boundaries especially for longitudinal data collection. However, understanding that a singular survey is a snapshot of the community and analysing the flux in the population can also provide invaluable information to the user. Survey professionals discussed ways in which this can be used as a data asset rather than a detraction.
- **SOGI data as contextual.** Disclosure of SOGI identities will vary upon the context of the survey, the institution providing the survey, and the trust the individual has in these institutions. SOGI data should be decoupled from access to resources but should be used post-hoc to identify how these resources are being distributed to LGBT+ individuals. Emphasising communication and trust on the part of the data collector has been shown to help with accurate data collection (though some may still not feel safe/able to disclose their identities in particular data collation contexts.)

- **SOGI data as sensitive.** The safety of LGBT+ individuals should be at the forefront of any data collection. Institutions are rightly extremely wary of this issue, and conscious that discoverability and "outing" of individuals is not a risk they are prepared to take. They are also conscious that the format and wording of SOGI items has the possibility to inflict harm if improperly executed. These risks can be mitigated with careful survey design and rigorous privacy protocols. The mechanics of these issues were discussed in detail.

A.2.6 Examining the existing evidence base

Participants reviewed an expanding evidence base on LGBT+ representation in STEM, within the broader context of emerging LGBT+ demographic data.

The majority of LGBT+ representation data has come from large national surveys from national governments. However, this isn't STEM-specific. Other essential quantitative and qualitative data sets have arisen from non-governmental organisations, academic researchers, and academic institutions. While harmonisation of data collection methods has remained a key hurdle in collection of SOGI data, there has been a growing body of evidence from multiple sectors on how to adapt SOGI items for the context of the survey. The analysis of the current evidence base also provides insights into the key barriers and gaps in data collection which have highlighted the methodological and ethical challenges to collecting this data.

- **National statistics agencies such as the UK Office for National Statistics and the US Census Bureau have recently begun implementation of SOGI items on large national surveys.**

National census surveys offer the potential of significant data on LGBT+ representation in the general public, which can in turn be used to analyse representation in STEM and other fields. The UK is well ahead of its peers on this issue. The English and Welsh census included SOGI items on the 2021 census[1-3], an extremely innovative and novel accomplishment. The National Records of Scotland also included SOGI items on the 2022 Scottish census[4-6]. The Northern Ireland census incorporated a sexual orientation question but not a gender identity question on its census in 2021[7-9].

By contrast, the US Census Bureau has yet to incorporate SOGI items on the US census or the American Community Survey (ACS). It does, however, allow for analysis of individuals sharing a household with a same-sex partner[10, 11] Incorporation of SOGI items is yet to be tested and implemented on further iterations of the ACS. (The census bureau did incorporate SOGI items on the Household Pulse Survey which measured household experiences during the COVID-19 pandemic. This study found that LGBT+ respondents were more likely than their non-LGBT+ counterparts to face food insecurity and economic insecurity[12].)

While these data sets are limited by their ability to only provide quantitative data, information on benchmark population sizes and cross-sectional analysis is critical to our understanding of various populations in the LGBT+ community and can be foundational in associating SOGI census items to economic items in order to identify LGBT+ representation in STEM fields at scale.

- **Funding agencies often are the first line of large-scale data collection on diversity and inclusion in STEM fields but largely have yet to include SOGI in their surveys.**

The largest source of governmental STEM funding in the UK is provided by UK Research and Innovation (UKRI). While UKRI has yet to include SOGI items on their demographic data collection, SOGI item inclusion in demographics is included in their equality, diversity, and inclusion strategic plan which will hopefully lead to SOGI data collection soon[13-15].

In the US, governmental funding is decentralised but relies upon the National Science Foundation (NSF) for demographic data collection and classification of marginalised identities as underrepresented in STEM[16]. NSF conducts a wide variety of surveys to collect demographics on the STEM workforce and education throughout different career stages including the National Survey of College Graduates, the Survey of Earned Doctorates, the Early Career Doctorates Survey, the Survey of Doctorate Recipients, and the Survey of Graduate Students and Postdoctorates in Science and Engineering[17]. Although NSF agreed to pilot SOGI items on their surveys, they ultimately decided not to include these items. Participants discussed the significance of this decision and researcher engagement with it. The National Science and Technology Council announced the first-ever Federal Evidence Agenda on LGBTQI+ Equity which urges that "data collection (on LGBT+ communities) must start immediately"[18]. The report follows the White House Summit on STEMM Equity and Excellence and its white paper urging improved data collection to achieve equity outcomes.

- **SOGI data collection has been rapidly developing in education agencies and provides a gold mine of opportunity for SOGI data analysis in both the US and the UK.**

Education agencies have the statistical power and capability to analyse a large section of the STEM population. These agencies also provide a unique opportunity to provide longitudinal data collection and analysis to follow individuals throughout their participation in the academic enterprise. The US Department of Education was one of the first national agencies to begin collecting SOGI data when it incorporated SOGI items on the 2016 follow up survey to the High School Longitudinal survey of 2009 using the Office of Management and Budget working group on SOGI data collection's recommendations[19, 20]. This study follows more than 23,000 students beginning in high school and through to postsecondary education, and beyond. The Baccalaureate and Beyond Longitudinal Study, which follows students for ten years after completion of a Baccalaureate degree, also incorporated SOGI metrics as of 2018[21]. The Beginning Postsecondary Students Longitudinal Study, which follows students through postsecondary education, incorporated SOGI metrics as of 2020[22].

In the UK, the Higher Education Statistics Agency (HESA), has collected SOGI items on their administrative census of all graduates of universities. HESA is a non-governmental organisation which adheres rigorously to UK statistical standards, allowing data harmonisation. SOGI data is incorporated in the Graduate Outcomes Survey, or its predecessors the DLHE and Longitudinal DLHE (Destinations of Leavers from Higher Education) records, which can both be linked back to the student record data, where the special category (EDI) personal information is held.*

* HESA publishes extracts of these datasets in a disclosure controlled manner as Open Data on their website: https://www.hesa.ac.uk/data-and-analysis. They supplement these data with a range of services, which are described here: https://www.hesa.ac.uk/services

- **Universities, professional societies, non-governmental organisations, and academic researchers have also led efforts to illuminate attrition and the challenges facing LGBT+ people in STEM.**

  Universities are in a strategically important position to alter the landscape of retention by increasing data collection and collation across institutions and sharing best practices to encourage a welcoming STEM environment. Professional societies and NGOs also collect SOGI data and often have high levels of trust from their membership leading to excellent survey-response data. Participants examined some examples of these, including university-led climate and perceptions studies which have identified important factors in poor LGBT+ retention in STEM at both the undergraduate and faculty levels.[23, 24] One such study determined that SOGI minorities were found to be 7% less likely to stay in a STEM degree than their peers, despite higher rates of participation in undergraduate research, a key predictor of STEM retention.[25] In the UK, a joint report from the Universities and Colleges Admissions Service and Stonewall did important work to identify the percentage of university applicants who are LGBT+. [26] At the professional level, a few key studies and surveys have examined climate in STEM workplaces.[27,28] Notably, the American Association for the Advancement of Science (AAAS) has launched a new SOGI data collection initiative, in addition to its SEA change programme.[29, 30] Participants encouraged transatlantic collaboration in ongoing phases of all of these to enrich data and share best practice.

Participants welcomed this trajectory of increased data collection. In order to translate this momentum into datasets which can support effective policymaking to increase retention, they recommended:

- **Increased analytical capability and policy intentionality**

  For the first time in history, SOGI data collection is gaining momentum. Participants cautioned against viewing this as the 'end' rather than the 'means' to increased retention for SOGI minorities in STEM. They recommended a focus on downstream analytical capabilities to ensure that data collected adequately answers user needs. Additionally, participants recommended clarifying policy intentionality at all stages of collection.[†]

- **Data harmonisation at a national and international level**

  Harmonisation of SOGI items will support data analysis and allow for systems to be nimble with respect to context and needs of the organisation /community. Harmonised standards have been created by the UK Office for National Statistics, the US Office of Management and Budget (OMB) working group on SOGI data collection, and the US Federal Committee on Statistical methodology. These standards, built in concert with LGBT+ communities, offer a framework for data collection but do not intend to be a rigid protocol on data collection. Additionally, participants recommended that the harmonised standards be continually reviewed in collaboration with the LGBT+ community to keep pace with the evolution of queer and trans identities over time. Participants emphasised harmonisation to enhance interoperability of data sets, noting that these remain flexible to respond to the specific questions being asked at individual institutions.

- **Disaggregation and qualitative methods**

[†] Participants considered the potentially circular issue of SOGI data in many institutions whereby sexual orientation and gender identity are not classified as underrepresented and therefore are not allocated resources for data collection. Of course, this leads to insufficient data collection, and the inability to show definitively that LGBT+ individuals are marginalised in STEM. This cycle must be broken to continue moving forward with allocation of resources and programming which addresses this issue.

Identities, especially intersectional identities, represent small subsets of the data and are therefore often left out of analysis which can lead to the exclusion of the needs of the most marginalised. Participants recommended that further work be done to address who is left out and how their experiences can be assessed through disaggregation or qualitative methods.

- **The UK and the US collect different types of data but taken together are more than the sum of their parts**

  The cultural, political, and structural contexts of the UK and US differ and have thereby led to differences in data collection on SOGI items, as described above. Attitudes towards the LGBT+ community, intrinsic community differences, education and funding structures, and the politicisation of SOGI data collection are just a few of the key differences when assessing the current landscapes in the respective countries. The combination of both countries' strengths in data collection can help cover some of the gaps that either country faces independently to create a more in-depth picture of LGBT+ representation and their experiences in STEM.

A.2.7 Recommendations for data collection at institutions

Participants agreed on the following eight tenets which might assist institutions in their first forays into collecting SOGI data. The Appendix includes supporting materials.

1. **Share best practices – Universities might be unique but they're not alone**

   Crafting sensitive questions, building community trust, overcoming legal barriers, ensuring robust privacy policy: All of these are issues that almost every institution faces

in first-generation efforts at gathering SOGI data.[‡] Participants agreed to help institutions informally connect with one another as they undertake these processes, and began this in earnest at Wilton Park. Participants formed continued informal working groups.

2. **Self-educate on the issues in advance**

   Institutions should recognise the cultural and political milieus which contextualise their collection efforts. Unfortunately, these still sometimes include active violence and attempts to delegitimise or leverage those with LGBT+ identities. Sensitivity to these issues in data collection and how this relates to other intersectional identities is key. Similarly, to avoid survey fatigue (particularly prevalent in campus climate surveys), the existing literature and data on LGBT+ experiences in STEM should be considered. Some resources are provided in the Bibliography.

3. **Involve LGBT+ communities in the entire process**

   Thoughtful co-production is key to developing trust and building relationships - both those being consulted and those being surveyed.[§] Ensure a clear plan for communicating the data uncovered about these communities back to the communities themselves. Participants recommended that institutions take careful note of the possibility of a small number of LGBT+ individuals taking on considerable burdens to assist universities in this work (often at personal cost). Institutions can mitigate against this by rewarding the consultation work. In general, clear communication and agreement upon the expectations,

[‡] Participants commended, for example, the open blog of Chief Statistician of Scotland sharing challenges to SOGI data collection candidly here: https://www.gov.scot/publications/data-collection-publication-guidance-sex-gender-identity-trans-status/

[§] Some groups emphasised that addressing LGBT+ retention in STEM must prioritise voices from the set of characteristics referenced in the Equality Act of 2010, including people of colour, women, trans, intersex, and asexual individuals, people with disabilities, and a mix of socioeconomic backgrounds. Doing so can help ensure that even those with the smallest numbers have a voice, and the experiences of the community can be defined by the most marginalised within the community.

outcomes, and accountability during the co-production process can ensure trust with the communities involved.

4. **Conduct an internal audit of available resources and capacity for change.**

   Prior to collecting SOGI data, an institution should have the resources to collect sensitive personal information, analyse it, distribute the results, and consider the downstream policy interventions accurately and safely. The process requires a myriad of professionals and resources including IT and analytics staff, communications departments, survey design professionals and others. Participants cautioned against the harms that can result in under-resourced or hasty data collection efforts, and highlighted the need for community involvement in survey development to mitigate some of the risks and harmful practices noted above.

5. **Design data collection with purpose.**

   It is valuable to define and communicate the institution's motivation for collecting the data as part of survey communications. As more institutions begin collecting data, there is a risk of collection for collection's sake and while more data might be helpful to researchers, institutions are unlikely to get buy-in from the communities they are trying to serve. When leadership is clear about data uses (in this case the improvement of the STEM system for all marginalised groups) those groups are more likely to respond. Harm reduction and the empowerment for change should be at the forefront of these data collection efforts.

   A considered approach to data collection will also help refine which survey questions are needed. For example, the question of "sex assigned at birth" is a topic of disagreement within the LGBT+ community and may not be necessary in circumstances

when gender is the primary demographic of interest. Additionally, the need for quantitative versus qualitative data should be assessed. If quantitative data is desired, is there sufficient sample size and statistical power to answer the question being asked? If sample sizes are insufficient, can the data be safely disaggregated to identify the needs of smaller subsets of the community?

6. **Employ rigorous methodologies.**

   Designing SOGI data collection and analysis requires balancing scientific and methodological rigour with flexibility and evolution of language. LGBT+ identities do not often fall neatly into a predefined set of categories, and the language used by the community is subject to change over time. Consideration must be given by professional teams to (1) data aggregation and analysis (2) use of mixed qualitative and quantitative methods, (3) reproducibility, (4) data interoperability, (5) sufficient statistical power in the questions to provide insight from the collected data, and (6) incorporation of relevant techniques for multidimensional demographic data such as relational data analysis and cluster analysis. Data analysts should have both technical and cultural competence.

7. **Ensure privacy and security.**

   Small sample sizes and the sensitive nature of SOGI data require particular attention to individuals' safety and protections against discoverability. Practitioners should remain vigilant and note that many social, cultural, and political contexts involve risks to the LGBT+ community. The collection of SOGI data requires investments in secure data systems and in IT staff, as well as accountability against data misuse.

8. **Use inclusive and flexible language in survey items.**

The topic of sexual orientation and gender identity is complex, with evolving language and disagreement even within the LGBT+ community as to the best ways to ask questions. Institutions collecting SOGI data should therefore be open to feedback and willing to adapt based on their needs. General guidelines include:

a. Organise response options alphabetically rather than putting “straight” or “male” first by default.
b. Avoid “other”. Instead, use “another identity not listed” or “write-in”. Resources exist for dealing with and coding free text responses.
c. Make all questions optional or include “decline to answer” options.
d. Include checkboxes to enable select-all-that-apply functionality for response items.
e. Avoid outdated or offensive terms. Poorly designed questions can cause harm or retraumatise respondents.
f. Recognise the fluidity of identities and language over time. Data should be harmonised for interoperability but not necessarily standardised.

A.2.8 Conclusions and next steps

Data is powerful, not just in helping understand the status quo in the STEM enterprise, but also in helping the scientific community design and deliver evidence-based actions to ameliorate it. Until now, a dearth of SOGI data has created challenges for understanding when and why LGBT+ people leave STEM and for designing data-driven policy interventions. The collection of this data has been fraught with challenges of technical, legal, cultural, operational natures. Social science and survey science have helped to overcome some of these challenges with rigorous and

sensitive methodology. These factors have led many, including the US National Science and Technology Council, to state that "data collection must start immediately."

The UK and the US are powerful partners on this issue on many fronts. Wilton Park participants highlight the following as key areas of continued work:

- sharing best practice on data collection and design
- highlighting synergistic datasets and working to share and learn from these
- continuing bilateral dialogue and collaboration on data-driven policy interventions to support retention
- establishing bilateral instruments to support UK-US leading social science research on this issue.

A.2.9 Acknowledgements

Kolin Clark and Shane Coffield served as rapporteurs for the Wilton Park conference and for this report. Wilton Park thanks Ronit Prawer and the UK Science and Innovation Network for their leadership of this bilateral initiative. Colbie Chinowski, Anna Dye, and Jacob O'Connor also contributed to an initial report on US/UK SOGI data collection in collaboration with the National Science Policy Network, which led to this event. Workshop participants and Garrett Dunlap contributed feedback and edits to the report. We also acknowledge the previous work of the Royal Society of Chemistry, Institute for Physics, and Royal Astronomical Society in their efforts to coalesce discussion around these topics.

Kolin Clark and Shane Coffield

Wilton Park | August 2023

Wilton Park reports are brief summaries of the main points and conclusions of a conference. The reports reflect rapporteurs' personal interpretations of the proceedings. As such they do not constitute any institutional policy of Wilton Park nor do they necessarily represent the views of the rapporteur. Wilton Park reports and any recommendations contained therein are for participants and are not a statement of policy for Wilton Park, the Foreign, Commonwealth and Development Office (FCDO) or His Majesty's Government.

A.2.10 References

1. For information on the UK ONS sexual orientation question addition to the English and Welsh census see https://www.ons.gov.uk/census/censustransformationprogramme/questiondevelopment/sexualorientationquestiondevelopmentforcensus2021
2. For information on the UK ONS gender identity question addition to the English and Welsh census see https://www.ons.gov.uk/census/censustransformationprogramme/questiondevelopment/sexandgenderidentityquestiondevelopmentforcensus2021
3. For information on the ONS topic consultation for incorporation of SOGI items on the English and Welsh Census see https://assets.publishing.service.gov.uk/government/uploads/system/uploads/attachment_data/file/765089/Census2021WhitePaper.pdf
4. For information on the NRS sexual orientation question addition to the Scottish census see https://www.scotlandscensus.gov.uk/media/nlugzlqn/sexual_orientation_topic_report.pdf
5. For information on the NRS gender identity question addition to the Scottish census see https://www.scotlandscensus.gov.uk/media/rguhe4ol/sex_and_gender_identity_topic_report.pdf
6. For information on the NRS topic consultation for incorporation of SOGI items on the Scottish Census See https://www.scotlandscensus.gov.uk/media/3w5b3fgi/topic_consultation.pdf
7. For information on the NISRA incorporation of sexual orientation on the Northern Ireland Census see https://www.nisra.gov.uk/sites/nisra.gov.uk/files/publications/sexual-orientation-topic-report.pdf
8. For information on NISRA's findings on gender identity items and their rationale for not including gender identity on the Northern Ireland census see https://www.nisra.gov.uk/sites/nisra.gov.uk/files/publications/Research%20on%20Measuring%20Gender%20Identity%20-%20Feb%202021.pdf
9. For information on NISRA's topic consultation on SOGI items see https://www.nisra.gov.uk/statistics/2021-census/consultation/topic-consultation
10. For information on the US Census see https://www.census.gov/programs-surveys/decennial-census/decade/2020/2020-census-main.html
11. For information on the American Community Survey see https://www.census.gov/programs-surveys/acs
12. For information on the Census Bureau's Household pulse survey see https://www.census.gov/data/experimental-data-products/household-pulse-survey.html
13. For information on UKRI's pilot of SOGI data collection see https://www.ukri.org/wp-content/uploads/2021/10/UKRI-071021-AddressingUnder-representationUpdate07Oct.pdf
14. For information on UKRI's draft of their equality, diversity, and inclusion strategy see https://www.ukri.org/publications/equality-diversity-and-inclusion-strategy-draft-for-consultation/ukri-equality-diversity-and-inclusion-strategy-draft-for-consultation/
15. The glossary attached to the UKRI draft of their equality, diversity, and inclusion strategy that lists SOGI items as diversity/demographic metrics https://www.ukri.org/publications/ukri-glossary-of-edi-terms/ukri-glossary-of-edi-terms/
16. The National Science Foundation's report on underrepresented groups used as a basis for classification by other federal agencies. https://ncses.nsf.gov/pubs/nsf21321/report
17. Listing of surveys conducted by the National Science Foundation https://ncses.nsf.gov/surveys
18. For information on the White House Federal evidence Agenda on LGBTQI Equity see https://www.whitehouse.gov/wp-content/uploads/2023/01/Federal-Evidence-Agenda-on-LGBTQI-Equity.pdf
19. For information about the US Department of Education's High School Longitudinal Survey see https://nces.ed.gov/surveys/hsls09/index.asp
20. The findings of the Office and Management and Budget's SOGI data working group that was used as a basis for question format in the US Department of Education's surveys. https://nces.ed.gov/FCSM/pdf/SOGI_Research_Agenda_Final_Report_20161020.pdf

21. For information about the US Department of Education's Baccalaureate and Beyond Survey see https://nces.ed.gov/surveys/b&b/index.asp
22. For information about the US Department of Education's Beginning Postsecondary Students Longitudinal Study see https://nces.ed.gov/surveys/bps/index.asp
23. Garvey, Jason C., Dian D. Squire, Brett Stachler, and Susan Rankin. "The impact of campus climate on queer-spectrum student academic success." *Journal of LGBT Youth* 15, no. 2 (2018): 89-105.
24. Bilimoria, Diana, and Abigail J. Stewart. "" Don't ask, don't tell": The academic climate for lesbian, gay, bisexual, and transgender faculty in science and engineering." *NWSA Journal* (2009): 85-103.
25. Hughes, Bryce E. "Coming out in STEM: Factors affecting retention of sexual minority STEM students." *Science advances* 4, no. 3 (2018): eaao6373.
26. For information on Stonewall's University Report see https://www.stonewall.org.uk/system/files/lgbt_in_britain_universities_report.pdf
27. Cech, Erin A., and Tom J. Waidzunas. "Systemic inequalities for LGBTQ professionals in STEM." Science advances 7.3 (2021): eabe0933. https://www.science.org/doi/10.1126/sciadv.abe0933
28. For information on the Royal Society of Chemistry's LGBT Report see https://www.rsc.org/new-perspectives/talent/lgbt-report/
29. Announcement of funding for the AAAS initiative on SOGI data collection in STEM https://www.aaas.org/news/aaas-awarded-nearly-20m-establish-three-distinct-initiatives-supporting-representation-stemm
30. For more information on the AAAS SEA Change program see https://seachange.aaas.org/

A.2.11 Bibliography and additional reading

Atherton, Timothy J., et al. "LGBT climate in physics: Building an inclusive community." American Physical Society, College Park, MD (2016). https://www.aps.org/programs/lgbt/upload/LGBTClimateinPhysicsReport.pdf

Barriers LGBTQI+ people face in the research funding process. TIGERS (2019) https://osf.io/dnhv8/

Barthelemy, Ramón S., et al. "Workplace climate for LGBT+ physicists: A view from students and professional physicists." *Physical Review Physics Education Research* 18.1 (2022): 010147. https://journals.aps.org/prper/abstract/10.1103/PhysRevPhysEducRes.18.010124

Bilimoria, Diana, and Abigail J. Stewart. "" Don't ask, don't tell": The academic climate for lesbian, gay, bisexual, and transgender faculty in science and engineering." nwsa Journal (2009): 85-103. https://www.jstor.org/stable/20628175

Campbell-Montalvo, Rebecca, et al. "" Now I'm not afraid": The influence of identity-focused STEM professional organizations on the persistence of sexual and gender minority undergraduates in STEM." Frontiers in Education. Frontiers, 2022. https://www.frontiersin.org/articles/10.3389/feduc.2022.780331/full

Cech, Erin A., and Michelle V. Pham. "Queer in STEM organizations: Workplace disadvantages for LGBT employees in STEM related federal agencies." Social Sciences 6.1 (2017): 12. https://www.mdpi.com/2076-0760/6/1/12

Cech, Erin A., and Tom J. Waidzunas. "Systemic inequalities for LGBTQ professionals in STEM." Science advances 7.3 (2021): eabe0933. https://www.science.org/doi/10.1126/sciadv.abe0933

Coon, Jaime Jo, et al. "Best practices for LGBTQ+ inclusion during ecological fieldwork: Considering safety, cis/heteronormativity, and structural barriers." Journal of Applied Ecology (2022). https://besjournals.onlinelibrary.wiley.com/doi/10.1111/1365-2664.14339

Exploring the workplace for LGBT+ physical scientists. Institute of Physics, Royal Astronomical Society and Royal Society of Chemistry (2019). https://www.rsc.org/globalassets/04-campaigning-outreach/campaigning/lgbt-report/lgbt-report_web.pdf

Formby, Eleanor. "How should we 'care' for LGBT+ students within higher education?." Pastoral care in education 35.3 (2017): 203-220. https://www.tandfonline.com/doi/abs/10.1080/02643944.2017.1363811

Freeman, Jon. "LGBTQ scientists are still left out." *Nature* comment (2018): 27-28. https://www.nature.com/articles/d41586-018-05587-y

Freeman, Jonathan B. "Measuring and resolving LGBTQ disparities in STEM." Policy Insights from the Behavioral and Brain Sciences 7.2 (2020): 141-148. https://journals.sagepub.com/doi/abs/10.1177/2372732220943232

Garvey, Jason C., et al. "The impact of campus climate on queer-spectrum student academic success." *Journal of LGBT Youth* 15.2 (2018): 89-105. https://www.tandfonline.com/doi/abs/10.1080/19361653.2018.1429978

Hughes, Bryce E. "Coming out in STEM: Factors affecting retention of sexual minority STEM students." Science advances 4.3 (2018): eaao6373. https://www.ncbi.nlm.nih.gov/pmc/articles/PMC5851677/

Maloy, Jeffrey, Monika B. Kwapisz, and Bryce E. Hughes. "Factors influencing retention of transgender and gender nonconforming students in undergraduate STEM majors." *CBE—Life Sciences Education* 21.1 (2022): ar13. https://www.lifescied.org/doi/full/10.1187/cbe.21-05-0136

Richey, Christina R., et al. "Gender and sexual minorities in astronomy and planetary science face increased risks of harassment and assault." Bulletin of the american astronomical society 51.4 (2019): 0206. https://assets.pubpub.org/cg3fekxj/51575918676654.pdf

Sansone, Dario, and Christopher S. Carpenter. "Turing's children: Representation of sexual minorities in STEM." *PloS one* 15.11 (2020): e0241596. https://journals.plos.org/plosone/article?id=10.1371/journal.pone.0241596

Sansone, Dario. "LGBT students: New evidence on demographics and educational outcomes." *Economics of Education Review* 73 (2019): 101933. https://www.sciencedirect.com/science/article/pii/S0272775719302791

Yoder, Jeremy B., and Allison Mattheis. "Queer in STEM: Workplace experiences reported in a national survey of LGBTQA individuals in science, technology, engineering, and mathematics careers." *Journal of homosexuality* 63.1 (2016): 1-27. https://www.tandfonline.com/doi/abs/10.1080/00918369.2015.1078632